THE LITHIUM ISOTOPE RATIO IN F AND G FIELD STARS

Thesis by

Judith Gamora Cohen

In Partial Fulfillment of the Requirements

For the Degree of

Doctor of Philosophy

California Institute of Technology

Pasadena, California

1971

(Submitted May 27, 1971)

Keep on trucking.

R. Krumb

ACKNOWLEDGMENTS

Steve and Karen Strom first got me involved in astronomical research. They've helped and encouraged me ever since, and I thank them.

Professor Guido Münch suggested this problem and supervised the research. He instructed me in the use of the interferometer. He faithfully came up to Mt. Wilson at the beginning of each of my runs to perform the delicate task of aligning the Fabry-Perot. He made many helpful comments on the earlier stages of the manuscript. I am very grateful for everything.

I had many helpful conversations with Professor Greenstein, whose vast store of spectroscopic wisdom has always impressed me. I also thank him for the use of many of his spectra. He and Prof. Oke were forced to listen to my many tirades on the unfortunate aspects of being a female at Caltech, and somewhat to my surprise as I look back on it, they listened patiently.

I thank Prof. Herbig for several helpful conversations and the loan of his spectra.

I am grateful to George Wallerstein, Arthur Vaughn, Dr. Conti, Prof. Sargent, and Prof. Fowler for helpful conversations on several topics.

I am grateful to the late Dr. Armin Deutsch for a chance to work with him and for much encouragement.

I thank Bob Kurucz, who with Steve Strom, wrote the model atmosphere programs.

I am grateful to Deane Peterson for many helpful conversations and the use of his computer program.

I thank Mt. Wilson Observatory for much 100" time and for a chance to sleep in the cook's cottage.

I thank Jerry and Vicky for all the good times I've had in their house in the Berkeley Hills, and for much encouragement.

While at Caltech, I have been supported by a NASA Traineeship, a California State scholarship, a GTA, and occasional gifts from my parents.

ABSTRACT

Theoretical profiles of the resonance line of Li I have been computed using an absorption coefficient which is the sum of that for each of the four components and a model stellar atmosphere. These profiles have been used to verify the lithium abundances derived by previous investigators with various approximations. A study of the feasibility of measuring the lithium isotope ratio with high dispersion photographic spectra was made, with negative results.

We obtain profiles of λ6708 Å of Li I, λ6717 Å of Ca I, and sometimes λ6710.3 Å of Fe I, and the D lines of Na I for a selected group of F, G, and early K field stars. These profiles were observed with the Fabry-Perot interferometer at the coudé focus of the 100" telescope with a resolution of 0.06-0.09 Å. Extensive checks of the accuracy of the wavelength scale, the instrumental profile, and the parasitic light level are made, including observations of the lunar spectrum. The D line profiles were used to test the accuracy of the computed theoretical profiles. The observed stellar line profiles are fit by calculated ones to determine the lithium abundance, calcium abundance, rotational velocity, radial velocity, microturbulent velocity, and lithium isotope ratio for the program stars. The rotational velocities are all greater than 2 km/sec, and range up to 10 km/sec. The microturbulent velocities in the program stars must be greater than zero. The isotope ratio Li^6/Li^7, determined by two independent methods, is zero in all the stars, with the possible exception of χ^1 Ori, for which we obtain $Li^6/Li^7 = 0.1\ (\pm 0.1)$.

Table of Contents

CHAPTER I

INTRODUCTION

In the last twenty years, a pattern of the relative chemical abundances in stars has become apparent. Let us define the metal deficiency of a star by the ratio

$$\frac{z_{\odot}}{z_{*}} = \frac{[\,N(Fe)/N(H)]_{\odot}}{[N(Fe)/N(H)]_{*}}. \qquad (1-1)$$

We have observed stars with metal deficiencies in their photospheres of almost 500. Yet the relative abundances of the elements heavier than beryllium with respect to iron are relatively constant, varying by no more than a factor of 5 for stars which are thought to be on or close to the main sequence. Lithium, beryllium, and perhaps helium do not obey this correlation. Stars with $z_{\odot}/z_{*}$ approximately unity may have lithium abundances with respect to hydrogen which differ by a factor of 200. Furthermore, the meteoritic and terrestial abundance of lithium is much higher than the lithium abundance of the solar photosphere. Lithium is very rare compared with other light nuclei such as C, N, and O.

The abundances observed in a stellar photosphere reflect the chemical composition of the gas out of which the star collapsed, any process of diffusion that may have occurred, nuclear reactions which may consume material convected downward as well as produce products which may mix to the surface, any surface nuclear reactions, mass loss, and other such phenomena. The light nuclei, such as deuterium, lithium, beryllium, and boron, are most susceptible to

nuclear burning, as they are destroyed at lower temperatures ($T \sim 8 \times 10^5$ °K) than the heavier elements. Furthermore, they are so rare ($N(Li)/N(H) \lesssim 10^{-9}$) that a relatively small additional amount produces observable changes in the lithium or beryllium abundance from star to star. In the cool stars, with deep surface convection zones, it is possible that material from the photosphere may be carried by convective currents to a depth where the temperature is sufficiently high that these light elements will be destroyed.

The abundance of these light nuclei at various stages of stellar evolution and in stars of different masses is therefore of considerable interest. Unfortunately, boron has never been observed in stellar spectra, and there is only one line in the spectrum of Be which is observable. This is the resonance line of Be II at 3130 Å, which is in a very inaccessible and a crowded region of the spectrum. The resonance line of Li I lies at 6708 Å, and no other lines of lithium are observable under normal conditions. Wallerstein and Conti (1969) review the observational material for Li and Be.

The isotopic ratio $N(Li^6)/N(Li^7)$ (which we abbreviate as Li^6/Li^7) is also a parameter of interest, as the isotopes of lithium have different cross sections for nuclear burning and different temperatures at which such burning commences. Isotopic data for stars are, however, very difficult to obtain. This is because the energy levels for atoms depend on the reduced mass μ, where

$$\mu = \frac{mM}{m + M}$$

and m is the mass of an electron, while M is the nuclear mass. Since $\mu \approx m(1 - \frac{m}{M})$ and m/M is at the maximum $1/1800$, the

separation of energy levels as μ changes for isotopes M to M + 1 is very small. Therefore the separation between lines of different isotopes of the same element is approximately $m\lambda/M$, which is very small. Furthermore, M increases rapidly as we go to atoms of larger atomic number. It is not surprising that only for D, He^3, and Li^6 (and Hg (Dworetsky 1970)) as compared with H, He^4, and Li^7 is the separation large enough that people have tried to determine isotopic abundances with atomic lines. (Peimbert and Wallerstein 1965a,b for D; Sargent and Jugaku 1961 for He^3). Molecular bands also show isotopic effects which depend on the reduced mass of the two atoms (for a diatomic molecule). C^{12}/C^{13} ratios have been measured in this way using the CH bands (McKellar 1960). Information about the distribution of Mg and Zr isotopes has been obtained using bands of MgH and ZrO (Schadee and Davis, 1968; Boesgaard 1968). G. H. Herbig (1964) initiated the work on the ratio Li^6/Li^7, although the possibility was mentioned in McKellar's (1960) review article, but dismissed as too difficult. Herbig used photographic spectra to observe the resonance line of Li I in late F and early G field stars. He claimed that the isotopic ratio ranged from 0.0 to 0.5 in the group of stars he studied. The isotopic ratio Li^6/Li^7 on the earth and meteorites is approximately 0.08, and the solar value is uncertain, but no larger than 0.2. Theories for production of Li predict $Li^6/Li^7 \approx 0.5$ when produced, and Li^6 burns more readily than Li^7.

We have measured the isotopic ratio Li^6/Li^7 using a Fabry-Perot interferometer built by Dr. A. H. Vaughn with a resolving power of more than 100,000 at the Coude focus of the 100" telescope.

The list of stars we observe includes most of those which Herbig (1964) discussed. In chapter II we describe the theoretical profiles of stellar lines which are necessary to interpret observed stellar line profiles. We attempt to derive Li^6/Li^7 from photographic spectra in chapter III. In chapter IV we rediscuss the observed data on lithium abundances.

A description of the Fabry-Perot interferometer is presented in chapter V, with special emphasis on its transmission as a function of wavelength, which we derive by observing laboratory sources. In chapter VI, we obtain profiles of the resonance line of Li I, λ6717 Å of Ca I, and sometimes λ6710 Å of Fe I for the observed stars. (Profiles of the D lines of Na I are given in appendix A.) This chapter also includes our observations of the lunar spectrum. We fit the observed stellar and lunar profiles to determine the abundance of lithium and calcium, the isotope ratio for lithium, the rotational velocity, and the microturbulent velocity of each star in chapter VII. In the last section, we present a brief discussion of the various theories of nuclear astrophysics for the production and destruction of lithium, and a summary of our conclusions. Appendix B discusses the feasibility of observing deuterium by means of the wings of the Balmer lines.

CHAPTER II

THEORETICAL PROFILES

A. Outline of Previous Investigations

No previous analysis of the resonance line of LiI in stellar spectra uses a correct method of calculating the theoretical line profile and equivalent width. The major studies of the Li abundance (Bonsack, 1959; Herbig, 1965; Merchant, 1967) have used two methods to determine the equivalent width of λ6707 Å, both originally suggested by Bonsack (1959). The lithium line, actually a blend of four components, is treated as though $Li^6/Li^7 = 0.00$, so that only the two fine-structure lines of Li^7 are considered. In Case I, it is assumed that the absorption coefficients for the two components should be added, and then the profile computed. Since LS-coupling predicts a ratio of 2:1 for the transition probability of these components, the method simply uses for the Doppler width of the blend a value 1.5 times that of the stronger component. Case II assumes $W_\lambda = W_1 + W_2$, where $gf_1 = 2gf_2$. In all previous analyses, a single layer approximation is used.

Obviously, neither of these methods is satisfactory. Furthermore the neglect of temperature stratification may introduce significant errors in determining the abundance of lithium.

The determination of the isotope ratio is based on the treatment given by Herbig (1964). Here the wavelength of the "center of gravity" of the resonance line is computed using the following

assumptions. Each isotopic line is assigned a wavelength which is that of the average of the two components, weighted by their 2:1 LS-coupling intensities. Thus the wavelength for a line of only the isotope Li^7 is 6707.811 Å, while that for pure Li^6 is 6707.971 Å. Then, if the isotopic ratio Li^6/Li^7 is denoted by R, the wavelength of the "center of gravity" of the whole line is given by

$$\lambda = \frac{6707.811 + R(6707.971)}{1 + R} \text{ Å} \qquad (2\text{-}1)$$

This treatment neglects the possibility of saturation in any of the components. Since the stars which were chosen by Herbig for determination of their isotopic ratio are those with a strong Li I line, it is possible that errors may in this manner be introduced.

We thus find that previous determinations of the theoretical provile of λ6708 Å of Li I, both in the form of its equivalent width and its central wavelength, have been inadequate.

B. Assumptions of Our Theoretical Profiles

Our theoretical profiles are based on an integration over optical depth of a summed line absorption coefficient. The line absorption coefficient is the sum of four Voigt functions. Let $\Delta\lambda_D(\tau)$ be the Doppler width corresponding to the depth τ. Then

$$\begin{aligned}\alpha(\lambda,\tau) = {} & \alpha_o(\tau) H[\lambda\text{-}6707.761)/\Delta\lambda_D(\tau), a(\tau)] \\ & + \alpha_o(\tau) 0.5 H[(\lambda\text{-}6707.912)/\Delta\lambda_D(\tau), a(\tau)] \\ & + \alpha_o(\tau) R H[(\lambda\text{-}6707.921)/\Delta\lambda_D(\tau), a(\tau)] \\ & + \alpha_o(\tau) R\, 0.5[(\lambda\text{-}6708.872)/\Delta\lambda_D(\tau), a(\tau)] \qquad (2\text{-}2)\end{aligned}$$

where $\alpha_o(\tau)$ is the absorption coefficient for the stronger Li^7 component (λ6707.761 Å) at line center for zero damping, and it depends on the ionization and excitation of lithium, as well as the lithium abundance. $a(\tau)$ is given by the relation

$$a(\tau) = \frac{\Gamma(\tau)}{4\pi\Delta\lambda_D}$$

where $\Gamma(\tau)$ is the damping constant. $H(\Delta\lambda/\Delta\lambda_D, a)$ is the Voigt function, and R is the isotope ratio $N(Li^6)/N(Li^7)$, which is assumed independent of depth. Note that the factors of 0.5 enter from the LS-coupling strengths of the fine structure components.

We have assumed that the profile of the absorption coefficient for each of the four components of λ6708 Å has the same $\Delta\lambda_D(\tau)$, i.e. the same microturbulent velocity at a given depth. These assumptions are reasonable and acceptable from the physical point of view. In practice, $R(Li^6/Li^7)$, $A(Li^7)$, and the microturbulent velocity are assumed independent of depth.

The actual value of the damping constant is the sum of Γ for radiative damping, van der Waals broadening, and electron broadening. Radiative damping gives a width proportional to the lifetime of the upper level, namely for λ6708 Å $\Gamma_\omega = 3.7 \times 10^7$/sec, or $\Gamma_\lambda = 4.5 \times 10^{-2}$ mÅ, which is negligible. H. R. Griem (1964) has tabulated the half width for electron broadening of λ6708 Å of LiI as a function of N_e and T. For typical values at $\tau \sim 0.5$ of $N_e \sim 10^{13}$ and $T \sim 5000\ ^oK$, we obtain $\Gamma_\lambda = 2 \times 10^{-2}$ mÅ, which is negligible. This result is not very sensitive to temperature and

is linear in N_e. Hence the major source of broadening must be collisions with neutral perturbers (van der Waals broadening). To evaluate this, we use an approximation given by Aller (1963) and the Rydberg correction for Li given by Herzberg (1944):

$$\Gamma_n = 17.0\, C^{2/5} v^{3/5} N_n \tag{2-3}$$

where N_n is the number of neutral atoms, and

$$C = 6.46 \times 10^{-34} \frac{r^2}{a_o^2}\ , \tag{2-4}$$

where a_o is the Bohr radius for the ground state of hydrogen. Aller (1963) gives an approximation for r as a function of the quantum numbers of the upper state, which we use for the D lines and λ6717 Å of Ca I. For λ6708 Å of Li I we obtain $C = 4.3 \times 10^{-33}$, while for the Na I D lines we obtain $C = 6.6 \times 10^{-33}$, and for λ6717 Å of Ca I we obtain $C = 8.0 \times 10^{-33}$. This leads to Γ_λ for λ6708 Å of 1 mÅ, which is much larger than that for electron broadening.

We now adopt the approximation of neglecting electron broadening, as both Γ_e and Γ_n are proportional to the density of perturbers. Therefore,

$$\Gamma = \Gamma_{rad} + \Gamma_n = \Gamma_{rad} + 17.0\, C^{2/5} N_n(\tau) v^{3/5}(\tau) \tag{2-5}$$

Figure 1 shows $\Gamma_n(\tau)/\Gamma_{c\ell}$ for a typical solar-type model, where $\Gamma_{c\ell}$ is the classical damping constant,

Figure 1. The ratio of the damping constant for van der Waals broadening to the classical damping constant as a function of τ_{5000} for the model (5500,4,1). The constant value of the radiative damping constant is indicated.

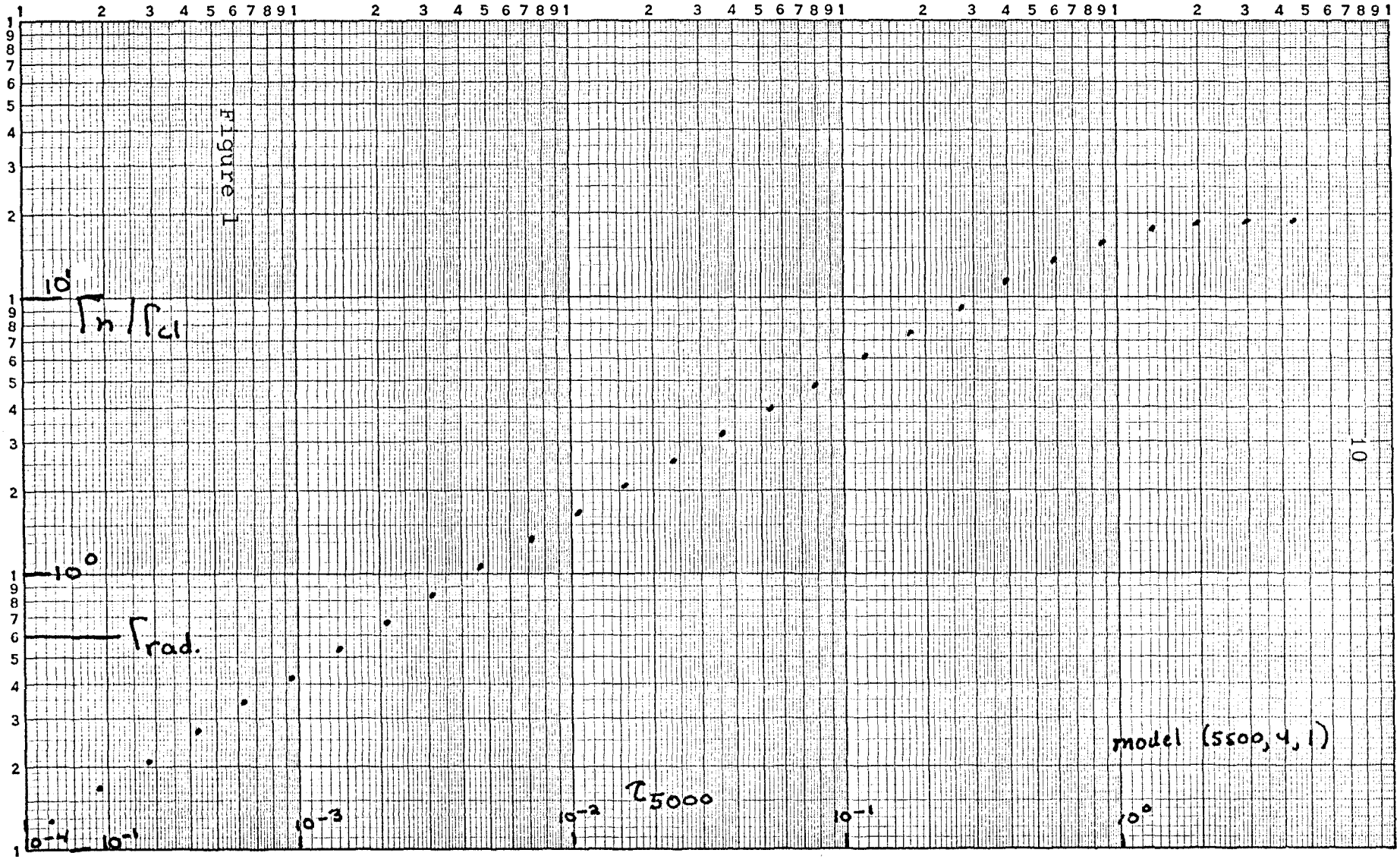
Figure 1
Γ_n / Γ_{cl}
10^1
10^0
$\Gamma_{rad.}$
τ_{5000}
10^{-4}
10^{-3}
10^{-2}
10^{-1}
10^0
model (5500, 4, 1)

$$\Gamma_{c\ell} = \frac{8\pi^2 \nu^2 e^2}{3mC^3} \qquad (2\text{-}6)$$

Ionization of hydrogen at large depths (which decreases N_n) produces the tendency for $\Gamma_n/\Gamma_{c\ell}$ to increase less rapidly beyond $\tau = 1$.

In the region from $\tau = 0.1$ to $\tau = 1$, Γ_n is from 10 to 20 times the classical value. Furthermore, the exact choice of the damping constant is irrelevant for a weak line whose equivalent width is less than 150 mÅ. We therefore set $\Gamma = 10\ \Gamma_{c\ell}$. We compute $\Gamma(\tau)$ using equation 2-5 only for the D lines of Na I, where the value of Γ is critical as the lines are so strong.

We must now use the line absorption coefficient of equation 2-1 together with a model atmosphere to produce a line profile. We recall that at the surface

$$I_\nu(\theta) = \int_0^\infty S_\nu(\tau_\nu) e^{-\tau_\nu \sec(\theta)} \sec(\theta)\, d\tau_\nu \qquad (2\text{-}7)$$

and

$$F_\nu = 2\int_0^\infty S_\nu(\tau_\nu) E_2(\tau_\nu)\, d\tau_\nu, \qquad (2\text{-}8)$$

where E_2 is the second exponential integral. Since our primary concern here is stellar, rather than solar, profiles, we require the emergent flux. In equations 2-7 and 2-8, τ_ν refers to an optical depth scale defined by the total absorption coefficient, which is the sum of the line and continuous absorption coefficients. We assume throughout that the source function is given by the Planck function at

$T(\tau)$; i.e. that there is no scattering. This point is discussed in more detail in section C.

We can then obtain the residual intensity and equivalent width from

$$RI(\lambda) = \frac{F^{line}(\lambda)}{F^{cont}(\lambda)} \tag{2-9}$$

and

$$W_\lambda = \int_0^\infty (1 - RI(\lambda))\, d\lambda \tag{2-10}$$

The models which we have used have been computed on the IBM 360 computer with a program (ATLAS) written by Dr. S. E. Strom and Mr. R. L. Kurucz. The basic methods used to generate the models are described in Strom and Avrett (1964, 1965). The assumptions on which these models are based are that the atmosphere can be represented by a plane parallel, semi-infinite model in hydrostatic and radiative equilibrium. Local thermodynamic equilibrium is assumed to hold. The opacity sources which are included are bound-free and free-free absorption by H^-, neutral hydrogen, neutral helium, and ionized helium, and electron scattering. Approximate opacities for bound-free absoprtion by C, N, O and Ne from the ground and low excited states of the first four ionization states have been added by Dr. D. M. Peterson (see Peterson and Scholz, 1971). Radiation pressure is treated as a perturbation on the gas pressure, and the Avrett-Krook temperature correction scheme is used iteratively to obtain a model with flux independent of depth.

The optical depth scale for the continuum is defined at a standard wavelength which corresponds to the frequency at which the atmosphere is most transparent; we have used $\tau_{5000\ \text{Å}}$ in all cases. With this choice of depth scale, convergence occurs within six iterations. The model atmospheres are characterized by the parameters of effective temperature, surface gravity, and chemical composition. The latter is represented by the factor $Z/Z_{\odot}$, where Z is an average over the heavy elements. We shall denote such models by the notation $(T_{eff}, \log g, Z/Z_{\odot})$. Note that the value of $Z/Z_{\odot}$ is used in calculating the electron pressure and continuous opacity, but does not affect the lithium abundance used to compute the line absorption coefficient. The helium content for all the models was assumed to be 0.10 by number. The exact choice of helium content is not relevant to the aim of this investigation.

We initially chose at random one model falling within the spectral range covered by the observational data, and computed a complete grid of profiles of λ6708 Å of Li I for it. The model chosen has an effective temperature of 6250 ^{o}K, a surface gravity of $\log g = 4.0$, and $Z/Z_{\odot} = 0.1$, corresponding approximately to an F8 main-sequence star with a moderate metal deficiency. Profiles were computed for $R = 0.01, 0.25, 0.50$, and 1.00 for a microturbulent velocity of 0, 1, and 3 km/sec. In addition to the standard adopted abundance of Li^7, denoted by $A(Li^7)$, $A(Li^7)$ was multiplied by 10, 0.1, and 0.3. The abundance $\log (N(Li)/N_H)$ corresponding to $A(Li^7)$ is -9.0, rather than the solar Li abundance. We note that the upper limit for the photospheric lithium abundance

is a factor of 200 less than the meteoritic abundance (Peach, 1968).

C. The Source Function of the Lithium Line

To construct our theoretical profiles, we have adopted the assumption that the source function in the lithium line λ6708 Å is given by the Planck function. This procedure requires some justification.

A more correct form of the source function is that given by Aller (1963)

$$S_\nu(\tau) = \left[\frac{1 + \epsilon\eta}{1 + \eta}\right] B_\nu(T(\tau)) + \left[1 - \left(\frac{1 + \epsilon\eta}{1 + \eta}\right)\right] J_\nu(\tau) \qquad (2\text{-}11)$$

where η is the ratio of line to continuous absorption coefficients and $(1 - \epsilon)$ is the fraction of all absorbed quanta which are reemitted as scattered radiation. In order to achieve our approximation that $S_\nu = B_\nu$, either of two conditions is sufficient; $\epsilon = 1$ or $J_\nu = B_\nu$. We may estimate ϵ for λ6708 Å using Ambartsumyan's (1956) result, (equation 14-19 of his text)

$$\epsilon = \frac{c_{2f}}{c_{2f} + A_{21}} \qquad (2\text{-}12)$$

where c_{2f} is the rate of photoionization processes from the upper level of the line. A reasonable estimate of c_{2f} combined with the value of A_{21} given by Wiese, Smith and Glennon (1966) leads to $\epsilon \sim 10^{-2}$, which is much too small for pure absorption to hold. We may also estimate ϵ by considering S_ν given by 2-11, assuming

that η is independent of depth, using a two stream approximation, and assuming that the Planck function is linear in τ and independent of ν over the width of the line,

$$B(\tau) = B_o + B_1(\tau) \tag{2-13}$$

to derive

$$RI_\nu = \frac{2}{\sqrt{3} + \frac{B_1}{B_o}} \frac{\sqrt{3L} + \frac{1}{1+\eta}\frac{B_1}{B_o}}{1 + \sqrt{L}} \tag{2-14}$$

where

$$L = \frac{1 + \epsilon\eta}{1 + \eta} \tag{2-15}$$

We now consider the center of very strong lines (which traditionally are considered to be formed by scattering) so that η is very large. The measured residual intensity of the center of a strong feature such as H and K of Ca II or the D lines in solar type stars is approximately 5%. Choosing a reasonable value of $B_1/B_o = 2$, we use equation 2-14 to obtain

$$L \sim \epsilon \sim 10^{-2}$$

Therefore ϵ is too small to force pure absorption to prevail.

We do not know enough about the mean intensity to validate the assumption of pure absorption through the behavior of $J_\nu(\tau)$. It is clear that a knowledge of this parameter is critical. We note that the limits of equation 2-14 when $L = 1$ or 0 (corresponding to pure absorption or pure scattering and large η respectively),

$$RI_\nu = \frac{\sqrt{3} + \frac{1}{1+\eta}\frac{B_1}{B_o}}{\sqrt{3} + \frac{B_1}{B_o}} \qquad \text{(for } L = 1\text{)} \qquad (2\text{-}16)$$

and

$$RI_\nu = \frac{2}{\sqrt{3} + \frac{B_1}{B_o}} \frac{1}{1+\eta}\frac{B_1}{B_o} \qquad \text{(for } L = 0\text{)} \qquad (2\text{-}17)$$

predict very different behavior for the line profile as a function of η.

Therefore our naive expectation is that scattering is very important in the source function for λ6708 Å and that the validity of our assumption that $S_\nu = B_\nu$ depends critically on how deep in the atmosphere does J_ν become equal to B_ν. To resolve this question we turn to the Na I D lines, which come from the same levels as the λ6708 Å fine structure doublet ($2\,^2S - 2\,^2P^o_{3/2}$, $2\,^2P^o_{1/2}$ for Li, and $3\,^2S - 3\,^2P^o_{3/2}$, $3\,^2P^o_{1/2}$ for Na). John Waddell III (1962a,b) studied the profile of each of the D lines from the center to the limb of the sun. He analyzed the cores of these profiles with three assumptions, $\eta_\lambda \gg 1$, η_λ proportional to gf, and $S_{D1}(\tau) = S_{D2}(\tau)$. The third assumption is the only one which can reasonably be questioned, and indeed if departures from LTE are important, it could be invalid. His derived relations for $I_{D1}(\mu)$ as a function of $I_{D2}(\mu)$ were obeyed extremely well by the observed profiles. This implies that even if the line source function for each line of the multiplet is not $B_\nu(\tau)$, the two source functions are identical. E. H. Avrett (1966) provided the theoretical understanding of

Waddell's observations. He discussed the problem of a three level atom plus continuum, where the three levels are a ground state (1) and two close-lying upper states (2 and 3) between which radiative transitions are forbidden. His solutions to the line transfer problem in such an idealized atom, made assuming detailed balance of each level, non-coherent scattering, and various functional forms for $B(\tau)$, demonstrate that in the interlocking 3-level atom $S_{31}(\tau) = S_{21}(\tau)$, and that $S_{31}(\tau)$ is equal to $B(\tau)$ at great depths, but less than $B(\tau)$ towards the surface (for T constant or increasing inward).

Let us apply these results to lithium. We denote the two components (λ6707.76 and 6707.91 Å) of the Li^7 line by A and B. Even if $S_A(\tau)$ is not equal to $B_\nu(\tau)$, we know $S_A(\tau) = S_B(\tau)$ and $S_A(\tau) \leq B_\nu(T(\tau))$. Hence, in effect, the worst that happens is that the temperature gradient given in the model with the assumption that $S_\nu = B_\nu(T(\tau))$ is too hot close to the surface, where we should use $S_\nu = B_\nu(T^*(\tau))$, and $T^* < T$. This would result in stronger lines than we predict with out simple theoretical profiles. We shall next show that in the case under consideration, $T^*(\tau)$ is very close to $T(\tau)$.

G. W. Curtis (1965), H. R. Johnson (1965), and D. Mugglestone (1965) have theoretically studied the Na I D lines in the sun. The most complete analysis is that of Curtis, which is based on Waddell's observations. With no a priori assumptions about the relationship between the source function and $B_\nu(T(\tau))$, they derive the continuum

source function $S_c(\tau)$ and the line source function $S_\ell(\tau)$ from the observed profiles. They assume $S_{D1}(\tau) = S_{D2}(\tau)$ and S_{D1} is independent of ν; $\alpha_{D1}(\nu) =$ constant $\alpha_{D2}(\nu)$, and S_c is independent of ν over the width of the line. Their final result is that for $\tau_{5000\,\text{Å}} > 10^{-2}$, $S_c = S_\ell$, and for $\tau_{5000\,\text{Å}} < 10^{-2}$, $S_\ell < S_c$ (as expected). Furthermore we know that the continuum is in LTE, and hence we obtain that for $\tau_{(5000\,\text{Å})} > 10^{-2}$, $S_\ell = B_\nu(T(\tau))$. Even the cores of the lithium lines, being much weaker than the D lines, are formed below $\tau = 10^{-2}$. Furthermore the atomic parameters of Li and Na are almost identical; they have similar ionization potentials, and the D lines are exactly analogous to the Li lines. None of the collisional transition rates involved in detailed balance of the Na I levels depends on the number of Na atoms, as the collisions are with electrons, H or H^-. Therefore, we may expect these results obtained by analysis of the D lines in the sun to be applicable to the lithium lines in stars whose atmospheric parameters are close to those of the sun.

We have therefore demonstrated that in the region of the atmosphere where the lithium lines are formed (with the possible exception of stars with exceedingly strong λ6708 Å, such as the T Tauri stars), $S_A(\tau) = S_B(\mu) = B(T(\tau))$, and hence pure absorption is a valid approximation.

D. Discussion of the Theoretical Profiles

The calculated profiles behave reasonably. If v_t (the microturbulent velocity) becomes as large as 3 km/sec, all detail in the profile is lost. This is not surprising, since the Doppler width corresponding to 3 km/sec is 0.07 Å, which is almost half of the wavelength separation between the components. Note that the thermal Doppler width at 6000 ^{o}K for this line is about 0.08 Å. The relative intensity of the two major components (at 6707.76 Å and 6707.92 Å) changes with R in the manner anticipated, while the third component at 6708.07 Å is never strong enough to be present, even when R = 1.0, although it can be observed as producing a slight asymmetry on the long wavelength wing of the line, but even this is marginally detectable. (Note that because $A(Li^7)$ was held constant, rather than $A(Li^6+Li^7)$, profiles with the same value of $A(Li^7)$ but different values of R, have different total lithium abundances.) At abundances corresponding to 10 $A(Li^7)$, it is obvious that the lines are completely saturated; however, none of the stars observed had lithium lines as strong as this profile. Even in the range from $A(Li^7)$ to 0.3 $A(Li^7)$, which covers the range of the observed profiles, there is some saturation, as the equivalent width at $A(Li^7)$ is less than $3 \times W(0.3\ A(Li^7))$.

In figures 2a-j we see samples of these profiles, all computed from the same model atmosphere. Table 1 presents the equivalent width for the calculated grid, while table 2 gives the wavelength at the point of minimum residual intensity, and table 3 gives the wavelength $\lambda_{1/2}$ such that

Figure 2. Computed Profile of λ6708 Å for the model (6250,4,0.1) with

a) $A(Li^7)$, R = 0.01, and $v_t = 0$

b) $A(Li^7)$, R = 0.25, and $v_t = 0$

c) $A(Li^7)$, R = 0.50, and $v_t = 0$

d) $A(Li^7)$, R = 1.0, and $v_t = 0$

e) $A(Li^7)$, R = 1.00, and $v_t = 3$

f) 0.3 $A(Li^7)$, R = 0.01, and $v_t = 0$

g) 0.3 $A(Li^7)$, R = 0.25, and $v_t = 0$

h) 0.3 $A(Li^7)$, R = 0.50, and $v_t = 0$

i) 0.3 $A(Li^7)$, R = 1.00, and $v_t = 0$

j) 10 $A(Li^7)$, R = 0.01, and $v_t = 0$

Figure 2

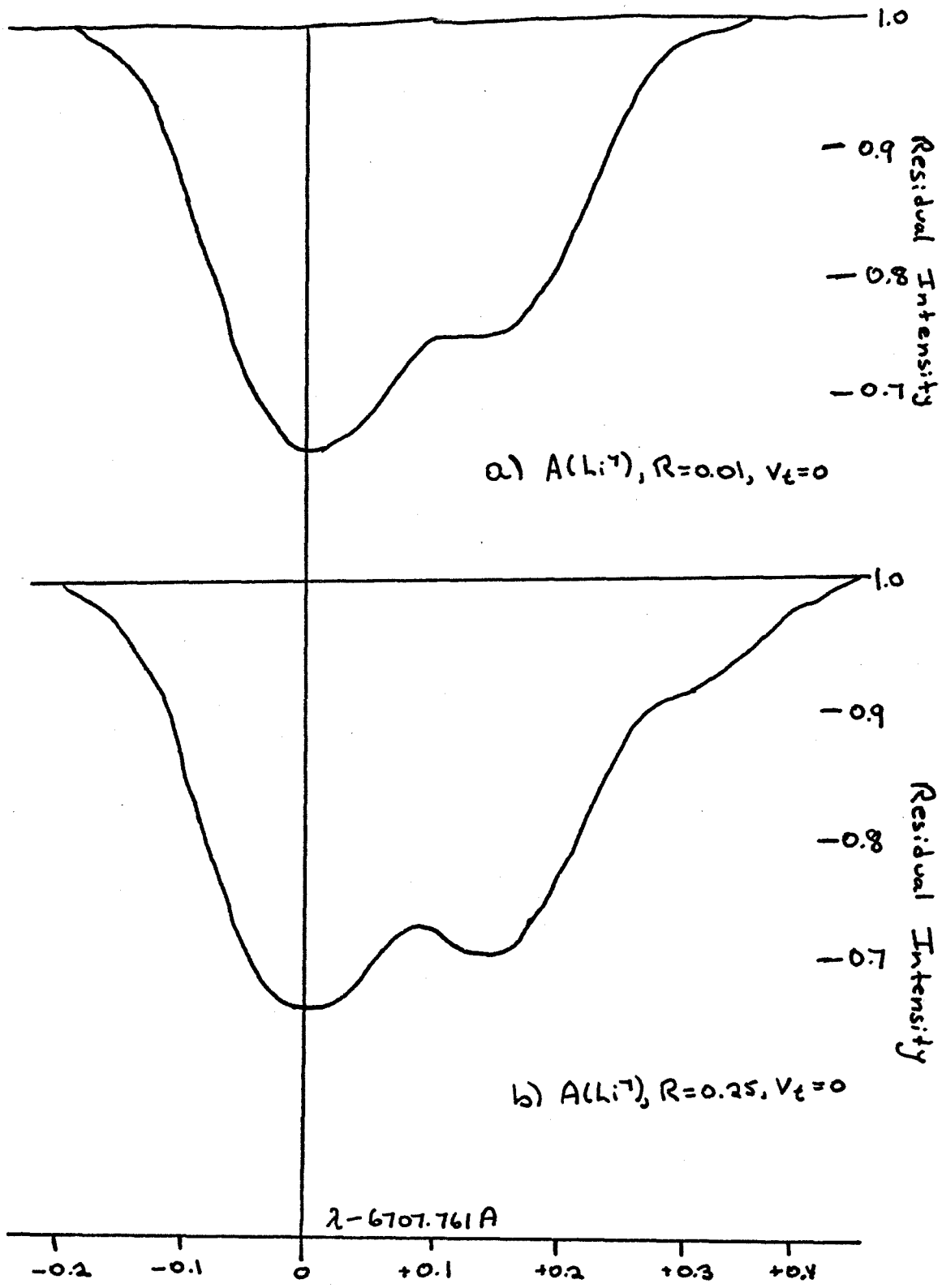
1.0
0.9
0.8
0.7
Residual Intensity
a) A(Li⁷), R=0.01, v_t=0
1.0
0.9
0.8
0.7
Residual Intensity
b) A(Li⁷), R=0.25, v_t=0
λ-6707.761 A
-0.2
-0.1
0
+0.1
+0.2
+0.3
+0.4

Figure 2

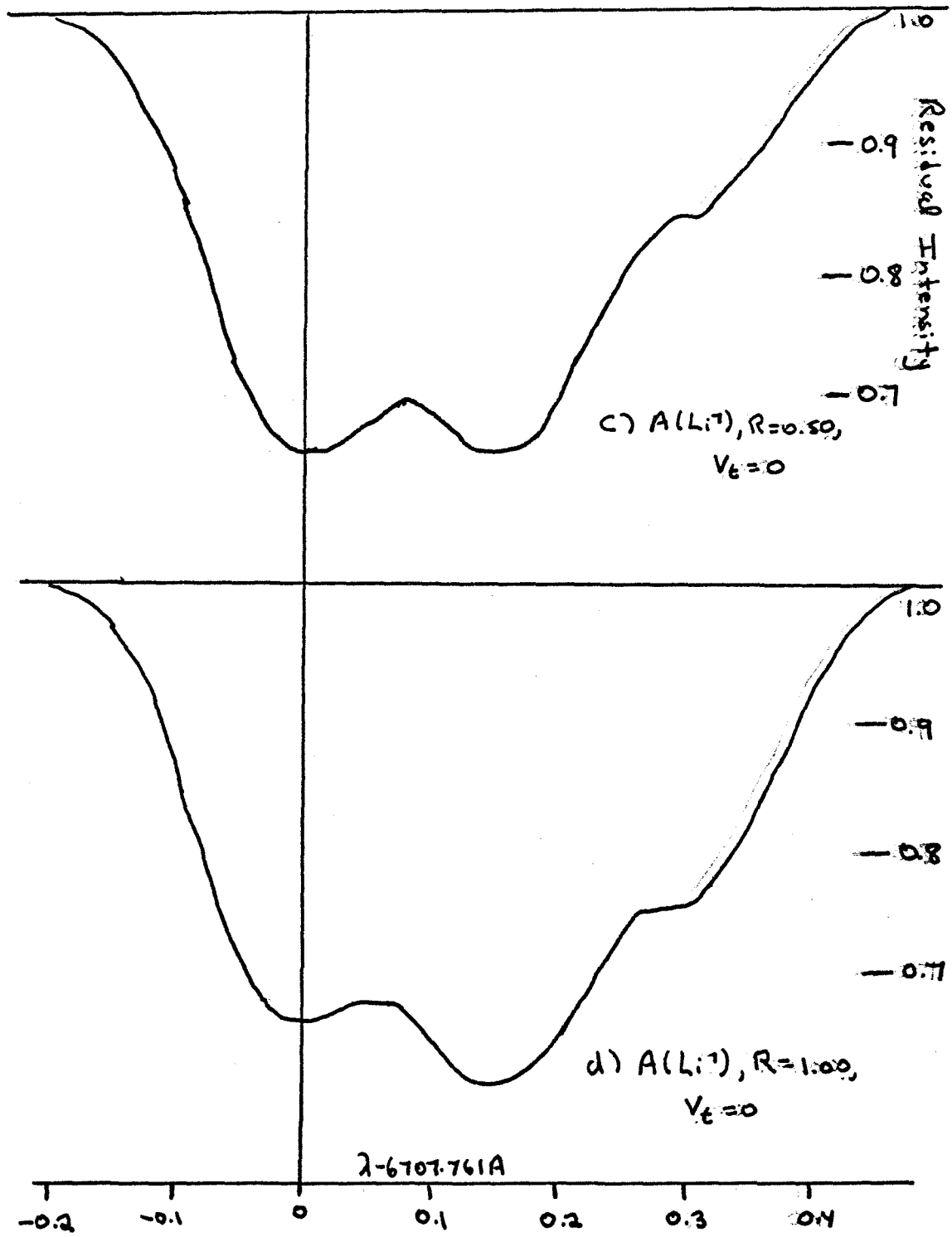
1.0
0.9
0.8
0.7
Residual Intensity
c) A(Li⁷), R=0.50, Vt=0
1.0
0.9
0.8
0.7
d) A(Li⁷), R=1.00, Vt=0
λ-6707.761A
-0.2
-0.1
0
0.1
0.2
0.3
0.4

Figure 2

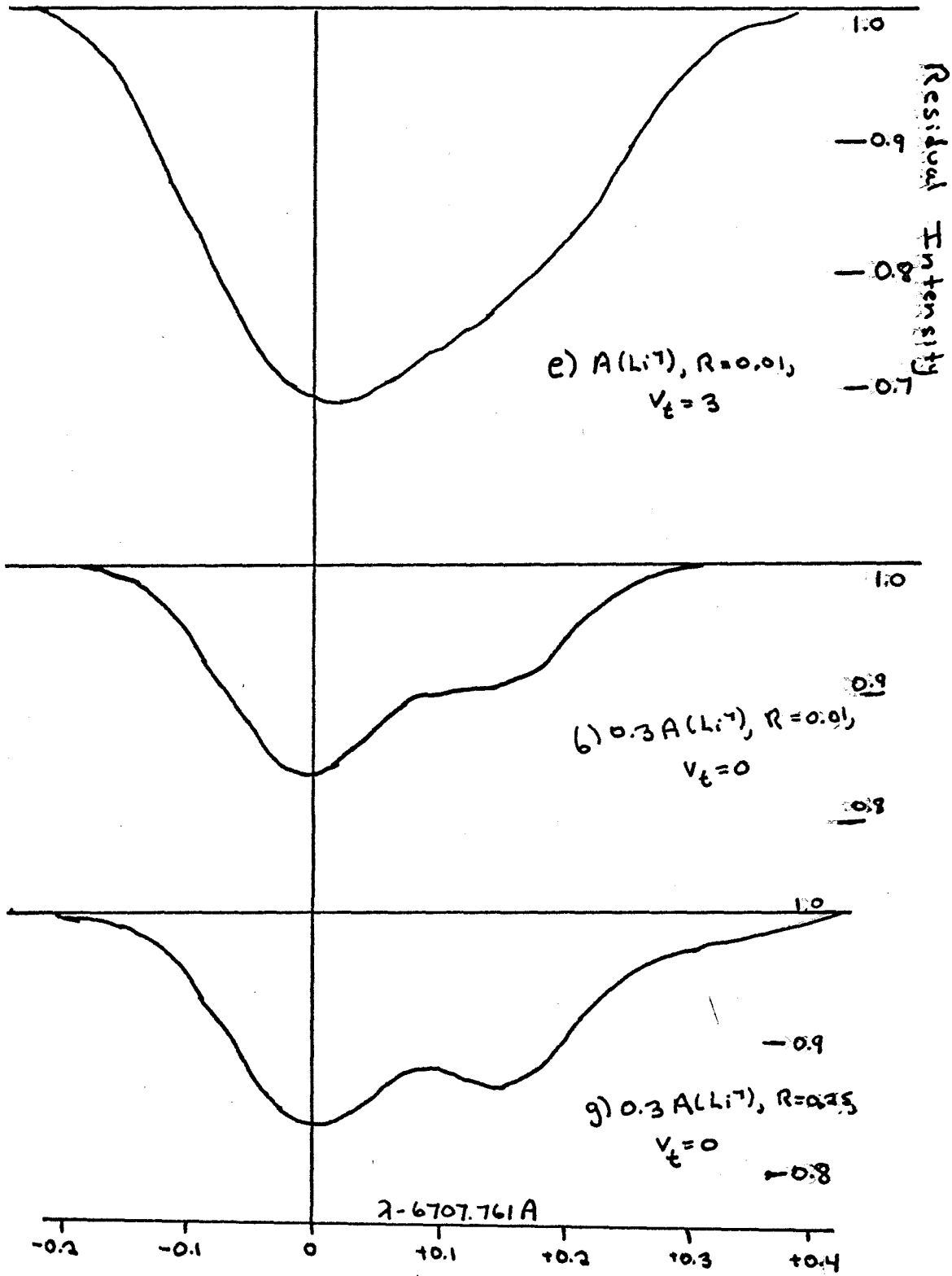
1.0
0.9
0.8
0.7
Residual Intensity
e) A(Li⁷), R=0.01,
$V_t = 3$
1.0
0.9
0.8
6) 0.3 A(Li⁷), R=0.01,
$V_t = 0$
1.0
0.9
0.8
g) 0.3 A(Li⁷), R=0.25
$V_t = 0$
λ-6707.761 A
-0.2
-0.1
0
+0.1
+0.2
+0.3
+0.4

Figure 2

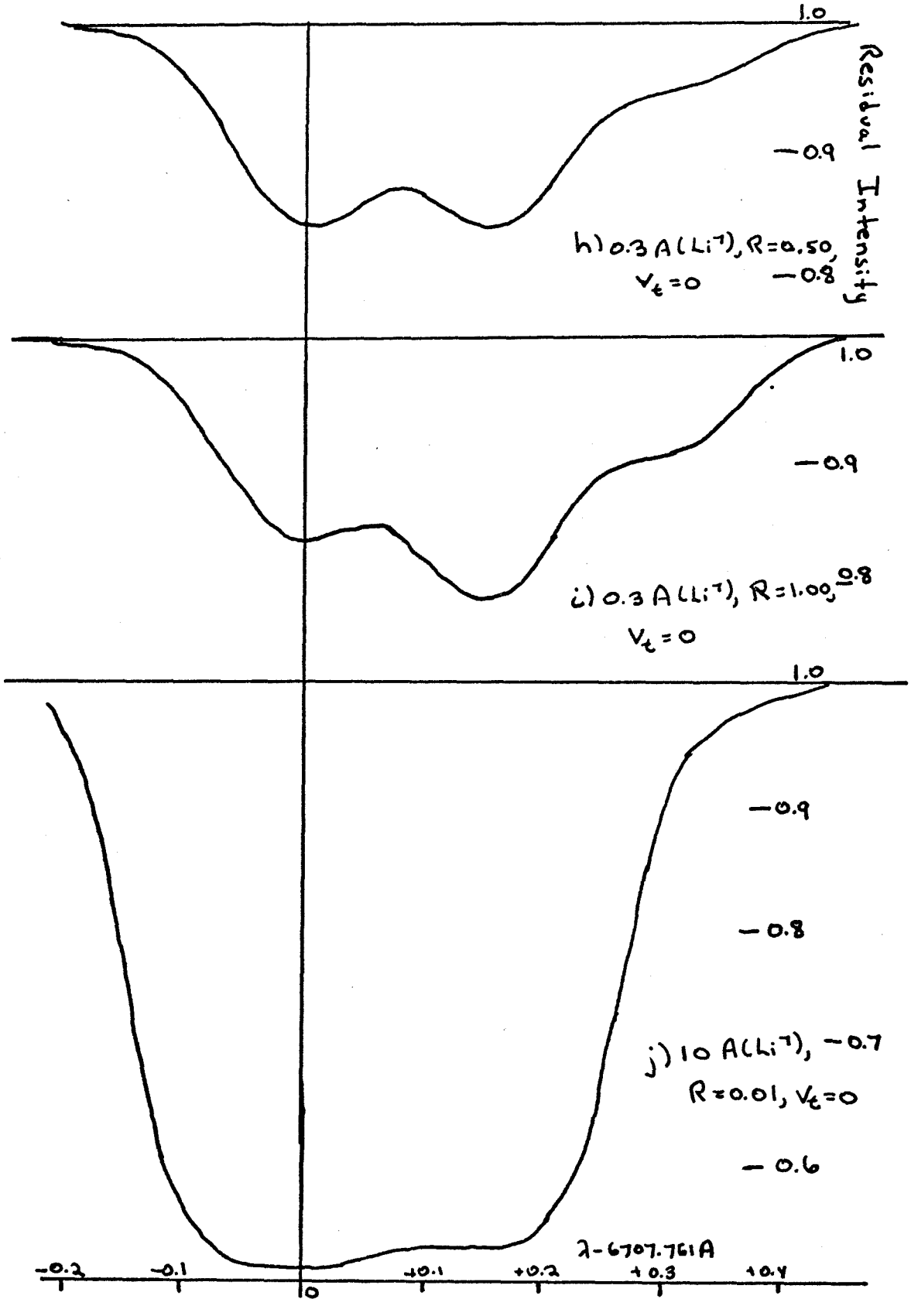
1.0
Residual Intensity
—0.9
h) 0.3 A(Li⁷), R=0.50,
V_t=0
—0.8
1.0
—0.9
i) 0.3 A(Li⁷), R=1.00, —0.8
V_t=0
1.0
—0.9
—0.8
j) 10 A(Li⁷), —0.7
R=0.01, V_t=0
—0.6
λ-6707.761A
-0.2
-0.1
0
+0.1
+0.2
+0.3
+0.4

TABLE 1

Equivalent Widths for λ6708Å Using the Model (6250,4,0.1)

(W_λ in mA is tabulated)

I. $A(Li^7)$

R	v_t		
	0	1	3
0.01	93	93	97
0.25	113	114	117
0.50	129	130	134
1.00	152	154	160

II. $10\ A(Li^7)$

R	v_t	
	0	3
0.01	201	224
0.25	246	266
0.50	262	283
1.00	276	301

III. $0.1\ A(Li^7)$

R	v_t
	0
0.01	15
0.25	18
0.50	22
1.00	28

IV. $0.3\ A(Li^7)$

R	v_t
	0
0.01	39
0.25	48
0.50	56
1.00	72

TABLE 2

Wavelength of the Minimum Value of $RI(\lambda)$
from Profiles for the Model (6250, 4, 0.1)

(λ-6707.761 Å is tabulated)

I. $A(Li^7)$

R	v_t		
	0	1	3
0.01	0.000	0.000	0.010
0.25	0.010	0.000	0.030
0.50	0.160 0.010	0.150 0.010	0.080
1.00	0.060	0.160	0.150

II. $10\ A(Li^7)$

R	v_t	
	0	3
0.01	0.000	0.030
0.25	0.000	0.060
0.50	0.150 0.000	0.080
1.00	0.120	0.120

III. $0.1\ A(Li^7)$

R	v_t
	0
0.01	0.000
0.25	0.000
0.50	0.150 0.000
1.00	0.150

IV. $0.3\ A(Li^7)$

R	v_t
	0
0.01	0.000
0.25	0.010
0.50	0.150 0.000
1.00	0.160

TABLE 3

Values of $\lambda_{1/2}$ for Profiles of λ6708 Å

for the Model (6250,4,0.1)

($\lambda_{1/2}$-6707.761 is tabulated)

I. A(Li^7)

R	v_t		
	0	1	3
0.01	0.05	0.05	0.05
0.25	0.08	0.08	0.08
0.50	0.11	0.11	0.11
1.00	0.14	0.13	0.13

II. 10 A(Li^7)

R	v_t	
	0	3
0.01	0.07	0.07
0.25	0.12	0.11
0.50	0.13	0.13
1.00	0.15	0.15

III. 0.1 A(Li^7)

R	v_t
	0
0.01	0.04
0.25	0.07
0.50	0.10
1.00	0.13

IV. 0.3 A(Li^7)

R	v_t
	0
0.01	0.04
0.25	0.07
0.50	0.10
1.00	0.13

$$\int_0^{\lambda_{1/2}} [1 - RI(\lambda)]\, d\lambda = \int_{\lambda_{1/2}}^{\infty} [1 - RI(\lambda)]\, d\lambda \qquad (2\text{-}18)$$

which is what Herbig (1964) meant by his expression "the wavelength of the center of gravity." (Herbig, 1970)

The equivalent widths given in table 1 do not depend strongly on microturbulent velocity even though the widths get to be so large that one expects the line to be on the flat part of the curve of growth. This is because, although the total width is large, the line is made of sufficiently many components that each is still in a certain sense on the linear part of the curve.

If we use Herbig's (1964) relation between $\lambda_{1/2}$ and the isotope ratio (equation 2-1), we obtain the values $\lambda_{1/2}$ (Herbig) given in table 4. We see that equation 2-1 satisfactorily predicts the "wavelength of the center of gravity," as $\lambda_{1/2}$ (Herbig) agrees very well with $\lambda_{1/2}$ determined from the computed profiles (see table 3). Thus assuming Herbig's (1964) measurements are correct, his results must be accepted.

TABLE 4

$\lambda_{1/2}$ as a Function of R

R	$\lambda_{1/2}$ (Herbig) (Å)
0.01	6707.761 + 0.05
0.25	6707.761 + 0.08
0.50	6707.761 + 0.11
1.00	6707.761 + 0.13

We now consider the validity of the assumptions which have been made in previous investigations regarding the equivalent width of the lithium line. Figure 3 shows 3 curves of growth. The first is a curve of growth for a single component. The second is that for the resonance line with $R = 0.01$ (essentially that for a blend of only two fine-structure components); the third is for $R = 0.50$, and is the curve for the complete line of four components. The abundance scale here is the total abundance of lithium, not $A(Li^7)$, so that the abundance is the same for all three curves. Note that the curves for $R = 0.01$ and $R = 0.50$ do not coincide; thus to some extent the equivalent width for a given Li abundance and hence the curve of growth depends on the isotope ratio. However, the range in W_λ as a function of R for values of W_λ that occur in stars (10 to 120 mÅ) is sufficiently small that the uncertainty in lithium abundance due to lack of knowledge of R is about 0.1 in the log.

We see that the curve of growth for the blend of several fine-structure components remains linear for much larger values of W_λ than does the curve for a single fine-structure component (i.e. a line with only one component). This is because a complex line with large equivalent width is in some sense a sum of lines of lower equivalent width, and hence each of the components is still on the linear part of the curve.

One of the standard approximations used in previous investigations to compute the equivalent width of the total lithium line is that $W = W_1 + W_2$, where $gf_1 = 2gf_2$, namely treating the line as a blend

Figure 3. Equivalent width versus total lithium abundance for λ6708 Å with only one fine-structure component, two fine-structure components (R = 0.01), and all four components (R = 0.50). The absolute scale of the lithium abundance is arbitrary but is the same for all three curves.

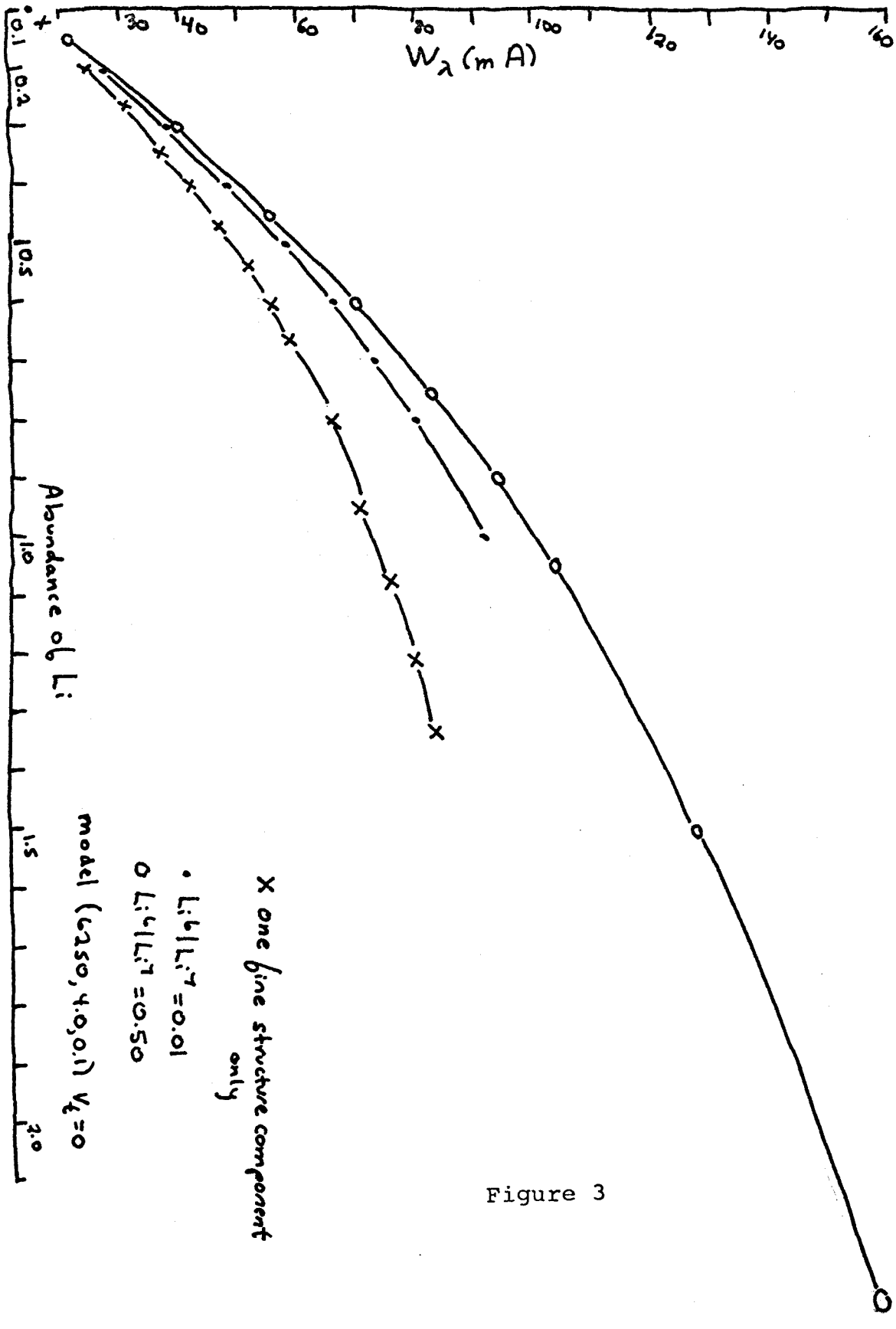
W_λ (m Å)
30
40
60
80
100
120
140
160
Abundance of Li
0.1
0.2
0.5
1.0
1.5
2.0
model (6250, 4.0, 0.1) V_t=0
• Li^6/Li^7 = 0.01
o Li^6/Li^7 = 0.50
x one fine structure component only

Figure 3

of two fine-structure components with $R = 0.00$. The accuracy of this approximation can be checked by using the curves of figure 3. Over the range $10\ \text{mÅ} \leq W_\lambda \leq 120\ \text{mÅ}$, which is the range of the strength of the line in most stars, this approximation predicts the total W_λ of the blended line to within 10%, and hence is of sufficient accuracy to predict abundances correct to within 0.1 in the log. Therefore, allowing for uncertainty in R, the approximation for W_λ used in previous studies leads to a maximum error of 0.2 in the logarithm of the lithium abundance, which is quite a tolerable value.

The accuracy of the single layer approximation is discussed later.

We thus find that the theoretical approximations used by previous investigators to obtain $\lambda_{1/2}$ and W_λ for the lithium line λ6708 Å are completely satisfactory. If their observational data are correct, we must accept their conclusions on the isotopic ratio and abundance of lithium in stars.

CHAPTER III

THE PHOTOGRAPHIC SPECTRA

A. Observational Material

We compiled a list of stars based on the following criteria: a) the star already had been included in Herbig's (1964) original paper on the isotope ratio Li^6/Li^7 or b) the star is bright, with a strong lithium resonance line (based on surveys by Bonsack (1959) and Herbig (1965)), and is expected to have reasonably narrow lines. The plate files of the Hale Observatories were searched for high dispersion spectra of stars on this list that were well exposed in the region near 6700 Å. In this manner, 19 plates of 10 stars were located, taken mostly by Dr. Bonsack and Prof. Greenstein. Fifteen additional spectra were taken by the author in March and September of 1970 with the 32" camera of the 100" telescope, producing a dispersion of 6.7 Å/mm near 6700 Å. In addition to the standard flashed IIaF plates, we used an experimental emulsion, Kodak 09801, which proved to be approximately two times as fastas preflashed IIaF plates. We thank Prof. Münch for making these fine plates available to us. The exposure times, even with the more rapid emulsion, ranged from 30 minutes to 2 hours. The plates were developed in MWP-2 for 5 minutes with the automatic rocker. Calibration wedges were made using the auxiliary wedge spectrograph. The comparison spectrum was produced by an iron arc. Because we lacked spectra for many stars included in Herbig's (1964) paper, nine spectra of 9

stars were borrowed from Prof. Herbig. We are very grateful for a chance to examine these beautiful spectra, which have a dispersion of 4.1 Å/mm, and were taken with the 160" camera of the 120" telescope at Lick Observatory. Table 5 lists the available observational material.

It was very simple to identify the lines using the plates in Herbig's (1965) article, the Atlas of the Spectrum of Arcturus (Griffin 1968) and the Revised Rowlend Tables (Moore, Minnaert, Houtgast 1966). The laboratory wavelengths of the stellar lines were taken from Moore's (1959) Revised Multiplet Tables. In most cases, the iron comparison spectrum was neglected, as the lines in this region are largely higher order blue lines. It was felt that the necessity of introducing a correction for the index of refraction of air could lead to errors where the utmost accuracy in wavelength was desired.

B. Grant Machine Measurements

All the plates were measured on the oscilloscope Grant machine in direct and reverse mode. A list of 20 unblended stellar features of varying strength from H_α to λ6767.78 Å was measured on each plate, plus all features between 6705 and 6710 Å. On the underexposed spectra, only half of these stellar features could be seen, and there were several plates where no lines were visible past λ6717 Å. For the reasons described above, the comparison spectrum was rarely measured. On some of the plates, the Li line

TABLE 5

List of Spectra

Star	Plate	Emulsion	Telescope	Dispersion A/mm	Observer
δ Eri	Pb 4961	IIaF	200"	6.7	JLG
	Pb 4962	IIaF	200"	6.7	JLG
	Pb 4966	IIaF	200"	6.7	JLG
$\nu^2 CM_j$	Pb 4963	IIaF	200"	6.7	JLG
	Pb 4968	IIaF	200"	6.7	JLG
η Cet	Ce 11671	103aF	100"	6.7	WKB
η Psc	Ce 11573	IIaF	100"	6.7	WKB
	Ce 12120	103aF	100"	15	WKB
HR 991	Ce 11629	103aF	100"	6.7	WKB
	Ce 20408	09801	100"	6.7	JC
χ Her	Ce 16995	IIaF	100"	6.7	BP
	Ce 16996	IIaF	100"	6.7	BP
	Ec 1909	fl.103aF	120"	4.1	GH
ι Peg	Ce 9971	103aE	100"	6.7	UVW
	Ce 10008	103aE	100"	6.7	MU
	Ce 13779	IIaF	100"	6.7	HEB
	Ce 9969	103aE	100"	6.7	UVW
	Ce 20204	09801	100"	6.7	JC
	Ce 20405	09801	100"	6.7	JC
ι Per	Pc 7775	IIaF	200"	15	RPK
	Ec 2342	fl.103aF	120"	4.1	GH
β Com	Ce 20259	09801	100"	6.7	JC
	Ce 20263	09801	100"	6.7	JC
	Ec 1840	fl.103aF	120"	4.1	GH
θ Per	Ce 17321	IIaF	100"	15	PSC
χ' Ori	Ce 16822	IIaF	100"	20	RPK
	Ce 20262	09801	100"	6.7	JC
ξ Boo A	Ce 20260	09801	100"	6.7	JC
	Ce 20264	09801	100"	6.7	JC
56 Aur	Ce 20252	fl.IIaF	100"	6.7	JC
	Ec 2523	fl.103aF	120"	4.1	GH
ψ UM_j	Ce 20253	fl.IIaF	100"	6.7	JC
	Ce 20258	09801	100"	6.7	JC

TABLE 5 (Continued)

Star	Plate	Emulsion	Telescope	Dispersion A/mm	Observer
ξ UM$_j$ A	Ce 20254	fl.IIaF	100"	6.7	JC
κ Cet	Ec 2394	fl.103aF	120"	4.1	GH
γ Lep A	Ec 2487	fl.103aF	120"	4.1	GH
ϕ^2 Cet	Ec 2393	fl.103aF	120"	4.1	GH
10 Tau	Ec 2430	fl.103aF	120"	4.1	GH
	Ce 20404	09801	100"	6.7	JC
δ Tri	Ec 2520	fl.103aF	120"	4.1	GH
	Ce 20407	09801	100"	6.7	JC
ξ Peg	Ce 20406	09801	100"	6.7	JC

Abbreviations for last column:

JLG	Prof. Greenstein
WKB	Prof. Bonsack
JC	present author
GH	Prof. Herbig
MU	Prof. Münch
UVW	Dr. van Wijk
HEB	Dr. Butler
RPK	Dr. Kraft
PSG	Dr. Conti
BP	Dr. Peterson

could clearly be seen as asymmetric. Normally, we attempted to measure the point of minimum residual intensity. However, if the line looked asymmetric, we attempted to measure "the center of gravity" of the line as defined by equation 2-18.

Because of the small range (only 200 Å) covered by our Grant machine measurements, a third order fit, $\lambda(y)$ where y is the measured position, and a fourth order fit gave essentially the same results, and so we used a third order least-squares fit to $\lambda(y)$ to obtain the wavelengths of features between 6705 Å and 6710 Å from their measured positions. In some cases, the unidentified solar line at 6707.45 Å was seen on the plates.

In general, the intrinsic resolution of the plate is about 20μ, or about 0.1 Å at 5Å/mm. We thus find it difficult to believe that the exact wavelength of the Li line can be determined to sufficient accuracy from only one plate. Herbig (1964) claims that with one plate of a star at 4.1 Å/mm, "the probable error in the wavelength determination for a single line is 0.3 - 0.5 km/sec" (or 0.006 to 0.010 Å). Thus we are working very close to the limit of resolution of the spectra, and one would suspect that one plate might not be sufficient.

Let us now examine the results of the Grant machine measurements to see if they conform to the above expectations. In table 6, we show the wavelength determined by Herbig for the line λ6707 Å through measurements on a comparator and the wavelength we obtained using the Grant machine for plates borrowed from Dr. Herbig. It is important to realize that in this case we are both measuring

TABLE 6

Comparison of My Measurements With Herbig's Measurements

Star	Plate	λ_{JC}-6707.00 Å	λ_{Herbig}-6707.00 Å*
κ Cet	Ec 2394	0.871	0.856
γ Lep A	Ec 2487	0.820	0.817
χ Her	Ec 1909	0.830	0.816
56 Aur	Ec 2523	0.809	0.818
ϕ^2 Cet	Ec 2393	0.834	0.810
ι Per	Ec 2342	0.816	0.850
10 Tau	Ec 2430	0.789	0.868
δ Tri	Ec 2520	0.839	0.866
β Com	Ec 1840	0.853	0.856

*Taken from Herbig (1964)

the same spectrograms. Here there is excellent agreement. The average value of the difference $|\lambda_{JC} - \lambda_{H}|$ is only 0.021 Å (1 km/sec). A similar difference was obtained when Margaret Katz measured several plates on a comparator which I had previously measured on the Grant machine, as shown in table 7. There the average value of $|\lambda_{JC} - \lambda_{MK}|$ is 0.022 Å.

TABLE 7

Comparison of My Measurements With Those of Margaret Katz

Star	Plate	λ_{JC}-6707.00 Å	λ_{MK}-6707.00 Å
χ Her	Ce 16995	0.828	0.805
β Com	Ce 20259	0.775	0.785
	Ce 20263	0.844	0.820
χ' Ori	Ce 20262	0.830	0.813

In a few cases, several lines of the comparison spectrum were measured. In the reduction of these measurements, we did not correct for the departure of the index of refraction of air from unity. Table 8 shows the radial velocities determined from our measurements of a maximum of four comparison lines per plate compared with the radial velocities given in the Yale Catalogue of Bright stars (Hoffleit 1964). The agreement is very satisfactory. Excluding the three spectroscopic binaries with variable radial velocities, the maximum difference is 5 km/sec, which corresponds to 0.1 Å on the spectra, while the average of the quantity $|v_r^{JC} - v_r^{Cat}|$

TABLE 8

Radial Velocity Determinations

Star	Plate	v_r(JC) km/sec	v_r(Catalog)* km/sec	Remarks
η Psc	Ce 11573	+ 11.2	+ 15	
	Ce 12120	+ 12.3		
HR 991	Ce 11629	- 2.4	+ 2	
	Ce 20408	+ 1.0		
ι Peg	Ce 9971	+ 14.8	- 4	Spectroscopic binary
	Ce 20404	- 49.5		
ι Per	Pc 7775	+ 14..8	+ 50	
β Com	Ce 20259	+ 3.0	+ 6	
	Ce 20263	+ 3.2		
χ' Ori	Ce 20262	- 15.2	- 14	
ξ Boo A	Ce 20260	+ 1.6	+ 4	
	Ce 20264	+ 1.7		
ψ UM_j	Ce 20258	- 1.6	- 4	
ξ UM_j A	Ce 20254	- 15.0	- 16	Spectroscopic binary
δ Tri	Ce 20407	- 3.5	- 6	Spectroscopic binary
ξ Peg	Ce 20406	- 5.7	- 5	
10 Tau	Ce 20409	+ 28.0	+ 28	

*Source: Hoffleit (1964)

is only 2 km/sec.

We thus reach the following conclusions: measurement on a comparator and measurement on an oscilloscope Grant machine gives the same wavelength for a line to within 0.02 Å; and measurement of the same plate at different times by different people gives the same wavelength for a line to within 0.02 Å. It does not follow however, that measurement of the same line in the same star on different spectra will give the same wavelength to within this accuracy.

Let us consider a weak unblended feature of Fe I at λ6710.32 Å. In some of the spectra, this line is too weak to appear. Table 9 shows, for this line, the average of the wavelengths measured in direct and reverse mode for the spectra where it was present. Here the average value of $|\lambda_{JC} - 6710.32|$ is 0.023 Å, only slightly larger than before.

TABLE 9

Measurements of λ6710.32 Å of Fe I

Star	Plate	λ-6710.00 Å	Star	Plate	λ-6710.00 Å
δ Eri	Pb 4961	0.298	HR 991	Ce 11629	0.291
	Pb 4962	0.309		Ce 20408	0.332
	Pb 4966	0.415	ι Peg	Ce 9971	0.338
ν^2 CM_j	Pb 4968	0.320	β Com	Ce 20263	0.365
	Pb 4963	0.316	ψ UM_j	Ce 20253	0.329
η Cet	Ce 11671	0.326		Ce 20258	0.315
η Psc	Ce 11573	0.346			
	Ce 12120	0.365			

Figure 4 shows a histogram of λ_{JC} for this line. (Note that the solar wavelength for this line is 6710.323 (Moore et al. 1966), and the Revised Multiplet Table (Moore 1959) has a less accurate wavelength of 6710.31 Å. The lack of sufficient accuracy in the laboratory wavelengths for many lines in the red presents a slight problem.) We thus see that wavelength measurements from spectrogram to spectrogram can be as consistent as the individual measuring error of 0.02 Å would suggest.

We now consider the Grant machine measurements for the lithium line. Table 10 presents a list of our measurements, while in figure 5 we plot $\lambda_{JC} - \lambda_H$ for each plate of those stars included in Herbig's (1964) study, excluding plates borrowed from Dr. Herbig. Figure 6 is a histogram of λ_{JC}, for all the spectra which were measured. We recall that 6707.811 Å is the predicted wavelength of the center of gravity of the line if $Li^6/Li^7 = 0$. Measurements of ι Peg are excluded from figures 5 and 6 as the star is a double-lined spectroscopic binary with a short period. It is obvious from these diagrams that measurement of the lithium line on different plates of the same star gives different wavelengths, and that the variation in wavelength from spectrum to spectrum is larger than the reproducibility of measurements on one plate, which was previously established as approximately 0.02 Å. Furthermore, contamination by the line at λ6707.45 Å is a problem; some of the measured wavelengths for the lithium line are less than the value 6707.81 Å for a zero isotope ratio.

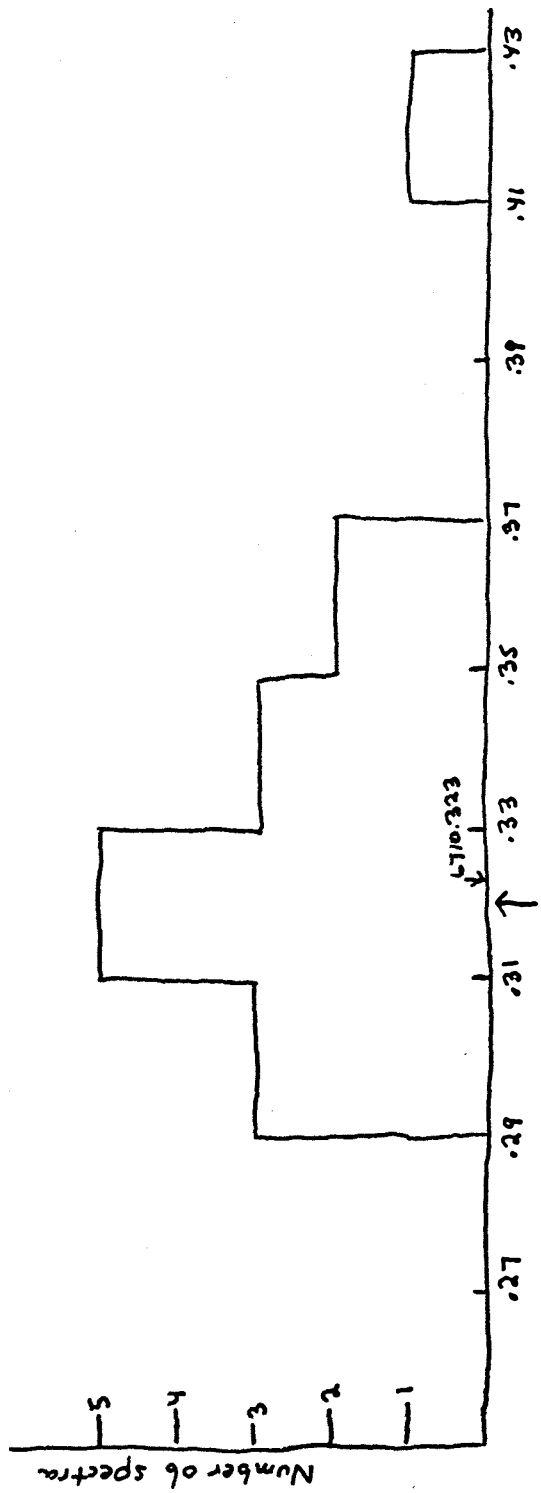

Figure 4 Histogram of wavelengths measured with the Grant machine for the FeI line at 6710.323 A.

TABLE 10

Measurements of λ6707 Å of Li I

Star	Plate	λ_{JC}-6707.00 Å	λ^{*}_{H}-6707.00 Å	Remarks
δ Eri	PB 4961	0.701		
	PB 4962	0.730		
	PB 4966	0.440[1]		
ν^2 CM_j	PB 4968	0.480[1]		
	PB 4963	0.584[2]		
η Cet	Ce 11671	0.755		
η Psc	Ce 11573	0.645[2]		
	Ce 12120	0.930		
HR 991	Ce 11629	0.597[2]		
	Ce 20408	0.601[2]		
χ Her	Ce 16995	0.828	0.816	
	Ce 16996	0.852		
	Ec 1909	0.830		
ι Peg	Ce 10008	0.730	0.861	double-lined SB
	Ce 13779	0.778		
	Ce 9969	0.815		
	Ce 20404	0.824		
	Ce 20405	0.801		
ι Per	Pc 7775	0.904	0.850	
	Ec 2342	0.816		
β Com	Ce 20259	0.775	0.856	
	Ce 20263	0.844		
	Ec 1840	0.853		
θ Per	Ce 17321	0.803	0.837	

TABLE 10 (Continued)

Star	Plate	λ_{JC}-6707.00 Å	λ^{*}_{H}-6707.00 Å	Remarks
χ' Ori	Ce 96822	0.848	0.809	
	Ce 20262	0.830		
ξ Boo A	Ce 20260	0.818	0.798	
	Ce 20264	0.799		
56 Aur	Ce 20252	0.838	0.818	
	Ec 2523	0.809		
ψ UM_j	Ce 20253	0.810		
	Ce 20258	0.807		
ξ Peg	Ce 20406	0.774	0.766	
ξ UM_jA	Ce 20254	0.787	0.844	
κ Cet	Ec 2394	0.871	0.856	
γ Lep A	Ec 2487	0.820	0.817	
ϕ^2 Cet	Ec 2393	0.834	0.810	
10 Tau	Ec 2430	0.789	0.868	
	Ce 20409	0.756		
δ Tri	Ec 2520	0.859	0.866	
	Ce 20407	0.904		

*from Herbig (1964)

(1) λ6707.45 Å

(2) probably a blend of λ6707.45 Å and λ6707 Å of Li I

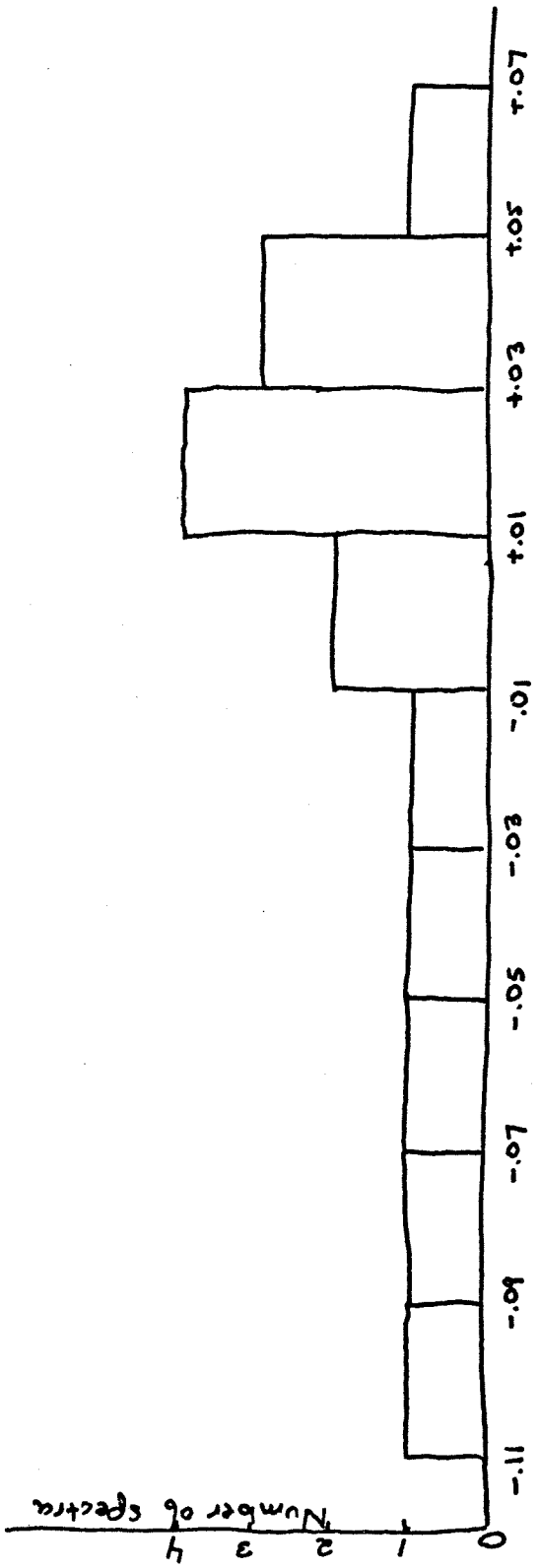

Figure 5 Histogram of the differences between the wavelength measured in this work and that obtained by Herbig (1964) for the LiI resonance line, excluding measurements of plates borrowed from Dr.Herbig and measurements of ι Peg.

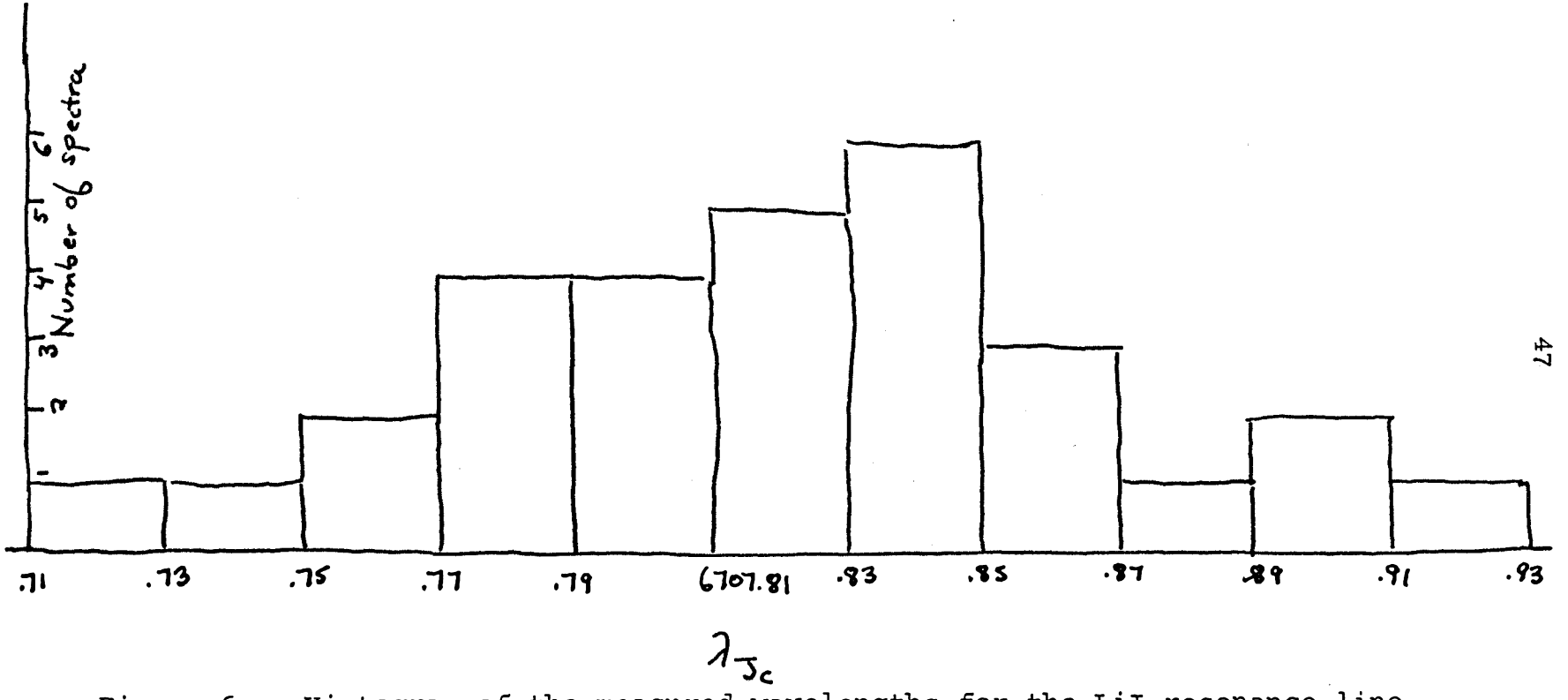

Figure 6 Histogram of the measured wavelengths for the LiI resonance line on all the spectra except those of i Peg.

A discussion of errors in radial velocity measurements was given by Dr. Petrie (1962). He states that "sporadic shifts of spectral lines, not explained by some errors of measurement, are familiar to everyone experienced in measuring Doppler shifts ...". The variation in wavelength of the lithium line λ6707 Å from spectrogram to spectrogram is a phenomenon obviously not unique to this line.

We see from figure 5 that there is no large systematic shift in our wavelength scale as compared with Herbig's--namely the curve $\lambda_{JC} - \lambda_{Herbig}$ is more or less symmetric about 0.00. It is possible that λ_{JC} is systematically higher by 0.01 Å, and this would explain why the mean wavelength for both the Fe I line and λ6707.811 Å appears to be about 0.01 Å higher than the laboratory wavelength. This could occur if the adjacent lines used for fitting have wavelengths which are too high by 0.01 Å, which is not impossible (though improbable), since many lines in the red lack laboratory measurements of great precision. The distributions of figure 5 and figure 6 may be compatible with the observations of the Fe I line 6710.33 on different plates in figure 4, when the effect of contamination by λ6707.45 Å is recalled. The average value of $|\lambda_{JC} - 6707.811|$ is 0.035 Å, which is greater than that for the Fe I line. Whether the effects of 6707.45 can explain all of this spread is unclear. Furthermore, there is no evidence for two discrete groups of stars, centered around R = 0.00 and R = 0.50, as claimed by Feast (1970). In fact, there are almost no stars with $\lambda_{JC} \geq 6707.87$, which is the theoretical value of $\lambda_{1/2}$ for R = 0.50.

We are thus forced to the following conclusions: one plate is not sufficient to determine the wavelength of the Li line accurately enough for evaluating Li^6/Li^7; the spread in wavelength of the Li line over all the observed plates may be consistent with the line having the unique wavelength of 6707.82 ± 0.01 Å, corresponding to Li^6/Li^7 near zero; and although the wavelengths measured by Herbig (1964) vary greatly from star to star and imply values of the isotope ratio which differ significantly from each other, since they are for the most part measurements on a single plate, they are unreliable. Our measurements show no evidence for a value of Li^6/Li^7 significantly greater than 0.1 in any star.

Therefore, unless many plates of the same star are averaged, the errors intrinsic in measuring wavelengths of a slightly blended weak line on a single photographic plate make spectra essentially useless in determining the isotopic abundance of lithium in stars.

C. Microphotometry of the Spectra

A selection of the photographic spectra were measured on the C.I.T. microphotometer. This included all of the plates taken with the 120" which we borrowed from Dr. Herbig and six of the spectra taken by us at the 100" Coude using the experimental Kodak emulsion 09801. The Lick plates have a dispersion of 4.1 Å/mm, while 100" plates have a dispersion of 6.7 Å/mm at Hα. The Lick plates were exposed with a strip calibration, and the strips on one spectrum were measured near 6700 Å to give the characteristic curve that was used to analyze all of the Lick plates. For the 09801 plates,

a wedge made with an auxiliary calibration spectrograph was used to provide the characteristic curve used to obtain intensity tracings of all the plates.

In tracing the plates, slits of 8 to 10μ at the plate were used. The resolution and granularity parameters of the 09801 emulsion are a few per cent worse than those of the F emulsion, but the 09801 plates are 3 to 4 times as fast. Typical resolving powers quoted by Kodak for medium resolving power emulsions such as 103aF or 09801 are 80 lines/mm, or 13μ (Kodak Publications, P-9, 1967). The Mount Wilson spectra were exposed with a slit of 0.11 mm (0.3" of arc) which corresponds to 15μ at the plate. At the higher dispersion, 15μ corresponds to 0.06 Å, while at 6.7 Å/mm it corresponds to 0.10 Å. Tracings were always made towards the right (lifting the weight) at a carriage speed of 1.40 mm/min (the slowest carriage speed) or 2.80 mm/min to provide the most uniform dispersion possible on the tracings. The wavelength scale on the chart paper near λ6708 Å was established by measuring the separation of a group of lines near λ6707 Å, including λ6717.69, λ6721.84, λ6705.10, and λ6703.58 Å. For the Lick plates, this was approximately 1.3 in/Å, while for the 100" plates it was 1.7 in/Å. The position on the chart paper corresponding to λ6707.81 Å was determined from the long and short wavelength side using the measured dispersion. In no case did this position disagree by more than 0.1 inches, and in most cases the two determinations agreed to within 0.05 in, which was the limit of our accuracy. Note that this procedure does not involve measuring the comparison arc spectrum. We are not interested in the radial

velocity of the star.

From each tracing we have measured the equivalent width of λ6708 Å and $\lambda_{1/2}$ by planimetry. We have also determined the minimum residual intensity of the Li I line and that of the Ca I line at 6718 Å. Some of these parameters will be useful in comparing our interferometric and photographic profiles. Here we are only concerned with $\lambda_{1/2}$, and we tabulate the measured values in table 11. λ_H is the value of $\lambda_{1/2}$ measured by Herbig (1964).

TABLE 11

Measurements of $\lambda_{1/2}$ for λ6708 Å from Microphotometer Tracings

Star	Plate	$\lambda_{1/2}$-6707.00 Å	λ_H-6707.00 Å
10 Tau	Ce 20409	0.81	0.87
	Ec 2430	0.81	
χ' Ori	Ce 20262	0.81	0.81
β Com	Ce 20259	0.79 ± 0.03	0.86
	Ce 20263	0.88	
	Ec 1840	0.89 ± 0.03	
δ Tri	Ec 2520	0.82	0.87
ι Per	Ec 2342	0.80	0.85
γ Lep A	Ec 2487a	0.88 ± 0.05	0.82
χ Her	Ec 1909a	0.82	0.82
56 Aur	Ec 2523	0.81 ± 0.02	0.82
ϕ^2 Cet	Ec 2393a	0.84 ± 0.03	0.81
ζ Boo A	Ce 20264	0.83 ± 0.03	0.80
	Ce 20260	0.81	

The errors which are quoted represent the cases where the low and high wavelength determinations of the position of 6707.81 Å on the chart paper disagrees by up to 1 mm. For γ Lep A, the error is large, as the nearby lines on the short wavelength side of λ6708 Å are too weak, so that the wavelength scale can only be determined from the high wavelength side.

We wish to examine these tracings to understand two phenomena. The first is that in one of the three cases with more than one plate for a star listed in table 11 there is a large range in the values for $\lambda_{1/2}$. The second problem is to determine what it is that makes the photographic process unsuitable for determining lithium isotope ratios, i.e. why do Grant machine measurements of different spectra of the same star yield badly divergent values for the lithium line wavelength. Let us consider the 3 plates of β Com which Herbig found to have $Li^6/Li^7 \sim 0.4$. In addition to one plate borrowed from Dr. Herbig, we have two 100" plates taken on March 14-15 and March 15-16, 1970. In figure 7, we show the intensity tracing of the Lick spectrum. The area which was planimetered to give $\lambda_{1/2}$ is exactly as indicated on figure 7, except that the short wavelength wing of λ6708 Å in Ec 1840 was taken as profile A of the sketch in this figure. Repeated tracings of the same plate give essentially the same results as appear in figure 7. The radial velocity of β Com does not seem to be variable. The lines are sharp and there is no evidence for it being a spectroscopic binary. The grain in Ec 1840 has an rms fluctuation of about 5 per cent (with occasional 8 per cent

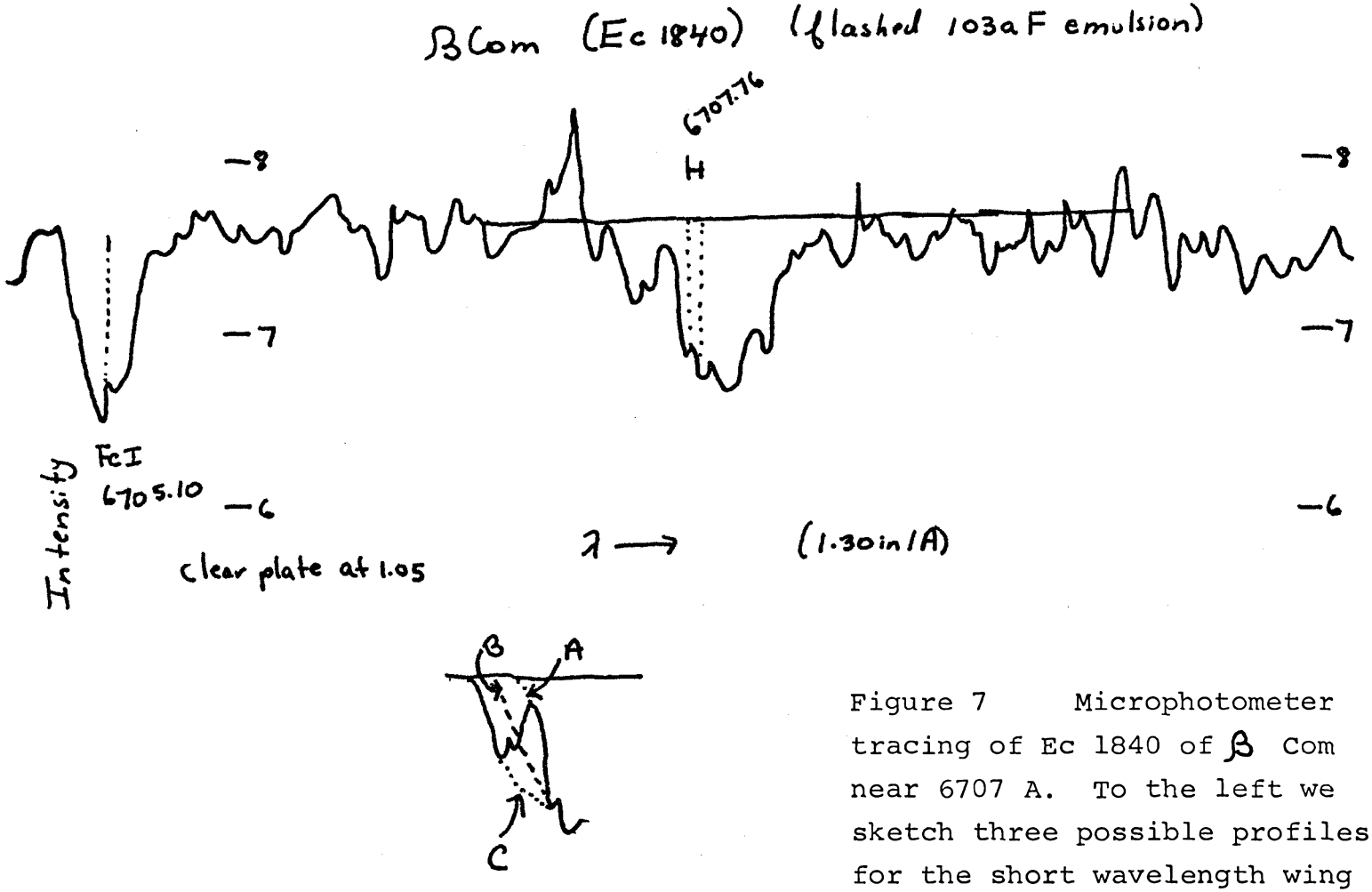

Figure 7 Microphotometer tracing of Ec 1840 of β Com near 6707 A. To the left we sketch three possible profiles for the short wavelength wing of the LiI resonance line.

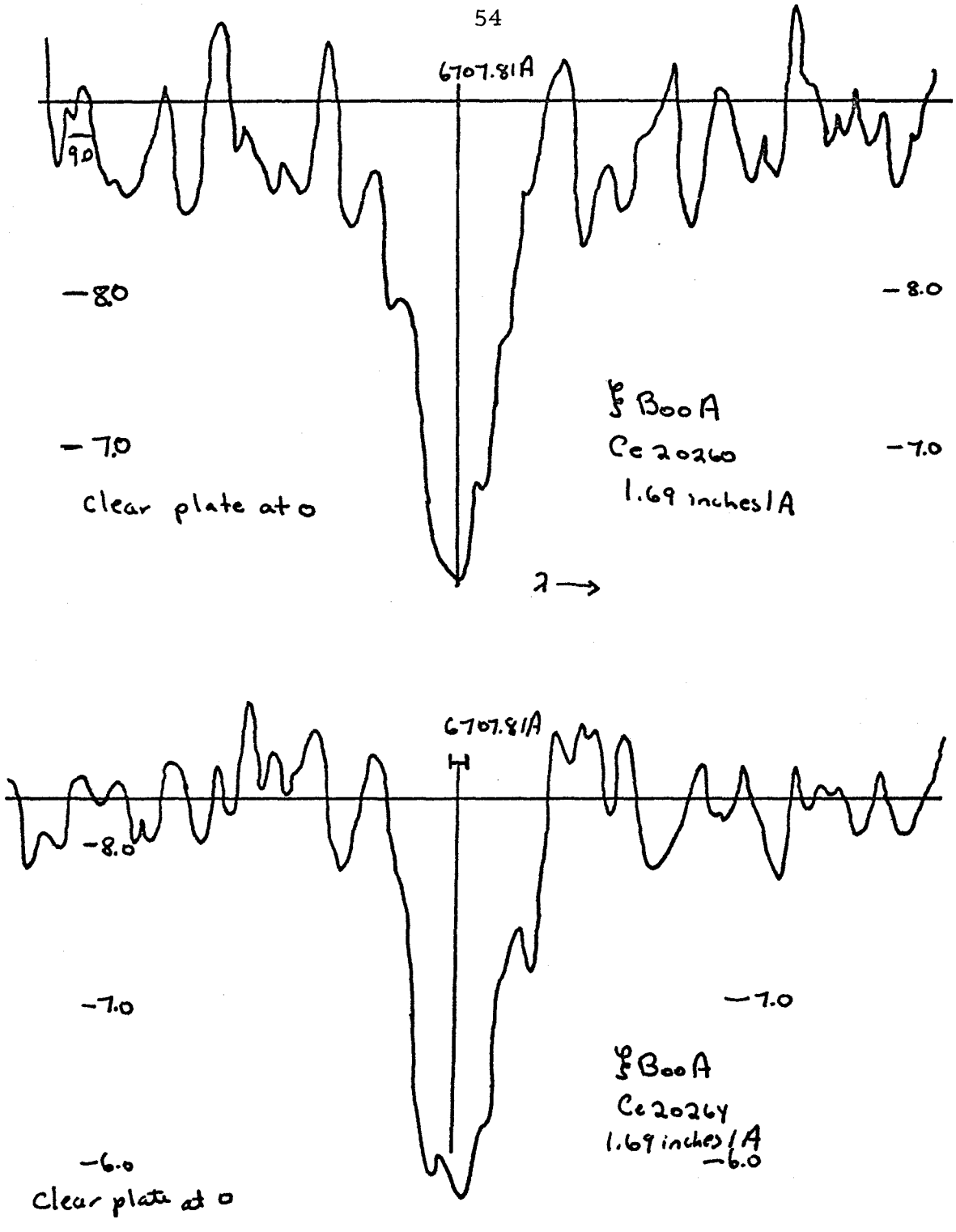

Figure 8 Microphotometer tracings of two 100" spectra (09801 emulsion) of λ Boo A in the region near 6707 A.

fluctuations) in intensity at the level of the continuum, whereas the lithium line is only 15 per cent deep at maximum. Note the critical nature of the short wavelength wing of the line. Three possible profiles at λ6708 Å in Ec 1840 are sketched in figure 7. We chose A, to obtain $\lambda_{1/2} = 6707.89 \pm 0.03$ Å. If we had chosen B, we would have measured $\lambda_{1/2} = 6707.85 \pm 0.03$ Å, while with C, we would have obtained $\lambda_{1/2} = 6707.82 \pm 0.03$ Å. β Com (GoV) is sufficiently hot that λ6707.45 Å is expected to be less than 5 mÅ in strength, and hence we cannot ascribe the bump in the profile to it.

Profiles of λ6708 Å from the two 100" spectra of ξ Boo A are shown in figure 8, and the full range of grain fluctuation for the 09801 plates can be seen. These spectra were taken on consecutive nights in March of 1970.

In looking at these tracings we see how difficult it is to determine $\lambda_{1/2}$ from a single spectrum or even a small number of spectra. The grain in the photographic process will reduce the resolving power for very weak features below the level which can be tolerated in determining the isotope ratio. Although the Lick spectra are at a slightly higher dispersion, we believe they suffer from the same defect. As evidence for this, we present in figure 9 a plot of $\Delta\lambda = |\lambda_H - 6707.81|$ from Herbig's (1964) paper versus the maximum depth of the Li I resonance line as determined from photographic spectra. With rms grain fluctuations of 5 per cent at the continuum, lines with a central residual intensity of more than 90 per cent are not easily measured. It is clear from figure 9 that the cases with the largest discrepancies tend to have the weakest lines. This

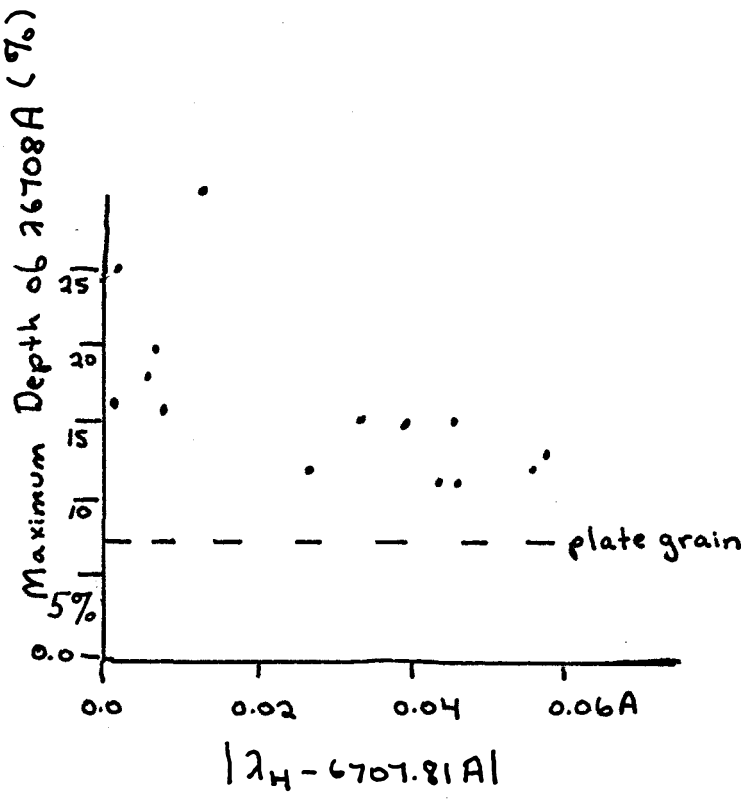

Figure 9 Plot of the absolute value of the difference between the wavelength measured by Herbig (1964) for the resonance line of LiI and λ for $N(Li^6)/N(Li^7) = 0.0$ and the maximum depth of the LiI line for those stars observed by Herbig (1964).

indicates that grain fluctuations may be important. If saturation of the two components were responsible for the observed cases where $\lambda_{1/2}$ is greater than 6707.82 Å, one would expect the strongest lines to show the maximum apparent isotope effect, which is contrary to the correlation shown in figure 9.

We therefore believe that grain fluctuations and other such effects make it difficult to determine accurately the mean-area wavelength ($\lambda_{1/2}$) of a broad weak feature such as λ6708 Å using photographic spectra. Although one can see from tracings of such spectra that the lithium line is wider than adjacent unblended weak lines, it is difficult to say anything further about the profile of λ6708 Å with photographic techniques.

CHAPTER IV

LITHIUM ABUNDANCE DETERMINATIONS

A. The Single Layer Approximation

Most previous investigations of the lithium abundance in stars have used the single layer approximation. In theory this approximation must be verified for each T_{eff} and logg within the region of interest. We shall choose a representative grid of models and compute the number of lithium atoms in the ground state of Li I. This involves the determination of the fraction of lithium which is not ionized and the fraction of Li I in the ground state. Let us denote by f_1, f_2 and f_3 the fraction of neutral, singly ionized, and doubly ionized lithium. Since the second ionization potential of Li is 75.6 eV, f_3 will be negligible. The first ionization potential of Li is 5.4 eV, so that we may expect that over the range of T_{eff} of interest (4500 - 6500 ^{o}K), f_2 will be large compared to f_1.

If the single layer approximation is to be valid, we require a smooth distribution of $f_1(\tau)$ with a relatively broad maximum at τ_m which must remain at the same τ from late F to early K stars. The single layer which is used must have a suitably chosen τ_{sl}. For the single layer of his analysis, Herbig (1965) chose the layer $\tau_{5500} = 0.35$. Figure 10 displays $f_1(\tau_{5000})$ for a number of model atmospheres. The ionization equilibrium is given by the Saha equation

$$\frac{f_2}{f_1} P_e = \frac{U_2}{U_1} \frac{2(2\pi m)^{3/2}(kT)^{5/2}}{h^3} e^{-\chi/kT} \qquad (4\text{-}1)$$

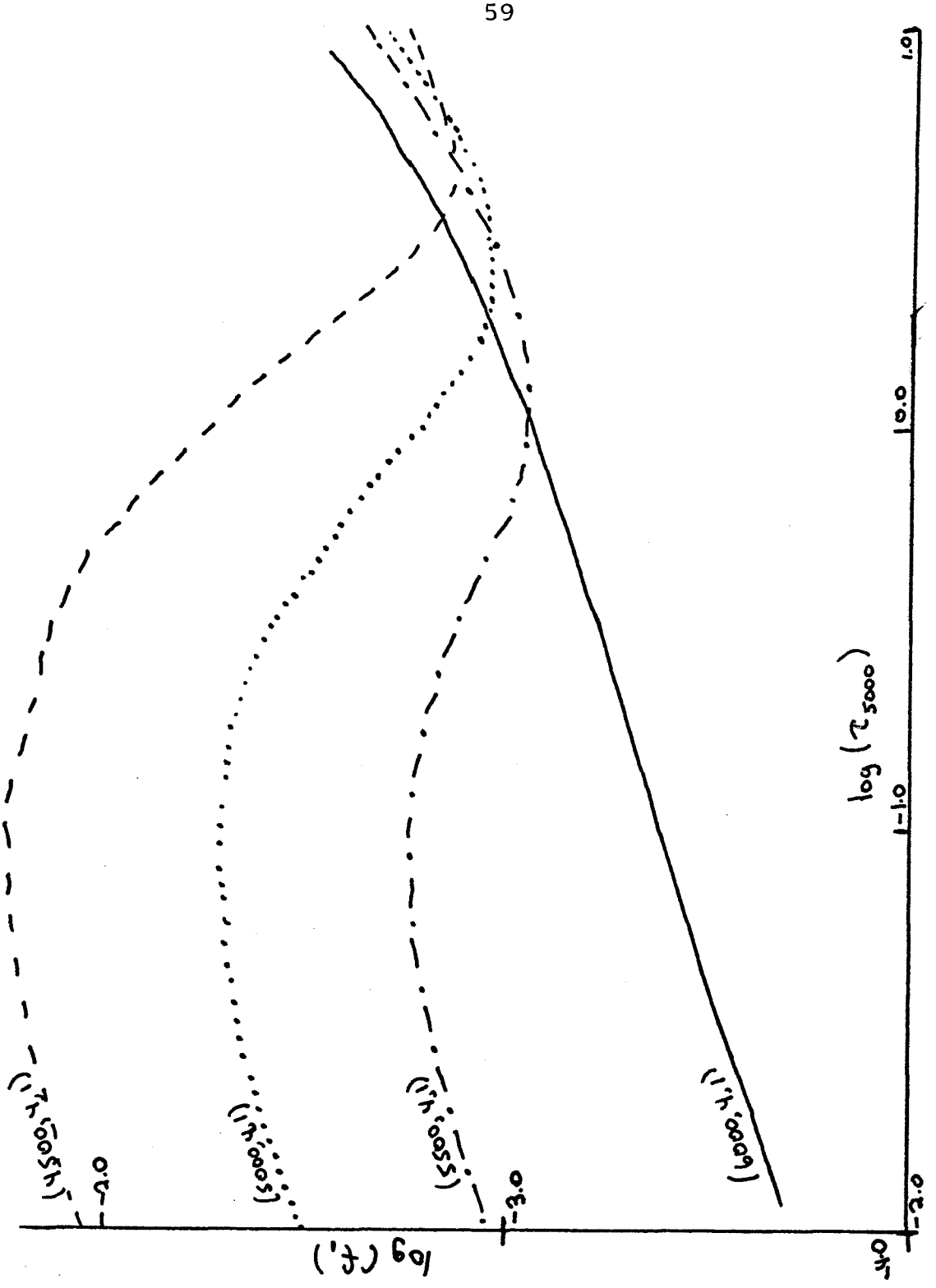

Figure 10: The fraction of lithium which is neutral as a function of optical depth for model atmospheres with T_{eff} from 4500 to 6000° K.

or

$$f_1 \propto \frac{f_2 P_e}{T^{5/2}} \; 10^{27.6/T_3}$$

Note that the predominant variation in f_2/f_1 is the factor P_e, which varies over two orders of magnitude from $\tau = 10^{-2}$ to $\tau = 10$, whereas T over most of that range may vary only by 1000^{o} or about 20%. The tendency of f_1 to increase with τ seen in figure 10 is due to the increase of P_e with τ, while the details of the curves are due to the effects of change in temperature with depth. Note that the maximum f_1 reached in any of the models is 1.73×10^{-2}, therefore even at $T_{eff} = 4500\ ^{o}K$, Li is 98% singly ionized. We also observe that the curves of $f_1(\tau)$ change in shape as T_{eff} decreases. They are not scaled versions of each other. This implies that we must doubt the validity of the single layer approximation. To demonstrate that factors such as the fraction of neutral lithium atoms which are in the ground state are not as important as changes in f_1, we show in figure 11 α_o(Li), which is the absorption coefficient of λ6707.76 Å at line center, and is defined by equation 2-2, for the model (6250,4,1). Note that α_o(Li) behaves in approximately the same manner as f_1 for the (6000,4,1) model.

To continue with our investigation of the validity of the single layer approximation, we shall define a mean $\overline{\tau}$ for the line. If the single layer approximation is to hold, τ_{sl} must equal $\overline{\tau}$. Since we have an absorption coefficient for each frequency point in the line (which is the sum of that for the four components), we can define an

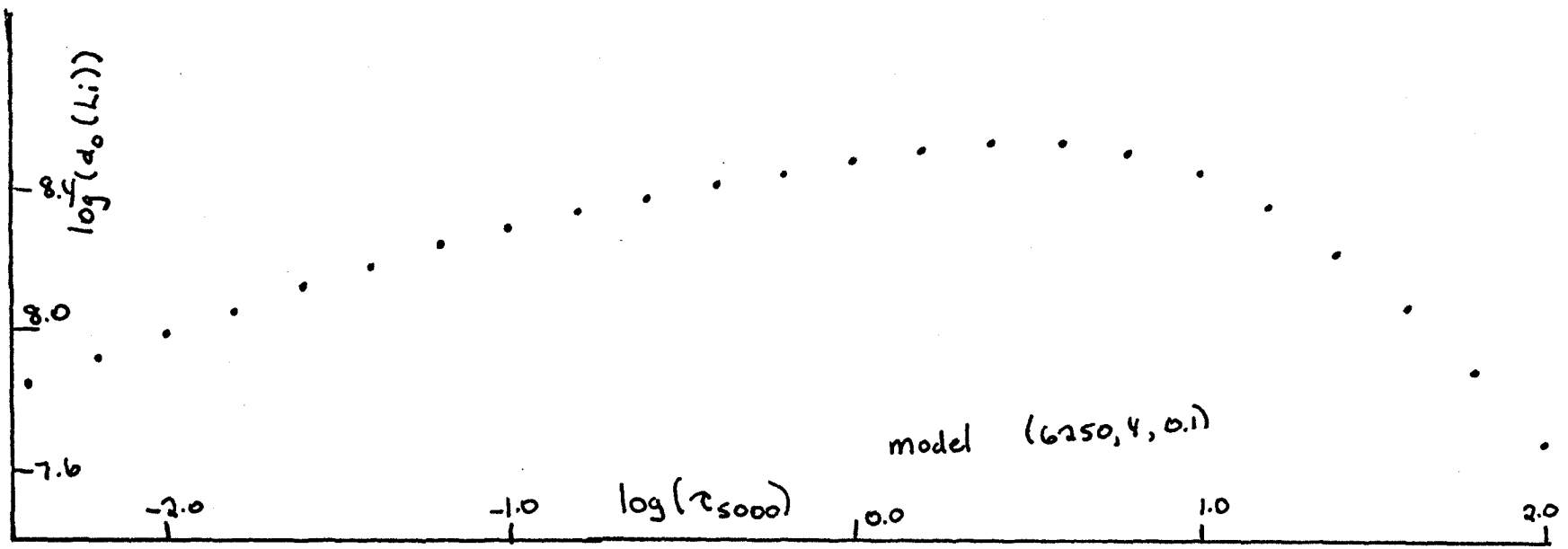

Figure 11: The absorption coefficient of the stronger fine structure component of the resonance line of Li^7 at line center as defined by equation 2-2 as a function of optical depth for the (6250,4.0,1) model.

optical depth scale at each line frequency by

$$d\tau_\lambda = d\tau_{5000} \frac{\kappa_{line}(\tau_{5000}) + \kappa_{cont,6707}(\tau_{5000})}{\kappa_{5000}(\tau_{5000})}$$

We can then set $\tau_1(\lambda)$ equal to the value of our reference $\tau\,(\tau_{5000})$ when τ_ν equals unity. We have thus defined a mean optical depth for each frequency. We then weight $\tau_1(\lambda)$ by $[1 - RI(\lambda)]$ and integrate over λ. Thus

$$\overline{\tau} = \frac{\int_0^\infty (1 - RI(\lambda))\,\tau_1(\lambda)\, d\lambda}{\int_0^\infty (1-RI(\lambda))\, d\lambda} \qquad (4\text{-}2)$$

Note that the denominator is equal to the equivalent width. Although there are other definitions of a mean optical depth with more transparent physical meanings, this definition is simplest to compute, and all reasonable definitions for a mean optical depth of a line give almost the same numerical values. We show in table 12 $\overline{\tau}$ for lithium lines of varying equivalent widths using several model atmospheres. The abundances have been varied over the models to produce a range of equivalent width. $\overline{\tau}$ appears to depend largely on equivalent width, with only a slight dependence on the model parameters. It seems clear that a choice of $\overline{\tau}_{sl}$ of 0.35 is moderately appropriate for a range of equivalent widths near 60 mÅ, but is not suitable for either stars with an extremely weak Li line or ones with a very strong line. If the line is extremely strong, there is a possibility that a large fraction of the line will be formed above $\tau_{5000} = 10^{-2}$, where the Boltzmann equation may no longer be valid and scattering may be important.

TABLE 12

Computed Mean Optical Depths for λ6708 Å

Model	R	W_λ (mÅ)	$\overline{\tau}_{5000}$
(6000,4,1)	0.01	176	0.13
(6000,2,1)	0.01	168	0.16
(4500,4,1)	0.01	129	0.25
(5000,4,1)	0.01	48	0.64
(5500,4,1)	0.01	17	0.75
(6000,2,1)	0.01	10	0.80
(5500,4,1)	0.50	25	0.74

B. Loci of Constant W_λ in the (T_{eff}, Abundance) Plane

We now study the variation in strength of the resonance line of Li I with temperature. Equivalent widths of λ6708 Å were calculated using a grid of model atmosphere, a constant value of R, and a constant lithium abundance. The results are shown in figure 12, which is a plot of equivalent width versus effective temperature of the model for a constant lithium abundance. In several cases, we obtained the line strength for more than one surface gravity, but the variation in W_λ with surface gravity (for a constant effective temperature) is relatively small. The variation in line strength with effective temperature for a constant Li abundance is very large, which we might have expected from consideration of the variation in $f_1(\tau)$ with effective temperature shown in figure 10. The equivalent width for a constant Li abundance changes from 4 mÅ at 6500° to 180 mÅ at

Figure 12: The equivalent width of the resonance line of Li I for a constant Li abundance as a function of T_{eff} of the model atmosphere. The curves for two values of the Li abundance, one a factor of 100 larger than the other, are displayed.

Figure 13: The lithium abundance required to produce a resonance line of Li I of constant equivalent width as a function of T_{eff} of the model atmosphere. The curve obtained by Wallerstein and Conti (1969) is indicated by the dotted line. Part of the curve for a line of Fe I is also shown.

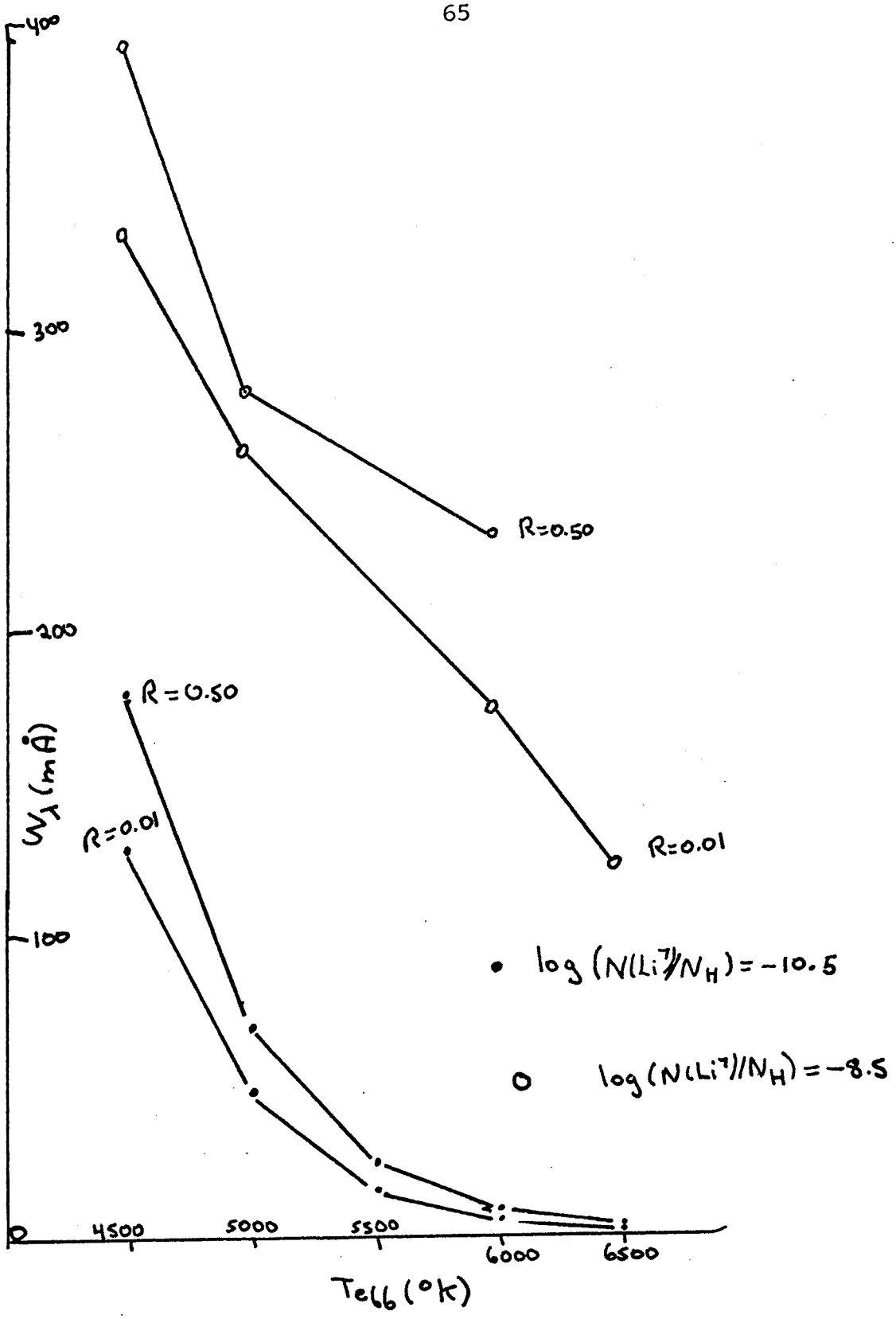
400
300
200
100
0
W_λ (mÅ)
R=0.50
R=0.01
R=0.50
R=0.01
• log (N(Li⁷)/N_H) = −10.5
o log (N(Li⁷)/N_H) = −8.5
4500
5000
5500
6000
6500
Teff (°K)

Figure 12

Figure 13

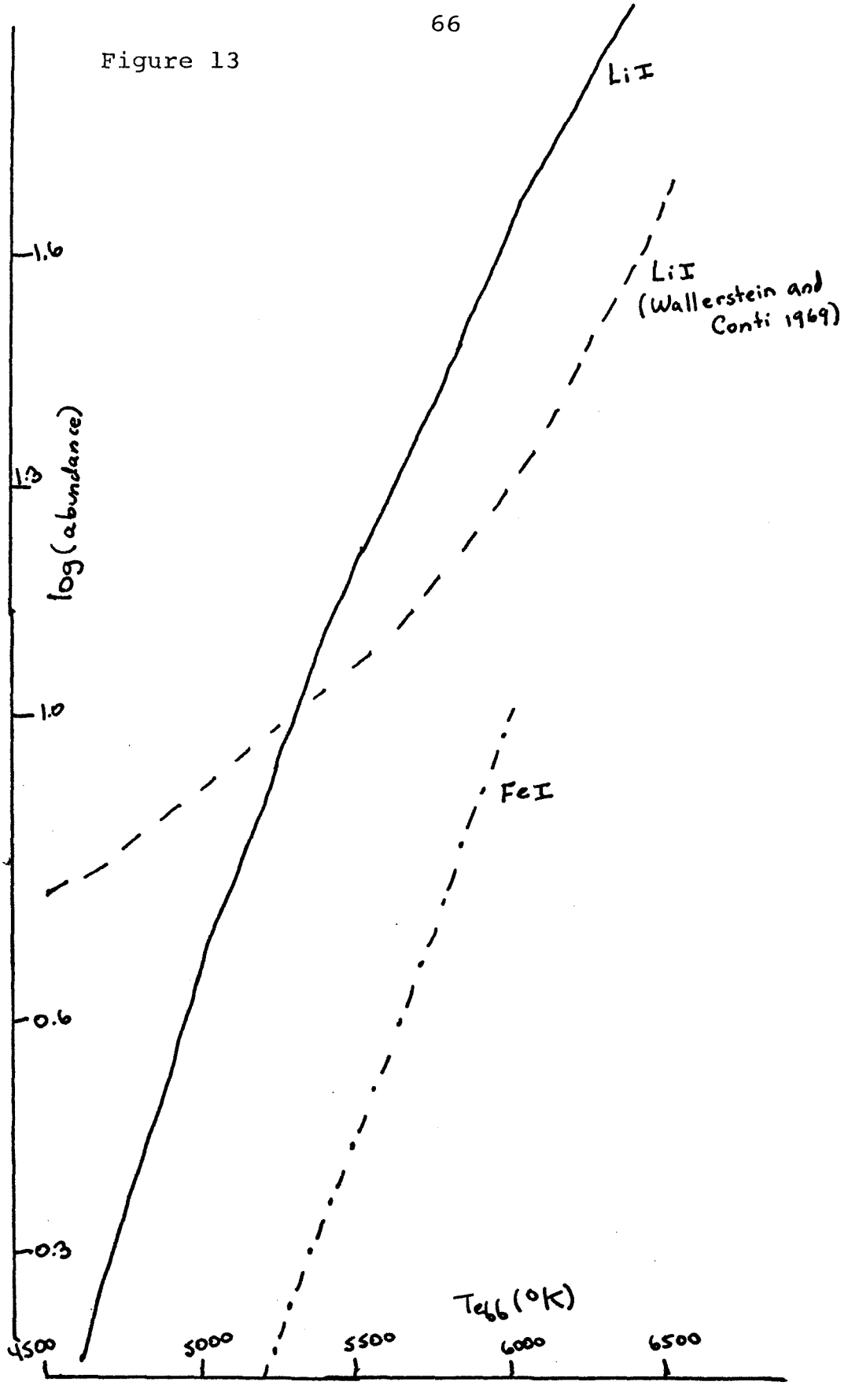
LiI
LiI
(Wallerstein and
Conti 1969)
FeI
log (abundance)
1.6
1.3
1.0
0.6
0.3
4500
5000
5500
6000
6500
Teff (°K)

4500 ^{o}K. This implies that it is critical to have a reliable effective temperature for the star before a lithium abundance can be determined. The difference between the curves for $R = 0.01$ and $R = 0.50$ can be understood by realizing that the curve of growth for the larger isotope ratio remains linear to larger values of W_λ than it does for $R = 0.01$. From figure 12, with the aid of a curve of growth for λ6708 Å (figure 3), we can construct a graph of the lithium abundance required to produce a fixed equivalent width for the resonance line as a function of effective temperature. The results are given in figure 13, where we also display a part of this curve for a Fe I line (extracted from some old calculations performed for another purpose several years ago). The abundance scale of figure 13 has been arbitrarily normalized. We also indicate in this figure the curve of lithium abundance for a constant W_λ of 4 mÅ given by Wallerstein and Conti (1969). Their original curve is given as a function of spectral type, and we have used the data given in Allen (1964) to convert this to effective temperatures. Note that our curve predicts a much larger range of lithium abundance, i.e. a much larger variation of W_λ with temperature than does the curve of Wallerstein and Conti (1969). The curve for iron, for the limited range of T_{eff} for which it is available has a slope almost equal to that of the lithium line. This is to be expected in view of the relatively close first ionization potentials of Fe and Li and the fact that the temperature is too low for there to be a significant amount of Fe III.

In a discussion with Prof. Conti over the source of the disagreement shown in figure 13, he discovered that an error had been

made in the preparation of the published figure. The line of abundance for a constant W_λ as a function of spectral type should have had a steeper slope, which is what we found. Upon comparing our results for a Hyades and Pleides with those of Wallerstein and Conti (1969), we realized that this error was not propagated throughout the published figure, and that just the one line was incorrectly drawn.

We can now obtain the lithium abundance for any star with known effective temperature and a measurement of W_λ for the resonance line. From figure 12, we can read off W_λ^{calc} at $A(Li^7) = -10.5$ (and $R = 0.01$) for the effective temperature of the star. Then from the curve of growth for $\lambda 6708$ Å (figure 3, with $R = 0.01$), we can obtain the abundance ratio which corresponds to a change in equivalent width from W_λ^{calc} to the observed value. Note that an uncertainty of 500 ^oK in T_{eff} can produce an uncertainty in the lithium abundance of a factor between 2 and 4, depending on T_{eff}. We have introduced one approximation in this procedure. The curve of growth shown in figure 3 was calculated for the model (6250,4.0,0.1). We assume that over the range from F7 to K0 the shape of this curve is the same, although obviously the curve of growth is shifted with respect to the log $(A(Li^7))$ axis. In effect, we neglect the slight change in the flat part of the curve due to the change in thermal velocity from 4500 ^oK to 6500 ^oK. This is a maximum of $\sqrt{6500/4500}$ or a factor of 1.2 in thermal velocity. Since we have ignored the possible presence of microturbulence, this is not an unreasonable procedure. Furthermore, most of the stellar lithium lines are so weak that they

are close to the linear part of the curve of growth.

C. Abundances for the Pleides and Hyades

In view of the large differences in figure 13 between our curve and that of Wallerstein and Conti (1969) we have redetermined the lithium abundance for stars in the Pleides and Hyades. Wallerstein, Herbig, and Conti (1965) have published equivalent widths of λ6708 Å for 23 stars in the Hyades cluster, as well as B-V colors. The relationship between B-V, spectral type, and T_{eff} in this cluster has been studied by Oke and Conti (1966), and from their results, we can convert B-V into T_{eff}, and therefore determine the lithium abundance. The relationships given by Oke and Conti (1966) include the effects of line blanketing. For ten stars in the Pleides, Danziger and Conti (1966) and Danziger (1967) have published the ratio of λ6708 Å to λ6717 Å of Ca I. We convert these measurements into approximate equivalent widths and use Oke and Conti's (B-V, T_{eff}) relationship to determine the Li abundance of these stars.

We now face the problem of the validity of our abundance scale. The absolute gf value given for the resonance line of Li I in Wiese, Smith and Glennon (1966) is log (gf) = 0.178. This is for both components of the Li^7 line, so that the value for λ6707.76 Å is 2/3 of the above, and that for λ6707.91 Å is 1/3. These are the transition probabilities we have used.

We check the accuracy of our system by considering the case of the sun. Peach (1968) has found that the equivalent width of

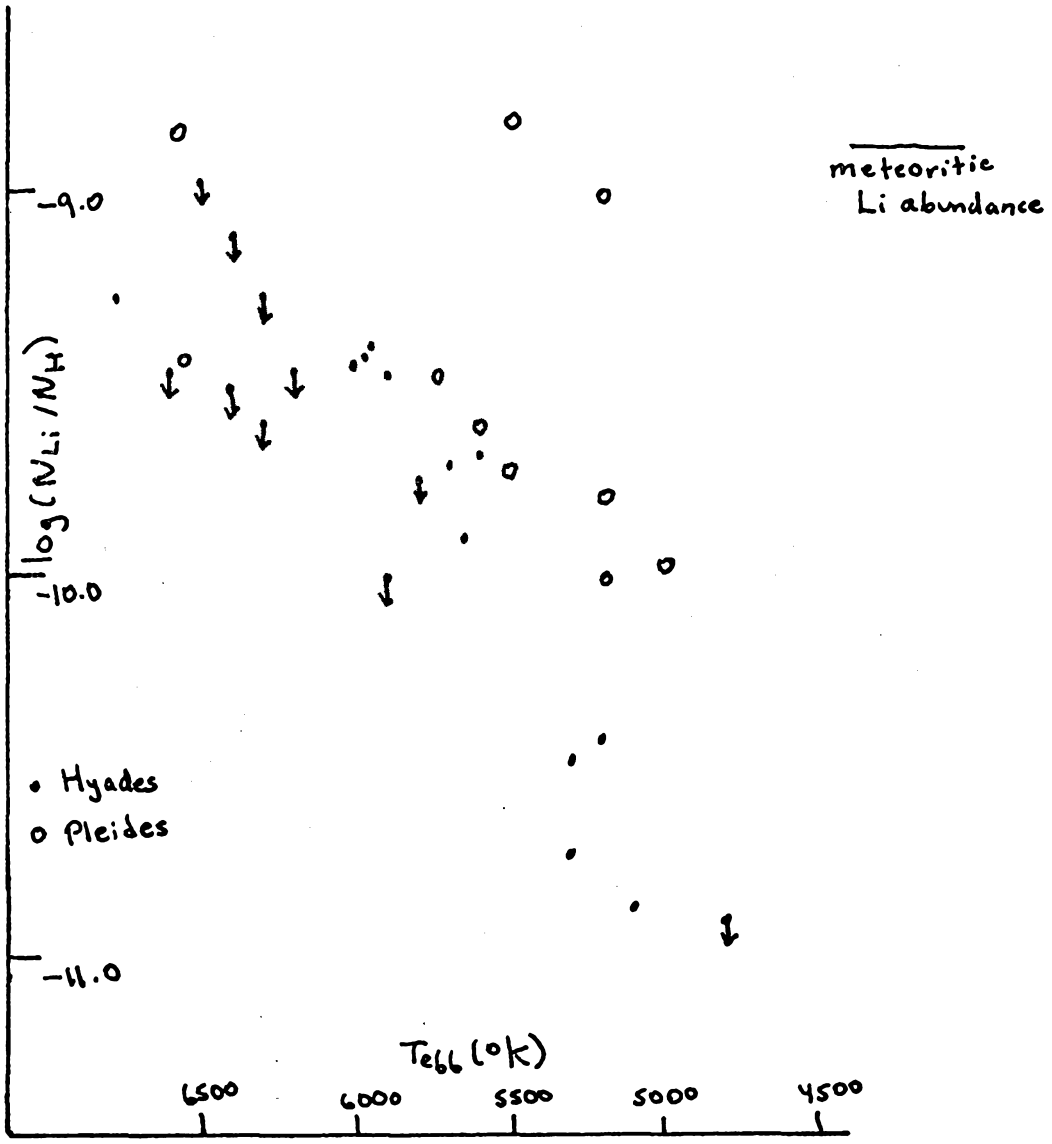

Figure 14: The lithium abundance for the Hyades (dots) and Pleides (open circles) stars, as a function of T_{eff} of the stars. The meteoritic lithium abundance is indicated.

λ6708 Å is less than 0.6 mÅ in the spectrum of the solar disc. Using an effective temperature of 5800 ^{o}K and this equivalent width, we obtain an abundance in our system of log [N(Li)/N(H)] ≤ - 11.85. The upper limit quoted by Peach (1968) is 0.38 on the scale of H = 12.00 or - 11.62. Our two determinations differ by less than a factor of 2, which is not bad when we recall that these are completely separate determinations, using different models and perhaps slightly different gf values. The solar Li line has been extensively studied, with model atmospheres and line profile fitting, so that this agreement is most encouraging.

With confidence in the accuracy of our abundance determinations, we plot in figure 14 our results for the Hyades and Pleides stars. This figure is to be compared with figure 1 of Wallerstein and Conti (1969). Note that the total range in abundance covered by the Hyades and Pleides in our figure is close to that in figure 1, whereas the 4 mÅ line in figure 1 of Wallerstein and Conti (1969) disagrees by more than an order of magnitude with our results. As previously remarked, a conversation with Prof. Conti revealed that the 4 mÅ line had been drawn incorrectly, but the rest of the published figure was correct.

D. T Tauri Stars

The presence of unusually strong λ6707 Å in several T Tauri stars is extremely interesting. Because these stars are so faint, (all are fainter than V = 9.0), it is difficult to secure high dispersion

spectra. Bonsack and Greenstein (1960) obtained several spectra at 27 and 31 A/mm at Hα and used these to deduce Li abundances in the T Tauri stars. Since 1960, our ideas of the nature of T Tauri stars have changed. Hence we shall rediscuss the problem of the lithium abundance of these stars.

The major problem is the determination of effective temperatures for the stars. Table 13 lists the spectral types assigned to these stars by Prof. Herbig at two times, and the next column is the effective temperature derived from the second (most recent) spectral type.

TABLE 13

Spectral Types and T_{eff} of T Tauri Stars

Star	sp. type[1]	sp. type[2]	T_{eff} °K	T_{eff}(Kuhi) °K
T Tau	dG5e	K1eV	5000	4100
RY Tau	dG0e	G5eV	5500	4400
RW Aur	dG5e	dG5e	5500	
GW Ori	dK3e	dK3e	4800	4250

[1]Herbig (1962)

[2]Herbig (quoted in Kuhi 1965)

[3]Kuhi (1964)

A change of 6 subclasses in the classification of T Tau and RY Tau introduces a large change in effective temperature.

A second method of determining T_{eff} is spectrophotometry. Here problems arise because of the unusual frequency distribution of the flux in these stars, the intense emission lines, and interstellar reddening and absorption. L. V. Kuhi (1964) has obtained effective temperatures for these stars by broad band photometry with filters designed to avoid the intense emission lines (J. Smak 1964). From these line-free colors, with corrections for absorption and reddening which are somewhat uncertain, Kuhi derives effective temperatures listed in the last column of table 13. The differences between these effective temperatures and ones based on the most recent spectral types are large. We shall use these to define the range within which the effective temperatures of the T Tauri stars must lie.

Kuhi (1964) was not aware of the strong infrared excesses of these stars, which were discovered by E. E. Mendoza V (1966). Integration of photometry out to 5 microns, together with the known distances of the cloud complexes in which the stars are embedded, revealed that the luminosity of T Tau, RY Tau, and GW Ori is from 24 to 50 times that of the sun (Mendoza V, 1968). If we adopt the T_{eff} given by high dispersion spectroscopy (the fourth column of table 13), we can use Iben's (1965) evolutionary tracks for contracting stars to estimate the masses and radii of these stars. We obtain masses of about 3 $M_{\odot}$ and R about $9 R_{\odot}$. The low T_{eff} values advocated by Kuhi (1964) seem to be too low to fit on Ibens tracks, and also put some of the stars in a region of very rapid evolution, which would perhaps not give the correct statistics for population of various segments of the tracks in the H-R diagram.

Equivalent widths of the resonance lithium line are given in Bonsack and Greenstein (1960), so we may obtain the abundances listed in Table 14.

TABLE 14

Lithium Abundance in T Tauri Stars

	W_λ(6708)	$T_{sp.}$	T_{colors}
T Tau	400 mÅ	-7.8	-8.8
RY Tau	350 mÅ	-7.8	-9.1
RW Aur	200 mÅ	-8.8	
GW Ori	150 mÅ	-10.1	-10.1

For comparison, the meteoritic abundance is -8.9. The uncertainty in the effective temperature of the T Tauri stars prevents us from definitely concluding that these stars have more lithium than do F5V Pleides stars or meteorites.

Another common belief about the lithium content of these young stars is that it shows only a small range of variation. Although the line strengths of λ6708 Å show large variations, from GW Ori, which has a relatively weak line of 150 mÅ to T Tau with a 400 mÅ line, the lithium abundance probably does not vary by as much as the factor of about 100 implied by the curve of growth and given in table 14. The different amount of veiling which obscures the absorption spectrum of GW Ori much more than it does that of T Tau must be taken into consideration.

Because of lack of any better information, Bonsack and Greenstein (1960) assumed that the T Tauri stars all have the same atmospheric structure as the sun. When we analyze the T Tauri stars using the effective temperatures from recent high dispersion spectroscopy, we obtain results within a factor of 3 of Bonsack and Greenstein's (1960) values, once their numbers are corrected for the decrease in measured W_λ of λ6708 Å in the sun from Greenstein and Richardson's (1951) original determination to Peach's (1968) value. The underabundance of barium which was obtained by Bonsack and Greenstein (1960) is probably a spurious result of the use of too hot an atmospheric model.

In one way, their method is more accurate, since they have used a curve of growth constructed from lines of Fe I, Ca I and Na I to determine the lithium abundance. We have instead relied on the measured W_λ and a theoretical curve of growth. However, in T Tauri stars "veiling" of the absorption spectrum by continuous emission occurs. This veiling is in part responsible for the early spectral types originally assigned to these objects, and it may significantly decrease the measured W_λ below the true value. This mechanism is quite possible operating in GW Ori, and may explain why it has such a weak lithium line.

One further point raised by Bonsack and Greenstein (1960) concerns the absence of any circumstellar lithium absorption, whereas absorption components are seen in H and K of Ca II, in the Balmer lines, and the D lines. They derive an upper limit to the

lithium abundance in the T Tauri nebula of $N(Li)/N(Na) \leq 10^{-4}$ or $\log (N_{Li}/N_H) \leq -9.8$. (Recall that -8.8 is the minimum lithium abundance we derive for T Tau.) They therefore conclude that the T Tauri nebula, from which the star condensed, contains less lithium than the star, and others have used this as evidence for the autogenic production of lithium on the surface of T Tauri stars. We have repeated the calculation of the upper limit for lithium in the circumstellar nebula, using the ultraviolet radiation field for a 5000 ^{o}K star, and ionization cross sections tabulated by R. D. Hudson and V. L. Carter (1967) for Li and Na. Unless the measured W_λ for the circumstellar D lines are substantially too large, the upper limit for Li/Na that we derive is the same as that obtained by Bonsack and Greenstein (1960). However, this argument for atuogenic production of lithium is not longer acceptable for other reasons.

Kuhi (1964) has studied the emission and absorption features of hydrogen and Ca II in T Tauri stars and has found that a) the ionization in the emission envelope is too large to be maintained by stellar radiation, b) substantial mass loss is occurring (the circumstellar lines are blueshifted with respect to the stellar lines), c) the absorption components show a large velocity dispersion, and d) the replacement times for the circumstellar envelopes are in all cases less than a year. Point a raises the question of how to calculate the ionization in the region where the absorption is occurring. (In the region where the emission lines are formed, all the lithium will be the unobservable ion Li II.) Although the discrepancy in the

source of ionization is reduced for the higher luminosities that were found by Mendoza (1966), this difficulty remains. In addition, a weak lithium absorption feature with such a large velocity dispersion may not easily be seen, as the central depth will be very small. Furthermore, the lithium abundance of the envelope should be the same as that of the photosphere, given the short replacement times. In view of all these difficulties, we do not consider that the determination of the lithium abundance in the T Tauri nebula is in serious disagreement with the lithium abundance of the star, neither of which can be said to be known to any great precision.

One possible way to obtain more information on the atmospheric parameters of T Tauri stars is to search for line pairs consisting of a resonance and subordinate line. We could try to look for λ6572 Å of Ca I (a zero volt line) and compare it with other Ca I lines near 2 eV that are seen in the spectrum, but λ6572 Å is masked by the H_α emission. There are few line pairs of a single element with large excitation potential separation and small wavelength separation, where both lines are present. Lithium has a subordinate line at 6103.6 Å. The excitation potential of the lower level of this line is 1.84 eV and its gf value (tabulated in Wiese, Smith, Glennon (1966)) is log $(gf_{6103}/gf_{6708}) = 0.4$. Therefore, for a strong resonance line, we can expect to see λ6103 Å. We have calculated with model atmospheres the expected line strength for the subordinate line in several cases shown below.

TABLE 15

Strength of λ6103 Å

Model	6708 (mÅ)	6103 (mÅ)	$f_{6103}N_1/f_{6708}N_0$
5500,4,1	16.8	0.54	0.032
4500,4,1	330	125	0.010

The strength for λ6103 Å was calculated assuming it was a doublet with the same separation as the resonance line (and R = 0.01). The numerical ratios in the last column of Table 15 agree fairly well with those calculated by the simple Boltzmann formula

$$\frac{N_1}{N_0} = \frac{g_1}{g_0}\ 10^{-\theta_{eff}1.84} \qquad (4\text{-}3)$$

whose results are shown below for various cases of interest.

Table 16

Strength of λ6103 Å Using equation 4-3

T	$f_{6103}N_1/f_{6708}N_0$
5500	0.07
5000	0.05
4500	0.03
4000	0.02
3500	0.0075
2500	0.006

The reason for the discrepancy of a factor of two or so is that the subordinate line is formed deeper in the atmosphere and hence has a larger $B_\nu(\bar{\tau})$ than expected by the simple assumption of the same temperature for the mean depth of λ6103 Å and λ6708 Å. In the sunspot spectrum, λ6708 Å has an equivalent width of 50 to 100 mÅ, while λ6103 Å is not detected, with an upper limit of 1 mÅ. This is consistent with a temperature of about 3500 ^{o}K. Lithium in sunspot spectra is discussed by Schmahl and Schroter (1965), Engvold, Moe and Maltby (1970) and Traub and Roesler (1971). Engvold, Moe and Maltby (1970) suggest a slight upward revision in the solar lithium abundance, to - 11.20 as compared to Peach's (1968) value of - 11.60. They note that in sunspots λ6708 Å is slightly blended with TiO. Furthermore, they obtain the isotope ratio Li^6/Li^7 less than 0.20, while Traub and Roesler (1971) obtain $N(Li^6)/N(Li^7) = 0.04 \pm 0.02$.

We have searched for λ6103.6 Å in the spectra of T Tau and RY Tau. This is difficult as there is a Ca I line at 6102.7 Å, which is quite strong in G and K stars. Furthermore, in G dwarfs, there are two strong iron lines at 6103.2 and 6102.18 Å. All of these are blended together with any λ6103.6 Å that might be present, as the spectra are of relatively low dispersion. The equivalent width of λ6122.23 Å of Ca I is given in Bonsack and Greenstein (1960), and from the appearance of the blend at 6103, the width of the blend, and the depth at 6103.6 Å, we can estimate an upper limit to the strength of the subordinate line, if present. This limit is 125 mÅ for RY Tau and 150 mÅ for T Tau. We predict below the equivalent width of λ6103.6 Å for two choices of T_{eff} for the stars.

TABLE 17

Predicted W_λ for λ6103.6 Å of Li I

	$T_{sp.}$	$W_{\lambda(6103)}$	T_{colors}	$W_{\lambda(6103)}$
T Tau	5000	160 mÅ	4100	140 mÅ
RY Tau	5500	180 mÅ	4400	125 mÅ

It is important to obtain spectra at slightly higher dispersion to reduce the upper limit on W_λ for the subordinate lithium line. There appears to be a marginal inconsistency between the strength of the resonance and subordinate lines of Li I if T_{eff} values based on the spectral types are adopted, but this is by no means certain. Also a lithium resonance line of 300 mÅ has $\overline{\tau} \approx 0.06$, which is not sufficiently deep in the atmosphere that we should not perhaps anticipate problems with uncertainties in the atmospheric structure due to mass loss, a large envelope, etc.

Let us summarize the results of the study of the T Tauri star spectra. The situation is quite complex, and the spectra deserve more study with regard to problems of "veiling" and the temperature structure of the outer layers of the atmosphere. Until we know more exactly the effective temperatures of these stars, we do not know whether their lithium abundance can be reduced to a value the same as or below the meteoritic abundance. Furthermore, there may be a spread in T Tauri star lithium abundances, although this effect may in part be due to different amounts of "veiling." It

is clear that these interesting objects deserve further study.

E. M Stars

Merchant (1967) conducted a survey of the strength of λ6708 Å of Li I in M stars and found abundances of lithium ranging from 2 to 10^{-2} that of the sun. Most C and S stars have lithium abundances within a factor of ten of that of the sun. There are, however, several very peculiar stars, including T Sgr, T Com, Case 621, T Ara, WX Cyg, WZ Cas and Y CVn which have huge lithium abundances ranging up to N(Li)/N(Na) ~ 10^{-2}, which, if Na is normal in these stars, is greater than the meteoritic value. Boesgaard (1970) has surveyed the S stars, while results for the C stars are summarized in Fujita (1970). All the abundances referred to above were derived from the resonance line.

Because for these super-lithium-rich stars the resonance line is so strong, we may expect to see the subordinate line at λ6103.6 Å. Dr. Dorothy Locanthi was kind enough to loan us tracings of Pc 8148 of R And (S6,6e) and Pb 9632 of T Sgr (S5,8e). The resonance line of Li I is undetected in R And, while its equivalent width is 1.5 Å in T Sgr. A search for the subordinate line was made on the tracings, and no line was seen in R And, while in T Sgr λ6103.6 Å was seen with an equivalent width about 1/4 of that of λ6122.2 Å of Ca I. If we adopt a temperature of 2500 ^{o}K, the observed strength of the subordinate line as compared with the resonance line seems a little low judging by table 16. However, if we derive a ratio N(Li)/N(Ca) from the subordinate line and λ6122.2 Å of Ca I (which has a lower

level with almost the same excitation potential as the lithium subordinate line) using very crude approximations, we obtain $N(Li)/N(Ca) = 0.5 \times 10^{-2}$ to within a factor of 5. This number is close to that derived by Boesgaard (1970). Thus, the huge overabundances of lithium derived from the resonance lines (usually compared to the D lines or Ca I lines) in these peculiar C and S stars must be accepted as correct.

F. Interstellar Lithium

G. H. Herbig (1968) analyzed the interstellar absorption lines in the spectrum of ζ Oph to obtain an upper limit to the interstellar lithium abundance. His upper limit to W_λ for the resonance line was 6 mÅ, which yielded an upper limit to the interstellar lithium abundance with respect to hydrogen of 9 times that in meteorites. Recently, Danziger and Vaughn (1969) observing with the same FP interferometer we used, have reduced this upper limit by a factor of 6. Thus the upper limit for interstellar lithium is now very close to the meteoritic lithium abundance. Dr. Vaughn (1971) states that there was a slight possibility that the interstellar line was present with W_λ just under 1 mÅ, but that they have been unable to repeat the measurements.

CHAPTER V

THE FABRY-PEROT INTERFEROMETER

A. Line Profiles of the Laboratory Sources

A Fabry-Perot interferometer offers several advantages over photographic spectra. Disregarding the question of resolving power, photoelectric detection offers the advantages of having digital and relatively noise free output with a linear response. Furthermore, the entrance aperture can be opened to accept the seeing disc of the star under average conditions without degrading the resolution.

A Fabry-Perot interferometer consists of a pair of semi-reflecting mirrors separated by a distance ℓ. The medium between the plates has an index of refraction μ, and light is incident nearly normally. The transmission of a FP interferometer near λ_0 is given approximately by the Airy formula:

$$T(\lambda) = \frac{T^o}{1 + \frac{4\mathfrak{F}^2}{\pi^2} \sin^2\left[\frac{\pi(\lambda - \lambda_0)}{FR}\right]} \qquad (5\text{-}1)$$

where FR is the free range. $\mathfrak{F}$, the effective finesse, depends on the reflectance of the etalons, the aperture, and the flatness of the plates. The transmission of such a device is sketched in figure 15.

Transmission maxima occur at integral interference orders m, where

$$m = \frac{2\mu\ell}{\lambda} . \qquad (5\text{-}2)$$

m is normally quite large. The free range (FR), or separation between maxima, is given by:

$$FR = \frac{\lambda}{m} = \frac{\lambda^2}{2\mu\ell} \tag{5-3}$$

The full width at half maximum (FWHM) is given by

$$FWHM = \frac{FR}{\mathfrak{F}} \quad \text{for} \quad \mathfrak{F} >> 1 \tag{5-4}$$

Note that we can scan (i.e. change the wavelength of the transmission maxima) by varying μ, which is in turn a function of the air pressure (P). To change the maximum by $\Delta\lambda$, we have

$$\Delta\lambda = \frac{\lambda}{\mu} \frac{d\mu}{dP} \Delta P \tag{5-5}$$

For a perfect gas, at 1 atmosphere pressure, and temperature of 0 ^{o}C,

$$\frac{d\mu}{dP} = \mu_0 - 1 \tag{5-6}$$

If we change the pressure of air by 1 atmosphere at λ = 10,000 Å, we scan over 3Å, which is more than sufficient for most purposes. Further technical details on the design and construction of FP interferometers can be found in the review article by Vaughn (1967).

The small separation of interference maxima is not a problem in emission line studies. However, for work on absorption lines, we must block off all but one of the maxima. This is done by using a grating as a premonochromator. We always use the 133B grating ruled at 900 lines/mm as it has the highest dispersion.

The exit slit of the Coudé scanner serves as the entrance aperture of the interferometer, which is mounted at the focus of the 114" camera. This slit is set to about 80% of the free range. We must then tune the FP and the grating such that the maximum transmission of the premonochromator is at exactly the same wavelength as the interference maximum of the FP. This is done by observing a lamp with widely separated lines and maximizing the count rate, scanning first the grating only, then the FP.

We can then observe any source by simultaneously scanning the FP (by changing the pressure) and rocking the grating at a rate such that the tune is maintained. The observation consists of the count of the photomultiplier together with the grating position (which is digitized as it is used in the Coudé scanner). Because it takes several minutes to an hour to complete a scan of length 1.0 Å in a star, which is a time long compared with seeing fluctuations, we must compensate for variations in the seeing. Therefore, a second photomultiplier counts the stellar photons in two bands, 16 Å wide, one on each side of the wavelength to which the Fabry-Perot is tuned. At each wavelength point in a scan, we count in the monitor band until a fixed count c_{fix} (usually 200,000 to 500,000) is reached, and the count in the photomultiplier behind the Fabry-Perot over this variable time interval forms the data. When c_{fix} is reached, after printing and punching the data for that point, the grating automatically steps to the next position, although the pressure must be changed by hand. If the time steps are uneven, which may

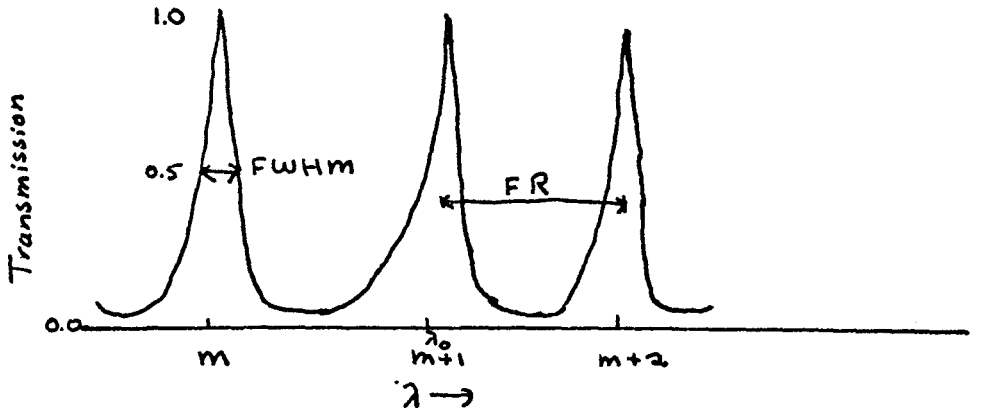

Figure 15: A sketch of the transmission of a Fabry-Perot interferometer as a function of wavelength.

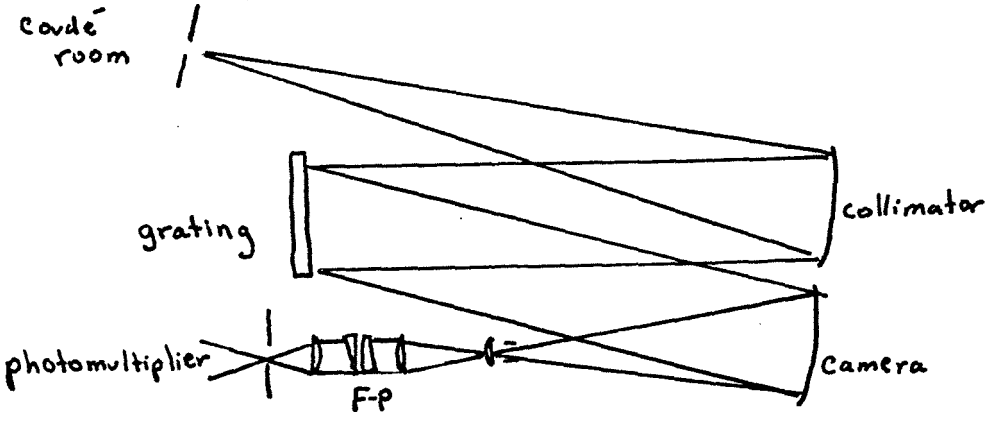

Figure 16: The instrumental arrangement for the data channel after figure 5 of Vaughn(1967). The moniter channel is not shown.

occur if the seeing varies drastically or if there are high clouds, the raw count must be corrected for the varying dark count. The Brown chart recorder provides a record of the integration time per count. We sketch in figure 16 the instrumental arrangement.

In table 18 we list the etalons and spacers used, together with their free ranges. The free range can be calculated from the spacer size, and also measured by keeping the grating fixed and scanning the Fabry-Perot from one maximum to another. We also list the slit size in the Coudé room, and at the camera focus.

TABLE 18

Etalons Used with the FP Interferometer

Name	Etalon	Spacer mm	FR Å	Slit in Coudé room mm	Slit in Coudé room sec of arc	Slit at Camera Focus Å
A	H_α (old)	1.21	1.87	1.4	3.8	1.22
B	H_α (old)	2.26	1.00	0.8	2.2	0.70
C	H_α (new)	1.13	1.90	1.0 1.4	2.7 3.8	0.88 1.22
D	D lines	2.26	0.78	0.5	1.3	0.44

The slit parallel to the dispersion was normally 1.5 mm in the Coudé room. Because the 14 layer dielectric coatings used on the etalons rapidly vary in reflectivity far from the central wavelength, a different set of etalons must be used for the D lines (5890) than for H_α or Li I λ6708.

The digital scale of the grating is a four digit number s, whose behavior $s(\lambda)$ is well known as it is used in the Coudé scanner. Furthermore $\Delta s/\Delta\lambda$ can be calibrated by observing two well separated lines with known wavelengths in a lamp. $\Delta s/\Delta\lambda$ was 155 steps/Å near the Li I line. The change in pressure $\Delta p/\Delta\lambda$ can be measured in a similar manner, once the free range has been measured. For the combination C above (which was used for the Li line after some initial experiments with A and B), $\Delta p/\Delta\lambda = 15.7$ in/Å. Therefore if we scanned by 5 steps in s, or 0.032 Å, we changed p by 0.5 inches per point. This was the usual scanning rate.

We now consider the profiles of the lines seen in the laboratory sources. Two hollow cathode lamps were used; one with sodium; the other contained Li, Ne, and Ca. Let us first examine the response of the instrument to a neon line, as it is sharper than the multi-component lithium line. The ideal line for this purpose is that of Ne I at λ6717.04 Å. This is in reality a doublet, as there are two abundant neon isotopes, Ne 20 and Ne 22, which are found on earth with a ratio of roughly 10:1. The isotopic structure of λ6717.04 Å has been studied by R. Ritschl and H. Schober (1937), who found that the line of the less common Ne 22 lies 0.03 Å to the blue of that of Ne 20. The net shift in wavelength for the blend is then of the order of 0.003 Å. This is negligible, and for our purposes we shall assume that the line is a singlet at 6717.04 Å.

To observe the lamp lines, we merely integrate for a fixed time (3 to 6 seconds) at each wavelength point in the scan. In figure 17 we show the premonochromator profile. This scan was

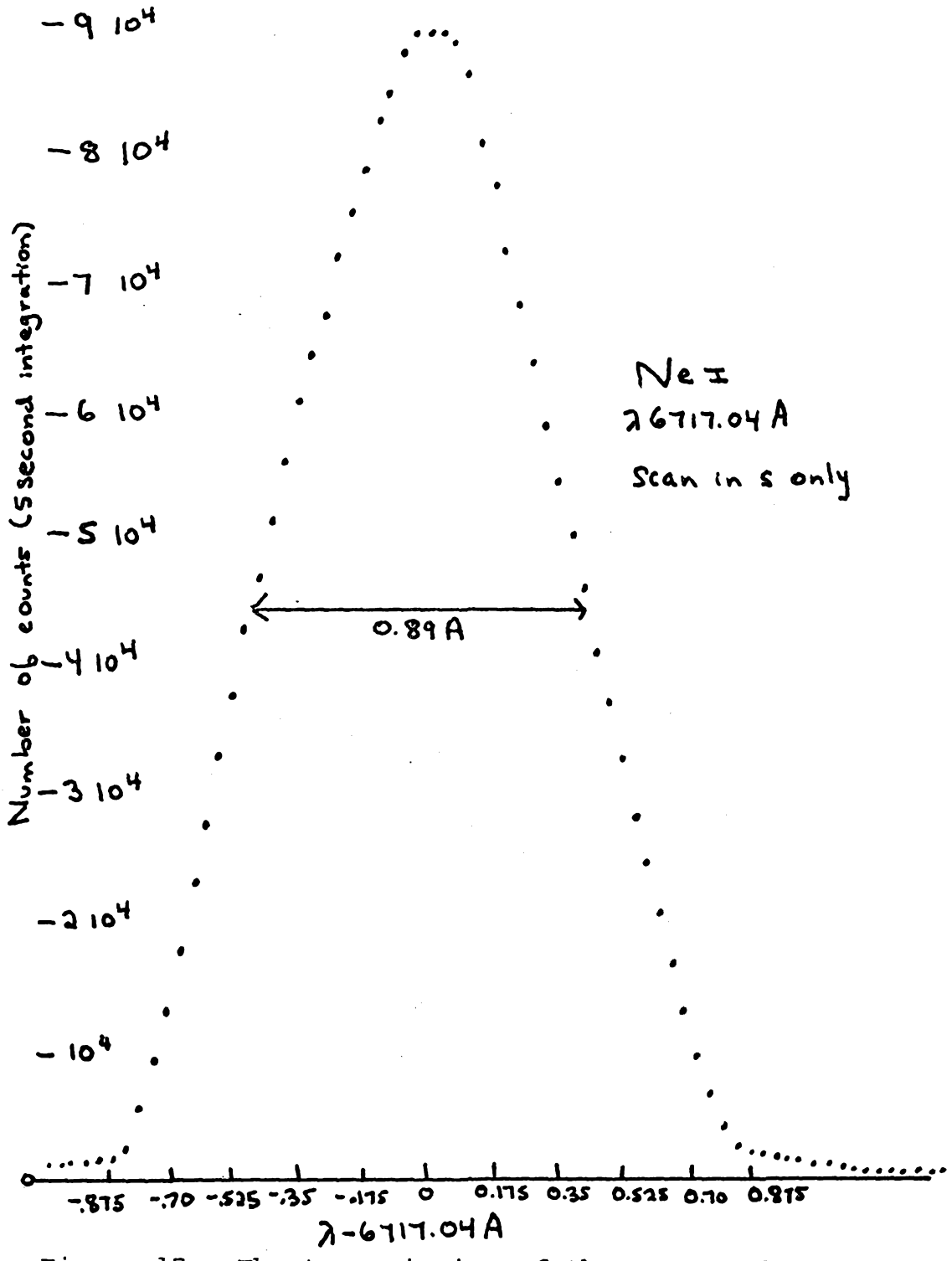

Figure 17: The transmission of the premonochromater. The Fabry-Perot was tuned to the center of λ6717.04A of Ne I and the grating position (s) was changed.

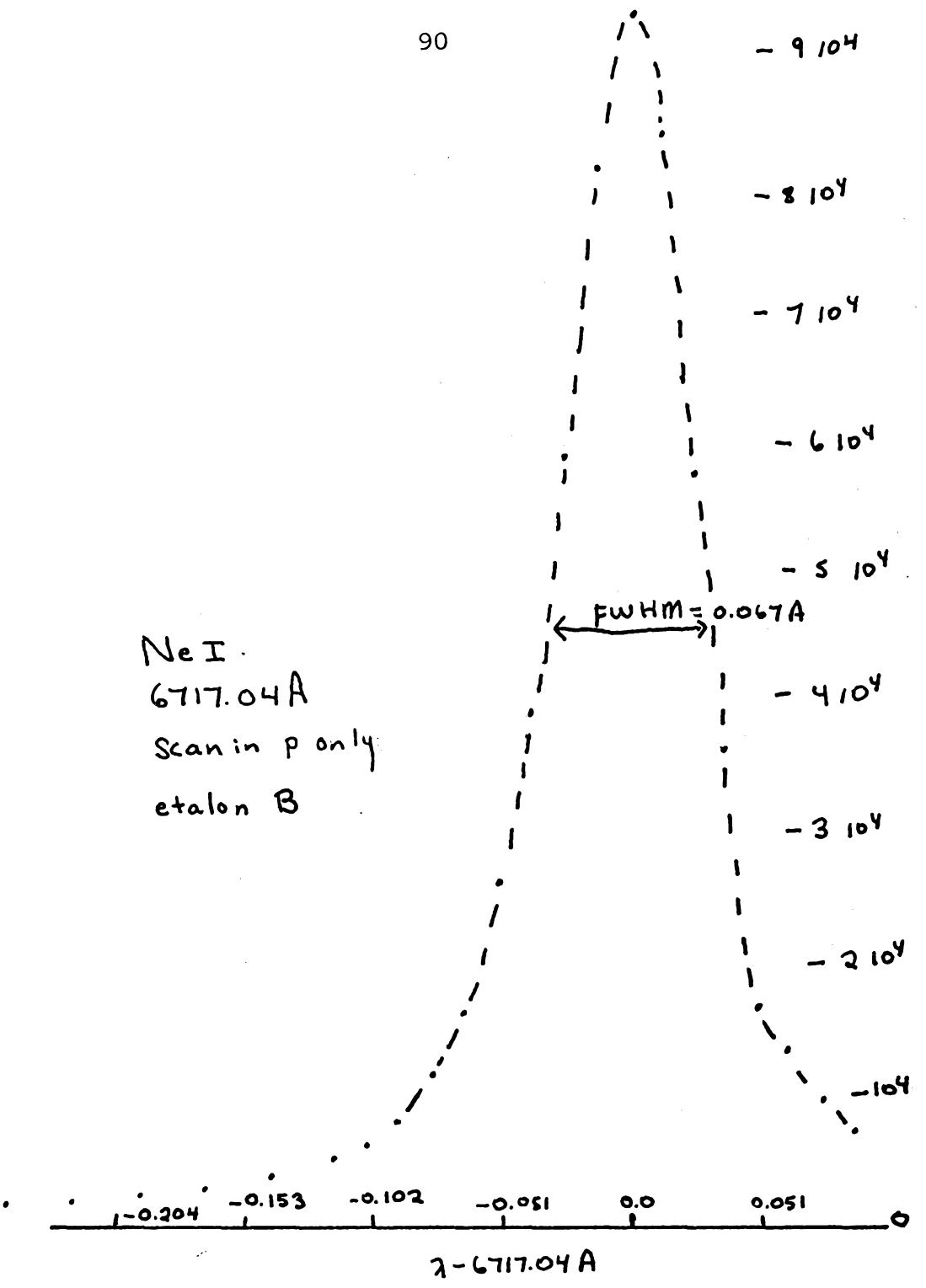

Figure 18: A scan of λ6717.04A of Ne I made by varying the pressure in the Fabry-Perot, with the grating position (s) fixed. Etalon B was used.

obtained by fixing the Fabry-Perot at the pressure corresponding to the line center and scanning the grating only. The FWHM of the profile is 0.89 Å, which is close to the calculated value of 0.88 Å for a 1 mm slit. Note that the premonochromator profile is quite smooth and symmetrical. If grating ghosts contribute significantly, they should show up in the scan of the neon line made with the Fabry-Perot. R. Griffin (1968) has photographically investigated the ghosts of the 133B grating. He found maximum ghost intensities of 10^{-3} of the central intensity, with a spacing of 2.34 Å from the main peak. We note that 2.34 Å is not an integral multiple of the free range of the etalons used for the lithium line. This, combined with the inherent low intensity of the ghosts relative to the main peak, shows that they are completely negligible in considering the interferometer profile.

Figure 18 shows the neon line profile obtained when the Fabry-Perot is scanned over λ6717.04 Å with etalon B of table 18. The peak of the profile (which is all that can be displayed on a linear scale) is symmetric with a FWHM of 0.067 Å. The neon line has a small but not quite negligible intrinsic width, so that the actual resolution of our instrumental setup is less than 0.067 Å.

To obtain an estimate of the intrinsic width of the Ne I line, we use some measurements made by Prof. Münch with an etalon of resolution 0.0238 Å at the D lines. This corresponds to a resolving power of 248,000, close to the design specification of 250,000. With this etalon, the neon line at λ5891 Å had an observed FWHM of 0.0379 Å, so that the intrinsic $\Delta\lambda$ due to pressure and

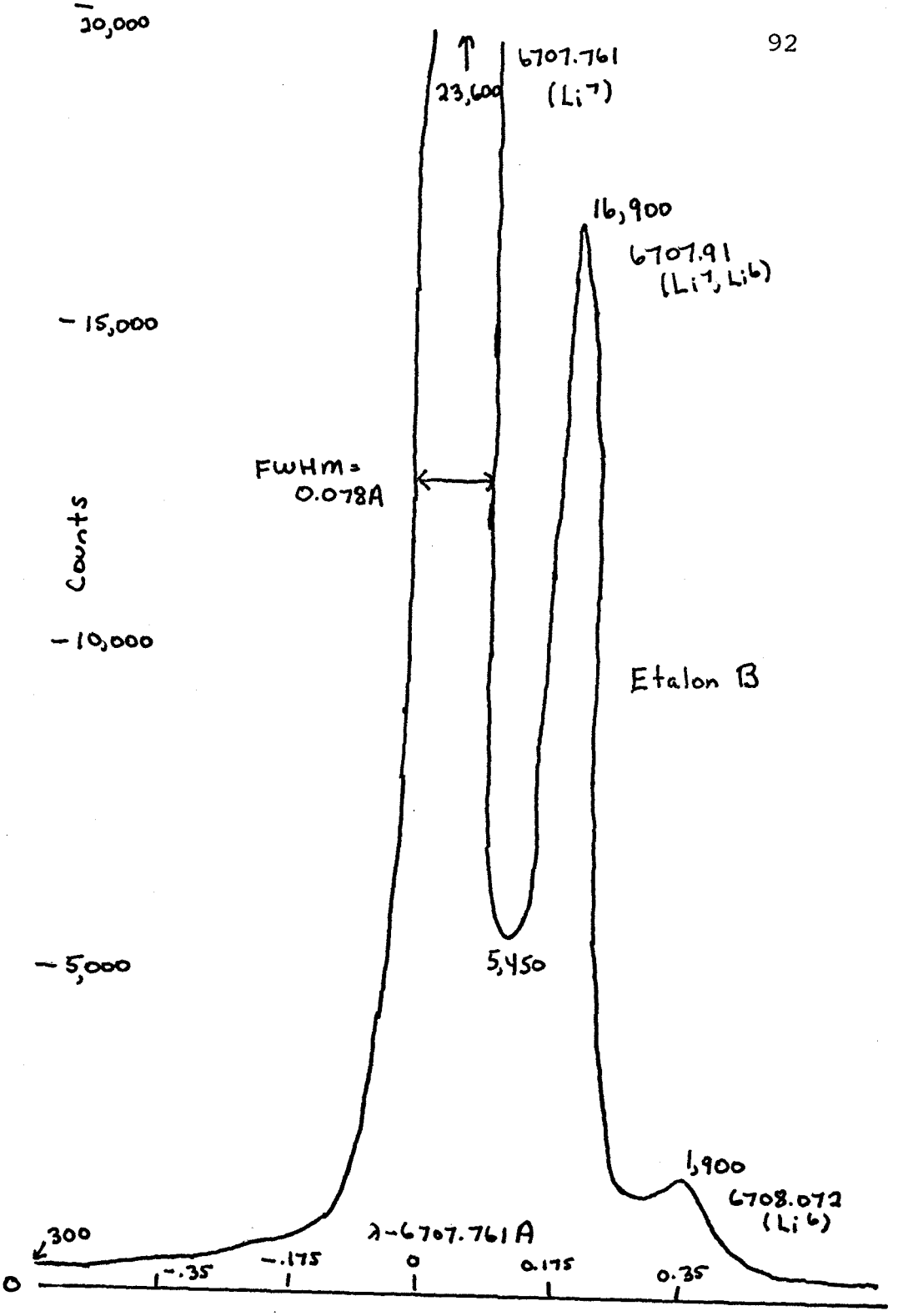

Figure 19: A scan in s and pressure of the resonance line of Li I seen in the calibration lamp. Etalon B was used.

thermal broadening in the lamp is

$$(0.0379)^2 = 0.0238^2 + \Delta\lambda^2$$

$$\Delta\lambda = 0.0295 \text{ Å}$$

At 6717 Å, $\Delta\lambda/6717 = (0.0295)/5891$ (a constant width in energy units), or $\Delta\lambda = 0.0334$ Å. Therefore, the FWHM of the etalon is

$$(0.067)^2 = (\text{FWHM})^2 + (0.0334)^2$$

or the etalon has an intrinsic profile with a FWHM of 0.058 Å. This corresponds to a resolving power of 115,000. This is all very impressive.

Let us now examine the profile of λ6708 Å of Li I in the lamp. The observed profile as seen with etalon B of table 18 is shown in figure 19. The wavelength scale is that given by $\Delta s/\Delta\lambda = 155$ step/Å and $\Delta p/\Delta\lambda = 15.7$ in/Å. The positions of the isotopic lines are within 0.01 Å of the position as determined from the wavelength scale. Notice the excellent separation between λ6707.76 Å and λ6707.91 Å, and also the weak presence of λ6708.07 Å. The observed FWHM of the line λ6707.76 Å is 0.078 Å. We can also predict this number from the neon lines, since, at least approximately, the intrinsic widths are related by

$$\Delta\lambda_{Li} = \Delta\lambda_{Ne}\sqrt{\frac{20}{7}} = 0.0334\sqrt{\frac{20}{7}} = 0.0565$$

The observed FWHM is then related to the intrinsic line width and etalon width by

$$FWHM^2 = (0.0565)^2 + (0.0580)^2 \quad \text{or} \quad FWHM = 0.081\ \text{Å}$$

The agreement between the predicted and observed width is striking. The new H_α etalon (C of table 18) was used over a period of 8 months. During that time, no change in the width or shape of the lamp profiles was noticed.

Another check on the accuracy of our lamp profiles can be made by determining the isotope ratio in the lamp from the profile of λ6708 Å. We use a ratio of gf values for the two components of 2:1. The weaker components are all seen against the wing of λ6707.76 Å; however a correction to each component for the wings of the other components leads to an isotope ratio in the lamp of $Li^6/Li^7 = 1/11.8$. This is very close to the terrestial ratio of ~1/12.5. Therefore self absorption in the lamp is not an important effect.

B. Parasitic Light

We now must define the off-band leakage of the Fabry-Perot system. In order to determine this, we require profiles of calibration lamp emission lines seen through a whole free range from the line center. Figure 20 shows on a logarithmic scale a scan of the neon line at 6717.04 Å from one order to the next made with etalon B. The grating was kept fixed at the line center and only the pressure was varied. We define the leakage as the central intensity of a line whose profile is a step function, with value 0 over the range w and value 1 elsewhere. It is obvious that the numerical value of the leakage depends on the width w, and hence w must be less than or

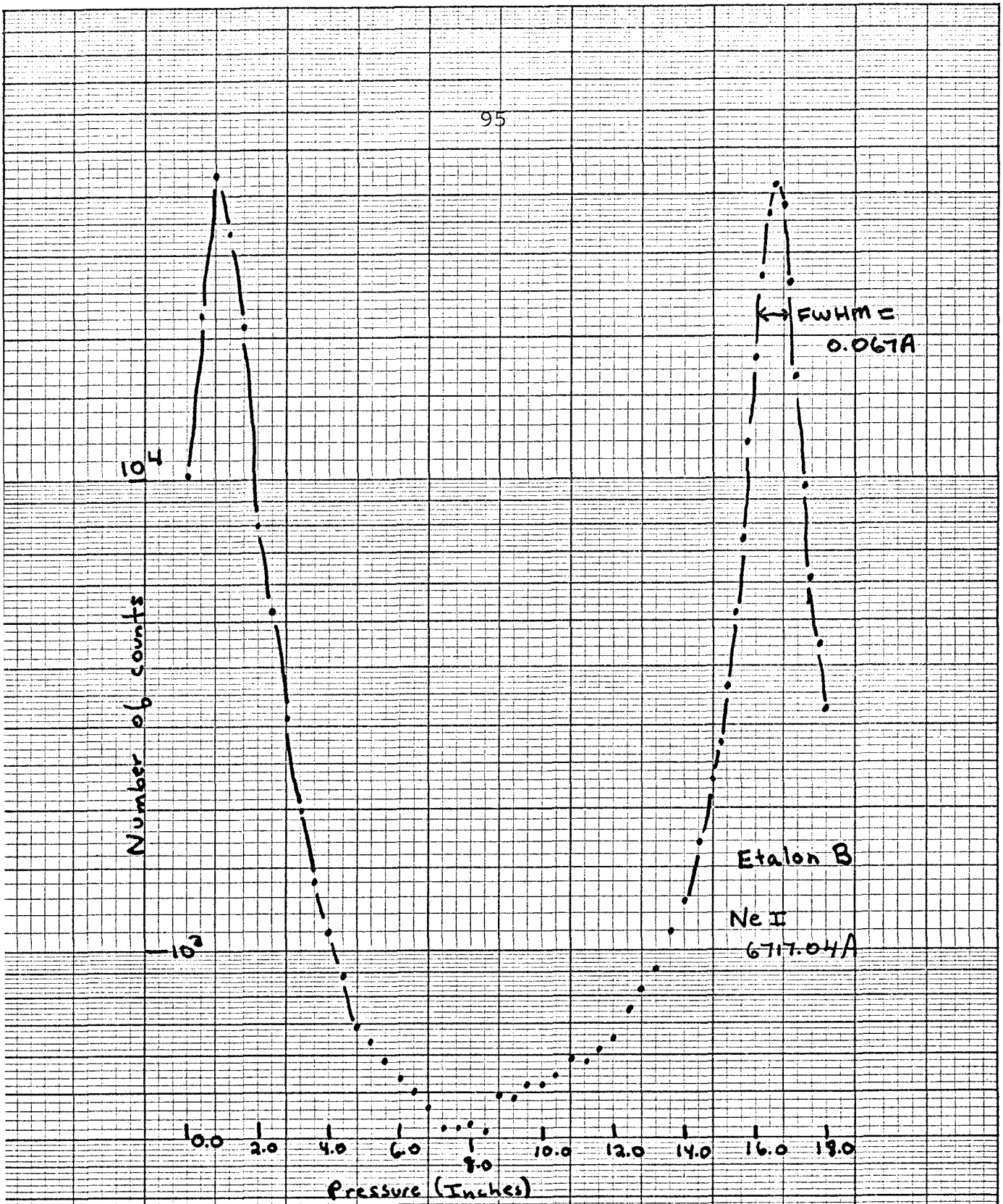

Figure 20: A scan in pressure only of λ6717.04A of Ne I with etalon B from the transmission maximum of one order to that of the next. The wavelength scale is such that $\Delta p/\Delta\lambda$ = 15.7 inches/A or 1 inch = 0.064 A.

equal to the width of the feature to be observed with the etalon. We can calculate the leakage from the profile in figure 20, as well as profiles where the grating and Fabry-Perot are scanned together. For w of 0.12 Å, only 15% of the total transmitted light is contributed by points more than 0.06 Å from the line center.

We now consider etalon C, which was used for a large part of the lithium line measurements. The neon line λ6717.04 Å has a FWHM of 0.097 Å when observed with this etalon, which implies a FWHM of the etalon itself of 0.091 Å, as compared with 0.058 for etalon B. A profile of the neon line as seen by etalon C when scanned in sand pressure is shown in figure 21. This etalon was in use for a period of more than a year, during which time the FWHM remained unchanged. The profile of the Ne I line shown in figure 21 is a composite of the observed profile in April 1970 and Nov. 1970. The total leakage derived from this provile, with w = 0.12 Å is also approximately 15%. This implies that about 15% of the total transmission is from points more than 0.06 Å from the central peak. If there is any continuous emission between the lines in the laboratory lamps, the leakage has been overestimated. However, we do not expect any significant continuum in these sources. Since the lithium line is a multi-component feature which is broader than 0.12 Å we may expect the leakage to be somewhat less for it. The calcium line λ6717 Å will have a slightly larger leakage, as it is a sharper feature.

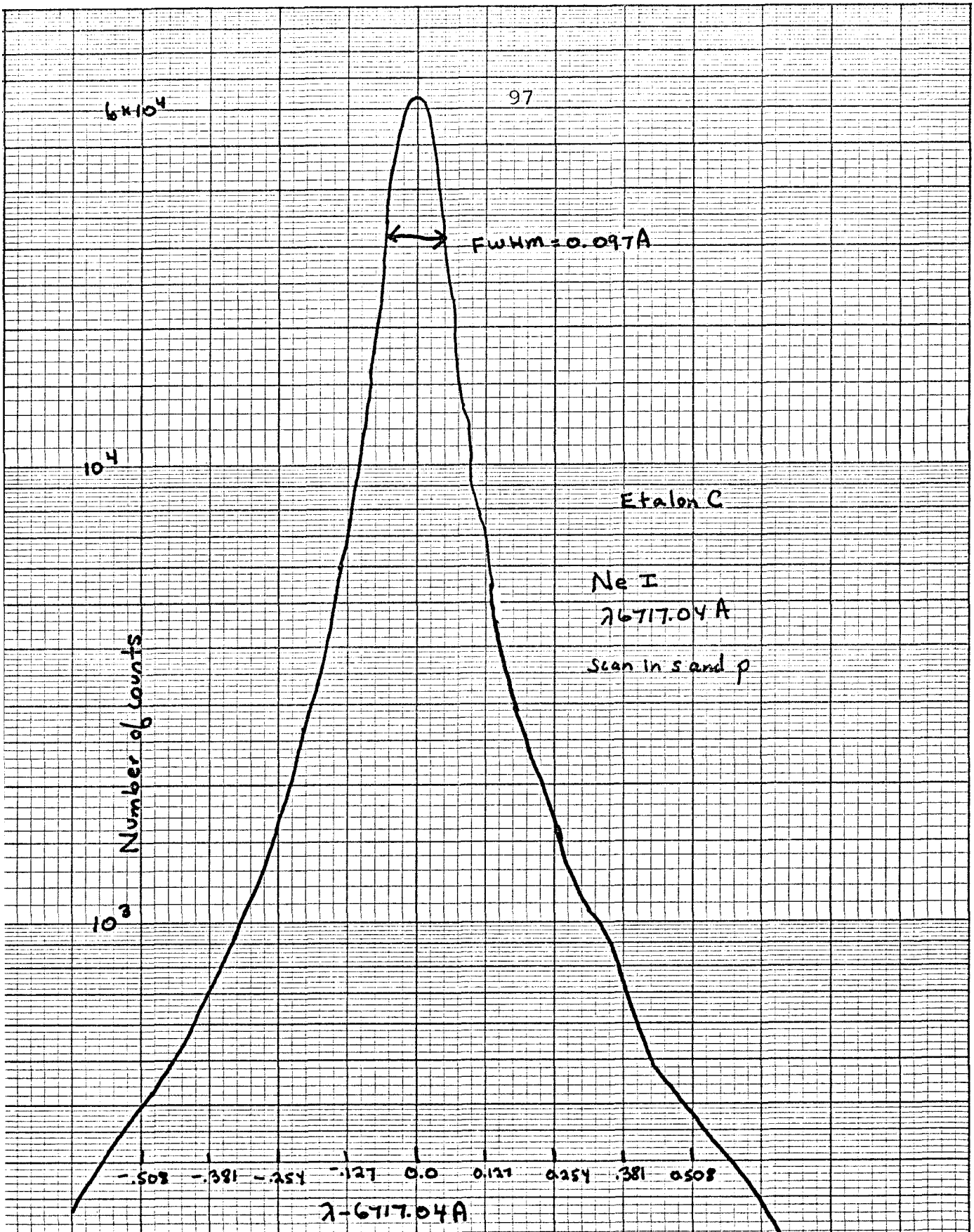

Figure 21: A scan of λ6717.04A of Ne I in the calibration lamp. Etalon C was used, and both the pressure and grating position were varied.

There is a second way to define the leakage. We are observing a spectral feature which is narrow compared to the free range of the instrument, and we wish to evaluate the fraction of the counts which come from the far wing of the instrumental profile. In effect, this leakage introduces a parasitic count, which fills in the absorption line profile.

We may evaluate $\mathfrak{F}$ from equation 5-4 for the FWHM. We can therefore express the instrumental response by

$$P(\Delta\lambda) = \frac{T^o}{1+\frac{4\mathfrak{F}^2}{\pi^2}\sin^2\left(\frac{\pi\Delta\lambda}{FR}\right)}\left(1 - \frac{|\Delta\lambda|}{S_\lambda}\right) \quad (|\Delta\lambda| < S_\lambda) \qquad (5\text{-}7)$$

where $2S_\lambda$ is the full width of the premonochromator slit. For etalons B and C respectively, we obtain $4\mathfrak{F}^2/\pi^2 = 96$ and 175. We then take two profiles; P_w is the complete profile given by equation 5-7 over the full range of $2S_\lambda$ (2.44 Å for etalon C), while P_s is the profile of the sharp central peak. In practice we take P_s to be the profile within 0.13 Å of the maximum and zero outside that range. We normalize both profiles and convolute them with theoretical profiles for λ6708 Å of Li I or λ6717 Å of Ca I. Obviously the wider profile P_w will give a shallower line than will P_s. If the central residual intensities of the theoretical line when convoluted are RI_w and RI_s, we may define the leakage L as

$$\frac{1.0 - RI_s}{1 - L} = 1.0 - RI_w \qquad (5\text{-}8)$$

Hence L is the fraction of the continuum which is spurious and is contributed by the far wings of the FP transmission profile outside the line of interest. L will depend on the width of the theoretical profile used in equation 5-8. Numerical calculations of L were made for etalon C. The results were 12% for Li I lines and 14% for Ca I lines. The difference in L is not surprising, as the Ca I lines are sharper than the lithium line.

We get an added dividend by this procedure. Our first estimate of the leakage using the observed profile of λ6717 Å of Ne I was based on the assumption that there is no continuous emission of the lamp to fill in the lamp profile between interference maxima. We know $\mathfrak{F}$ from equation 5-4, and from equation 5-1 we can calculate the ratio of the peak transmission to the minimum transmission between orders as

$$\frac{T^o}{T_{min}} = 1 + \frac{4\mathfrak{F}^2}{\pi^2} . \qquad (5\text{-}9)$$

If continuous emission is present in the lamp, the observed value of T^o/T_{min} will be less than $1 + (4\mathfrak{F}^2/\pi^2)$. We show in table 19 the comparison between T^o/T_{min} predicted and observed.

TABLE 19

Values of T^o/T_{min}

	etalon B	etalon C
predicted	97	178
observed	100	160

Therefore any continuous emission in the lamp must be less than 10% of the minimum transmission, or about 0.1% of the peak transmission.

For etalon C, we shall adopt a leakage correction of 10% for λ6708 Å and 12% for λ6717 Å. Places in the analysis where such corrections have been applied will be indicated in the text. Leakage corrections will never be applied to observed profiles which will always be plotted in counts/channel (N), with the dark count removed. Such corrections are applied to theoretical profiles (RI(λ)) which may be fitted to the observed profiles. If the apparent continuum of the observed profile is N_c, then the theoretical profile will give $N(\lambda)$, where

$$N_c - N(\lambda) = (1 - L)N_c RI(\lambda) \qquad (5\text{-}10)$$

We adopt this procedure so that the reader will see the observed profiles exactly as observed, instead of seeing them after several steps of reductions.

The profile of the D line etalon, which is of higher resolution than the etalons used for the lithium line, is shown in figure 22. Its half width is approximately 0.04 Å. If we use as w the FWHM of the D line etalon, the leakage calculated from figure 22 is approximately 8%. The value in practice is even less, as the D lines in the stars under consideration have half widths much greater than the FWHM of the etalon. Therefore the D line profiles are not noticeably affected by leakage. We can verify this by noting that several of the observed stellar D lines had central residual

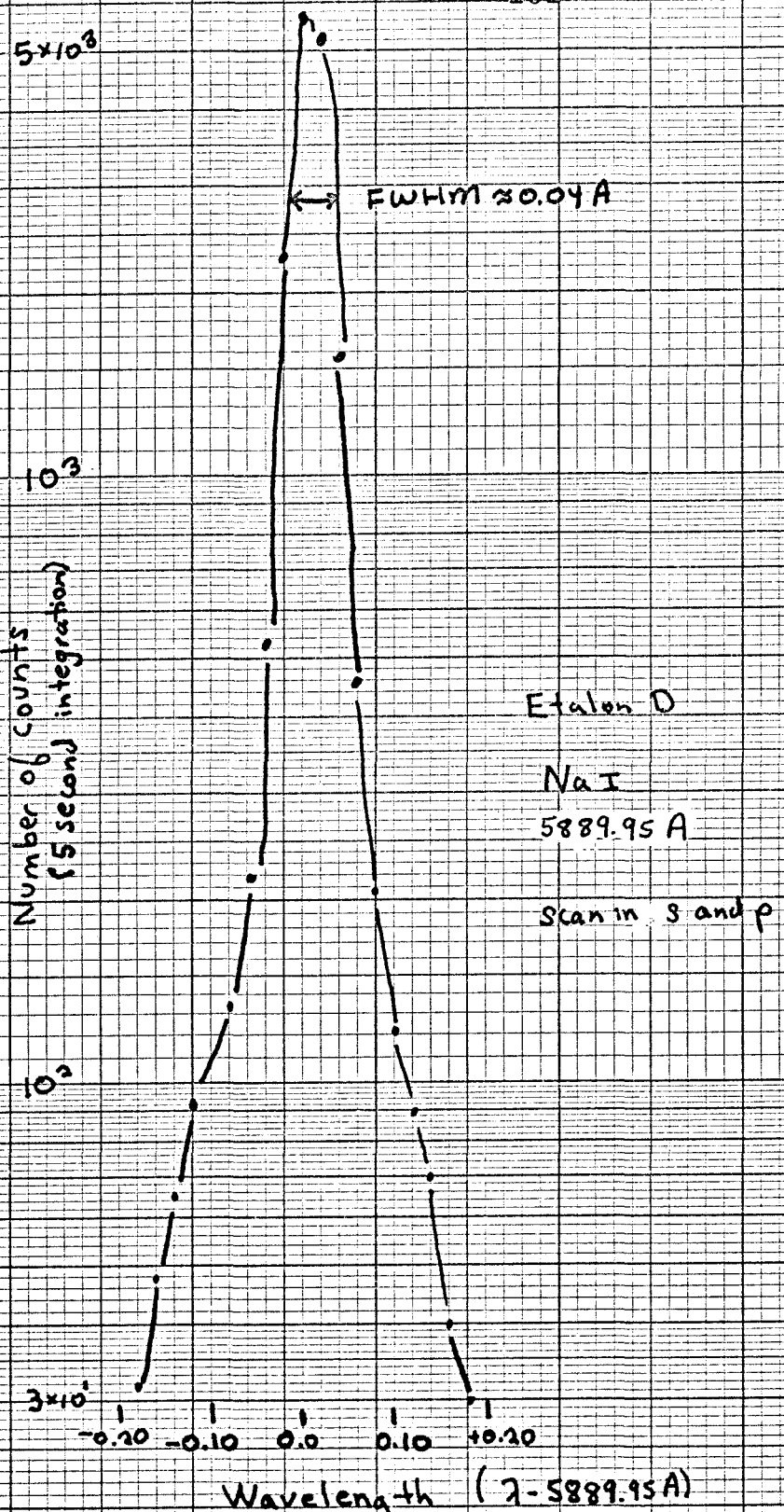

Figure 22: A scan of D_2 of Na I in the calibration lamp using etalon D. Both p and s were varied.

intensities of 10%.

C. Efficiency of the Interferometer

We conclude this chapter by evaluating the efficiency of the Fabry-Perot. First we consider the efficiency of the interferometer itself. We may determine this by comparing the counting rates of the data and monitor channel. For 10 Tau, we obtain 650 counts (corrected for dark count) in 15 seconds with etalon C in the channel, while in the same time interval we obtain 200,000 counts in the monitor channel. The ratio of the pass bands is approximately 2(16.5)Å/0.09 Å or 367. The efficiency (ϵ) of the FP is then

$$\epsilon = \frac{200,000}{367(650)} = 84\%$$

However, the efficiency of the entire system including telescope and camera optics is much less. We evaluate this by recalling our count rate for 10 Tau, which is an F6V star with V = 4.3 mag. The number of photons/sec/Å/cm^2 received above the earth's atmosphere from an AoV star with V = 0.0 is 1.24×10^3 photons/sec/cm^2/Å at 5500 Å (Oke and Schild 1970). If we multiply this number by 80% of the area of the 100" telescope (the secondary obscures 20% of the area of the primary), the time interval, the passband of the interferometer (0.09 Å), and a factor of 53 to compensate for the apparent magnitude of 10 Tau, we obtain a predicted count. The ratio of the observed value to the predicted count is the efficiency which comes out as $\epsilon = 0.6 \times 10^{-3}$. At first sight, that is a distressingly small

number. If we attempt to isolate the factors involved in it, we note that the quantum efficiency of an S-20 photo cathode at 6700 Å is only 10%; atmospheric transmission at the hour angle at which the star was observed is about 80% (somewhat less at Mt. Wilson probably); the FP efficiency is 80%. Then we have 5 mirrors, and a grating used far from the blaze along the light path. If these are fairly clean, with 80% reflectivity for each mirror and 20% reflectivity for the grating in this order, perhaps 5% of the light at the top of the telescope tube survives to the entrance slit of the FP. These factors combined give 3×10^{-3}. It is not clear exactly where the remaining factor of 5 originates; perhaps the Mount Wilson sky lacks transparency; most likely the mirror reflectivity is lower than assumed. We must recall that photography will have all of these factors except for the efficiency of the photo cathode and the FP, which are 8%. Photographic emulsions at 6700 Å are not extremely efficient either, and there will also be a corrector plate in the light path.

Let us compare the time required to observe the Li I line photographically and with an interferometer for 10 Tau. If we wish to scan over 1 Å, we need 30 points (spaced 5 steps apart), which gives 8 minutes per scan of the star. The resolution of this scan will be 0.09 Å, although the scan will be noisy. This one scan will have a resolution and a noise level comparable to that of a spectrum at 4.5 Å/mm (assuming the resolution on the plate is 20μ). Even with the new 09801 emulsion, it takes an exposure of about 1-1/4 hours to

obtain a spectrum at 6.7 Å/mm of 10 Tau. To obtain a photographic spectrum at 4.5 Å/mm would require an exposure of almost 2 hours. Thus we require almost 2 hours to observe a line profile with conventional photographic spectroscopy of quality comparable to that obtained by a Fabry-Perot in 8 minutes.

CHAPTER VI

THE STELLAR PROFILES

A. Observational Technique

At the beginning of each night, the Fabry-Perot is tuned by observing the λ6708 Å of lithium and λ6717 Å of neon. This gives us the pressure and grating position (s) corresponding to the center of the laboratory lines. This calibration is measured several times each night; it drifts very little in pressure and slightly more in s; since the transmission of the premonochrometer is much broader than that of the Fabry-Perot, it is the drift in pressure which must be accurately measured. However, recall that s is digitized and recorded, whereas p is not. Figure 23 shows a typical set of calibration readings over a night. It is apparent that the drift is fairly smooth and that more frequent calibrations are not necessary. The constants for the scanning rates $ds/d\lambda$ and $dp/d\lambda$ can be measured from the separation of the Ne and Li lamp lines or they can be determined from properties of the etalon and grating. Both methods give similar results, and these numbers are constant from run to run.

We measure the dark count of the data channel several times per night. It is generally 1-2 counts per second. For both data and monitor channels, S-20 photo cathode surfaces are used.

Once each run the instrumental profile is determined by observing the profile of the Li and Ne lines (see chapter V).

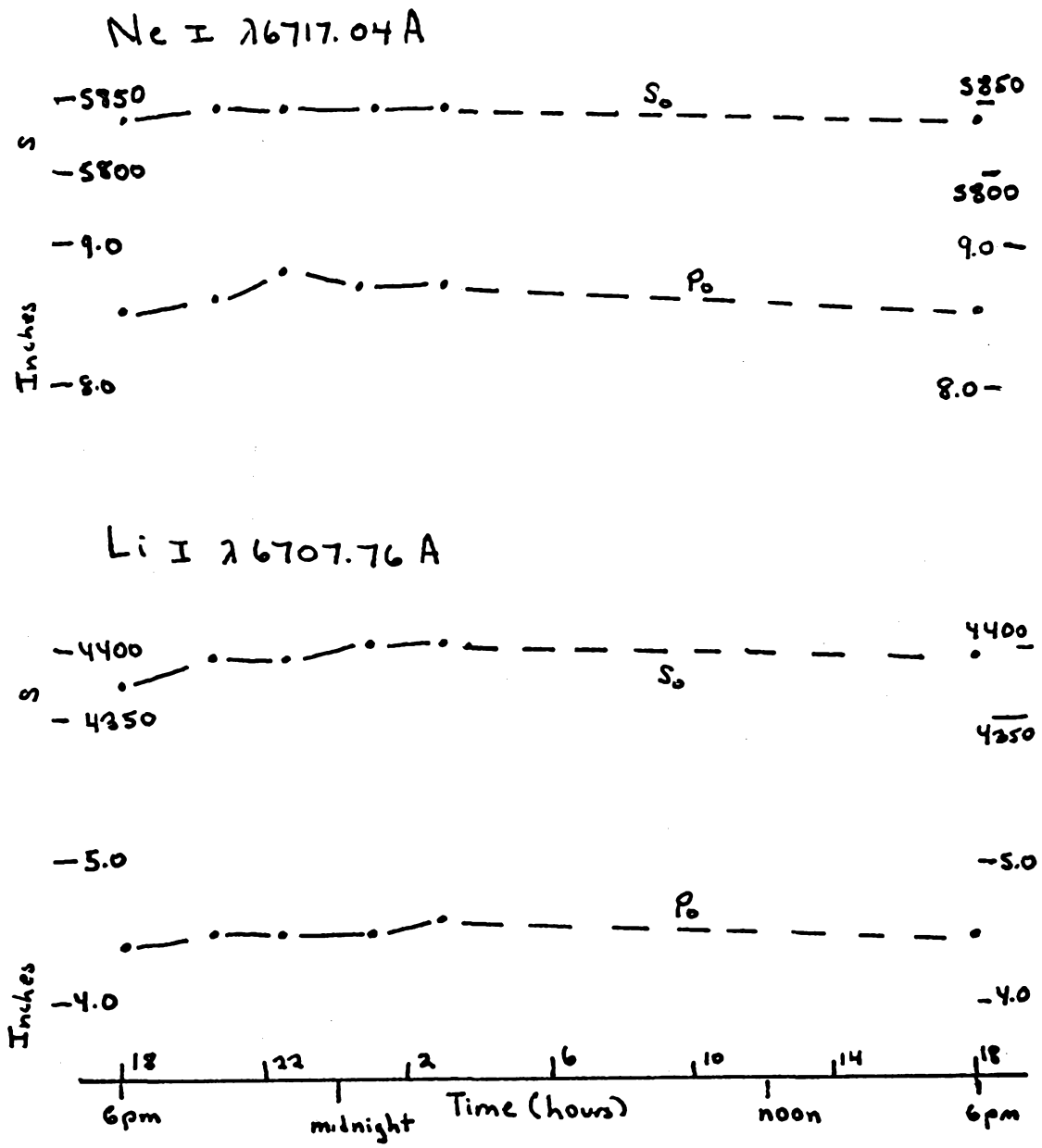

Figure 23: s_o and p_o (the s and pressure corresponding to the center of a calibration line) for λ6707.761A in the lithium lamp and λ6717.04A of NeI over a 24 hour period.

For each star, we have a radial velocity from the Yale Catalogue of Bright Stars (Hoffleit 1964) and an approximate correction to v_r for the orbital motion of the earth. These, together with the (s_o, p_o) calibration using laboratory lamps, gives an approximate (s_*, p_*) for the center of the line we wish to observe. It is important to have some idea of (s_*, p_*) as it is very time consuming to have to search for a feature over a large wavelength range. The stellar line is then scanned 3 to 5 times, with the monitor gate set at a level determined from experience to a yield roughly 900 counts per channel in the continuum (more if the star is very bright). The Brown chart recorder provides a record of the integration time in seconds for each count so that the dark count can be subtracted; the cards from the key punch are used in the data reduction program; the printer provides a convenient listing of all the data.

The range that is scanned is chosen from experience for the first scan of a given star; it is then adjusted if the continuum does not appear to be reached at the beginning and end of the scan. Of course, we cannot include very much of the spectrum outside the line, as that is time consuming too. Typically we go at least 0.5 Å from the line center.

All the scans are made in the same direction in wavelength with the pressure increasing. We usually observe the Li line, then calibrate the Li line with the lamp, then calibrate the Ne line, and finally observe the Ca line. In the next star, the order is

reversed and the Ca line is observed first. On a good night, this requires about 2-1/2 hours for a fifth magnitude G star. Guiding is sometimes tricky, as the compensation is better if the star is held in a fixed position with respect to the entrance aperture. If the seeing is very good, the entire disc goes in the slit with the exception of the diffraction spikes, which can be used to guide. The companions of close doubles can also be used to guide. Note that we must guide in <u>two</u> dimensions; our entrance aperture is almost a square and we do not trail. In general, the 100" drive is not accurate to 1" in 10 minutes and frequent corrections are necessary.

For each line in each star on each night, the scans are averaged at each value of s. We then obtain the exact radial velocity correction due to the orbital motion of the earth for the date and time of the observation and compute $(s_* - s_o, p_* - p_o)$ more exactly. We thus have for each night (s_o^i, p_o^i) and $(s_* - s_o^i, p_* - p_o^i) = (\Delta s^i, \Delta p^i)$, where i is the index for the number of the night. We then average over the nights of a run by averaging channels which have the same values of $(s - s_o^i - \Delta s^i, p - p_o^i - \Delta p^i)$. This insures that the shifting between nights is such that channels corresponding to the same wavelength in the rest frame of the star are averaged. When necessary, weights are assigned, as the scans do not cover exactly the same range in wavelength, and if the monitor setting is changed from one night to another, an averaging procedure without weights will give discontinuous jumps where the number of nights which include a particular channel changes.

This same averaging procedure (with the shifting to the rest frame of the star and weighing) is repeated when we average the averages from each run to get the final line profile for each star. This procedure was not used for the spectroscopic binaries. For these objects, separate averages were retained for each run.

In table 20 we list the nights which were devoted to obtaining observations and the etalons used each night (see table 18 for a description of the etalons). A total of 26 nights on the 100" telescope was assigned for interferometry, of which 18 were suitable for observation, although on many of these nights the seeing was poor (0-1), and the counting rate was very slow. The relatively few nights of superior seeing provided a large fraction of the data.

An unforseen problem developed in the course of the investigation. We had assumed that the radial velocities listed in the Yale Catalogue of Bright Stars (Hoffleit (1964)) would be of sufficient accuracy (± 0.5 km/sec), except for the spectroscopic binaries. However, lines often appeared several km/sec away from their predicted positions. We therefore decided to observe the Ca I line at 6717 Å as well as λ6708 Å to obtain an idea of the error in the radial velocity. We recall that this is the first time that the Fabry-Perot has been used for work on weak stellar lines, rather than interstellar lines. Furthermore errors of 1 km/sec could easily occur in the standard radial velocity measurements. Dr. Arthur Vaughn informs me that he encountered several similar problems in observing λ3984 Å of Hg I in Ap stars, which are exceedingly

TABLE 20

Observing Record with the Fabry-Perot Interferometer

Date	Etalon	Remarks
Nov 1969		
24-25	A	clouded out after midnight
25-26	B	
26-27	"	clouded out after midnight
27-28	"	
29-30	D (for Na I lines)	
30-Dec 1	"	cloudy all night
Apr 1970		
15-16	C	cloudy all night
16-17	"	cloudy all night
17-18	"	cloudy until 9 pm
18-19	"	
Sept 1970		
9-10	C	
10-11	"	
11-12	photography	instrumental troubles
12-13	C	
13-14	"	
Sept 1970		
22-23	D (for Na I lines)	
23-24	"	
Dec 1970		
4-5	C	
5-6	"	clouds after midnight
6-7	"	clouds after 3 am
7-8	"	clouds all night
8-9	"	clouds all night
Mar 1971		
4-5	C	wind 35 mph after midnight
5-6	"	
6-7	"	
7-8	"	

sharp lined objects and hence should have accurately known radial velocities. Evidence will be given in the next section that this "velocity shift" is indeed an error in the previously catalogued v_r and not an instrumental effect.

We now come to the problem of the errors in the profiles. Except for the cores of the Na I D lines, the count per channel per scan (n) is about 900 and the dark count n_d is generally about 50. This gives a flucutation due to photon noise of $\sqrt{n}$, and a fractional error of $\sqrt{n}/(n-n_d)$ which is 4% for the numbers quoted. However, the compensation of the interferometer for seeing fluctuations as well as placement of star on the slit is far from perfect. Tests by counting at a fixed s and p and watching the fluctuation in the count rates show that the compensation can be described as introducing a fluctuation about the true count rate of about 4%. (As the error in compensation must be measured with a star rather than a lamp source, the fluctuations in the observed count rates during this test contain a considerable contribution due to photon noise.) This gives a final error per scan of

$$\epsilon = \sqrt{\frac{n}{(n-n_d)^2} + (0.04)^2}$$

or 5.6% for the numbers quoted. If n_s is the number of scans that are averaged to give the final line profile, then the rms error of each channel of the final scan is

$$\delta = \frac{\epsilon}{\sqrt{n_s}}$$

A typical value of n_s is 15, which gives $\delta = 1.5\%$. If we assume that the center of the line has a residual intensity of 75%, then the same analysis as above also gives δ less than 2%. It is only when the line becomes extremely deep that the errors significantly increase.

B. The Width of the Stellar Profiles

There is a gravitational redshift of spectral features emitted by a massive body as seen by a distant observer. This redshift will occur in our stellar spectra when compared in wavelength with a laboratory source on earth. We can calculate the shift using the physical dimensions of the sun, as these are typical of the stars we have observed. Then

$$h\Delta\nu_g = \frac{GM_\odot(h\nu/c^2)}{R_\odot}$$

and $\Delta\lambda_g = 0.014$ Å at 6707 Å. No correction for this shift has been applied to the observation. (It occurs in such a sense that, if it is present, we will overestimate the amount of Li^6.)

We now consider the expected width of the stellar profile. We neglect rotation. (The rotational velocity of the sun is approximately 2 km/sec.) Classical damping theory (i.e. a harmonic oscillator) gives a width of 0.06 mÅ, and in chapter II we indicated that 10 times the classical damping constant is a reasonable approximation to the damping constant resulting from radiative, electron, and van der Waals broadening. Hence collisional and radiative broadening gives a width of 0.6 mÅ. There is also a shift in wave-

length, which is 2/3 of the collisional width. This shift is much smaller than the gravitational redshift.

The thermal widths are much larger. If we take $\sqrt{2kT/m}$ as the mean velocity, then for 5000 ^{o}K we obtain 1.4 km/sec for Ca and 3.4 km/sec for Li. We must also allow for a microturbulent velocity of 1.5 km/sec, as is found in the sun. Hence

$$v = \sqrt{v_{thermal}^2 + v_{mt}^2}$$

$$= 2.0 \text{ km/sec for Ca and } 3.7 \text{ km/sec for Li}$$

For a weak line whose profile can be approximated by a Gaussian, we expect a FWHM of approximately 0.09 Å for Ca and 0.16 Å for Li. We now recall that the instrumental profile has a FWHM of 0.06 to 0.09 Å. We therefore expect a weak observed line to have a FWHM of $\sqrt{0.09^2 + 0.09^2} = 0.13$ Å. The solar Ca I line at λ6717 Å is not a weak feature, and furthermore we have not allowed for the rotational velocity of 2 km/sec. Thus, it is not surprising that the observed width (discussed in the next section) is somewhat larger than the derived figure.

Because we are working over a narrow range in spectral type and hence in temperature, any variation in the observed width of the lines must be due mostly to variation in rotational velocity. We can therefore use the observed width of λ6717 Å to derive the rotational velocity of a star. The lithium line has too many components and the Na I D lines are too broad to be used for this purpose.

C. Observations of the Moon

To further test the accuracy of the apparatus, we observed the moon on March 4-5, 1971. The seeing was extremely poor with high clouds. Even with the telescope in focus, no craters could be seen on the lunar surface. The same slits as were used for stars were used here, except that the number of counts in the monitor band before advancing to the next channel was set very high, so that approximately 3000 counts per channel were obtained in relatively short integration times. The rate of the telescope drive was not adjusted; the slit was set on one limb of the moon and then several scans could be made before the other limb was reached.

There are several components of the total radial velocity of the moon which can contribute to a possible Doppler shift of the lunar spectrum relative to a laboratory source. The first of these is any radial motion of the moon with respect to the earth. We have estimated this by differentiating tables giving the semi-diameter of the lunar disc every half-day in the 1971 Ephemeris. (We thank Prof. Schmidt for this suggestion.) This gives a recessional velocity of 0.06 km/sec. There is also a component of the rotation of the earth, which is a recession of about 0.4 km/sec, since the moon was observed when it was over 3 hours west of the meridian. We therefore expect a total v_r of -0.46 km/sec which corresponds to a redshift of 0.01 Å. There may also be a gravitational redshift between the sun and a laboratory source of 0.01 Å. Hence we expect the lunar lines to be approximately 0.02 Å to the red of a laboratory source.

Figure 24 shows λ6717 Å of Ca I as observed in the reflected solar spectrum. Note that the lunar line is ~ 0.03 Å to the red of the laboratory source, which is very close to its expected position. We can compare this profile with data from the Photometric Atlas of the Solar Spectrum (Minnaert, Mulders, and Houtgast (1940) and from Moore, Minnaert, and Houtgast (1966), which refer to the center of the solar line and hence should be close, but not exactly identical, to the lunar spectrum. Recall that the center of the solar disc has no component of v_{rot} along the line of sight. The lunar spectrum has the rotational velocity of the sun, 2 km/sec. The equivalent width of the F.P. line profile is 105 mÅ, which becomes 120 mÅ when corrected for a 14% leakage. Moore, Minnaert and Houtgast (1966) quote 131 mÅ as the total width of λ6717.69 Å (Ca I) and λ6717.83 Å (Fe I). The Utrecht atlas has an instrumental profile whose FWHM is approximately 0.05 Å. We therefore expect the central residual intensity and FWHM of the Utrecht and interferometer profile for λ6717 Å to be about the same. Table 21 shows this comparison, where the same 14% correction in leakage has been applied.

TABLE 21

Comparison of Utrecht and FP Profiles for λ6717 Å

	FP	Utrecht
RI_{min}	55%	48%
FWHM	0.21 Å	0.17 Å

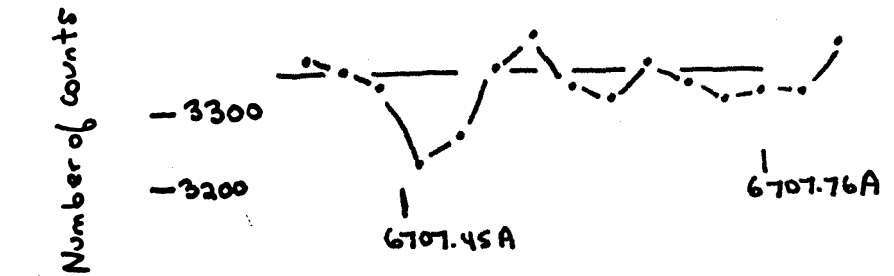

Figure 25: A scan of the region near 6707.7A in the lunar spectrum. The points are separated by 0.032A. The wavelengths indicated were obtained directly from the lamp calibration, assuming the radial velocity of the moon with respect to the earth is zero.

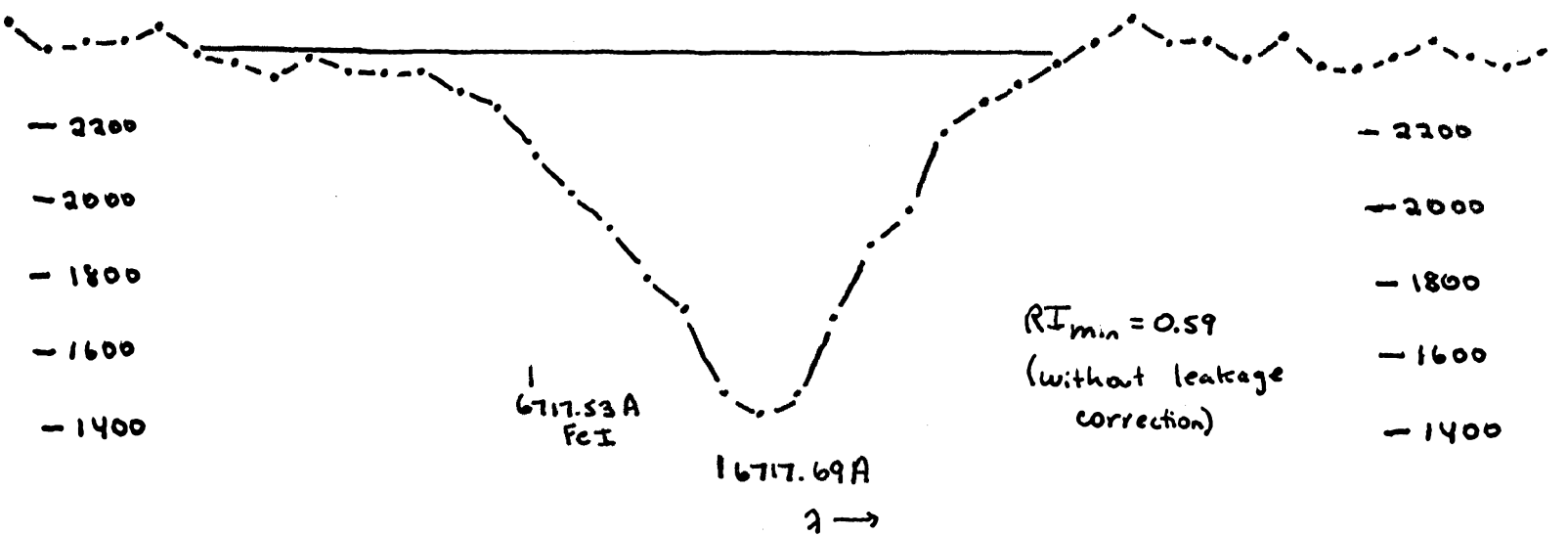

Figure 24: A scan of the region near λ6717.69A of Ca I in the lunar spectrum. Points are separated by 0.032A. The wavelength of the line center is indicated assuming v_r of the moon with respect to the earth is 0.

The agreement is very reasonable. The Utrecht profile is sharper, as we expected for the center of the disc compared to the entire disc.

Figure 25 shows a scan of the region of λ6707.76 Å in the lunar spectrum. We do not expect the lithium line to be observed, and its presence on the scan is marginal at best. However we can see λ6707.45 Å, an unidentified solar line, which is ~ 0.02 Å to the red of its laboratory position, as expected. In table 22, we make the same comparison of parameters as was done for the Ca I line. (The colon denotes data of large uncertainty.)

TABLE 22

Comparison of Utrecht and FP Profiles for λ6707.45 Å

	FP	Utrecht
W_λ	2.5 mÅ	5:
RI_{min}	96%	95%
FWHM	0.08 Å:	0.10 Å

The agreement is extremely good.

This investigation of the lunar spectrum gives us great confidence that the equipment does indeed work properly and that the instrument does not introduce spurious wavelength shifts into the star as compared with a laboratory source.

D. Basic Parameters of the Program Stars

The program stars were chosen to obey several basic criteria which are listed below.

a) strong λ6708 Å of Li I

b) sharp lines

c) $V \leq 5.0$ magnitudes

d) λ6707.45 Å is expected to be weak

It is surprising how few stars there are which satisfy these conditions. An effort was made to observe as many of Herbig's (1964) stars as possible; however several were too faint and one (ι Peg) is a double-lined spectroscopic binary (period = 10.2 days) whose velocity curve has a very large amplitude (total range of 90 km/sec) (Curtis (1904)). The literature contains several surveys of Li I line strength (Herbig 1965 for example) which were used as a basic starting list.

In table 23 we list the star name, apparent magnitude, spectral type, radial velocity (Hoffleit 1964), the number of scans of λ6708 Å that were made, information on the H-K emission of Ca II (Wilson 1966), v_{rot} given by Kraft (1967), remarks, and the isotope ratio given by Herbig (1964). Note that the list includes all but 4 of the 15 stars observed by Herbig (1964), and that of the four missing, only one (ι Peg) had an isotope ratio greater than 0.10. All the doubles were observed on nights of good seeing and if necessary the image rotator was used to keep the companion off the entrance slit. Contamination of the profiles by light from a companion is expected to be negligible.

TABLE 23

Program Stars

Name	V	type[1]	v_r[1]	n_s	H-k emission[2]	v^{rot} Kraft[3]	remarks	R_{Herbig}[4]
γ Lep	3.6	F6V	-10	15				0.04
ξ Peg	4.2	F7V	- 5	10	none	9		0.01
10 Tau	4.3	F8V	+28	17				0.55
χ Her	4.6	F9V	+55	11	none	≤6		0.03
χ' Ori	4.6	G0V	-14	23	strong	5-7		-0.01
ξ UMjA	4.4	"	-17	20			SB	0.21
β Com	4.3	"	+ 6	21	moderate	3-5		0.39
δ Tri	4.9	"	- 6	3	weak		SB	0.52
ι Per	4.0	"	+50	12	none			0.32
κ Cet	4.8	G5V	+19	6	strong			0.39
ξ Boo A	4.5	G8V	+ 4	18	strong			-0.08
η Psc	3.7	G8 III	+15	2	weak			
ψ UMj	3.2	K1 III	-20	13				
η Cet	3.4	K2 III	+12	10	strong			

1) Hoffleit (1964)
2) Wilson (1966)
3) Kraft (1967)
4) Herbig (1964)

E. The Stellar Profiles

In this section we present in figure 26 the final profiles of λ6708 Å of Li I and λ6717 Å of Ca I which were measured with the Fabry-Perot interferometer. The profiles of the Na I lines are given in Appendix A. The Li and Ca profiles were measured with etalon C. All of the figures are drawn with the same scales. Wavelength increases to the right, and one centimeter on the λ axis is 0.064 Å. Data were obtained at points separated by 0.032 Å (corresponding to $\Delta s = 5$ and $\Delta p = 0.5$ inches, with etalon C). The vertical scale is number of counts (the dark count has been removed) in a single scan. This axis can be multiplied by an arbitrary factor. The point on the wavelength axis marked v_o is the wavlength at which the line is expected to fall using the radial velocity of table 23 and the correction for the earth's orbital motion appropriate for each day. The wavelength denoted by v_o is 6717.69 Å for the Ca I line, and 6707.76 Å for Li I. If the radial velocity of table 23 is correct, then the center of the Ca I line, and the strongest component of λ6708 Å should fall at the indicated positions. For each Li I line, we indicate the minimum residual intensity, the equivalent width, and $\lambda_{1/2}$ (defined by equation 2-18). A planimeter was used to measure $\lambda_{1/2}$ and W_λ. For each Ca I profile, we indicate the minimum residual intensity and the FWHM. These scans and the derived parameters have not been corrected for leakage of the interferometer. Some remarks on the profiles for each star are given below.

γ Lep A: This star is a wide double, whose separation is 95", with $\Delta m = 3.0$. In the Yale Catalogue of Bright Stars (Hoffleit 1964), its v_r is listed as "-10 V?." We have used $v_r = -10$ km/sec to obtain the points marked v_o. It appears that from Sept. 1970 to March 1971 the radial velocity was closer to -8.6 km/sec, as the Ca I line center is noticeably offset from the v_o position. We have adopted a 5 step (0.032 Å) shift due to the error in v_r in computing $\lambda_{1/2}$.

ξ Peg: This star obviously has broad lines. The Ca I profile is very poor, being a mean of only 2 scans. We therefore include the core of the D lines as seen by the Fabry-Perot to give additional evidence that there does not appear to be any error in the radial velocity for this star. The lithium profile is a mean of only 10 scans. so that the rms error per point of the final scan is 2%, somewhat larger than for most profiles of λ6708 Å.

10 Tau: This star is a critical star, as Herbig (1964) asserted that $Li^6/Li^7 = 0.55$. We therefore show the core of the D lines again as well as the Li and Ca profile. (The scale of the D line profiles is 0.041 Å/pt.). The Na I and Ca I lines all indicate a slight velocity error of 1.4 km/sec (5 steps) in the sense that the tabulated velocity is too small. If this were an error in the other direction, one could assert that the very high layers of the atmosphere in which the D line cores are formed are moving outward from the star, and that a velocity correction as determined from the D lines of Na I is not

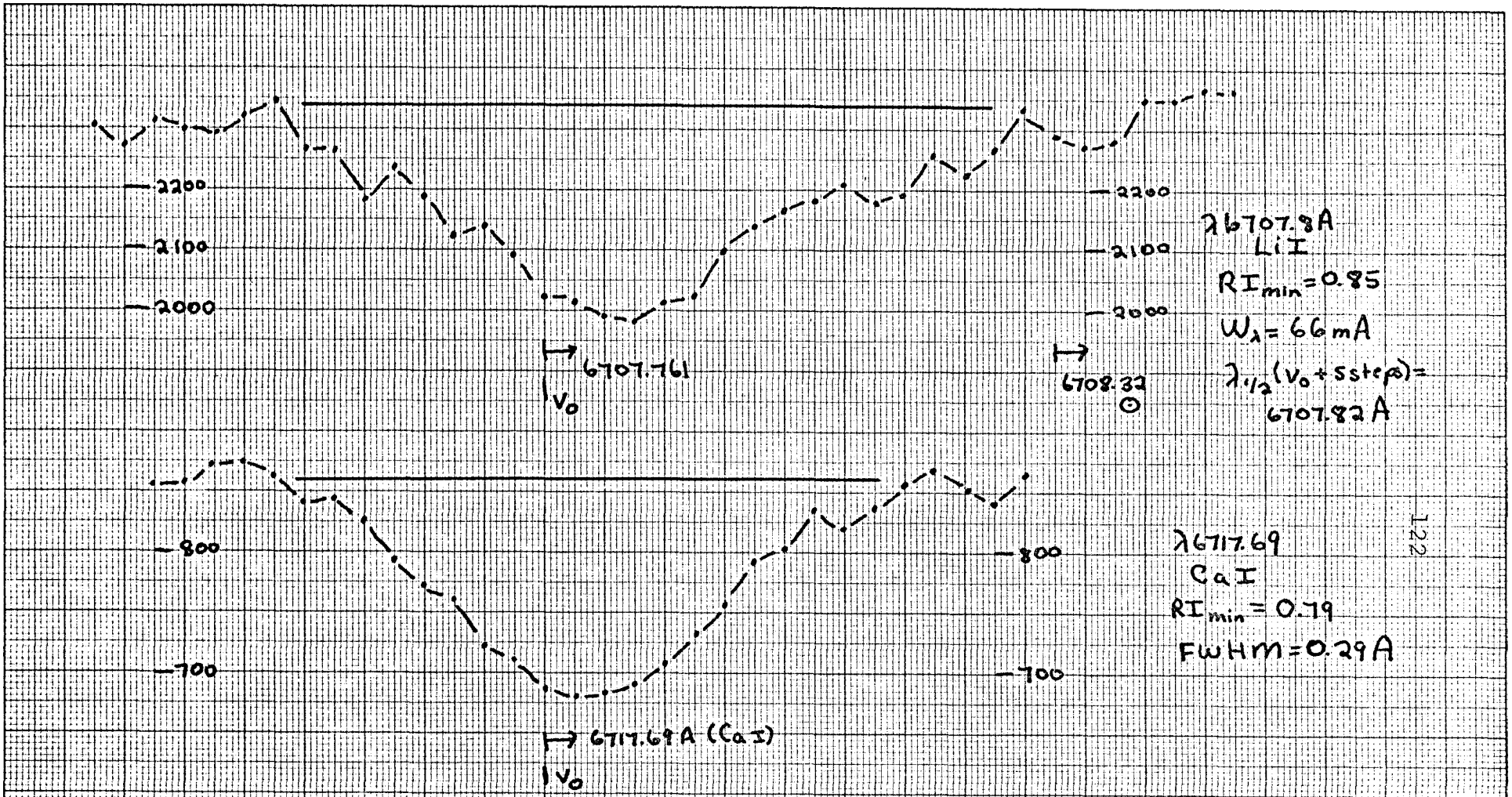

Figure 26a: The profiles of the resonance line of Li I and λ6717.69A of Ca I in γ Lep (F6V) observed with the FP. Etalon C was used. Points are 0.032A apart.

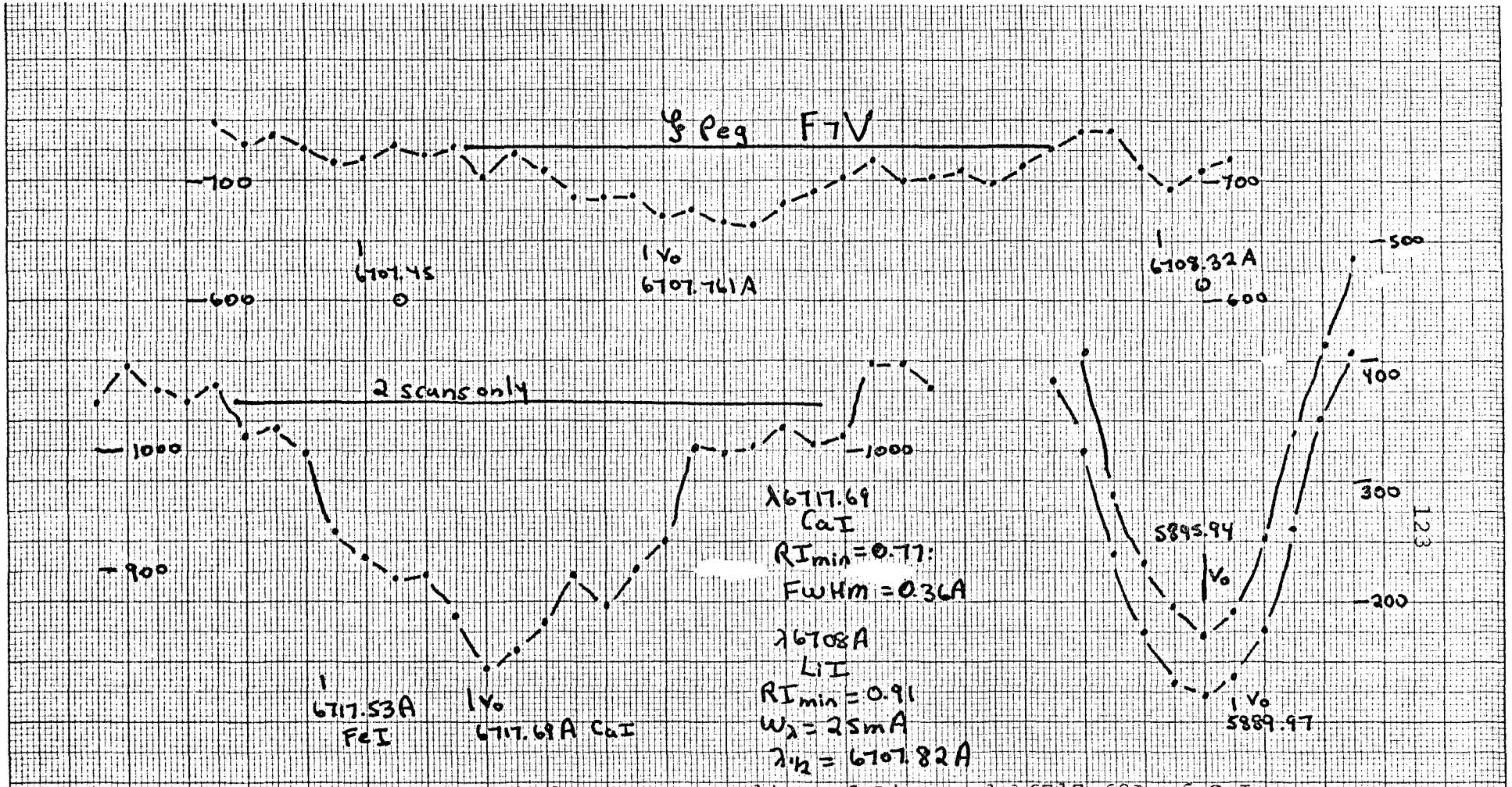

Figure 26b: The profiles of the resonance line of Li I and λ6717.69A of CaI in ζ Peg (F7V) observed with the FP. Etalon C was used. Profiles of the cores of the D lines of NaI observed with etalon D are also shown. The wavelength scale is 0.032A/point except for the D lines, where it is 0.041A/point.

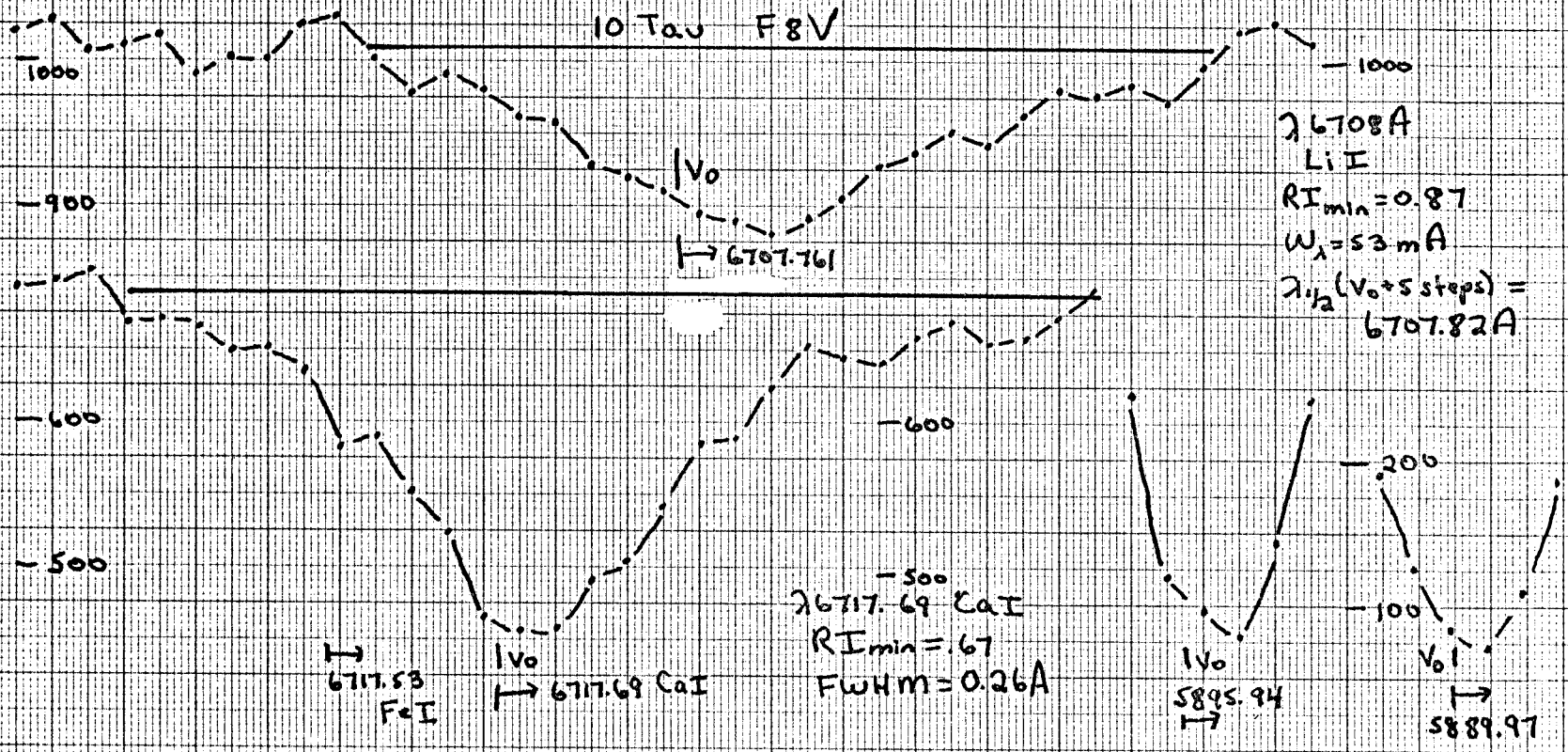

Figure 26c: The profiles of the resonance line of Li I and λ6717.69A of Ca I in 10 Tau (F8V) observed with the FP. Etalon C was used. Profiles of the cores of the D lines of NaI observed with etalon D are also shown. The wavelength scale is 0.032A/point except for the D lines, where it is 0.041A/point. The points marked v_o were calculated assuming the tabulated radial velocity.

applicable to the Li I line. However, no such argument is possible given the sign of the correction that is required. It is possible that the velocity correction is as large as 2.3 km/sec, but doubtful. A 1.5 km/sec error in v_r was used in computing $\lambda_{1/2}$. Seventeen scans were averaged to obtain the profile of λ6708 Å, so that it should be of high accuracy; only 6 scans were made of λ6717 Å.

χ Her: This star has a very large v_r (+55 km/sec from the Yale Catalogue of Bright Stars (Hoffleit 1964). It appears that the tabulated v_r is too large by about 3 km/sec. We have applied a 10 step correction (equivalent to - 2.9 km/sec) in determining $\lambda_{1/2}$. If the correction were not this large, $\lambda_{1/2}$ would become less than 6707.81 Å and we would later obtain a negative isotope ratio.

χ' Ori: This star has broad lines. The Ca I profile indicates a possible 5 step (1.4 km/sec) error in the velocity in the sense that the tabulated velocity is too small. We use this 5 step shift in measuring $\lambda_{1/2}$. It is unfortunate that the lines are so broad, as this makes determining the central wavelength of λ6717 Å rather difficult. Slight errors (of the order of 2%) in the profile will be very noticeable in the core of such a broad feature.

ξ UMa A: This star is a close double (Δm = 0.9 and separation 3.4"; period = 60 years). We were able to avoid contamination by the secondary by using the image rotator to place the secondary out of the entrance aperture. The brighter component is a spectroscopic binary with a 669 day period (Berman 1931). (The fainter

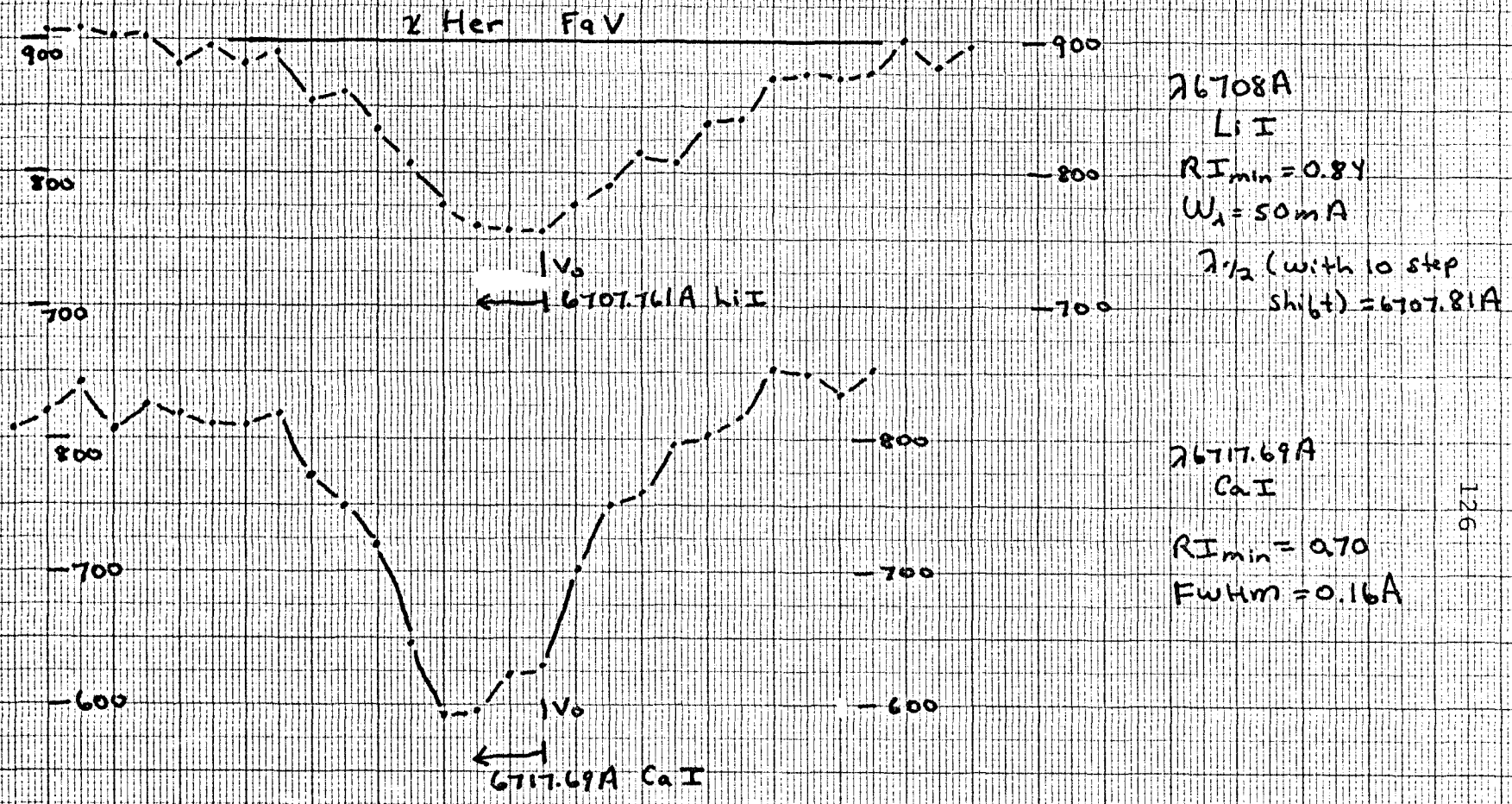

Figure 26d: The profiles of the resonance line of LiI and λ6717.69A of CaI in χ Her (F9V) observed with the Fabry-Perot interferometer. Etalon C was used. Points are 0.032A apart.

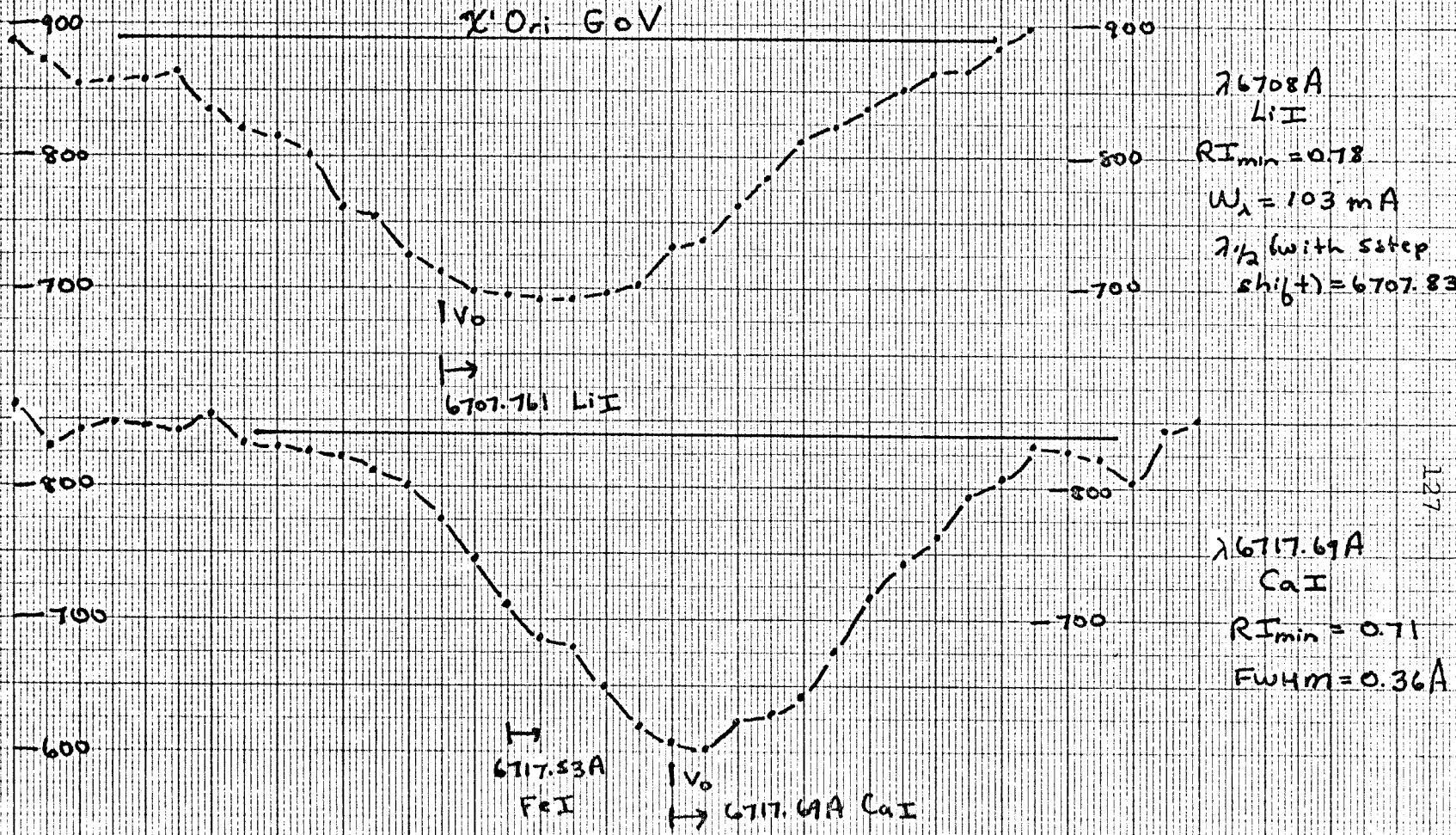

Figure 26c: The profiles of the resonance line of LiI and λ6717.69A of CaI in χ' Ori (G0V) observed with the Fabry-Perot interferometer. Etalon C was used. Points are 0.032A apart.

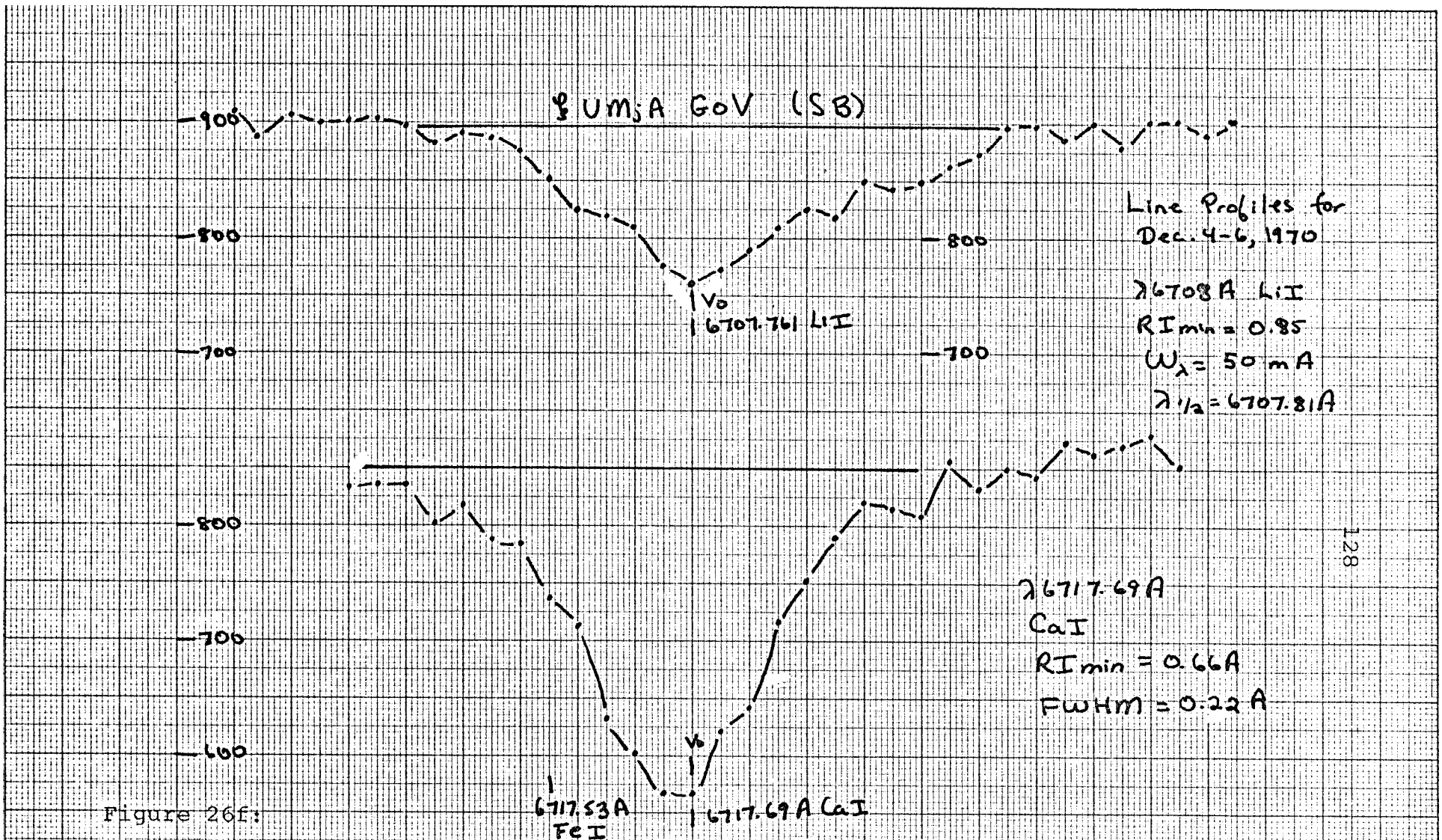

Figure 26f:
The profiles of the resonance line of LiI and λ6717.69A of CaI in the spectroscopic binary ξ UMj A (GoV) observed with the FP. Etalon C was used. Points are 0.032A apart. The profiles shown are averages over the period Dec.4-6,1970.

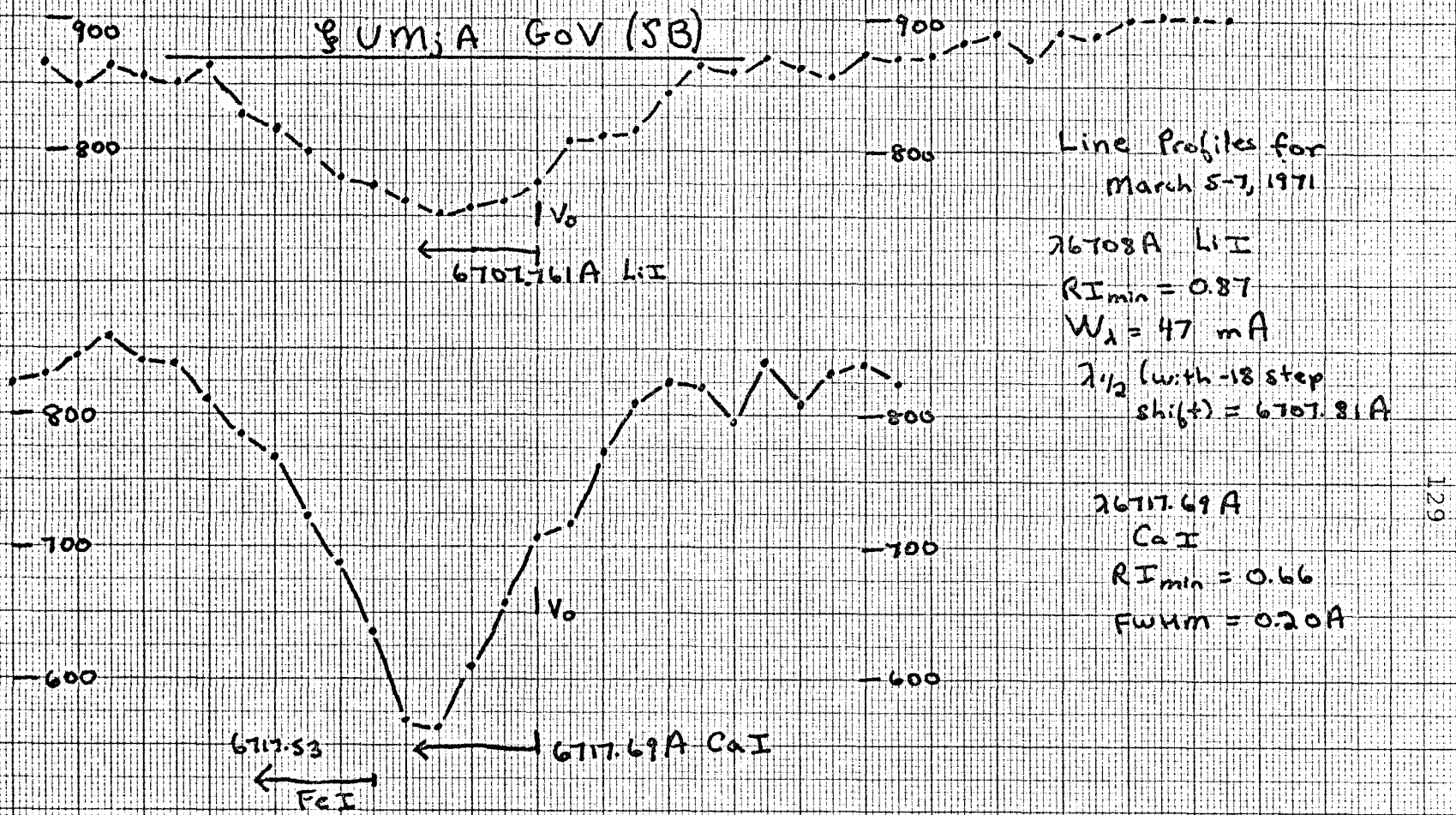

Figure 26g: The profiles of the resonance line of LiI and λ6717.69A of CaI in the spectroscopic binary ξ UMj A (GoV) observed with the FP. Etalon C was used. The profiles shown are averages over the period March 5-7, 1971. Note the good agreement with the December profiles (fig.26f). Points are 0.032A apart.

component is also a spectroscopic binary.) We therefore present separate averages for the Dec. 1970 and March 1971 observing runs. The corrections to v_o required to get to the center of λ6717 Å of Ca I are - 4.9 km/sec for March 5-7, 1971 and 0 for Dec. 4-6, 1970. Using the parameters of the spectroscopic binary orbit (P = 1.8321 ± 0.002 yr, T = 1909.754) given by van den Bos (1927), we obtain the phase of 0.4 for Dec. 4, 1970. The predicted velocity change from Dec. 4, 1970 to March 4, 1971 using a diagram of v_r(phase) given by van den Bos is - 3 km/sec, whereas that observed is - 4.9 km/sec. This agreement is quite reasonable. Several poor scans were made on April 18, 1970, which indicated a v_o correction of +11.5 km/sec. The change from April to Dec. in radial velocity of + 11.5 km/sec is in good agreement with the predicted change of 12 km/sec read off van den Bos' (1929) velocity curve. The parameters of the orbit given by him based on data from 1897 to 1924 have not changed over a 50 year interval. Note that aside from the shift due to a change in radial velocity, the December and March profiles agree very well. The residual intensity at the center of the Ca I line is exactly the same, while in the March profile of λ6708 Å it is 2% larger than in the Dec. one.

β Com: There is perhaps some indication of a v_o shift of -1.0 km/sec. We quote $\lambda_{1/2}$ as determined with and without this shift.

δ Tri: This star is a double-lined spectroscopic binary (period = 9.929 days) whose orbit is given by Pearce (1924). Unfortunately

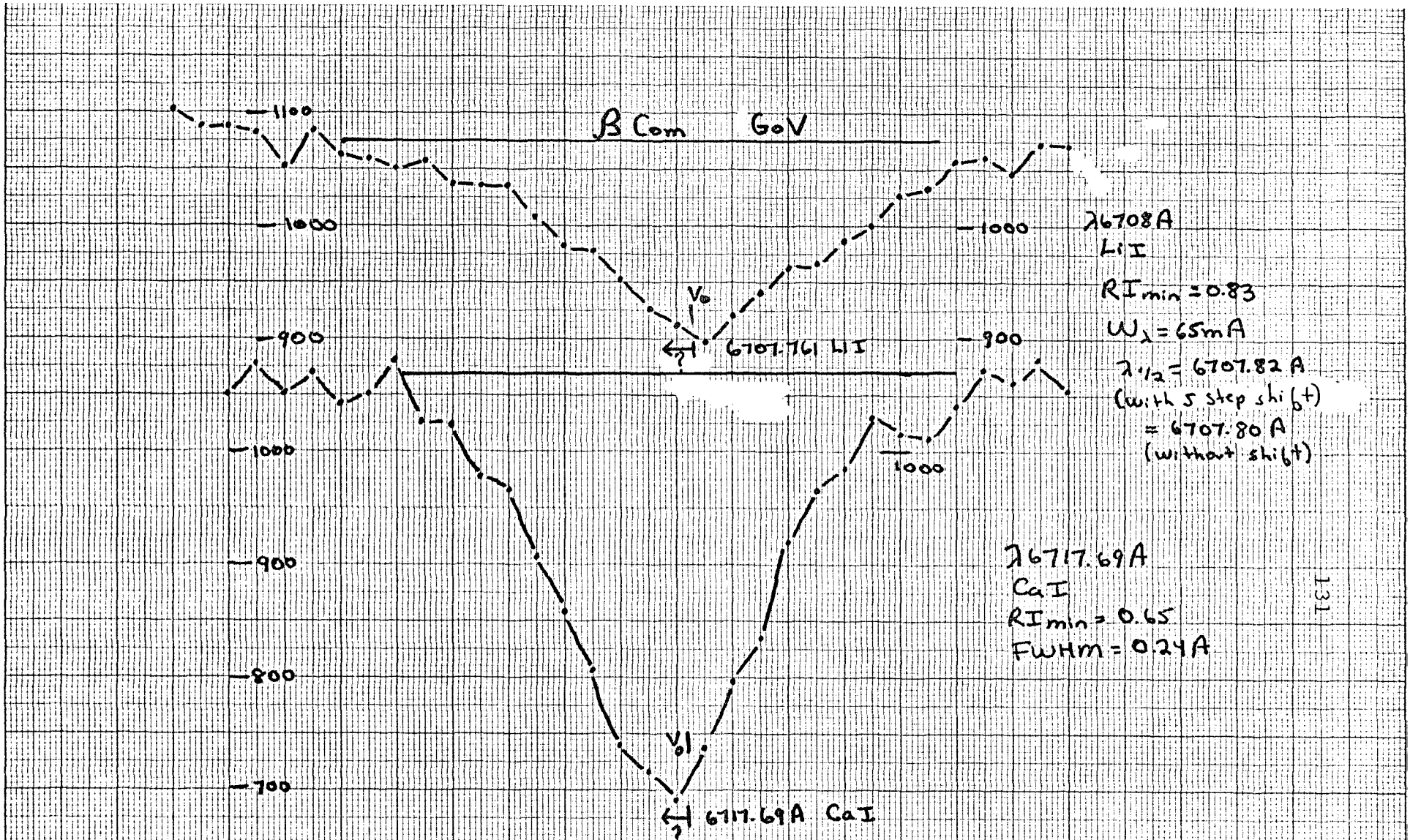

Figure 26h: The profiles of the resonance line of LiI and λ6717.69A of Ca I in β Com (GoV) observed with the Fabry-Perot interferometer. Etalon C was used.

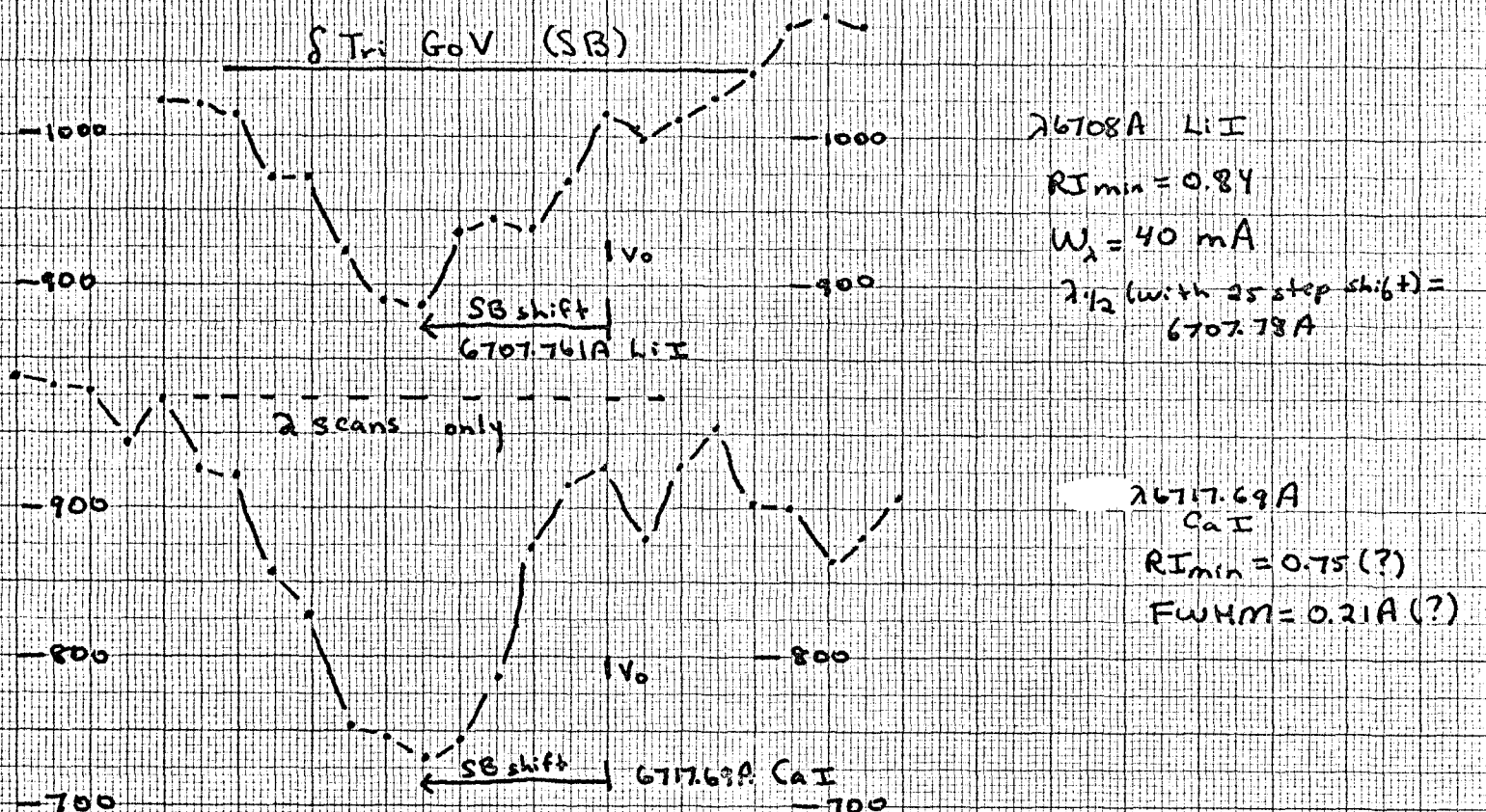

Figure 26i: The profiles of the resonance line of LiI and λ6717.69A of CaI in the spectroscopic binary δ Tri (GoV) with the FP. Etalon C was used. The profiles shown are averages for the night of Dec. 6-7, 1970. The CaI profile is a mean of only 2 scans.

when the star was observed in Sept. of 1970, the observed Ca I line profile indicated that the two components were not well separated. Hence the only scans that are useful are those made in Dec. of 1970. Furthermore the star is rather faint, hence n_s for Li I is only 3, and only 2 scans were made of the Ca I line in Dec. of 1970, so that the traces are rather noisy. The phase calculated using the period given by Pearce (1924) ($P = 9.92912 \pm 0.00009$ days) appears to give corrections to v_o which do not agree with those observed, as shown in table 24, where v_o is taken with the radial velocity of the center of mass of the system.

TABLE 24

v_r for δ Tri

	correction to v_o (km/sec)	
Date	observed	predicted
Sept. 13-14, 1970	+8.6	- 9 km sec
Dec 6-7, 1970	-7.2	+ 6 km/sec

If we assume that the period is wrong so that the phase at midnight Sept. 13-14 1970 is 0.6 instead of 0.9, then the predicted corrections to v_o come out very close to those observed. This corresponds to a loss of 3 days over 17,561 days (48 years), which seems reasonable, considering the short period. Since Herbig (1964) was the first to observe the lines of the secondary, there is no velocity curve for it, and we cannot predict the velocity difference between the primary and secondary on Dec. 6-7, 1970.

ι Per: There is marginal evidence for a +5 step (+1.4 km/sec) shift in v_o. The value of $\lambda_{1/2}$ was determined with and without that shift.

κ Cet: This faint star with a very weak Li I line has only 6 scans of its profile. A velocity shift of +3 steps (+0.8 km/sec) is possible, and we determine $\lambda_{1/2}$ with and without this shift.

ξ Boo A: This star is a well separated double (Δm= 1.9, separation = 7.1"). There is a -8 step (- 2.3 km/sec) shift in v_o as determined from the Ca I line.

η Psc: There are only 2 scans of λ6708 Å in this star, and none of the Ca I line λ6717 Å. We therefore include the observations of the D line cores to demonstrate that the tabulated v_r is accurate. Note the first appearance of λ6707.45 Å, the unidentified solar line, which will become even stronger in later type stars. (The scale of the D line profiles is 0.041 Å per point.)

ψ UMj: There appears to be a four step error (+1.0 km/sec) in v_r. Note how strong λ6707.45 Å has become; this makes determination of the short wavelength side of the profile of λ6708 Å very difficult and hence $\lambda_{1/2}$ is somewhat uncertain. Because the Ca I line at λ6717 Å is so strong, its FWHM will not help in determining the rotational velocity. We therefore include a profile of λ6710.32 Å of Fe I which was taken with etalon B.

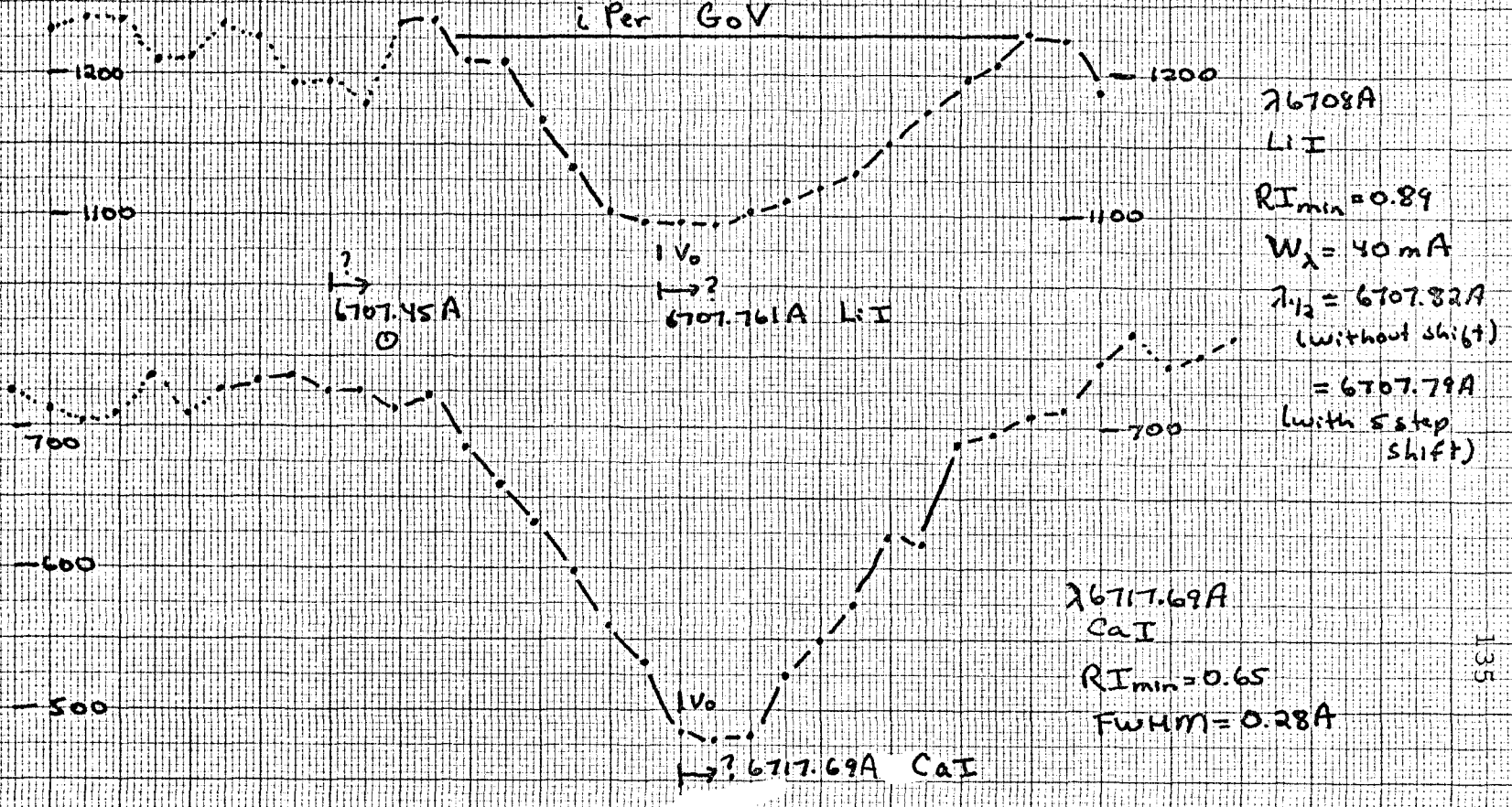

Figure 26j: The profiles of the resonance line of LiI and λ6717.69A of CaI in i Per (GoV) observed with the Fabry-Perot. Etalon C was used, and the points are 0.032A apart. There may be a 5 step error in the tabulated v_r. Points connected by dots are less accurate than points connected by lines.

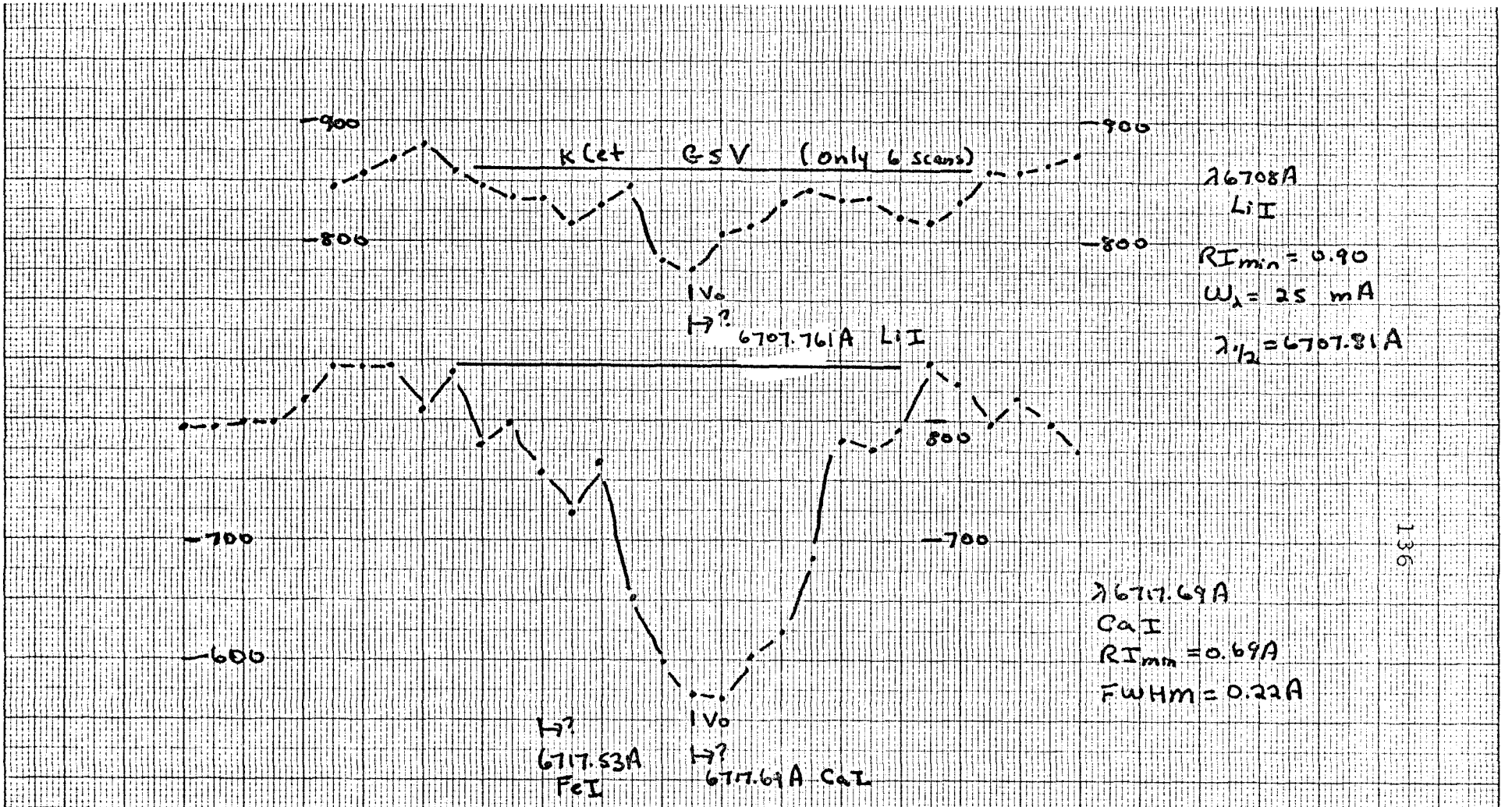

Figure 26k: The profiles of the resonance line of LiI and λ6717.69A of Ca I in K Cet (G5V) observed with the FP. The Li and Ca profiles are an average of only 6 scans and hence are somewhat noisy. Etalon C was used. Points are 0.032A apart.

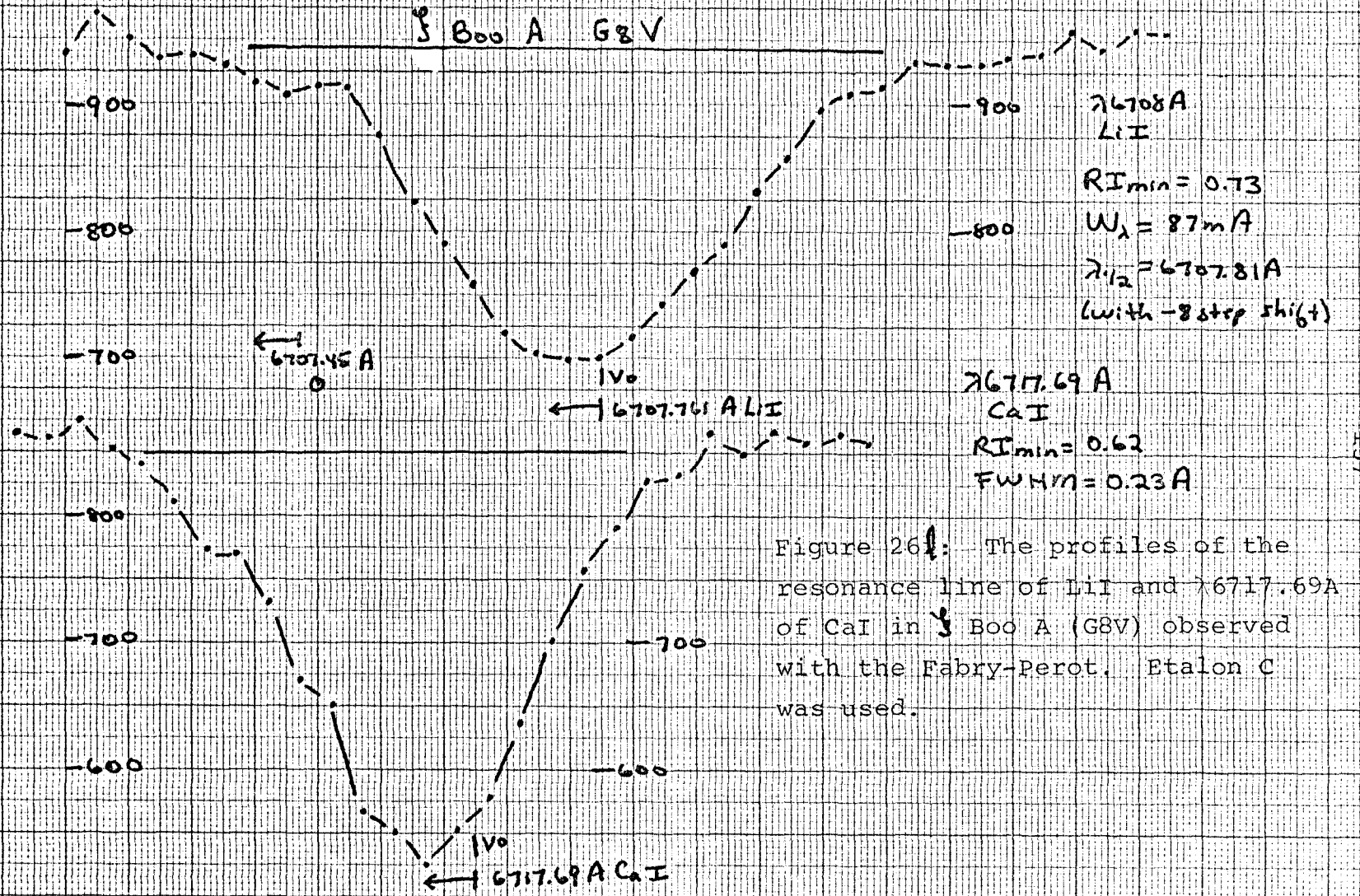

Figure 26: The profiles of the resonance line of LiI and λ6717.69A of CaI in ζ Boo A (G8V) observed with the Fabry-Perot, Etalon C was used.

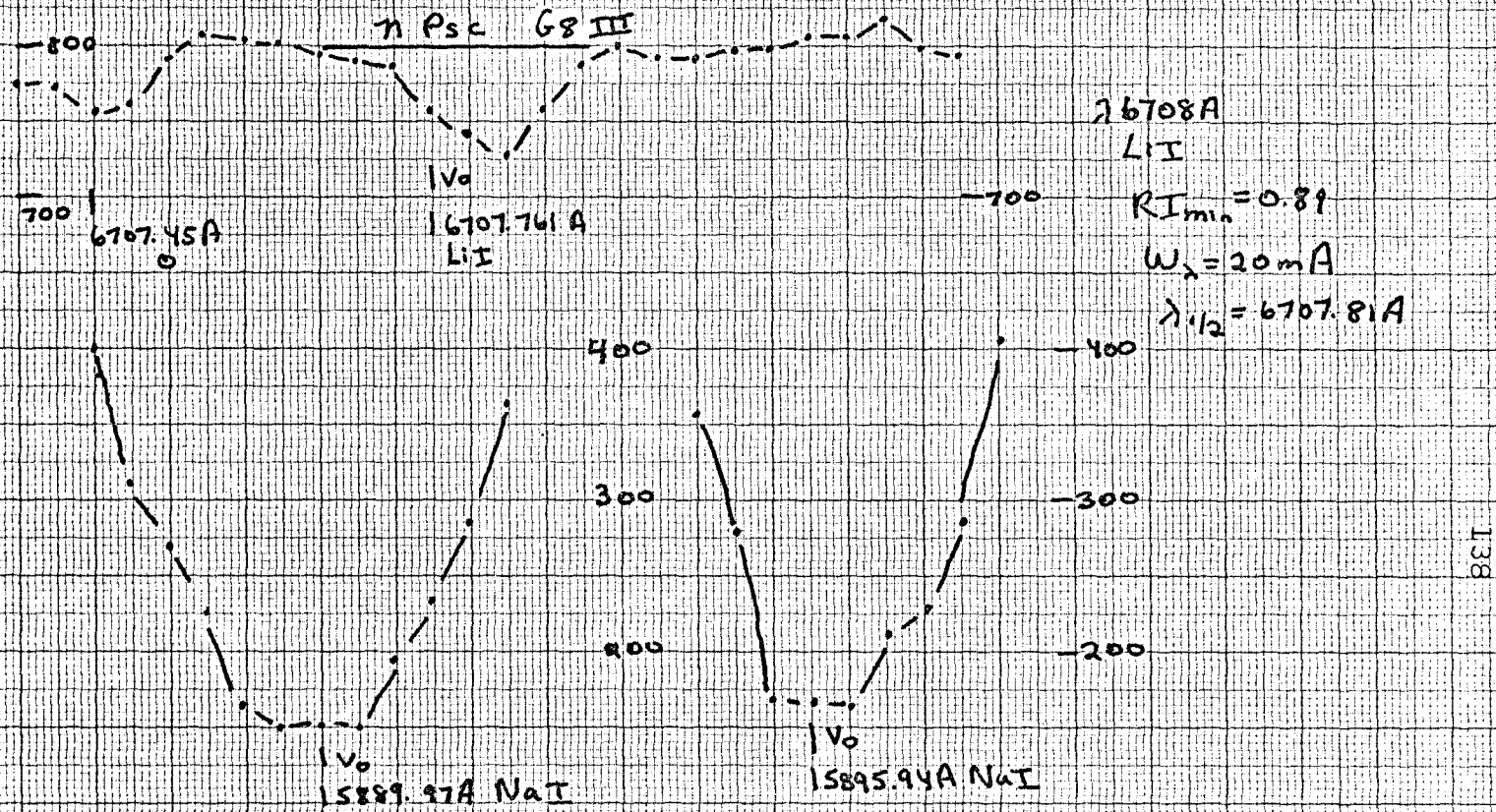

Figure 26m: The profiles of the resonance line of LiI and the cores of the D lines of NaI observed in η Psc (G8III) with the FP. Etalon B was used for the lithium line (which is a mean of only 2 scans) and etalon D for the D lines. Thus points in the lithium profile are 0.032A apart and those in the D line profile are 0.041A apart.

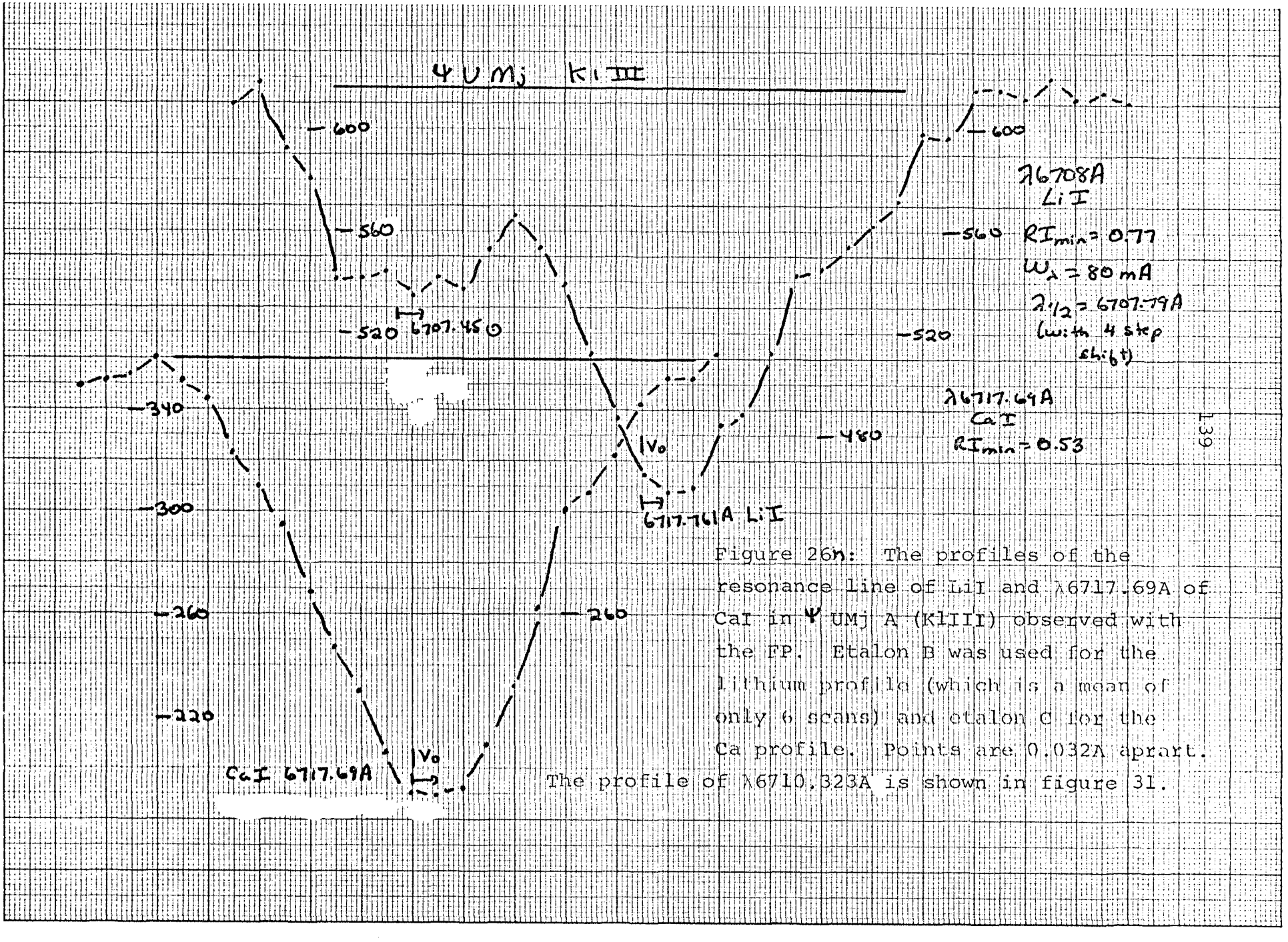

Figure 26h: The profiles of the resonance line of LiI and λ6717.69A of CaI in ψ UMj A (KIII) observed with the FP. Etalon B was used for the lithium profile (which is a mean of only 6 scans) and etalon C for the Ca profile. Points are 0.032A aprart. The profile of λ6710.323A is shown in figure 31.

η Cet: This star shows no evidence for a velocity error. Note the strength of λ6707.45 Å, so that $\lambda_{1/2}$ is poorly determined. For reasons similar to those discussed above, we include a profile of λ6710.32 Å of Fe I observed Nov. 25, 1969 with etalon B.

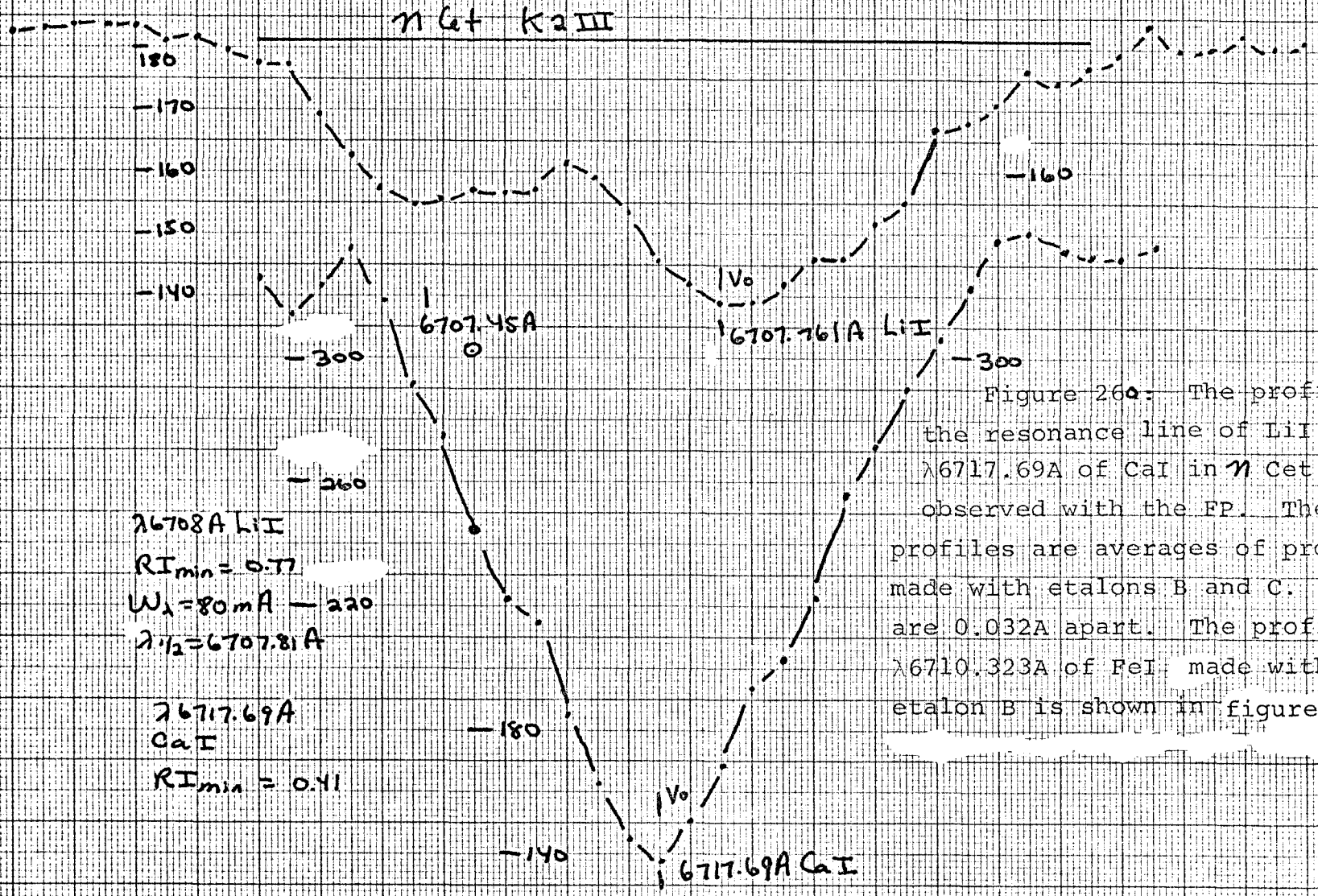

Figure 26a: The profile of the resonance line of LiI and λ6717.69A of CaI in η Cet(K2III) observed with the FP. These profiles are averages of profiles made with etalons B and C. Points are 0.032A apart. The profile of λ6710.323A of FeI made with etalon B is shown in figure 31m.

CHAPTER VII

DISCUSSION OF THE STELLAR PROFILES

A. Comparison of Interferometric and Photographic Profiles

We have described in chapter VI the lithium line profiles that were measured with Fabry-Perot interferometer. Although profiles cannot be derived photographically, measurements of the equivalent width of a line, which is a parameter of the integrated profile, determined with these two techniques can be compared.

Table 25 presents the equivalent width and maximum depth of the line as measured from the photographic and interferometric profiles. The interferometer measurements have been corrected for off-bond leakage by the factors of 10% of the continuum for Li I lines and 14% of the continuum for λ6717 Å of Ca I, as discussed in chapter V. It is probable that the equivalent width measurements on the 6.7 A/mm spectra are systematically too large as compared with the 4.1 A/mm spectra (which are the Lick plates borrowed from Dr. Herbig).

The agreement in equivalent width is very good. Only in two cases of 13 does W_λ as measured with the interferometer differ from W_λ from the photographic spectra by more than 15% of W_λ. It is interesting to note that photographic determinations of W_λ for the same line on different spectra show a variation of 10 to 20% (Wright, Lee, Jacobson and Greenstein 1964). The central depths of the lines do not agree as well. There are 6 cases out of 13 where the photographic and interferometric values differ by 4% or more,

TABLE 25

Comparison of W_λ and Central Depth

		Photography		F.P. Interferometry	
Li I λ6708 Å		W_λ (mÅ)	maximum depth (%)	W_λ (mÅ)	maximum depth (%)
6.7 Å/mm spectra					
10 Tau	Ce 20409	67	16	59	14
χ' Ori	Ce 20262	125	25	114	24
ξ Boo A	Ce 20264	5	29	97	30
	Ce 20260	141	33		
4.1 Å/mm spectra					
10 Tau		52	13	59	14
δ Tri		36	13	44	18
ι Per		45	16-22	44	12
β Com		65	15	71	19
γ Lep A		58	~ 20	73	16
χ Her		59	18	55	18
Ca I λ6717					
6.7 Å/mm spectra					
χ' Ori	Ce 20262	143	33	134	33
4.1 Å/mm spectra					
β Com		160	36	180	41
ι Per		180	49	186	41
χ Her		103	33	87	35

and in 5 cases out of 13 the error is more than 15% of the measured central depth. This is not surprising, as the central depth is a parameter of the profile, not of the integrated profile. Furthermore the instrumental profile of the interferometer is perhaps narrower than that of the photographic spectra. This will affect the central depths but not the integrated equivalent widths.

The agreement of the equivalent widths as measured photographically and with the FP interferometer is encouraging. Photographic spectrophotometry can yield accurate measurements of the integrated line profile. However, as expected, photographic spectra cannot define accurately the central depth or the line profile of a weak feature.

B. Interpretation of the D Line Profiles

The profiles of the D lines of Na I were observed with the Fabry-Perot using etalon D (see table 18), which has a resolution of at least 0.05 Å. The profiles thus obtained are illustrated in appendix A.

The D lines are the resonance doublet in the spectrum of Na I, and the excitation potential of the upper level is 2.10 ev. The ionization potentials of sodium are 5.12 and 47.1 ev, so that the ionization fractions of sodium and lithium should be almost identical in stars cool enough such that there is a negligible amount of Na III. The ratio of the gf values for the two components of the D lines is 2:1, with λ5889.95 Å the stronger. Thus D_1 and D_2 are precisely

analogous to the two components of the Li^7 line, λ6707.76 Å and λ6707.92 Å. If we can satisfactorily fit a theoretical profile generated from a model to the observed D line profiles, this will give us evidence that our theoretical profiles are correct.

Theoretical profiles of the D lines were calculated using the same grid of model atmospheres and line profile program previously described. The theoretical profiles depend strongly on the damping constant; we have evaluated Γ as a function of optical depth as described in chapter II. We assume a sodium abundance of log (N_{Na}/N_H) = - 5.78. The microturbulent velocity is irrelevant as the lines are so broad.

We assume that the lines are formed under the mechanism of pure absorption. This approximation fails in the highest layers, where the core of the line is formed. The minimum possible residual intensity with our assumptions is

$$\frac{B_\nu(\tau_c=0)}{B_\nu(\tau_c=0)} = \frac{T(\tau_c=0)^4}{T(\tau_c=1)^4}$$

where τ_c is the optical depth defined by the continuous absorption coefficient. This is approximately 33%, whereas our observed D lines have central residual intensities of 10% or less. We therefore cannot fit the cores until they are formed sufficiently deep that our assumption of pure absorption prevails. We have adopted the criterion of RI > 40% (corresponding to $\tau_{5000} \approx 0.01$) as the region we will try to fit. A more complete discussion of the source function of the D lines was given in chapter II.

Let us assume that the line absorption coefficient is given by $\alpha = \alpha_o H(\Delta\lambda, a)$. Then

$$0.5\,\alpha_{D_1}(\Delta\lambda) = \alpha_{D_2}(\Delta\lambda)$$

Since we have neglected scattering,

$$\frac{I_\nu(5889)}{I_\nu(5895)} \approx \frac{B_\nu[\,0.5(\tau_{5895}=1)]}{B_\nu[\,\tau_{5895}=1]}$$

Therefore, given the observed intensity of one of the D lines at a fixed $\Delta\lambda$ from the line center, we can predict from a model atmosphere the intensity of the second component and compare it with the observed value. We shall call this comparison the $D_2(D_1)$ test. This is a test of the accuracy of $T(\tau)$ in our model atmosphere.

Because the D lines are so broad, the calculated residual intensity varies very slowly over the width of the instrumental profile (FWHM less than 0.05 Å). Convolution with the instrumental profile changes the residual intensity at any wavelength in the line by less than one per cent. Furthermore, there is no need for an off-band leakage correction. However, the rotational broadening profile may be considerably wider than the instrumental one, and may change the predicted residual intensity by 2-3% in the region where $RI(\Delta\lambda)$ varies rapidly.

Since the damping width is only 1 mÅ and the Doppler width perhaps 0.05 Å, the absorption coefficient in the region beyond 0.1 Å from the line center can be approximated by

$$\alpha(\Delta\lambda) = A/\Delta\lambda^2$$

where A is a constant. This is the asymptotic form of a Lorentz profile for large $\Delta\lambda$. The constant is linear in $N(Na)gf$. Hence for any other value of the constant, A',

$$\alpha'(\Delta\lambda) = A'/\Delta\lambda^2$$

and $\alpha' = \alpha$ at

$$\Delta\lambda' = \sqrt{\frac{A'}{A}}\ \Delta\lambda$$

Therefore, we can express the profile, beyond the core, of any D line for any reasonable sodium abundance as a fixed profile $f(\Delta\lambda_o)$ which is transformed along the $\Delta\lambda$ axis by a line transformation

$$\Delta\lambda = \frac{\Delta\lambda_o}{\sqrt{N(Na)gf}}$$

Thus the two D lines have profiles of the same shape, but the stronger one has a $\Delta\lambda$ axis which is stretched out with respect to the weaker one. We assume that rotational broadening affects the two profiles similarly. This is not a good assumption, but the effect of rotational broadening is small. Hence we may compare the observed profiles of D_1 and D_2 at the same $\Delta\lambda$ with the theoretical ones in the manner described above, even though we must compare them with theoretical profiles at $\Delta\lambda'$, such that $RI^{D_1}_{calc}(\Delta\lambda') = RI^{D_1}_{obs}(\Delta\lambda)$, as the calculated profiles are not as broad as the observed ones. Any problem we may have in the width of our profiles is merely a problem with the scale of $\Delta\lambda$ and is not relevant to the D_2 (D_1) test described

TABLE 26

The $D_2(D_1)$ Test for ξ Peg and ι Per

ξ Peg (F7V)

Observed Profile			Predictions of Profiles from (6000,4,0.01) Model			
Δλ(Å)	RI(5889)	RI(5895)	Δλ(Å)	RI(5889)	Implies	RI(5895)
0.09	0.27	0.37	0.24	0.69		0.80
0.17	0.52	0.49	0.33	0.80		0.89
0.25	0.69	0.79	0.45	0.87		0.93
0.34	0.80	0.90	0.59	0.93		0.97
0.42	0.88	0.95				
0.51	0.93	0.97				
0.59	0.96					

ι Per (G0V)

Observed Profile			Predictions of Profiles from (6000,4,0.01) Model			
Δλ(Å)	RI(5889)	RI(5895)	Δλ(Å)	RI(5889)	Implies	RI(5895)
0.09	0.19	0.21	0.18	0.63		0.72
0.17	0.41	0.47	0.26	0.72		0.83
0.25	0.63	0.69	0.31	0.78		0.87
0.34	0.72	0.83	0.34	0.82		0.90
0.42	0.78	0.87	0.42	0.86		0.93
0.51	0.82	0.89				
0.59	0.86	0.92				

above.

From table 26 we see that the $D_2(D_1)$ test gives excellent results outside the core, but that $RI^{D_1}_{obs}(\Delta\lambda)$ is less than $RI^{D_1}_{calc}(\Delta\lambda)$. There are six stars with observed D_1 and D_2 profiles, and the test has been carried out for all of them. The agreement is very satisfactory, with the poorest results encountered for η Psc (G8III) and η Cet (K2III). These two stars are problematical partially because the models are poor there, and also because the profiles are so broad in these cool stars that they span more than one free range and we did not observe far enough from the line center to be sure of the position of the continuum, since there are many atmospheric lines in this region. However, even in these two cases the agreement is reasonable.

We can also try to compare the plot of observed residual intensity as a function of log $(\Delta\lambda)$ for one of the D lines with a computed plot. We call this the D_1(obs)-D_1(calc) test. As we have previously argued, these plots should agree except for a constant in the log $(\Delta\lambda)$ scale. The agreement is not too good, even excluding the core. For the case of ι Per, much better agreement is found when a theoretical profile is convoluted with a rotational broadening profile with v_r of about 5 km/sec, and the D_1(obs)-D_1(calc) test is then performed. The importance of convoluting with $P_{rotation}$ is not surprising.

We have remarked that the calculated profiles are too narrow, and yet by obtaining good results with the D_1(obs)-D_1(calc) test we know that the theoretical profiles have the correct shape. Our

adopted transition probabilities for the D lines are those of Corliss and Bozman (1962). The gf values given by Kohl (1964) are a factor of 1.4 larger. This is about the right size to increase the width of the profiles (without changing their shapes) to the observed values.

This agreement encourages our belief that the T-τ relation of our models compares favorably with that of the stars and that for residual intensities greater than 40%, the assumptions which go into our line formation program are at least approximately valid.

We can use the D lines in another way to determine the accuracy of the interferometer profiles. There are several fairly strong atmospheric lines near 5890 Å, unlike near 6708 Å. We can predict the positions of these lines in different stars relative to the line center by using the radial velocity of the stars. The apparent wavelength of atmospheric lines are of course not affected by the radial velocity of the star. We therefore can test the accuracy of our transfer of wavelength scale from the sodium calibration lamp to the star by looking for these atmospheric features. The stronger of the expected lines appear in the proper places in several of the D line profiles as illustrated in figure 27, which presents the observed D_1' and D_2 profiles of 10 Tau. The position of the wavelength of the sodium line center is derived from the sodium lamp calibration, v_r of the star, and the solar correction to the stellar radial velocity. The positions corresponding to the wavelengths of the atmospheric features were derived from the lamp calibration only. The coincidence of the expected positions of these weak, sharp atmospheric features and their observed positions are good. This agreement

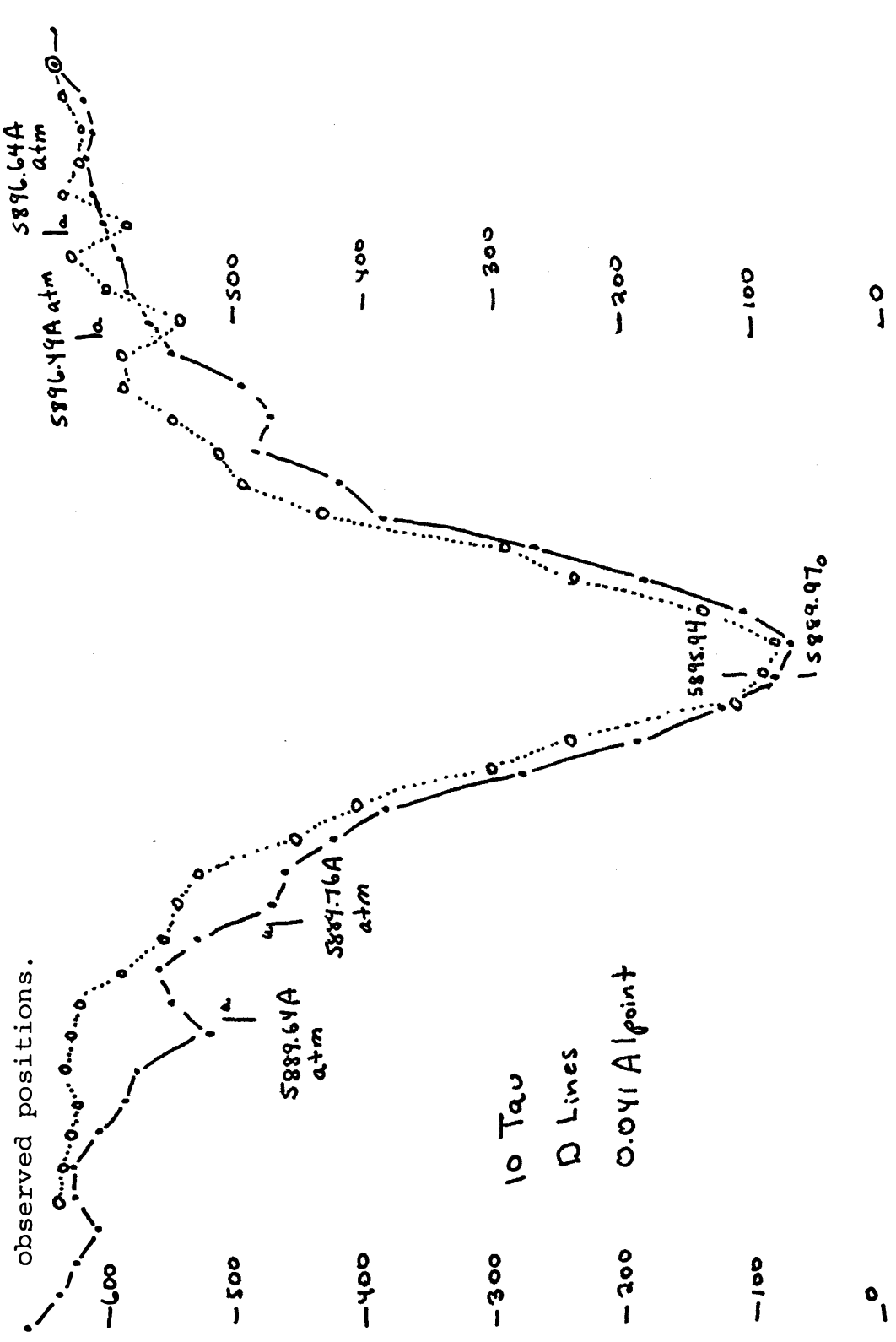

Figure 27: The profiles of the D lines of Na I in 10 Tau. These profiles, made with etalon D, have points 0.041A apart. Note the good coincidence between the expected positions of the atmospheric lines, indicated by the letter "a", and the observed positions.

holds to a similar degree for the rest of the stars and gives us additional confidence in the accuracy of our wavelength scale.

C. Profile Fitting Using λ6717 Å of Ca I

In order to fit the observed profiles $O(\lambda)$ with theoretical profiles $\psi(\lambda)$ that were described in chapter II, it is necessary to take into account rotational broadening and the transmission of the instrument $(T(\lambda))$. If we denote the broadening function for rotation by $R(\Delta\lambda)$, where $\Delta\lambda$ is measured from the line center, then

$$O(\lambda) = \int_{-\infty}^{\infty} T(\Delta\lambda_2) \int_{-\infty}^{\infty} R(\Delta\lambda_1)\psi(\lambda + \Delta\lambda_1 + \Delta\lambda_2)\, d(\Delta\lambda_1) d(\Delta\lambda_2) \tag{7-1}$$

It is difficult to invert this equation and solve for $\psi(\lambda)$ from the observed profile $O(\lambda)$. Instead we take a computed $\psi(\lambda)$, which is a function of the lithium isotope ratio, lithium abundance, the model atmosphere, etc. and compute $O'(\lambda)$ from equation 7-1. We adjust $\psi(\lambda)$ until a good fit is obtained between the observed $(O(\lambda))$ and calculated $(O'(\lambda))$ profiles.

As a first attack on this problem, we adopt the approximation that, for a given star, the observed profile of the Ca I line at λ6717 Å $(O_{Ca}(\lambda))$ corrected for leakage as described in chapter V is the instrumental response (i.e. the central peak without the far wings of the instrumental profile) to a single component of the intrinsic stellar lithium line λ6708 Å, where rotation is included in the intrinsic stellar profile. Thus we assume

$$O_{Li}^{Ca}(\lambda) = \int_{-\infty}^{\infty} O_{Ca}(6717.69\text{Å}+\Delta\lambda)\psi(\lambda+\Delta\lambda)\, d\Delta\lambda \qquad (7\text{-}2)$$

The main error here lies in assuming that the Doppler width of a lithium component is the same as for a calcium line. However, the thermal width is small compared to the instrumental width and possibly the rotational width. With this approximation, we avoid having to determine the rotational velocity, and thus we have one less parameter to adjust. This is a great simplification of the problem.

We normalize the observed profile of λ6717 Å corrected for leakage so that $\int_0^{\infty} O_{Ca}(\lambda)\, d\lambda = 1$. Then we pick a model atmosphere whose effective temperature is close to that of the star, as determined from the spectral type (using Allen (1964) to convert spectral type to T_{eff}). We then pick of value of Li^6/Li^7 and a lithium abundance, and compute $\psi(\lambda)$. After convoluting the theoretical profile with the calcium profile using equation 7-2, we adjust $\psi(\lambda)$ if necessary, until a satisfactory fit is obtained. This fit is done with a 10% leakage correction to the computed profile using equation 5-10. This must be done separately for each star.

There are ten stars with profiles of λ6717 Å where λ6707.45 Å is not sufficiently strong to distort the lithium line profile. We have carried out the above procedure for each of these stars, except κ Cet which has a noisy profile for λ6708 Å. The results are shown in figures 28a-e. The wavelength scale of these figures is 0.032 Å/point of the observed profile or 0.064 Å/cm. Note that this fitting of the profile of λ6708 Å is done independently of the wavelengths determined from

the lamp calibration. Since each point in the theoretical profile has a wavelength $\Delta\lambda$ from the line center, and we know where the line center (corresponding to λ = 6707.76 Å) is in the theoretical profile, this fitting determines a second wavelength scale for the observed profile. The best fit for each star therefore gives us an additional determination of any error in the tabulated radial velocity, which was previously determined by the position of the center of the observed stellar Ca I line as compared with the lamp calibration. The position of the wavelength of 6707.761 Å in the theoretical profile is denoted by the subscript "p" in figures 28a-e. Table 27 presents a comparison of the error in tabulated v_r as deduced by these two methods. The agreement between the two determinations is extremely good. Furthermore, the corrections to v_r of table 27 are of both signs, so that there is no systematic trend introduced by our interferometer.

Although there are many parameters to vary, if Li^6/Li^7 = 0.50 we find that the calculated lithium lines ($O_{Li}^{Ca}(\lambda)$) are broader than the observed profiles. In general, very good fits can be obtained with an isotope ratio of 0.01. There are several cases, such as χ' Ori and ξ Peg where perhaps some additional absorption on the long wavelength side is present, but it is not more than 15% of the main line.

We note that the isotope ratios obtained by this process of line fitting using the calcium line profile are independent of the wavelength scale and thus of errors in radial velocity. Hence it is

TABLE 27

Difference Between v_r and the Tabulated Values of v_r

Star	v_r tab.(1)	Remarks	Ca line center Δv steps	Ca line center Δv km/sec	Li line fitting Δv steps	Li line fitting Δv km/sec
γ Lep	-10		+5	+1.4	+4	+1.1
ξ Peg	-5		0	0	+3	+0.8
10 Tau	+28		+5	+1.4	+4	+1.1
χ Her	+55		-10	-2.9	-9	-2.6
χ' Ori	-14		+5	+1.4	+6	+1.7
ξ UMjA	-17	SB Dec 4-6,70	0	0	-2	-0.6
		Mar 5-7,71	-17	-4.9	-21	-6.0
β Com	+6		-4	-1.1	-5	-1.4
δ Tri	-6	SB Sept 13-14,70	+30	+8.6		
		Dec 6, 70	-25	-7.2		
ι Per	+50		+5?	+1.4?	+2	+0.6
κ Cet	+19		+3?	+0.8?		
ξ BooA	+4		-8	-2.3	-12	-3.5
η Psc	+15		0	0		
ψ Umj	-20		+4	+1.1		
η Cet	+12		0	0		

Source

1) Hoffleit (1964)

gratifying that such good fits of the lithium line profile can be made using this simple technique with $Li^6/Li^7 \sim 0.0$.

Figure 28a. Observed profile (solid line) of λ6708 Å in γ Lep and ξ Peg. Theoretical profiles convoluted with the stellar calcium line profiles are indicated by dotted lines. The theoretical profiles are generated from the model (6250, 4.0, 0.1) with $Li^6/Li^7 = 0.01$, and Li^7 abundance of 0.510^{-9} for γ Lep and 0.210^{-9} for ξ Peg. Zero microturbulent velocity is assumed.

Figure 28b. Observed profile (solid line) of λ6708 Å in 10 Tau and χ Her. Theoretical profiles convoluted with the stellar calcium line profile are indicated by dotted lines. The theoretical profiles are calculated from the model (6250, 4.0, 0.1) with $Li^6/Li^7 = 0.01$ and Li^7 abundance of 0.410^{-9} for 10 Tau and 0.510^{-9} for χ Her. For χ Her a profile with $Li^6/Li^7 = 0.5$ and Li^7 abundance of 0.410^{-9} is indicated by the wiggly line.

Figure 28c. Observed profile (solid line) of λ6708 Å in χ' Ori and ξ UMjA. The profile given for ξ UMjA is the average from the March 1971 observing run. Theoretical profiles convoluted with the stellar calcium line profile are indicated by dotted lines. The models used to calculate the theoretical profile are (5500, 4, 1), $Li^6/Li^7 = 0.01$, Li^7 abundance = 0.301^{-9} for ξ UMjA. Zero microturbulent velocity is assumed.

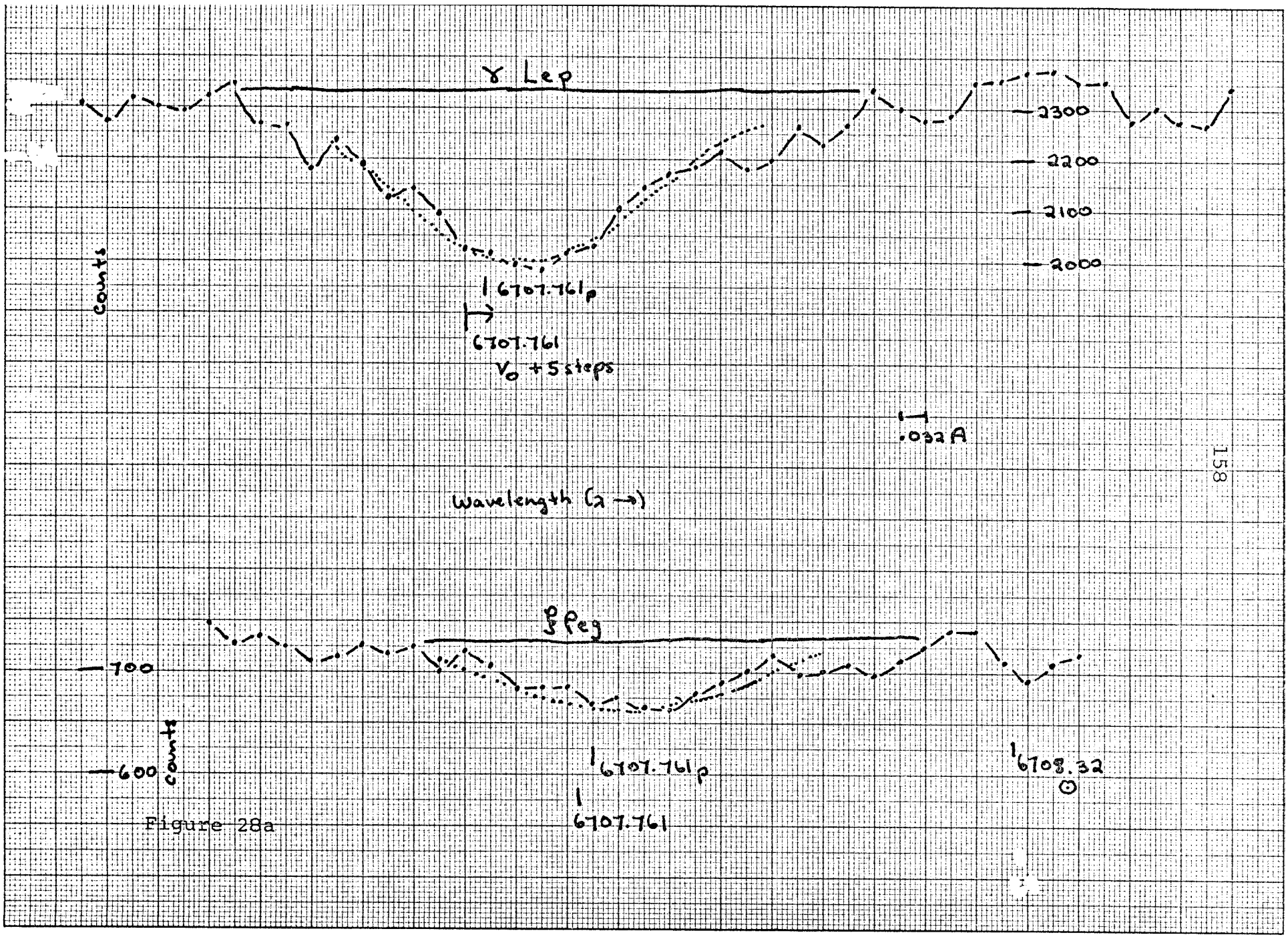
γ Lep
2300
2200
2100
2000
counts
6707.761p
6707.761
V_0 +5 steps
.032 A
Wavelength (λ →)
β Peg
700
600
counts
6707.761p
6707.761
6708.32

Figure 28a

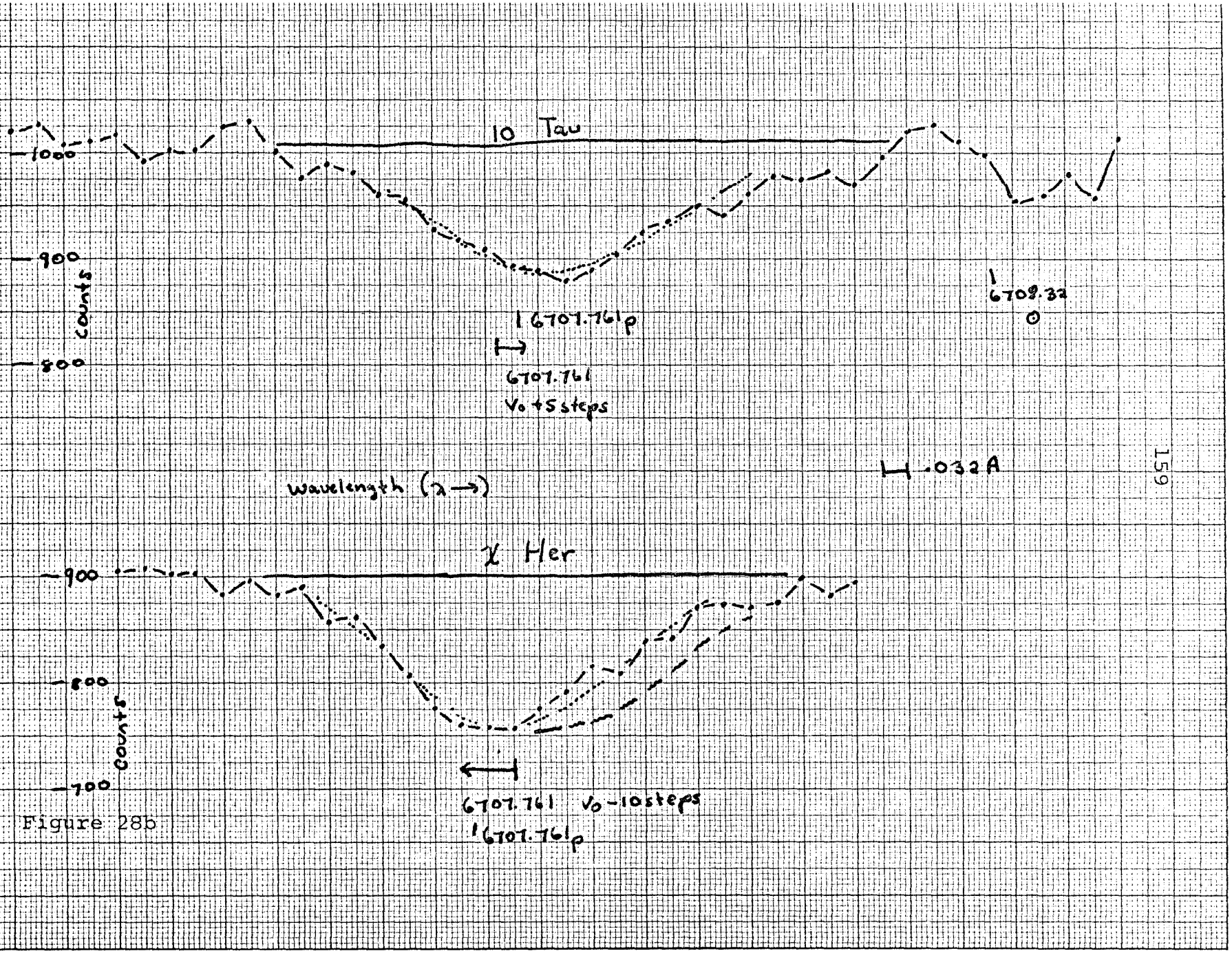
10 Tau
1000
900
800
counts
6709.32
6707.761p
6707.761
V₀ +5 steps
.032 A
Wavelength (λ →)
χ Her
900
800
700
counts
6707.761 V₀ -10 steps
6707.761p

Figure 28b

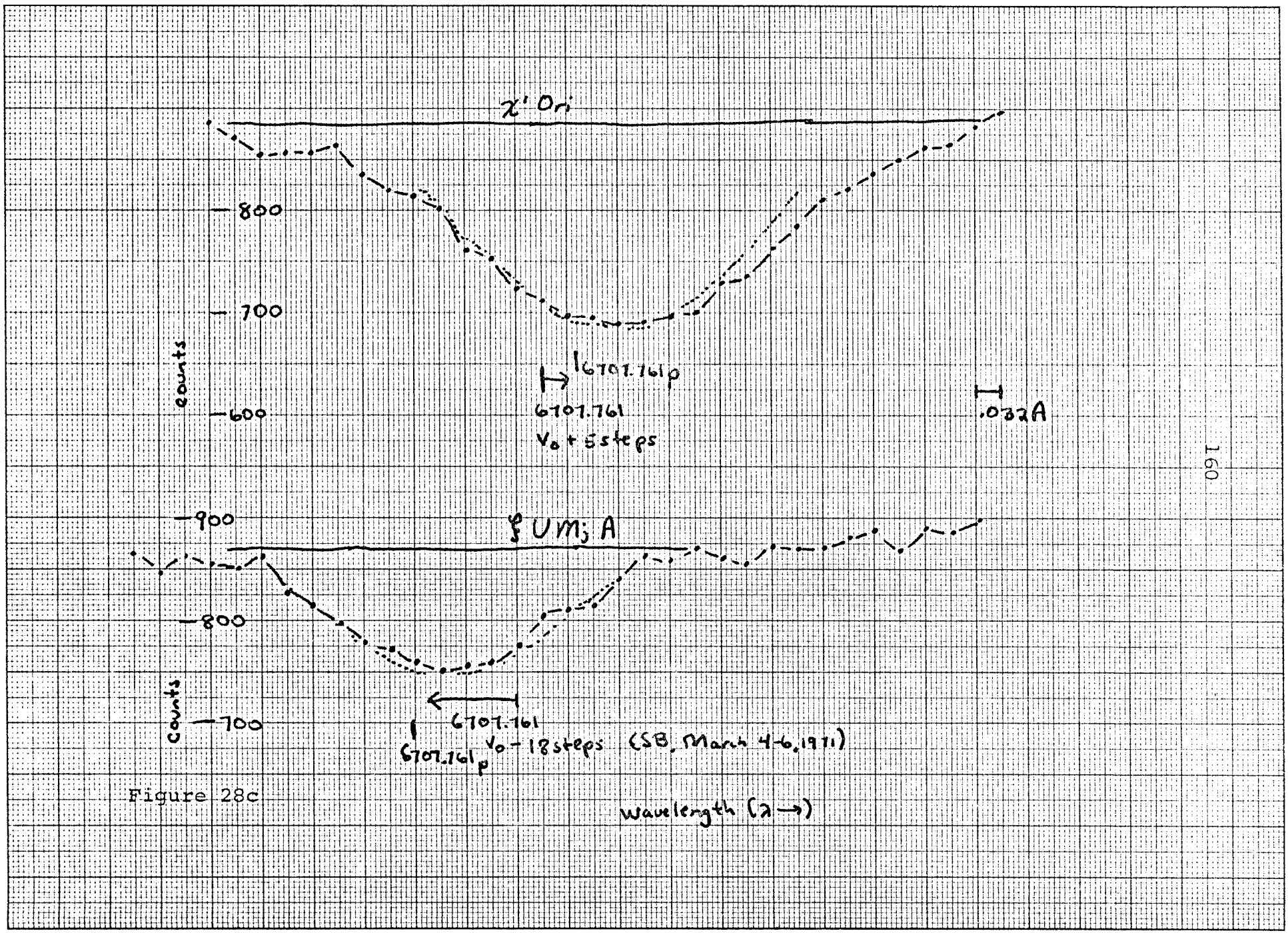
χ' Ori
800
700
600
counts
6707.761ρ
6707.761
V₀ + 5 steps
.032A
900
ζ UMj A
800
700
counts
6707.761
6707.761ρ
V₀ - 18 steps
(SB, March 4-6, 1971)
Wavelength (λ →)

Figure 28c

Figure 28d. Observed profile (solid line) of λ6708 Å in β Com and ¿ Per. Theoretical profiles convoluted with the stellar calcium line profile are indicated by dotted lines. The theoretical profiles are calculated from the model (6250,4.0,0.1) with $Li^6/Li^7 = 0.01$ and Li^7 abundance = 0.510^{-9} for β Com and 0.410^{-9} for ¿ Per. For β Com, we also show a profile of $Li^6/Li^7 = 0.50$ and Li^7 abundance = 0.510^{-9} computed from the same model. The continuum as determined from this profile is somewhat higher than that indicated on the figure.

Figure 28e. Observed profile (solid line) of λ6708 Å in ξ Boo A, The theoretical profile from the model (4500,4.0,1), $Li^6/Li^7 = 0.01$, and Li^7 abundance = 0.0310^{-9} was convoluted with the stellar calcium line and the result is indicated by the dotted line.

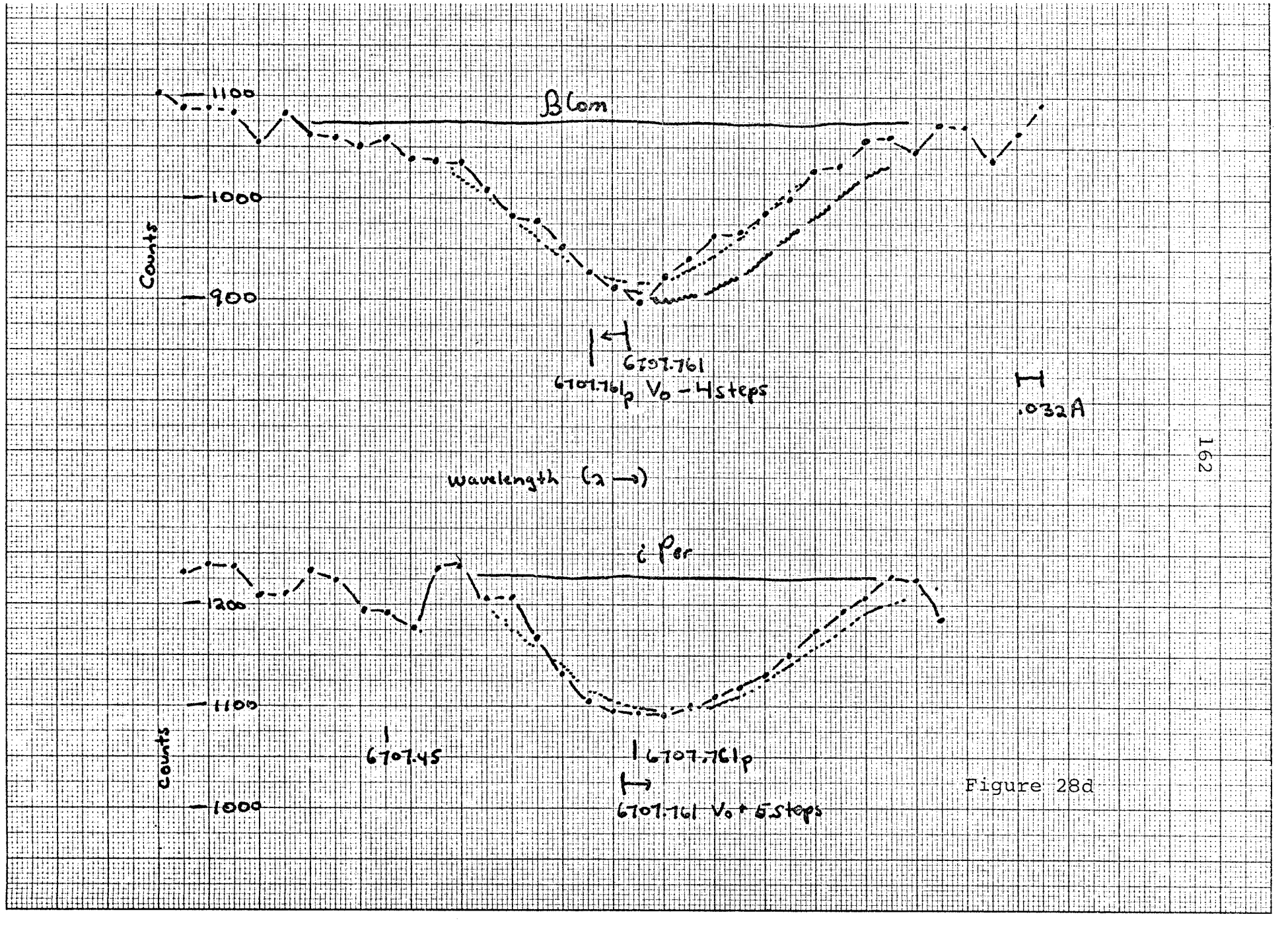
1100
1000
900
Counts
B Com
6707.761
6707.761p V₀ - 4 steps
.032 A
Wavelength (λ →)
i Per
1200
1100
1000
Counts
6707.45
6707.761p
6707.761 V₀ + 5 steps

Figure 28d

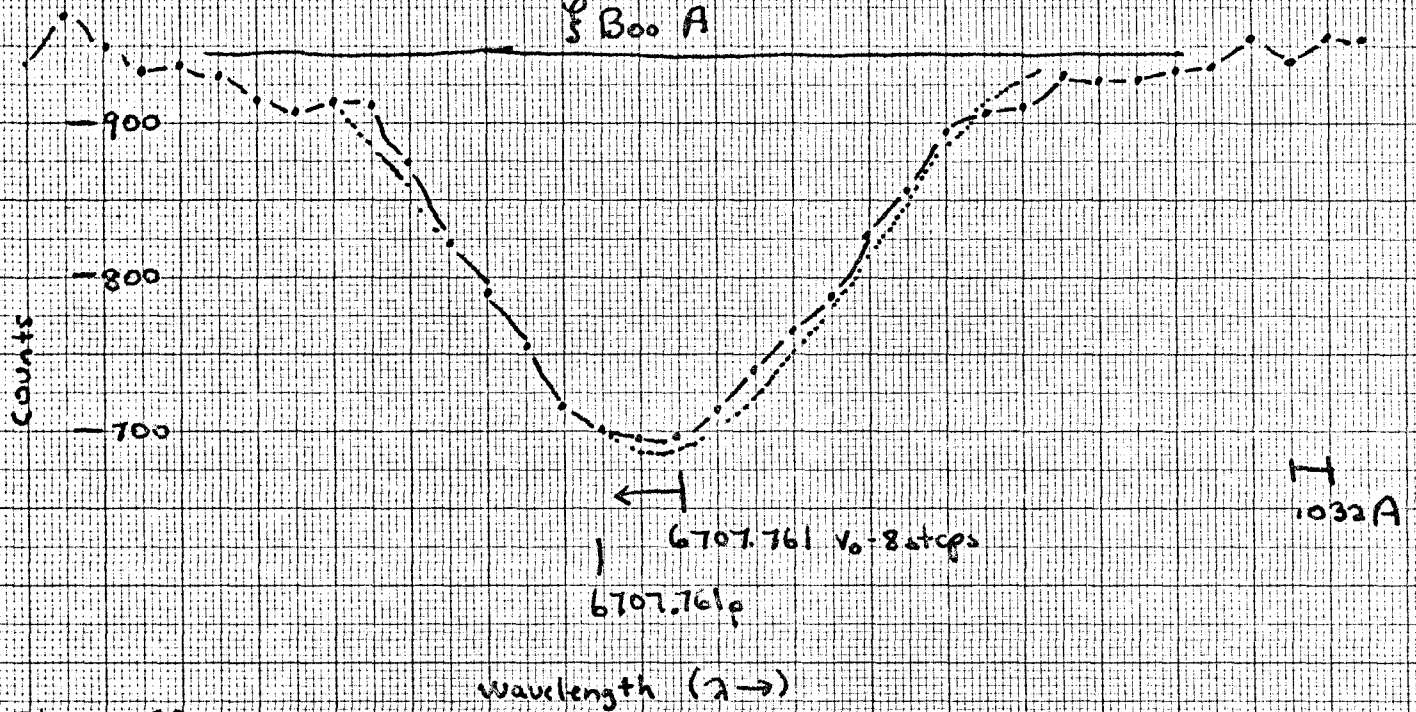
ζ Boo A
900
800
700
Counts
6707.761 V_0 -8 stqs
6707.761 ρ
.1032 A
Wavelength (λ →)

Figure 28e

D. Profile Fitting of λ6717 Å and λ6708 Å

We now try to fit the observed profiles using equation 7-1, without resorting to the simplification involving the Ca I profiles as introduced in equation 7-2. With such a procedure involving two convolutions, there are many free parameters which can be adjusted to improve the fit of the calculated and observed profiles. For example, in matching an observed profile for λ6717 Å, we must choose a model atmosphere. We can then vary the rotational velocity of the star (v_{rot}), the microturbulent velocity (v_t), the calcium abundance, the damping constant, and the correction for leakage in the observations. In calculating theoretical profiles for λ6717 Å of Ca I, we have computed the damping constant for van der Waals broadening as a function of optical depth, and have used equation 2-5 to obtain the total damping constant, rather than use ten times the classical value. Therefore, the damping constant may be varied only by about a factor of 4. Since the Ca I line is too weak to be on the damping part of the curve of growth, such a variation in Γ does not noticably affect the theoretical profile. Furthermore, the leakage (which was calculated in chapter V as 10-13%, depending on the width of the line) has an uncertainty of (+5%, - 4%), and is therefore a relatively well determined parameter. Thus the parameters we can vary in trying to fit an observed profile are the abundance (i.e. Ngf), v_{rot}, and v_t.

Since we have observed only two lines per star, it does not seem necessary to construct a complete grid of profiles with all possible values of the above parameters. Instead, with an educated guess at the parameters, followed by slight adjustments from the

initial choices, if necessary, we can produce a reasonable fit. This means that there will be some uncertainty in the final value of the parameters which control the profile, as for instance, $v_{rot} = a$, $v_t = 0$ may produce approximately the same profile as $v_{rot} = a - b'$, $v_t = b$. With certain reasonable restrictions on the calcium abundance, we will be able to obtain unique values of v_{rot} and v_t.

Let us first try to fit the profile of $\lambda 6717$ Å of Ca I observed in the lunar spectrum. We adopt the known solar rotational velocity (2 km/sec) and microturbulent velocity (1.4 km/sec). We take the solar calcium abundance $N^{\odot}_{Ca}$ as $\log \left[N(Ca)/N_H\right] = -5.78$ and adopt $\log (gf) = -0.78$ (Corliss and Bozman 1962) for the line under consideration, so that

$$\log(Ngf) = -6.56 \qquad (7\text{-}3)$$

The instrumental profile of the etalons is taken from observations of the Ne I line. We compute the rotational profile from the equation of Huang and Struve (1953):

$$p_{rot}(x) = \frac{1}{2}\left[\frac{2}{\pi}(1-x^2)^{1/2} + \frac{3}{4}(1-x^2)\right] \qquad |x| \leq 1.0$$

x is the wavelength from the line center measured in units of the rotational width $\Delta\lambda_r$, where

$$\Delta\lambda_r = \frac{v_{rot}\lambda_o}{c}$$

We have adopted the value of 1.5 for the limb-darkening coefficient. Note that the FWHM of a rotational-broadening profile is closer to

$1.5\,\Delta\lambda_r$ than to $\Delta\lambda_r$ and that $p_{rot}(x)$ is much broader than a Gaussian. We use a (5500,4,1) model for the sun.

The transition probability given by Corliss and Bozman (1962) for this line seems to be too small, as we cannot achieve a reasonable fit without taking the calcium abundance as $4\,N^{\odot}_{Ca}$. For the increased calcium abundance, with the above choices for v_{rot} and v_t, a reasonable fit may be obtained to the observed profile, as shown in figure 29.

We recall that there are many weak features of CN in this region and also λ6717.53 Å of Fe I, which shows up as an asymmetry of the observed profile such that the long wavelength wing fits the calculated profile, while there is an additional feature in the short wavelength wing. The strength of this extra feature agrees well with the equivalent width of 13 mÅ given by Moore, Minnaert and Houtgast (1966) for λ6717.53 Å of Fe I, and it appears at the correct wavelength. Therefore we feel justified in ascribing it to the line of Fe I. If we try to increase v_{rot} to 5 km/sec, the computed profiles for λ6717.69 Å become wider and shallower than the observed profiles, and even a gross change in the choice of the calcium abundance will not produce a reasonable fit.

To summarize our results for the moon, we can satisfactorily fit the observed profile of λ6717.69 Å of Ca I with the usual rotational and turbulent velocity if we increase the calcium abundance (i.e. increase the transition probability) and if we recall that there is an iron line at 6717.53 Å.

Figure 29: The profile of λ6717A of CaI observed in the lunar spectrum with etalon C. This profile is fit by a calculated profile (the dotted line) with v_t=1.4 km/sec and v_{rot}= 2 km/sec using a (5500,4,1) model and a calcium abundance 4 times that given by equation 7-3.

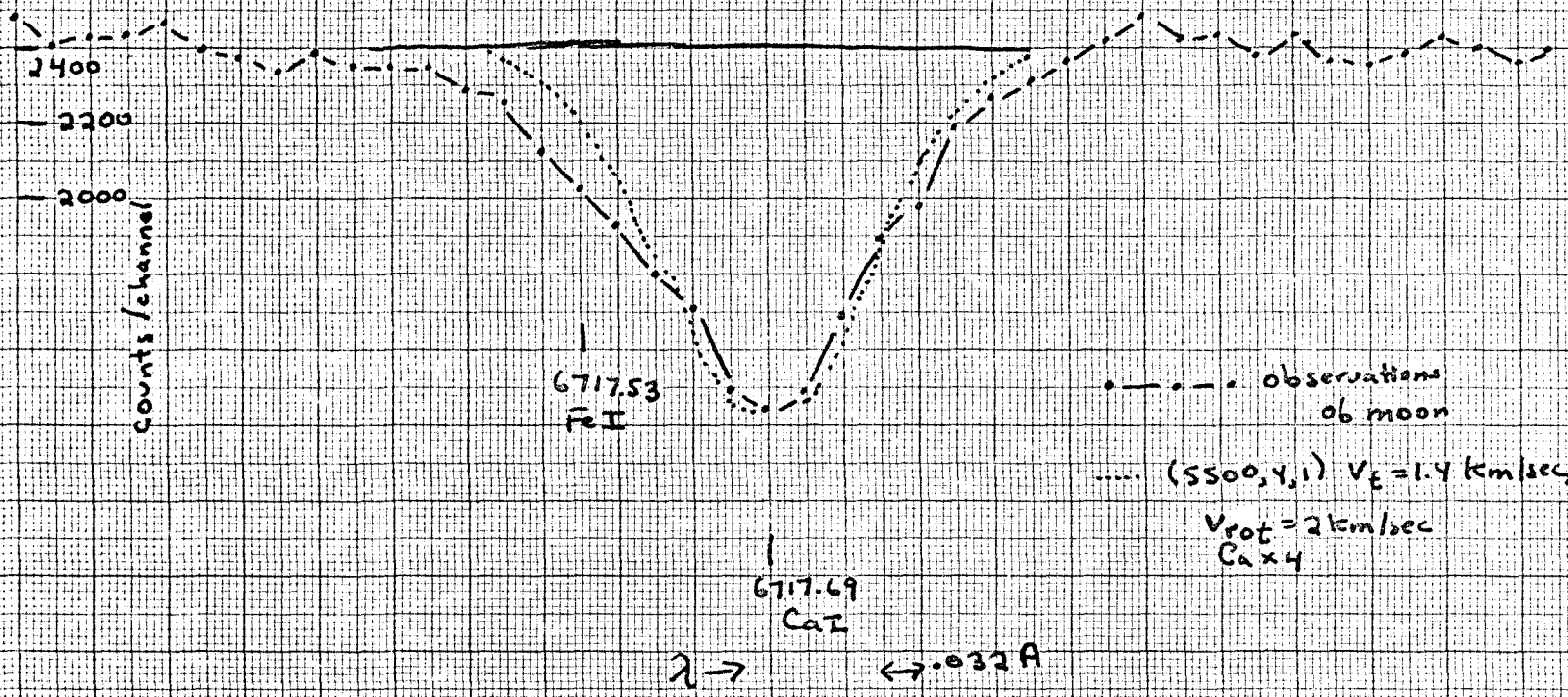

We now discuss the results of profile fitting for the stellar observations. The lithium line profile is not very sensitive to v_t for reasons discussed in chapter III, and is slightly, but not extremely, sensitive to the choice of v_{rot}, as it is much broader than the calcium line. In the cooler stars, the calcium line becomes so strong that the center of the line is probably not formed in a region where pure absorption prevails. The central residual intensity of 40% observed for λ6717 Å in η Cet surely implies that the intrinsic stellar profile, not convoluted by the instrumental response, must be less than 40%, which is below the minimum allowed value for pure absorption. This problem does not become serious until we reach the K stars. Therefore, for the G and F stars, we may determine v_{rot} sin (i) and v_t from the calcium line profiles. We shall denote v_{rot} sin (i) by v_{rot}.

In figure 30, we present the calculated curve of growth for λ6717 Å of Ca I for models with a range of effective temperatures. We see that allowing for the difference on T_{eff} between the sun and a 5500 ^{o}K model, the solar calcium abundance corresponds to $5\, N^{\odot}_{Ca}$ on our previous scale. We now redefine our scale and change our notation so that this is $Ca_{\odot}$. The Ca I line is on the flat part of the curve of growth, and its equivalent width depends on v_t. Unless we are prepared to accept a rather large range in $Ca_*/Ca_{\odot}$ none of the stars can have $v_t = 0$. This is because if we adopt $v_t = 0$, the computed profiles for λ6717 Å are too weak, and to reach the observed line strengths, we must take $Ca_*/Ca_{\odot}$ up to 5. It is not reasonable

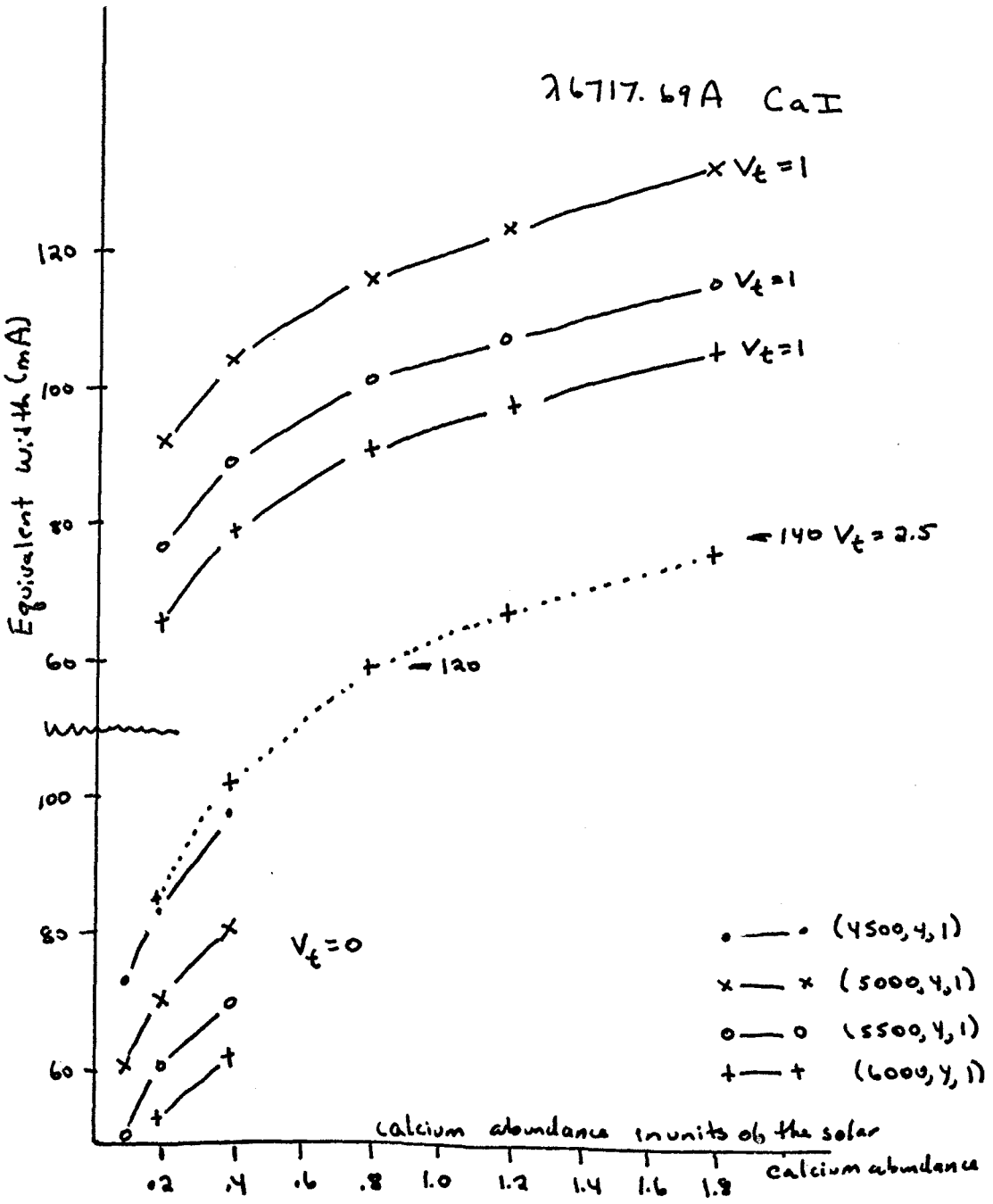

Figure 30: Portions of curves of growth of λ6717.69A of CaI for various models and values of the microturbulent velocity. The abundance scale is our revised scale for calcium, so that 1.0 corresponds to the solar abundance. Note the drastic increase in W_λ for a given model and N_{Ca} as v_t increases.

to assume that most of these stars are super-metal-rich by a factor of 2 to 5. Hence, we shall use $v_t = 1.4$ km/sec as a minimum value.

In table 28, we list the rotational velocities v_{rot} deduced from the line fitting for λ6717 Å, v_{rot} measured by Kraft (1967), the calcium abundances obtained from line fitting plus any necessary temperature corrections made with figure 30, and values of v_t. The values of v_t are very uncertain. If there was some uncertainty in v_{rot} arising from the noise in the observed Ca I line profile, we indicate the limits on v_{rot} and the approximate calcium abundance in parenthesis. The spectroscopic binary δ Tri has a period of 9.9 days. If the radius of the primary is close to that of the sun, then with v_{rot} of about 6 km/sec, the rotational period is the same as the orbital period. The other spectroscopic binary, ξ UMjA, has a much longer period of 660 days, and the rotational period is shorter than the orbital period. Perhaps the separation is wider and tidal effects are not as important in this system.

Note that for some of the stars, we were forced to adopt $v_t > 1.4$ km/sec in order to avoid obtaining very large calcium abundances. χ' Ori, 10 Tau, and perhaps ι Per belong to this group, with v_t greater than the solar value, or, if $v_t = v_t^{\odot}$, then $Ca_*/Ca_{\odot}$ is at least 4. It is interesting to note that these are among the stars with the largest rotational velocities for their spectral types. With the choices for v_t given in table 28, the final calcium abundances are then close to $Ca_{\odot}$, except for δ Tri, for which we have only 2 scans of λ6717 Å averaged to form the very uncertain final profile.

The comparison of our rotational velocities and those of Kraft

TABLE 28

Rotational Velocities, Calcium Abundances, and Values of v_t for the Program Stars

Star	Spectral type	v_{rot} km/sec	v_t km/sec	Ca abundance	v_{rot} (Kraft)[1]
moon	G2V	2	1.4	$Ca_\odot$	
γ Lep	F6V	9	1.4	0.8 $Ca_\odot$	
ξ Peg	F7V	9	1.4	$Ca_\odot$	9
10 Tau	F8V	7 (6,7)	2.5	$Ca_\odot$	
χ Her	F9V	5	1.4	0.6 $Ca_\odot$	$\leq$ 6
χ' Ori	G0V	10	2.5	0.8 $Ca_\odot$	5-7
ξ UMjA	G0V	4 (4,5)	1.4	0.5 $Ca_\odot$	
β Com	G0V	5	1.4	1.4 $Ca_\odot$	3-5
δ Tri	G0V	6 (3-6)	1.4	(0.2 $Ca_\odot$)	
ι Per	G0V	6	1.4	2 $Ca_\odot$	
κ Cet	G5V	5 (4,5)	1.4	(0.5 $Ca_\odot$)	
ξ BooA	G8V	5	1.4	0.8 $Ca_\odot$	
η Psc	G8III	$\lesssim$ 4			
ψ UMj	K1III	3*	1.4		
η Cet	K2III	3*	1.4		

*Obtained from λ6710.32 Å of Fe I

Source
[1]Kraft (1967)

(1967) is good for the four stars in common, except for χ' Ori. Unless v_t for this star is even greater than 2.5 km/sec, it is difficult to avoid the larger value of v_{rot} given in table 28. Kraft (1965) normalized his scale of v_{rot}, which had previously been defined only for larger values of v_{rot}, by a downwards interpolation from the previous scale, and also by using spectra of the star with the sharpest lines he could find (H1 in the Hyades). This scale appears to be correct. Kraft has suggested that stars with emission in the cores of the H and K lines tend to rotate faster than do field stars of the same spectral type without emission. We take measurements of H-K emission from Wilson (1966) and from Kraft (1967) to construct v_{rot} (spectral type, emission strength). We obtain, with an inadequate number of stars, some support for Kraft's suggestion. It appears that in the range from F8 to G0, v_{rot} begins to increase rapidly towards earlier spectral type.

None of the stars had lines as sharp as the sun. The difference in central intensity and width of λ6717 Å between $v_{rot} = 2$ and 5 km/sec is very noticable. While v_{rot} may have an uncertainty of $\pm$ 20% due to variations in v_t and uncertainties in the instrumental profile, v_{rot} for these stars is definitely greater than that of the sun.

The theoretical fits to the observed calcium and lithium line profiles are shown in figures 31a-m. The theoretical profiles have wavelength scales associated with them, and we allow sliding of the computed profiles along the wavelength axis in trying to fit them to the observed profiles. Therefore, if there are errors in v_r, such a translation along the wavelength axis will be necessary. Thus we may

construct table 29 which lists the errors in v_r as deduced from fitting the lithium and calcium lines; the data of table 29 are derived by essentially the same method as was used for table 27. The agreement among the various methods of determining the error in the tabulated radial velocity, and hence the accuracy of our wavelength scale, is good.

The wavelengths of the Ca I line center and 6707.761 Å on the theoretical profiles are indicated in the figures by the subscript "p," while the subscript "o" denotes the wavelength scale from the tabulated radial velocity and the lamp calibration. The calcium abundance of the theoretical profile is indicated on our original scale (equation 7-3). The wavelength scale is 0.032 Å/point or 0.064 Å/cm on the paper in figures 31a-m. Some remarks on the fitting process for individual stars are now given.

<u>χ' Ori:</u> For the Ca I line we had to adopt $v_t = 2.5$ km/sec to avoid an abnormally large calcium abundance. If we attempted to fit the profile of λ6708 Å using a theoretical profile with $v_t = 0$, the calculated profile using equation 7-1 was not as broad as the observed one. An additional source of broadening could be added by making Li^6/Li^7 greater than 0. The value required to produce the observed profile was $Li^6/Li^7 \approx 0.2$. However, when we use theoretical profiles for λ6708 Å calculated with $v_t = 2.5$ km/sec and we use equation 7-1 to convolute the profile, the calculated profile for $Li^6/Li^7 = 0.01$ is as broad as the observed profile. Since v_{rot} of the star is so large, there is no detail in the profile beyond its width. It seems reasonable

TABLE 29

Errors in the Tabulated Radial Velocities Deduced by Fitting Theoretical Profiles

Star	Δv_r (Li fit) steps[1]	Δv_r (Ca fit) steps	Δv_r (Ca line center) steps
γ Lep	+ 5	+ 7	+ 5
ξ Peg	+ 2	+ 5	0
10 Tau	+ 2	+ 5	+ 5
χ Her	-10	-10	-10
χ' Ori	+ 9	+ 4	+ 5
ξ UMjA[2]	-20	-16	-17
β Com	- 4	- 4	- 4
δ Tri[3]	-30	-26	-25
ι Per	+ 2	+ 5	+ 5?
κ Cet		+ 3	+ 3?
ξ BooA	-10	- 7	- 8

[1] At 6708 Å, there are 155 steps per angstrom.

[2] For this spectroscopic binary, we fit the March 1971 profiles; the Dec. profiles are almost identical.

[3] Spectroscopic binary

Figure 3la: Observed (dots) and computed (wriggly lines) profiles for γ Lep.

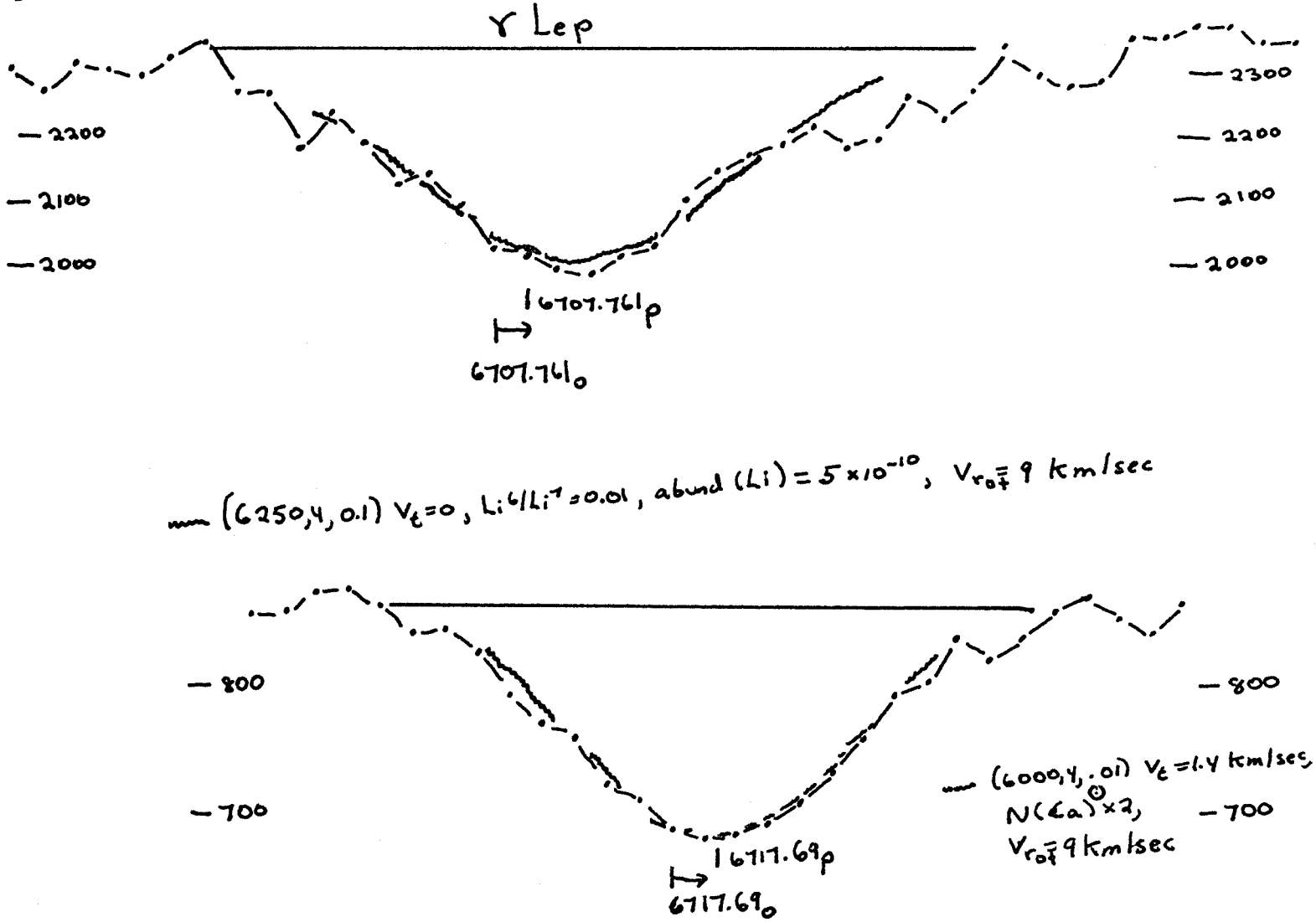

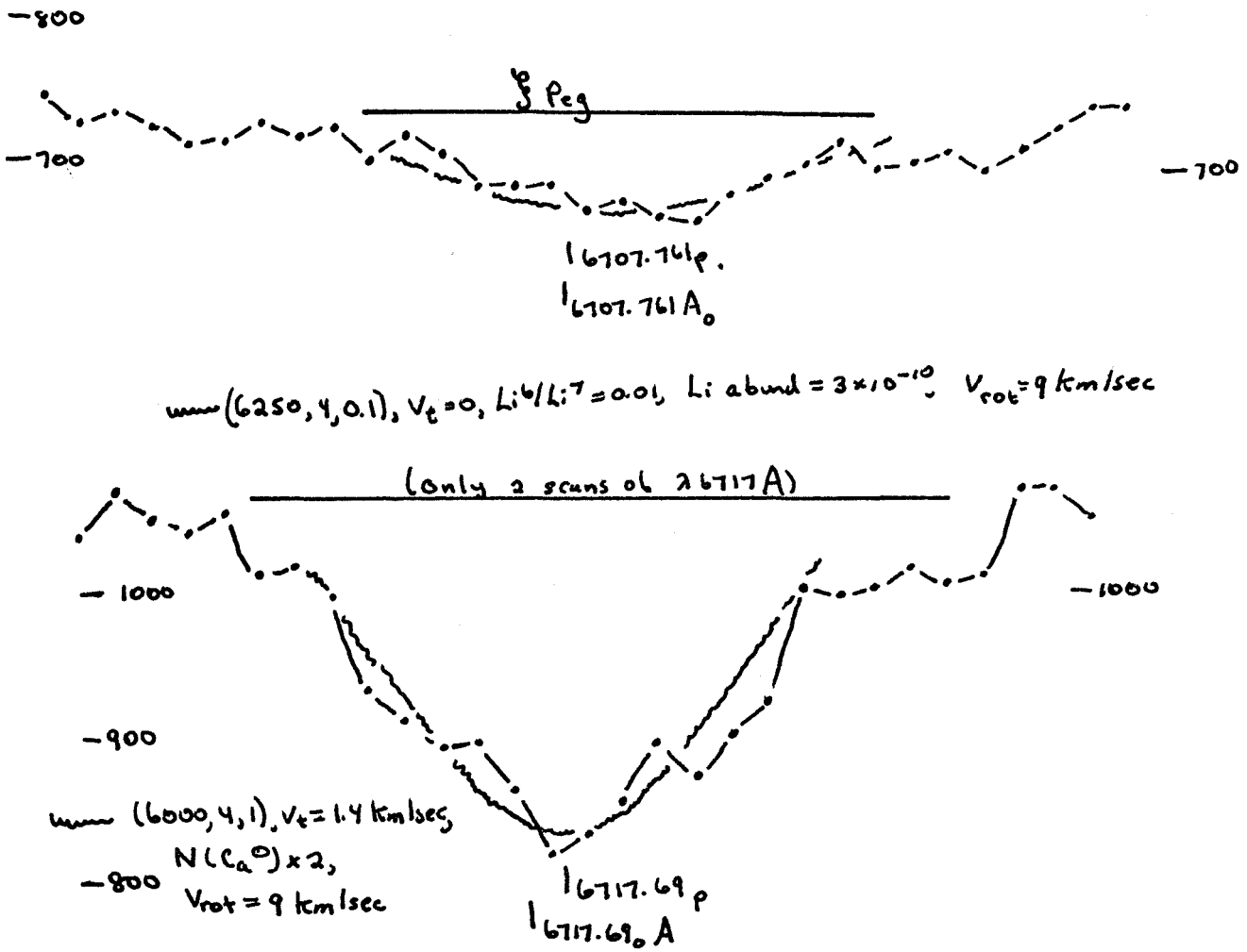

Figure 31b: Observed (dots) and computed (wriggly lines) profiles for ζ Peg.

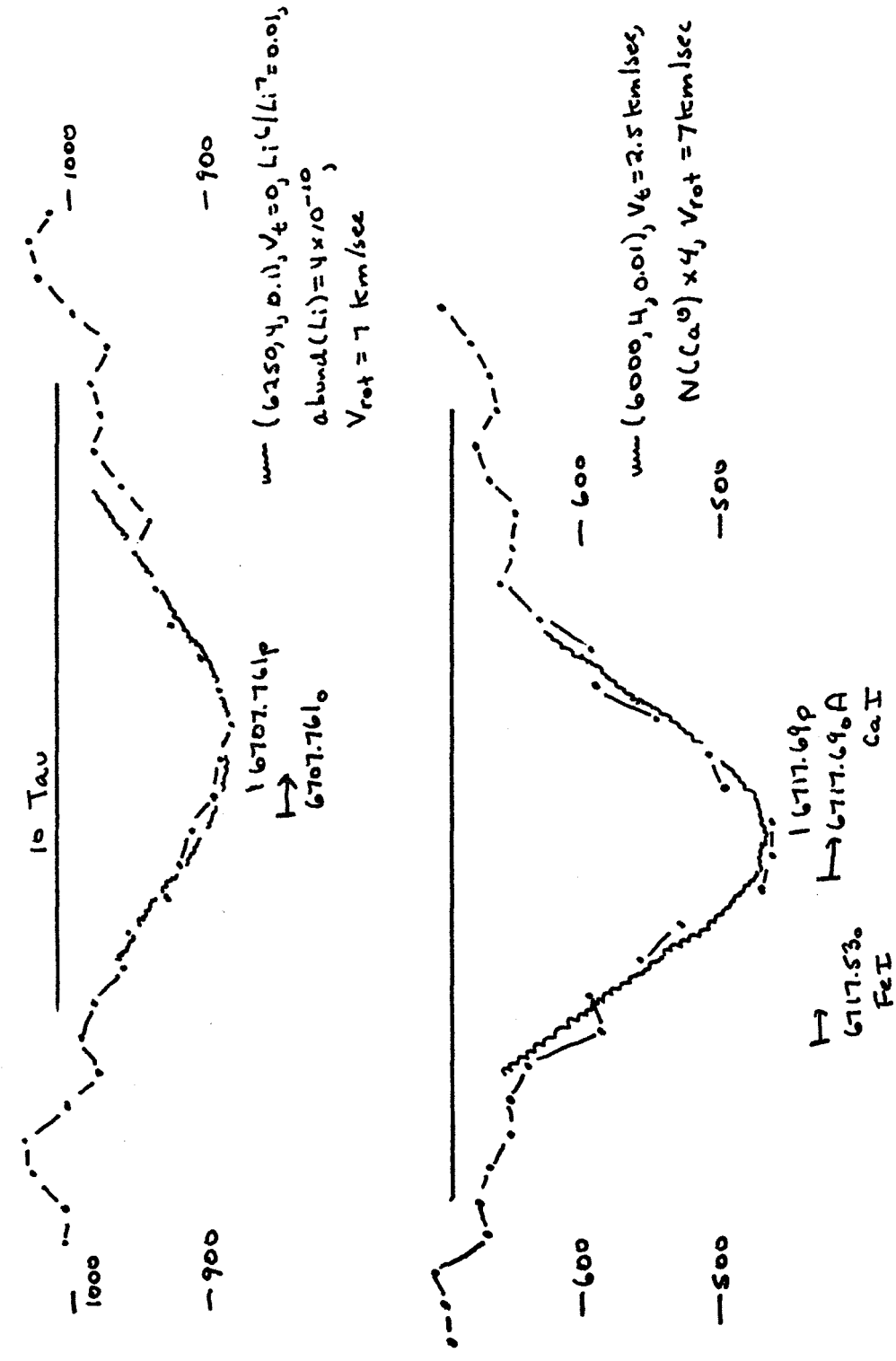

Figure 31c: Observed (dots) and computed (wriggly lines) profiles for 10 Tau.

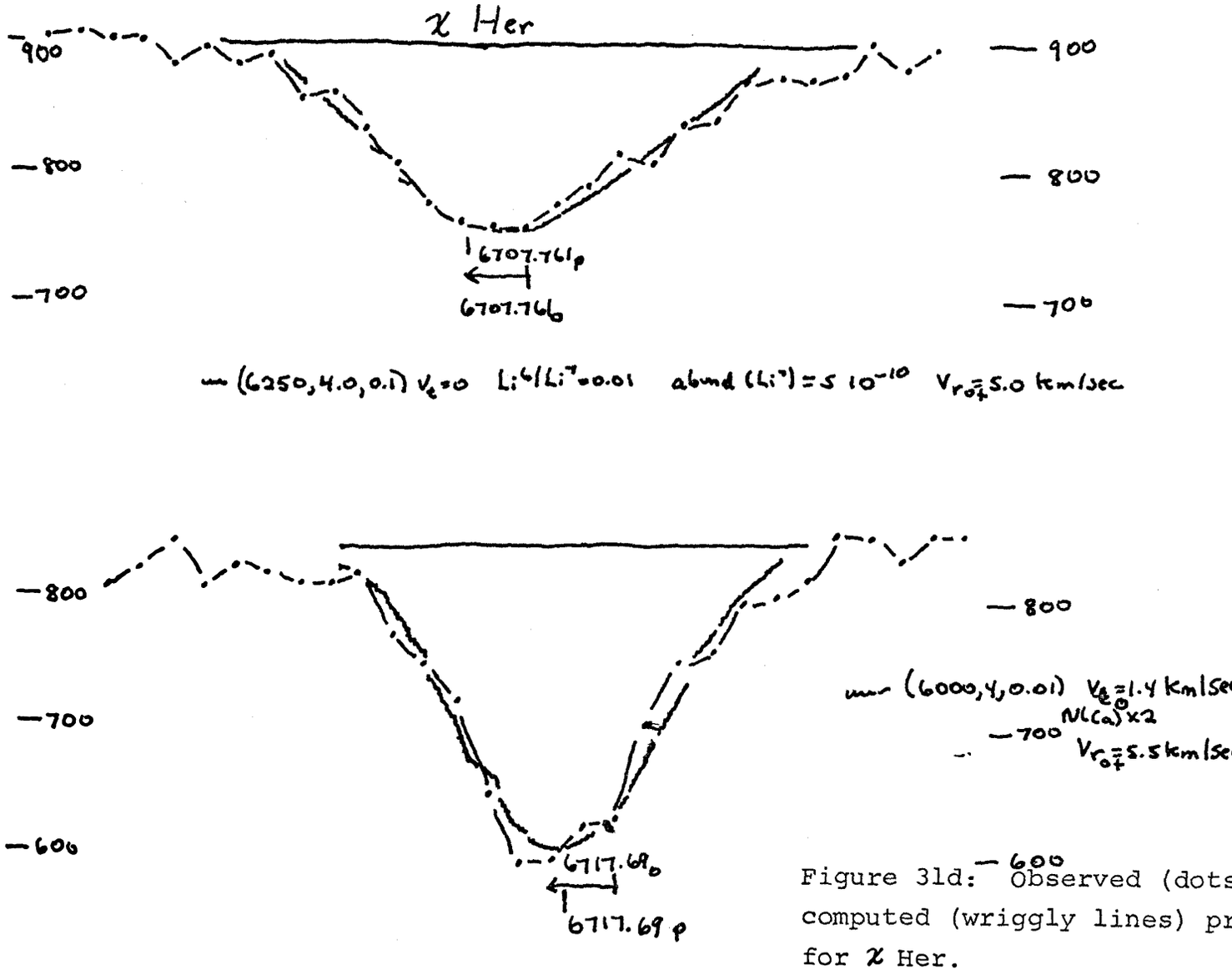

Figure 31d: Observed (dots) and computed (wriggly lines) profiles for χ Her.

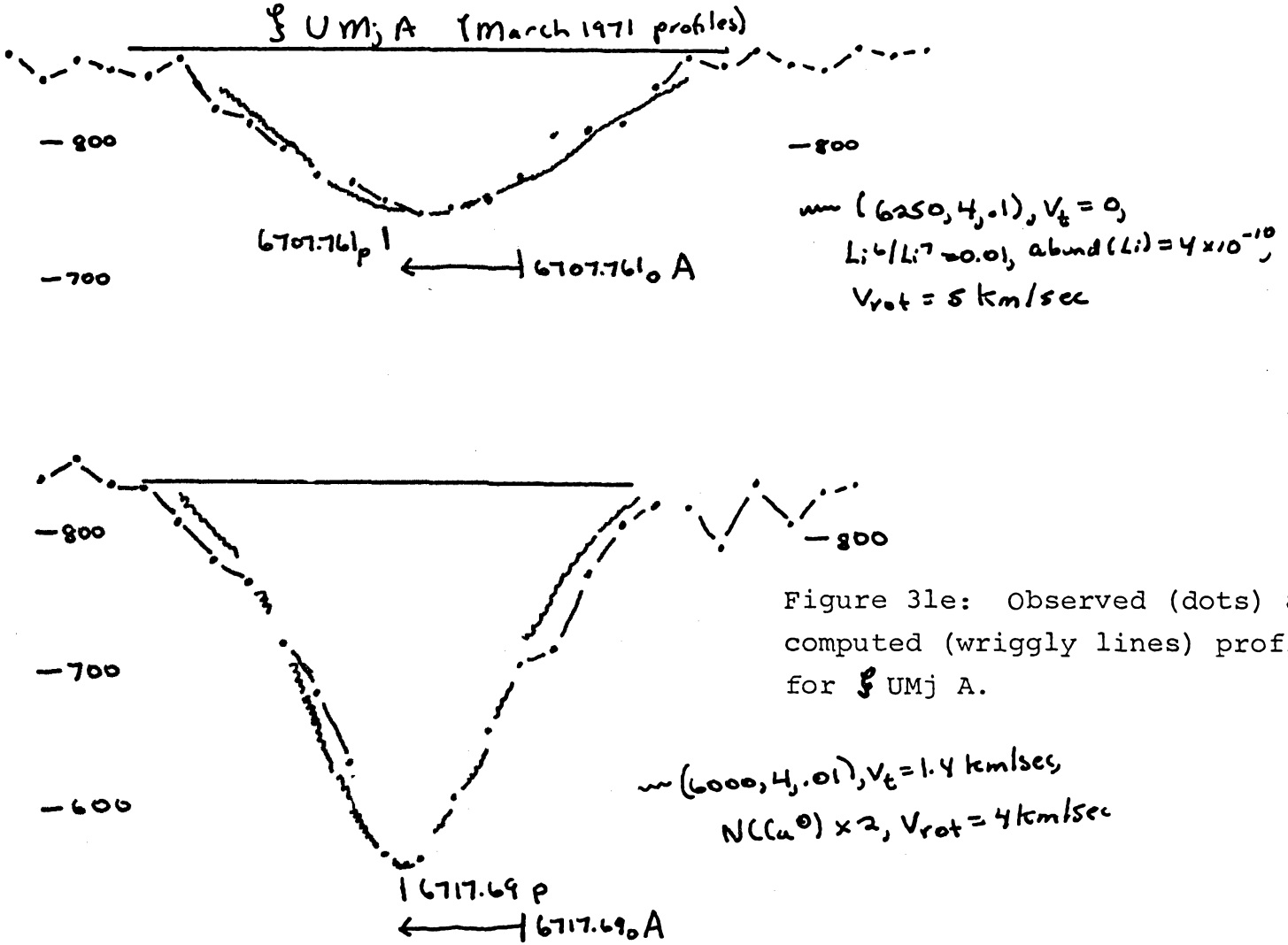

Figure 31e: Observed (dots) and computed (wriggly lines) profiles for ζ UMj A.

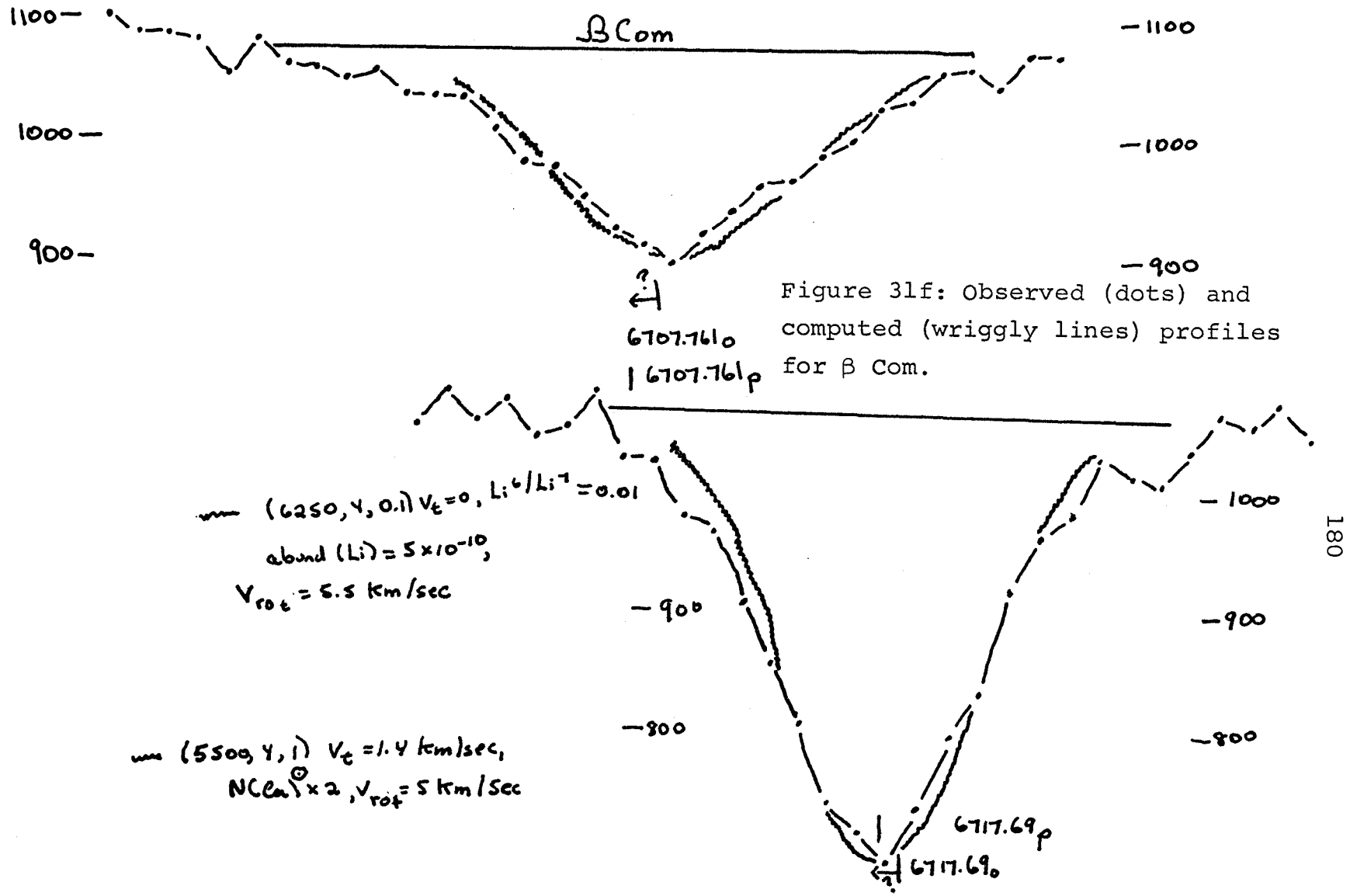

Figure 31f: Observed (dots) and computed (wriggly lines) profiles for β Com.

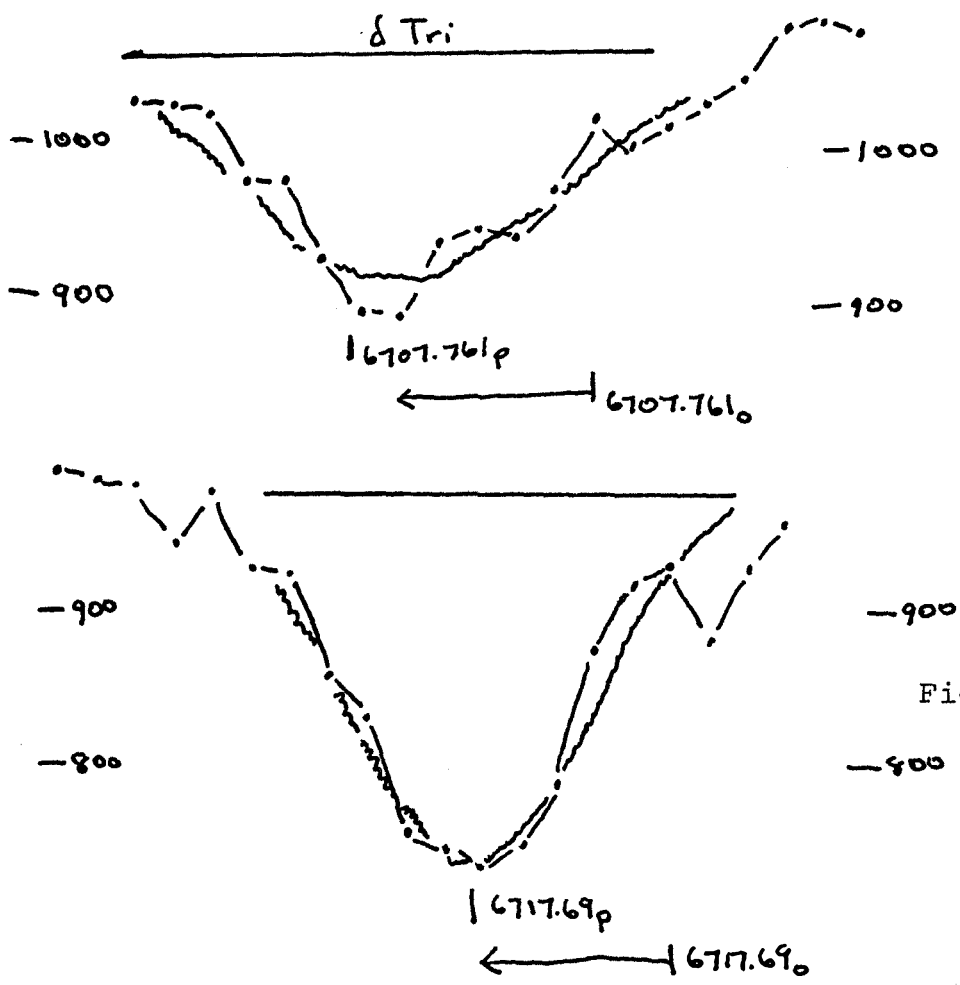

Figure 31g: Observed (dots) and computed (wriggly lines) profiles for δ Tri.

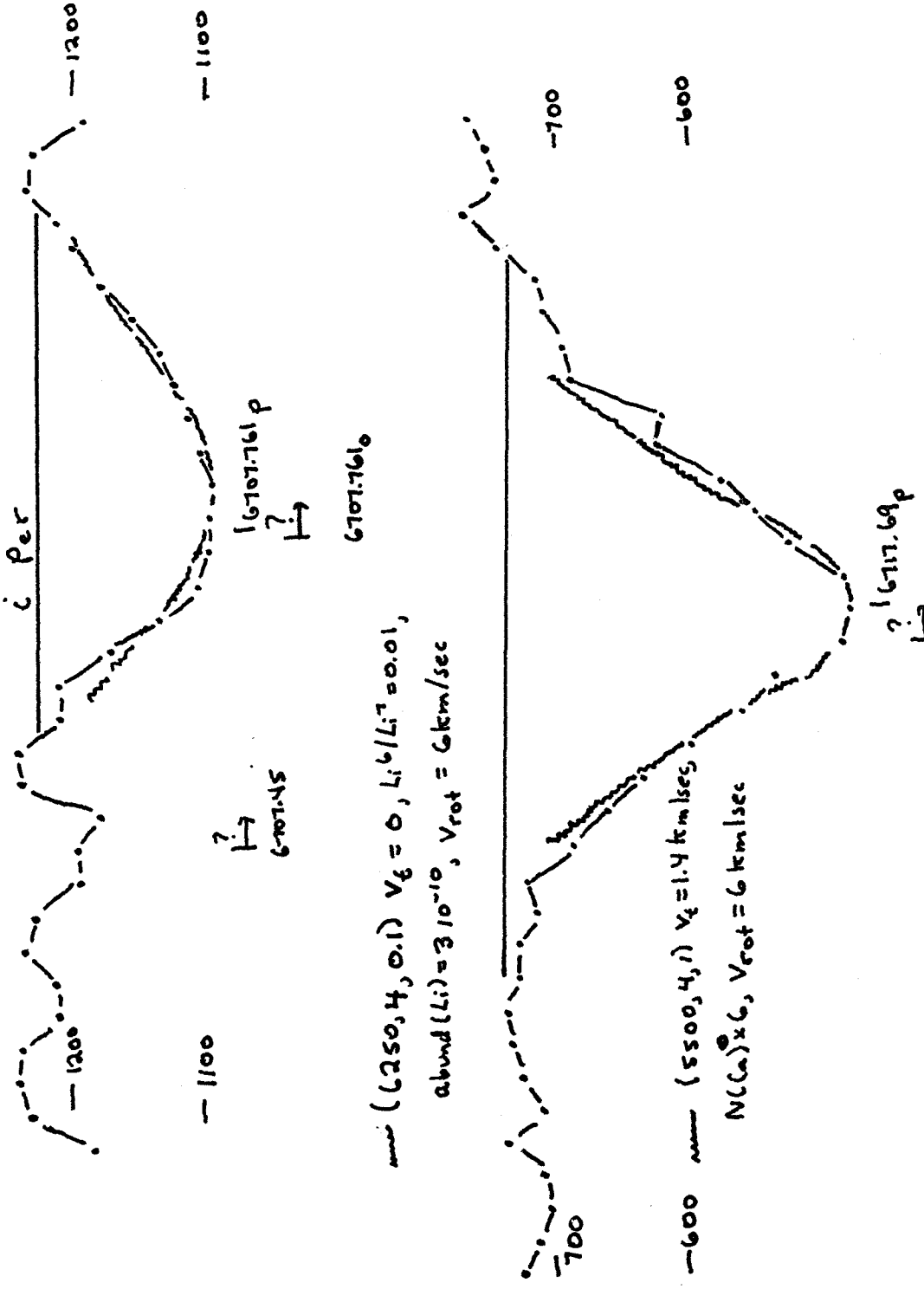

Figure 31h: Observed (dots) and computed (wriggly lines) profiles for ζ Per.

Figure 31i: Observed (dots) and computed (wriggly lines) profiles for χ' Ori.

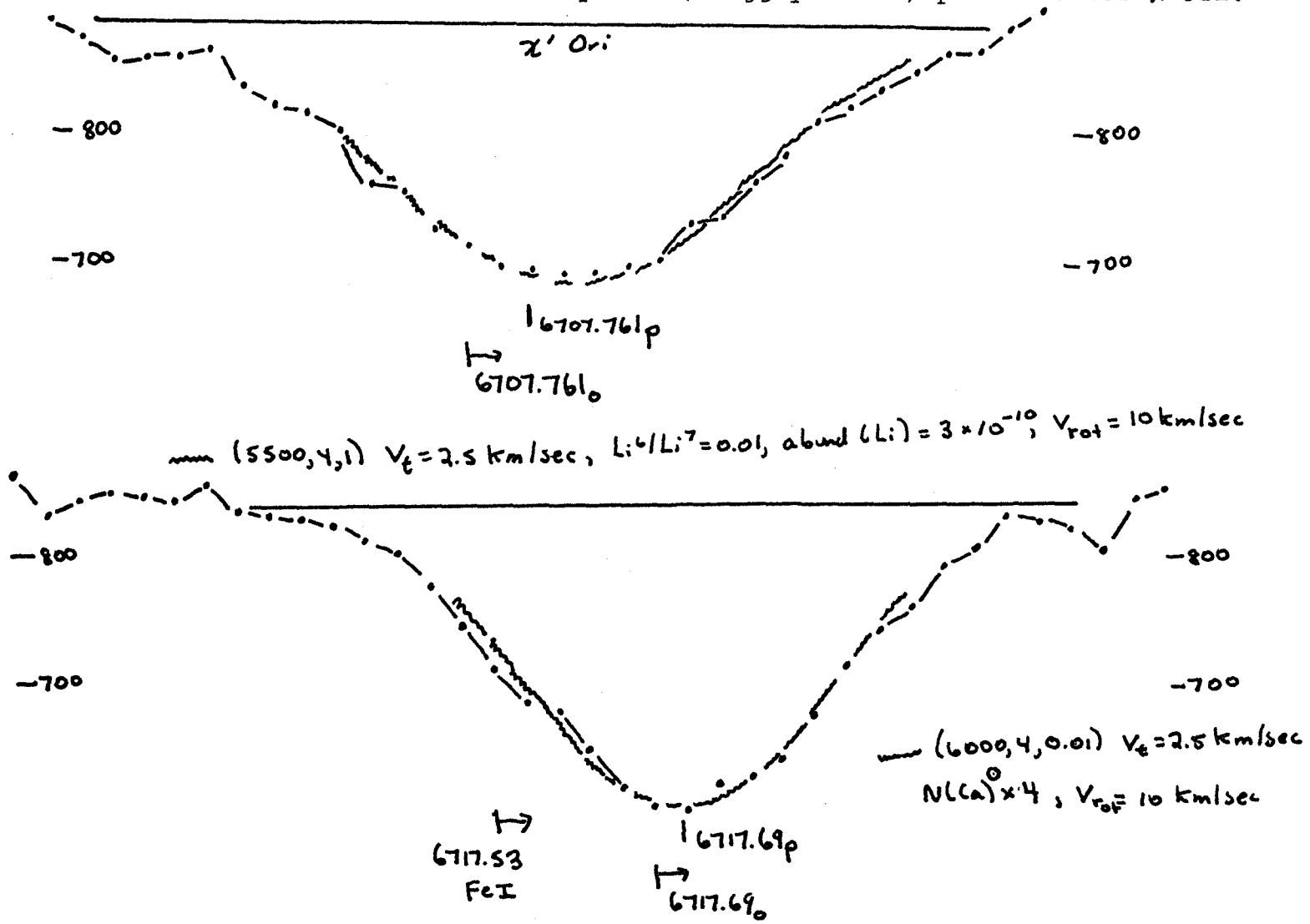

Figure 31ℓ: Observed (dots) and computed (wriggly lines) profile for KCet. The lithium profile was too noisy and could not be fit.

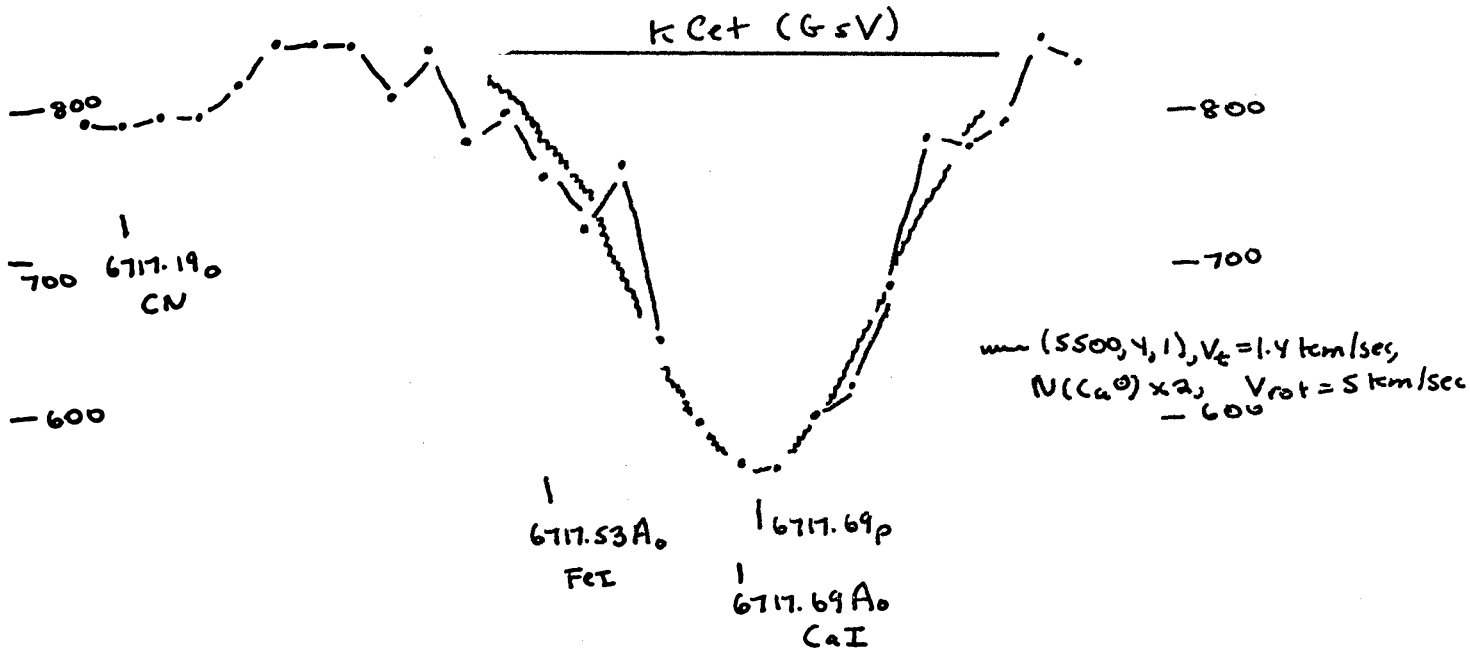

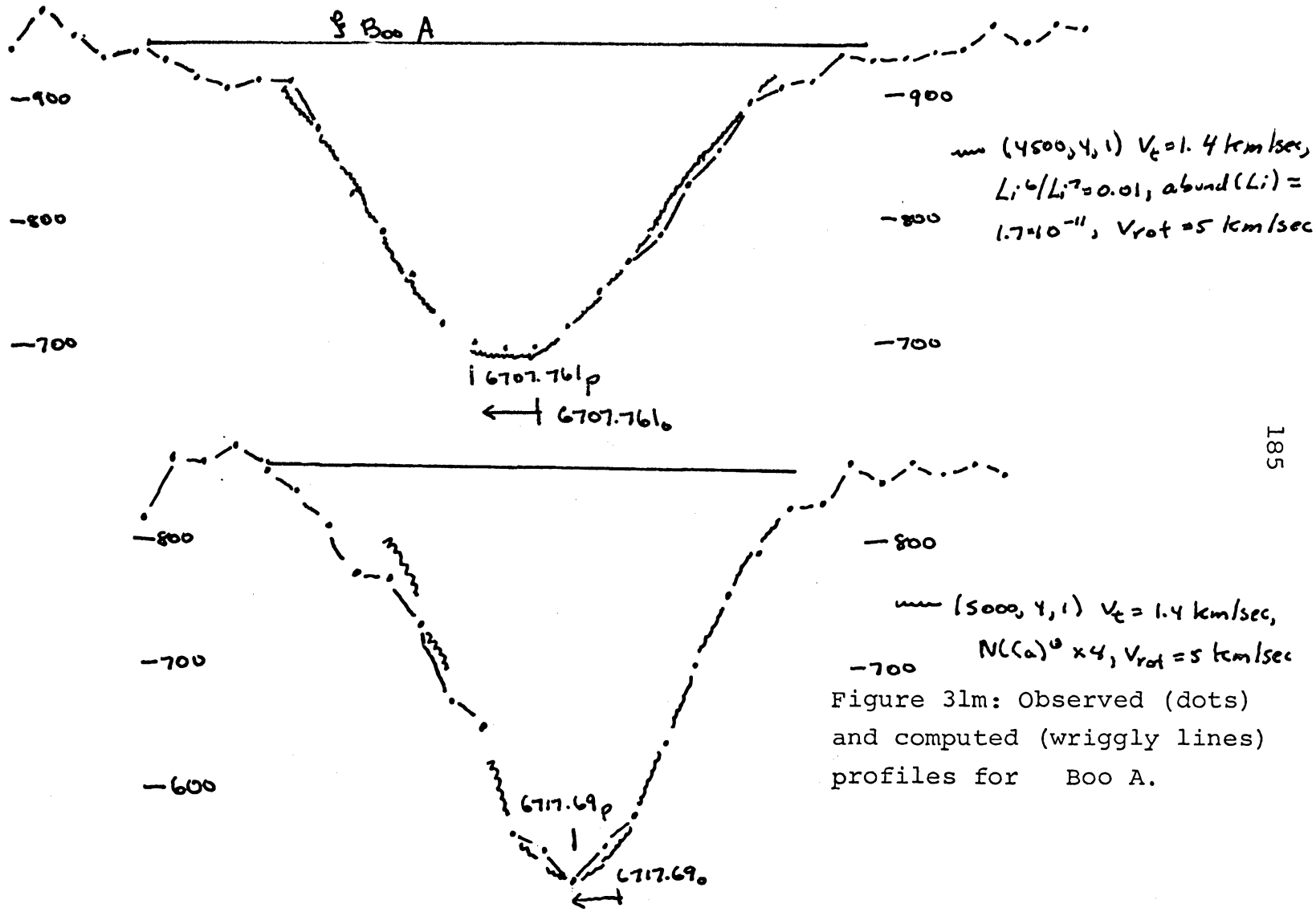

Figure 31m: Observed (dots) and computed (wriggly lines) profiles for Boo A.

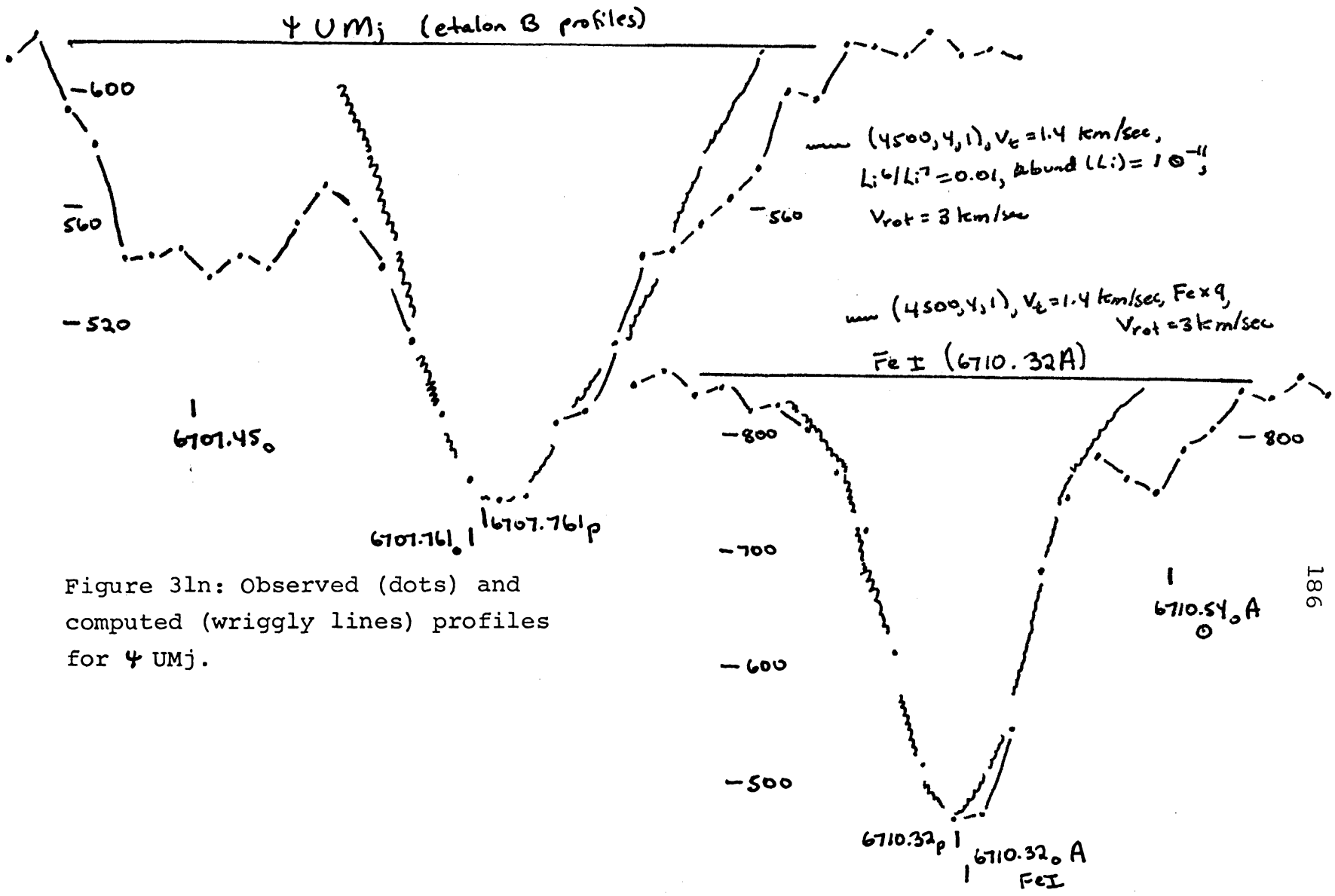

Figure 31n: Observed (dots) and computed (wriggly lines) profiles for ψ UMj.

Figure 31o: Observed (dots) and computed (wriggly lines) profile for η Cet. We do not fit the lithium line due to blending with λ6707.45A.

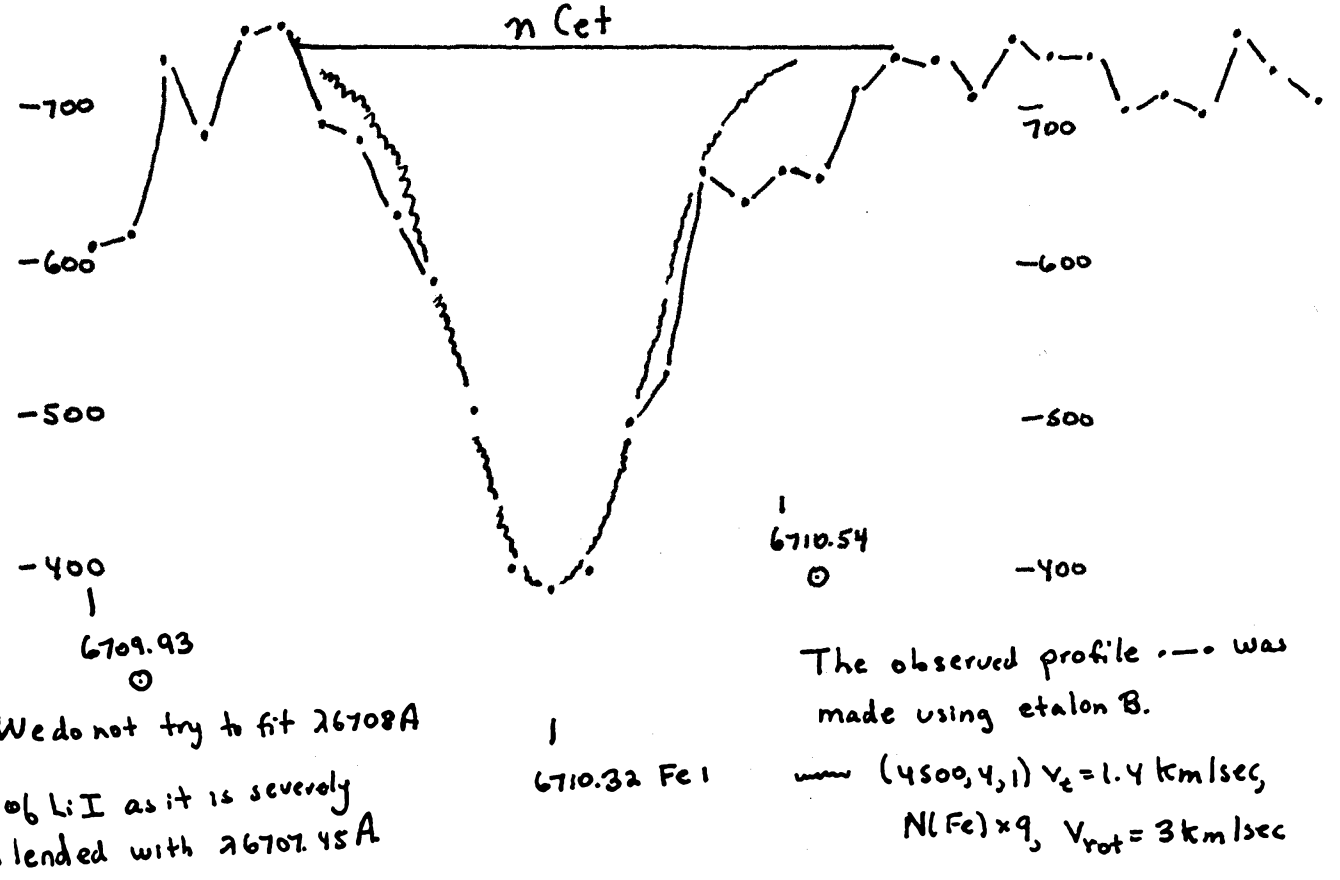

to choose the same microturbulent velocity for λ6708 Å as for λ6717 Å, and hence we accept the value $Li^6/Li^7 = 0.0$, with an uncertainty which could permit R to be as large as 0.2. The isotope ratio will be poorly determined in those stars where the profile of λ6708 Å is so broadened by rotation that it is almost symmetrical about a wavelength near 6707.82 Å.

κ Cet: We cannot fit the lithium line, as its profile is too noisy. The problem is that the long wavelength wing shown by all the theoretical profiles is not seen in the noisy observed profile, shown in table 26k. The lithium line in this star is a mean of only 6 scans, and the line is very weak.

ξ UMjA: The observed profiles for March, 1971 were used for this spectroscopic binary. The profiles observed in Dec. 1970 are the same as those of March, 1971 except for a shift in radial velocity.

ξ BooA: The Ca I line is asymmetric. This is probably due to a blend with the weak line of Fe I at 6717.53 Å, as in the lunar spectrum.

η Psc: The observed profile of λ6708 Å shown in figure 26m could not be fit. This star has the same problem as κ Cet--there was no long-wavelength wing on the observed profile. There are only 2 scans of λ6708 Å for η Psc. Since λ6707.45 Å is seen in the expected place, the wavelength scale must be correct.

ψ UMj: We determine v_{rot} from the profile of λ6710.32 Å of Fe I which was observed with etalon B. The calcium lines (λ6717 Å and λ6572 Å were observed in this star) are much too strong for this

purpose. The wavelength scale near the Fe I line is not well known, as the laboratory lamps do not show the iron spectrum. The nearest line observed in the calibration lamp was the lithium resonance line. We therefore cannot determine the accuracy of the tabulated v_r by fitting λ6710.32 Å. Note that the profile of λ6708 Å was also made using etalon B. We can satisfactorily fit this profile except in the far wings. It is probable that there are many weak molecular features in this region which produce the additional absorption observed beyond 6707.96 Å.

η Cet: The rotational velocity was determined from λ6710.32 Å of Fe I. We do not fit the lithium profile, as blending with λ6707.45 Å is very severe.

E. The Isotope Ratio

We list in table 30 the various determinations of the isotope ratio and lithium abundance for the program stars. The lithium abundance as determined using the measured equivalent width of λ6708 Å and the curve of growth is more accurate than that determined by fitting profiles and correcting for the difference between T_{eff} of the star and of the model using figure 13. Still the agreement between the two lithium abundances is quite good. It is also encouraging to note that values of $\lambda_{1/2}$ less than 6707.81 Å (i.e. $Li^6/Li^7 < 0$) were obtained only for those stars with exceptionally poor profiles. There are 3 determinations of the isotope ratio, 2 of which are independent. We measured $\lambda_{1/2}$ as discussed in chapter VI. This

TABLE 30

The Isotope Ratio and Lithium Abundance of the Program Stars

Star	$\lambda_{1/2}$ -6707.00 Å (1)	Li^6/Li^7 from $\lambda_{1/2}$	Li^6/Li^7 from Ca fitting	Li^6/Li^7 from v_{rot} fitting	Remarks	Li abund from W_λ	Li abund (fit)
γ Lep	0.82	0.06	0	0		- 9.2	- 9.4
ξ Peg	0.82	0.06	0-0.2	0		- 9.9	- 9.5
10 Tau	0.82	0.06	0	0		- 9.6	- 9.4
χ Her	0.81	0.00	0	0		- 9.7	- 9.3
χ' Ori	0.83	0.125	0-0.2	0-0.2		- 9.3	- 9.2
ξ UMjA	0.81	0.00	0	0		- 9.9	- 9.4
β Com	0.80-0.82	0.00-0.06	0	0		- 9.8	- 9.3
δ Tri	0.78	< 0.00	0		3	- 9.9	- 9.7
ι Per	0.79-0.82	<0.00-0.06	0	0		- 9.9	- 9.7
κ Cet	0.79-0.81	<0.00-0.00			3	-10.6	
ξ BooA	0.81	0.00	0	0		-10.0	-10.1
η Psc	0.81	0.00			3	-10.8	
ψ UMj	0.79	< 0.00	0		2	-10.5	-10.6
η Cet	0.81	0.00			2	-10.5	

1 From figures 26a-o.

2 The Li resonance line is blended with λ6707.45 Å, making determination of $\lambda_{1/2}$ difficult.

3 Noisy profile of λ6708 Å. The lithium line for these stars is an average of less than 7 scans.

measurement is independent of the shape of the line, and uses only the tabulated radial velocity, any corrections to v_r as determined by the position of the center of λ6717 Å of Ca I, and the lamp calibration. The line fitting procedures are independent of the wavelength scale of the line (although they provide information on the accuracy of the tabulated radial velocity), but depend on the exact shape of the observed line profiles of the lithium resonance line and of λ6717 Å of Ca I, especially on the widths of the lines.

In all cases, $Li^6/Li^7 = 0$, with an uncertainty which we discuss later. The one possible exception is χ' Ori, for which we shall adopt $Li^6/Li^7 = 0.1$. This star has the broadest lines, and hence the isotope ratio is difficult to determine. Since the lines are broad and shallow, the profile of λ6717 Å near the center of the line is that of a region 0.15 Å wide with almost constant residual intensity. The effect of even a 2% rms fluctuation on the determination of the line center of such a profile is severe. Hence, it is possible that χ' Ori does have $Li^6/Li^7 = 0.0$.

The possible errors in the isotope ratio are difficult to assess. Certainly if Li^6/Li^7 were 0.2, we would notice that the calculated lithium lines were too narrow when fitted to the observed lines. However, if Li^6/Li^7 in a few stars were 0.1, the effect on the profiles would be too small to detect in this manner, although such ratios would show up in the determinations of $\lambda_{1/2}$. If Li^6/Li^7 were 0.1 in all the stars, then the effect of Li^6 on the line widths perhaps would have been noticed.

We therefore adopt as our final determination of the isotope

ratio $Li^6/Li^7 = 0.1$ ($\pm$ 0.1) for χ' Ori (the star with the broadest lines), $Li^6/Li^7 = 0.05$ ($\pm$0.1) for γ Lep, ξ Peg and 10 Tau (which are all stars with large rotational velocities and broad lines), and $Li^6/Li^7 = 0.0$ ($\pm$0.1) for the remainder of the stars. Li^6/Li^7 could be 0.0 for all stars, and the difficulties discussed above for broad-lined stars could produce the cases where measurements seem to indicate Li^6/Li^7 slightly larger than zero. The isotope ratio Li^6/Li^7 cannot be greater than 0.2 in any of the stars we observed.

CHAPTER VIII

The Nuclear Astrophysics of the Light Elements

A. The Nuclear Astrophysics of the Light Elements

Reeves (1969) has written a useful summary of the nuclear astrophysics of the light elements which we have relied on extensively in preparing this brief summary. The most critical nuclear property of the light elements is their marginal stability; they have very low binding energies against break-up into the largest possible number of α particles. No nucleus of mass 5 or 8 is stable. Beryllium has only one stable isotope, Be^9, and only its nuclear ground state is stable.

Thus these elements are difficult to form, and can be readily destroyed. Lithium, in particular, undergoes the reactions

$$Li^6 + H^1 \rightarrow He^3 + He^4 \qquad (8\text{-}1)$$

and

$$Li^7 + H^1 \rightarrow 2\ He^4 \qquad (8\text{-}2)$$

Both of these are exothermic reactions, so that the protons do not need large initial energies. For thermal protons, these reactions proceed rapidly at temperatures of about 10^6 °K. (Of course, nonthermal protons with sufficient energy work just as well.) Since Li^6 is less stable than Li^7 with respect to break-up into the largest number of particles, the cross section for reaction 8-1 is larger than for reaction 8-2. The cross section for destruction of Be^9 at low proton energies is smaller than that for Li due to the larger coulomb repulsion between the Be nucleus and the incoming proton. At larger proton energies,

where the coulomb repulsion no longer determines the cross section, the fragility of Be^9 leads to

$$\sigma(Be^9) > \sigma(Li^6) > \sigma(Li^7) \quad \text{for} \quad E_p > 100 \text{ keV} \qquad (8\text{-}3)$$

Therefore, any lithium present in a stellar interior where $T > 10^6\ ^oK$ is rapidly destroyed by reactions 8-1 and 8-2, with Li^6 being burned more rapidly. Be^9 is not significantly destroyed for $T < 3 \times 10^6\ ^oK$.

A second means of decreasing the lithium abundance of a star is the phenomenon of mass loss. Since Li is concentrated toward the surface in a main-sequence star, mass loss from the surface will deplete lithium.

Although the light elements are produced by nuclear reactions in stellar interiors, it is very unlikely under normal circumstances that such material could reach the stellar photosphere. The most accepted mechanism for formation of these elements involves spallation of targets of medium weight (and relatively abundant) nuclei such as C^{12}, N^{14}, and O^{16} with high-energy protons. These protons must have energies of at least 100 meV each, which implies that they cannot be thermal protons, and must have been accelerated by some non-thermal mechanism. Over the range of energy $E_p > 100$ meV, the cross sections for spallation have constant ratios such that

$$\sigma_{sp}(Li^7)/\sigma_{sp}(Li^6) \approx 2, \quad \sigma_{sp}(Li)/\sigma_{sp}(Be) \approx 20, \quad \text{and}$$
$$\sigma_{sp}(B^{11})/\sigma_{sp}(B^{10}) \approx 3 \qquad (8\text{-}4)$$

where "sp" denotes spallation.

Spallation is clearly the dominant nuclear mechanism, as the meteoritic Li/Be and B^{10}/B^{11} ratios agree closely with the experimental results for spallation. Also the meteoritic abundances of the light elements are constant to within a few per cent, and agree with the terrestial values. We therefore deduce that the solar nebula from which the planets condensed must have separated from the sun after the light elements were formed. The remaining question is where these light elements were produced.

Big-bang nucleosynthesis calculations of such ratios as Li/Be disagree with the observed values, so that the observed light elements are not likely to be remnants of the initial fireball. Solar flares are known to be accompanied by the production of high-energy protons. By extension to stars, stellar flares are a possible source of such particles. Furthermore, solar flares are a phenomenon of the chromosphere, rather than the photosphere, and the T Tauri stars, which have very high lithium abundances, also show evidence of very active chromospheres. Bonsack and Greenstein (1960) suggested that these young stars produce their own lithium by surface spallation reactions (autogenic production). The energy requirements for the production of such a large amount of Li ($N_{Li}/N_H \approx 10^{-9}$) are large. Most of the high-energy protons will be decelerated by interactions with the hydrogen and electrons in the stellar photosphere (heating up the medium) before they hit a target nucleus such as C^{12}. It is therefore necessary to provide about 10^6 meV in high energy protons to produce one Li nucleus. Thus to produce the amount of Li observed in T Tauri stars requires a large fraction of the gravitational energy of the star.

Reeves, Fowler, and Hoyle (1970) suggest production by spallation on medium-weight target nuclei with galactic cosmic-ray protons. Recent observations imply that residual modulation of the cosmic-ray spectrum may exist even at solar minimum, and thus make this suggestion plausible.

By the time the star reaches the T Tauri phase, it has somehow acquired an initial amount of Li ($N_{Li}/N_H \approx 10^{-9}$). As the star contracts toward the main sequence, convection may carry the light elements to regions that are hot enough for them to be destroyed by reactions such as 8-1 and 8-2. Bodenheimer (1965, 1966) has carried out approximate calculations of the destruction of Li and Be through such convective currents as a function of time in pre-main sequence models. He finds no significant depletion of Be until stars later than K5V, but non-negligible destruction of the initial Li content by the time the star reaches the main sequence. The fraction of initial Li destroyed increases as the mass of the star decreases. However, his calculations predict a 50% survival of Li in the sun, whereas the sun has 1/200 the lithium abundance of meteorites. A comparison of the Pleides and Hyades Li abundances (figure 14) shows that there is additional depletion of Li while on the main sequence. The convection zone must somehow reach down to temperatures high enough to destroy Li, but not Be. Studies of the Be abundance (Wallerstein and Conti 1969 summarize previous work on Be) indicate that Be is depleted in early F stars, but has values close to the meteoritic Be abundance in G stars. Reeves (1969) has suggested a mechanism for destroying Be by low-energy surface nuclear reactions (see equation 8-3) in stars

without deep convection zones; in the G stars these convection zones do not reach high enough temperatures to burn Be, while they shield Be from surface nuclear reactions.

Previous measurements of the Li isotope ratio by Herbig (1964) led to an inconsistency in that Li^6 was observed in stars where Be had its meteoritic abundance, yet Li/Be is less than the spallation value. This implies some depletion of Li in these stars, and the observed Li abundances support this. But then we would expect $Li^6/Li^7 \ll 1/2$, which is the spallation ratio, since Li^6 is destroyed more readily than Li^7. Our observations of a low ratio Li^6/Li^7 remove this difficulty.

It is clear from the discussion in chapter IV and previous work (see Boesgaard 1970, for example) that the huge Li overabundances in some very cool evolved stars such as WZ Cas cannot be errors in the analysis. Autogeneration of Li must occur in these super-Li-rich C and S stars. Those evolved stars also sometimes show lines of Tc. Somehow material from the interior is getting out to the surface (or being produced on the surface) in a short time scale. If it can happen for Tc, it could happen for Li also. The details of this process are unclear.

B. Conclusions

The stars we have observed were selected to have high lithium abundances. They show some Li depletion, in that they have less Li than the T Tauri stars or meteorites, but much more than the sun has. The percentage of stars with high and moderate strength of H-K

emission among our program stars is larger than the percentages given by Wilson (1963) for stars of various spectral types randomly selected from the general field. The rotational velocities which we have obtained are certainly larger than that of the sun. If Kraft's (1965) results for stars near G0V may be taken as typical of a random selection of field stars, the rotational velocities of our stars are larger than his mean for stars near G0V.

Most of the program stars are probably relatively young objects with ages between the Pleides and Hyades. We can understand the observed Li^6/Li^7 ratios assuming even a small Li depletion, as Li^6 is so readily destroyed. Although the uncertainty in Traub and Roesler's (1971) determination of the isotropic ratio in the sun as $Li^6/Li^7 = 0.04 \pm 0.02$ is probably larger than quoted, we can understand why the solar isotope ratio is small. We still do not understand the low value of Li^6/Li^7 in meteorites.

It is clear that there is a correlation between the presence of a deep convection zone, rotational velocity and lithium abundance. There may also be a correlation (near G0V at least) between the rotational velocity and microturbulent velocity. The microturbulent velocity in the sun is a reflection of the convective cells which may be related to the energy source for the chromosphere and corona. The rotational velocity appears to be correlated with H-K emission. Hence such a correlation is at least plausible.

For the benefit of the reader who has bogged down in the morass of this long treatise, we summarize the main conclusions:

1) It is difficult to obtain reliable measurements of Li^6/Li^7 from photographic spectra.
2) The previous Li abundance determinations, including those in the C and S stars, are correct to within factors of 3, which are irrelevant in view of the large observed range in lithium abundances.
3) It is still not clear whether the lithium content of T Tauri stars is greater than the present upper limit for the interstellar Li abundance.
4) Kraft's work on rotational velocities, even for $v_{rot} < 10$ km/sec, is correct.
5) Li^6/Li^7 is very small in the program stars.

APPENDIX A

Profiles of the D Lines

We show in figure 32 the profiles of the D lines of Na I which were observed for some of the stars. Profiles of the D lines in 10 Tau were shown in figure 27, and in figure 32a-e we show those of ξ Peg, (F7V), 99 Her A (F7V), ι Per (G0V), η Psc (G8II), and η Cet (K2III). Points in these profiles, made with etalon D, are 0.041 Å apart, and the scale on the paper is 0.082 Å/cm for the first three stars and 0.164 Å/cm for η Psc and η Cet. The other axis is counts per channel (with the dark count removed). No correction for leakage was made, and the level of parasitic light is probably less than 2% of the continuum.

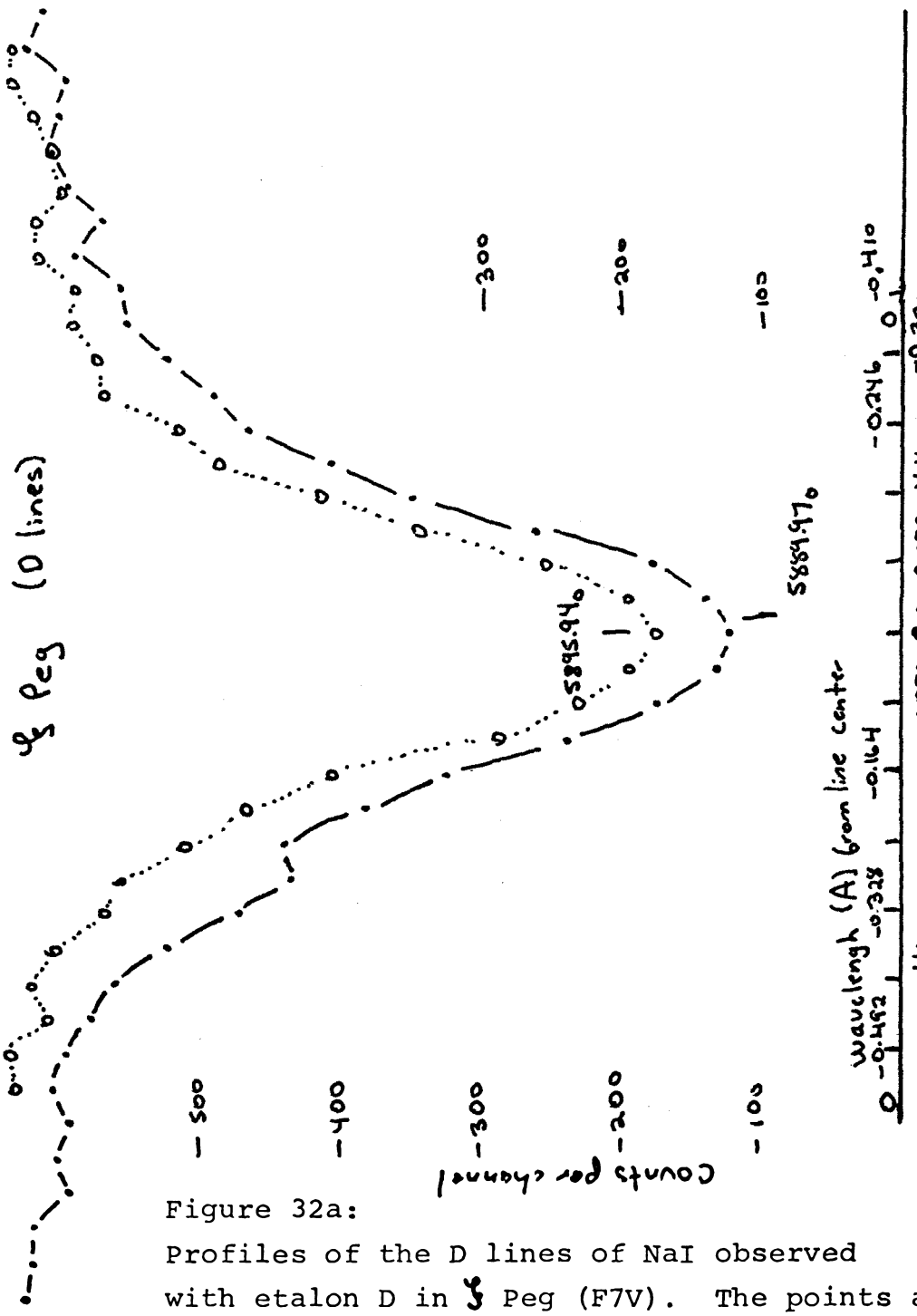

Figure 32a:
Profiles of the D lines of NaI observed with etalon D in ζ Peg (F7V). The points are 0.041A apart and the scale on the paper is 0.082A per centimeter.

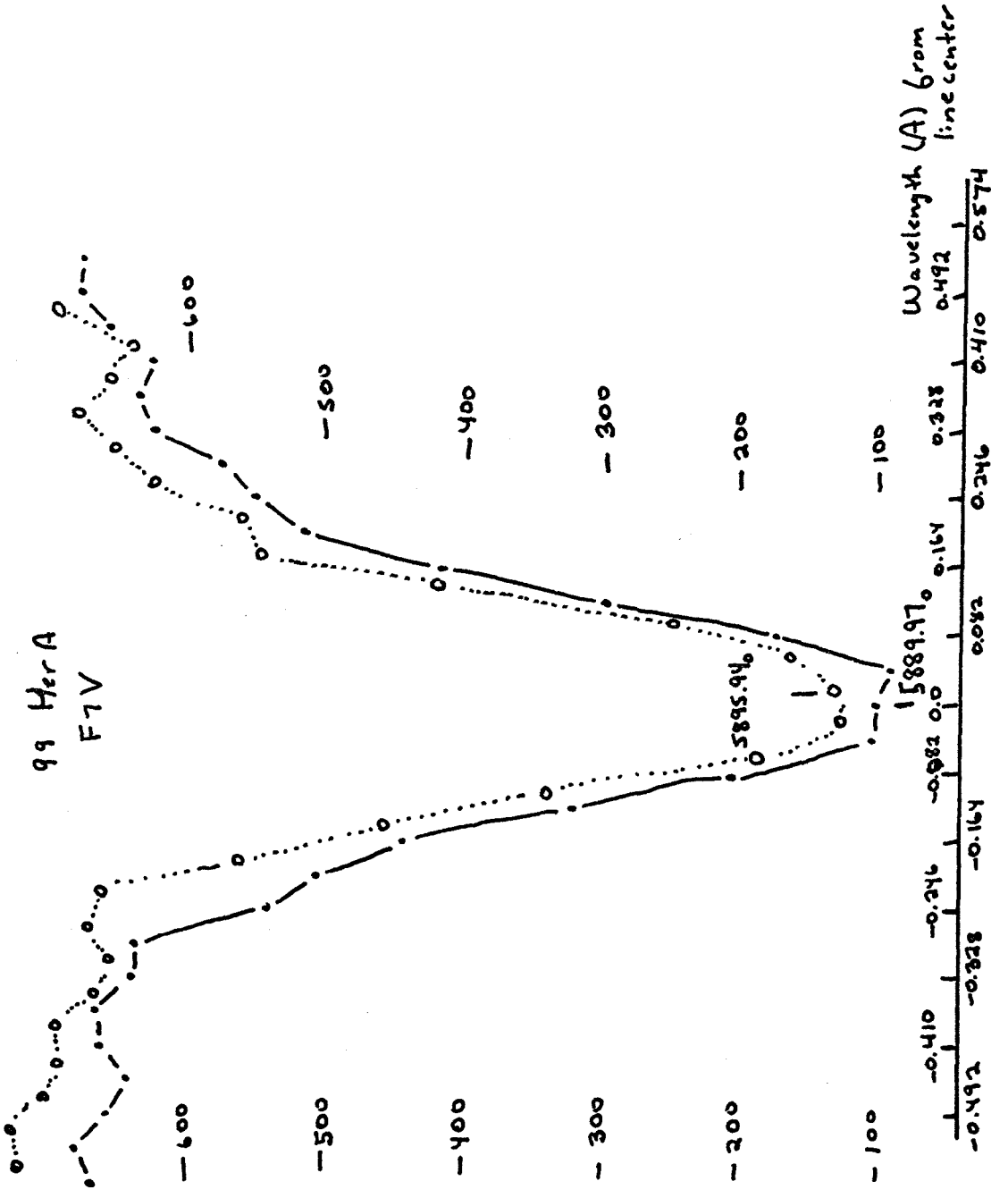

Figure 32b: Profiles of the D lines of NaI observed with etalon D in 99 Her A (F7V). The points are 0.041A apart and the scale on the paper is 0.082A/cm. Note the sharpness of the D lines compared with those of ξ Peg (figure 32a).

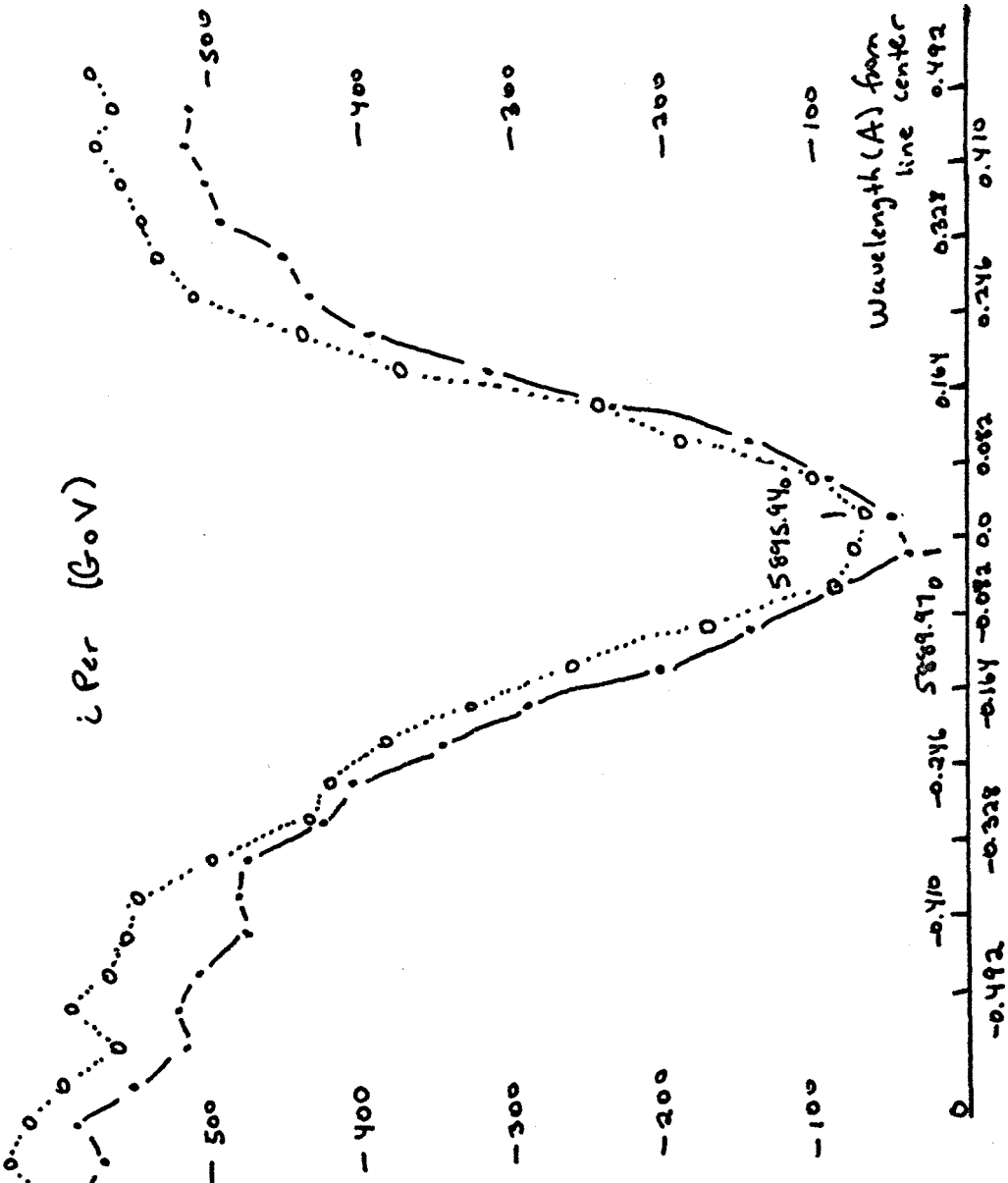

Figure 32c: Profiles of the D lines of NaI observed with etalon D in ι Per (G0V). The points are 0.041A apart and the scale on the paper is 0.082A/centimeter.

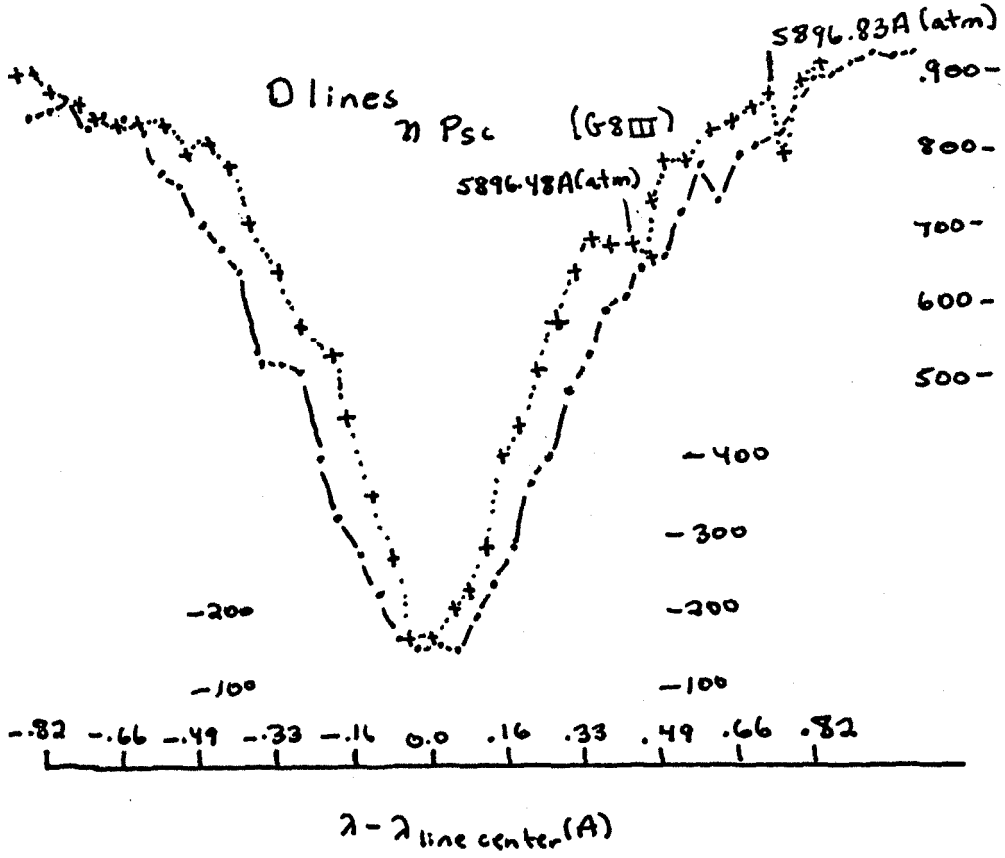

Figure 32d: Profiles of the D lines of NaI observed with etalon D in η Psc (G8III). Points are 0.041A apart, and the scale on the paper is 0.164A/cm. The cores of the lines are shown on a larger scale in figure 26m.

Figure 32e: Profiles of the D lines of NaI observed with etalon D in η Cet (K3III). Points are 0.041A apart, and the scale on the paper is 0.164A/centimeter.

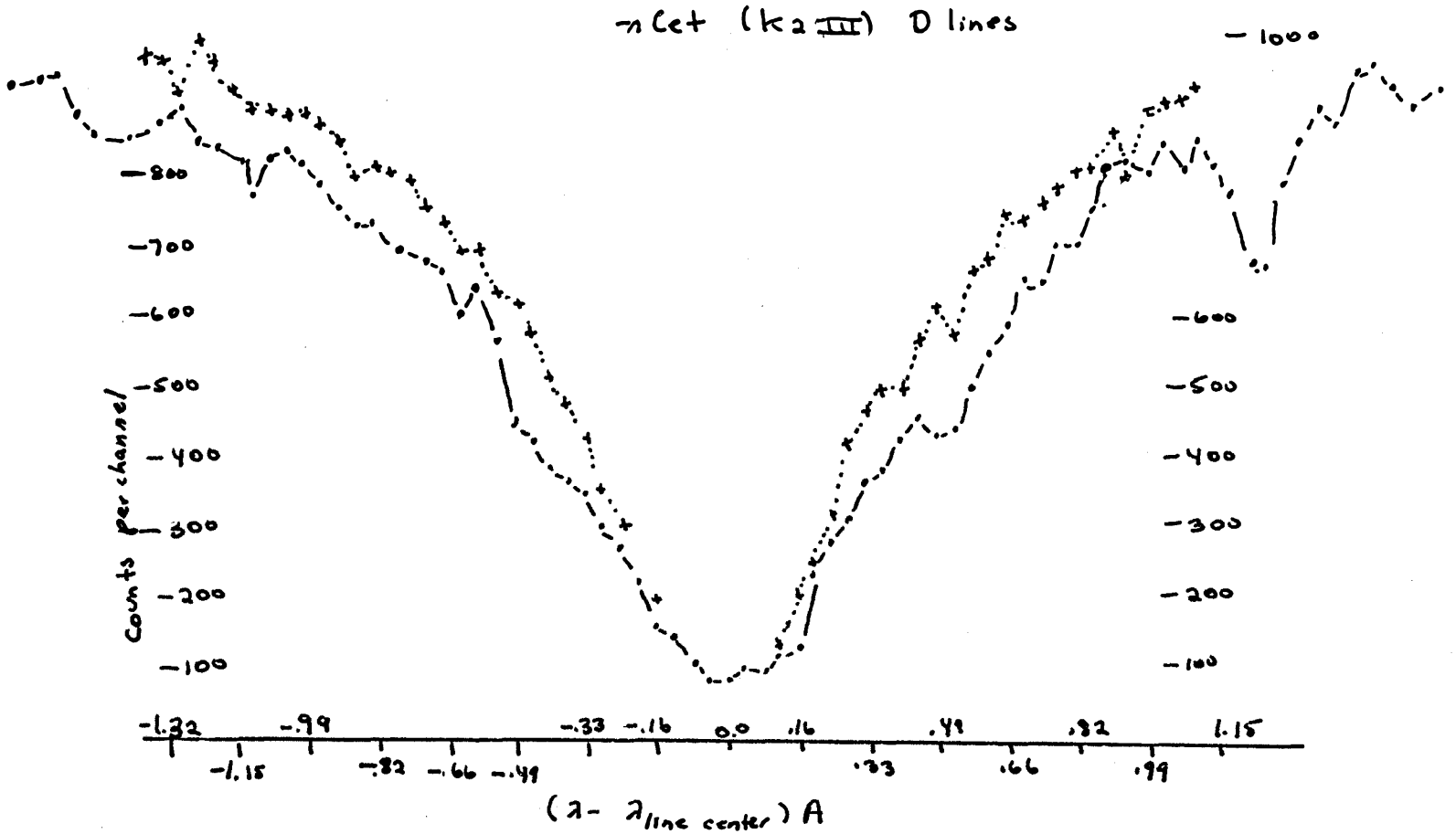

APPENDIX B

Deuterium

The computer programming techniques we used to obtain the absorption coefficient of the lithium resonance line (which is a blend of 4 components) are essentially the same as those required to obtain the absorption coefficient of a Balmer line of hydrogen blended with a deuterium line. The difficult part is to obtain the absorption coefficient for the Balmer line of hydrogen. We had available the computer program BALMER, written by Dr. Deane Peterson, which does this. The program is described in Dr. Peterson's unpublished thesis and in Strom and Peterson (1968). It therefore seemed easy and educational to compute deuterium profiles. Such profiles have been described recently by Peimbert and Wallerstein (1965a,b).

We modified the existing program by adding to the hydrogen line absorption coefficient at each depth and frequency point the deuterium line absorption coefficient κ_D. We scaled the hydrogen line absorption by a factor of 10^{-2} to 10^{-4} to obtain κ_D; we also took into consideration the fact that the Doppler width for deuterium is $1/\sqrt{2}$ that of hydrogen due to the difference in atomic weight. Furthermore, Γ for resonance (self) broadening for deuterium must be scaled by the isotope ratio. κ_D is then shifted in frequency relative to the Balmer hydrogen line by the appropriate amount, and the emergent flux is computed by the usual means. Such deuterium-Balmer line profiles have been calculated using several model atmospheres and

isotope ratios for H_α, H_β and H_γ. We show some typical ones in figure 33. Note that D/H for the H_α profile is a factor of 3 less than D/H for the H_β and H_γ profile.

We see that it is much more reasonable to search for deuterium using H_α rather than H_γ, which is more commonly tried. This is because the H_α line has the largest isotope shift (1.785Å), and the line is least broadened by the Stark effect. Thus H_α is sharper and narrower than H_γ and hence the ratio of κ_D(D line center)/κ_H(D line center) is a maximum. This produces a much larger deuterium feature at H_α for a given D/H than at H_γ, as is shown in figure 1.

The cores of the theoretical profiles are not expected to be very accurate, as they are formed so high in the atmosphere that the models are no longer reliable. At the center of a Balmer line, $\tau_\nu = 1$ is reached at $\tau_{5000} = 10^{-4}$ to 10^{-5}. However at 1 Å from the line center, $\tau_\nu = 1$ is reached at $\tau_{5000} = 0.005$ for H_α and 0.03 for H_γ. This is probably deeper than the temperature minimum and therefore the deuterium line profiles are qualitatively reliable, excluding the core, for deuterium abundances less than 10^{-3} = D/H. If D/H is larger than this, the part of the Balmer line near the deuterium central wavelength is formed so high up that the atmospheric model is not valid.

If the rotational velocity is large, then the deuterium line will be even more difficult to observe.

Deuterium has never been observed in any extraterrestial object. Upper limits to D/H for several Ap stars were derived from

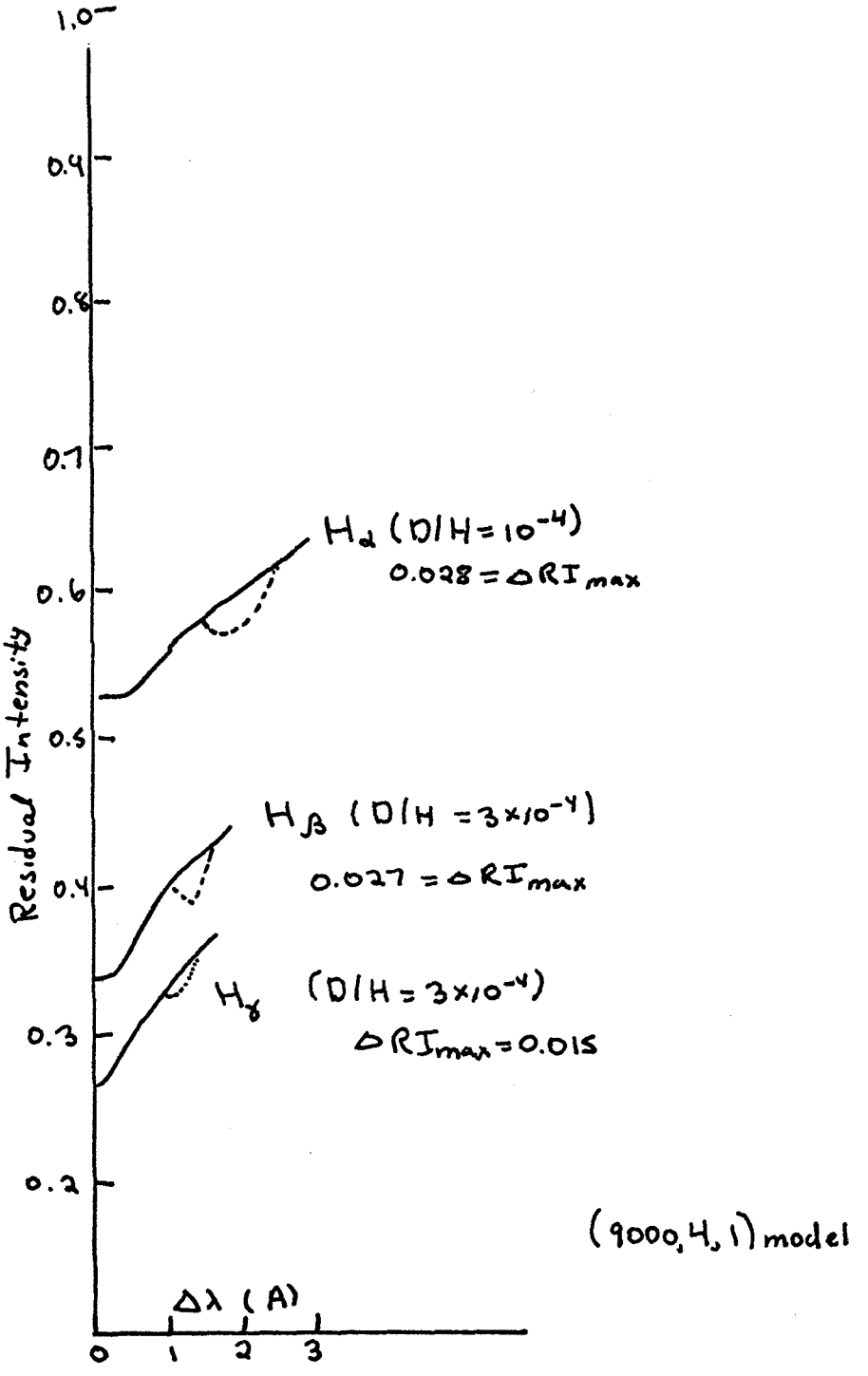

Figure 33: Profiles near the line center for Balmer lines (solid lines) and for Balmer lines blended with deuterium lines (dotted lines) for a (9000,4,1) model.

averaged photographic H_γ profiles obtained by Profs. Sargent and Greenstein. These limits are $D/H \leq 6 \times 10^{-4}$ for HD 204411, 112 Her, and 53 Tau. The upper limits of Peimbert and Wallerstein (1965a), using their second (more accurate) method, are about the same for the Ap stars they observed. Peimbert and Wallerstein's (1965a) first estimate of upper limits for D/H is too low by an order of magnitude.

REFERENCES

Allen, C. W. (1964) Basic Astrophysical Quantities, (2nd ed., London, Athlone Press).

Aller, L. H. (1963) Astrophysics, the Atmosphere of the Sun and Stars, (New York, Ronald Press).

Ambartsumyan, V. A. ed. (1959) Theoretical Astrophysics, (London, Pergamon Press).

Avrett, E. H. (1966) Ap. J., 144, 59.

Berman, L. (1931) LOB, 15, 109.

Bodenheimer, P. (1965) Ap. J., 142, 451.

Bodenheimer, P. (1966) Ap. J., 144, 103.

Boesgaard, A. M. (1968) Ap. J., 154, 185.

Boesgaard, A. M. (1970) Ap. J., 161, 83.

Bonsack, W. K. (1959) Ap. J., 130, 843.

Bonsack, W. K. and Greenstein, J. L. (1960) Ap. J., 131, 83.

Corliss, C. H. and Bozman, W. R. (1962) Experimental Transition Probabilities for Lines of Seventy Elements, NBS Monograph 53.

Curtis, G. W. (1965) in SAO Special Report No. 174, p. 301.

Curtis, H. D. (1904) LOB, 2, 169.

Canziger, I. J. (1967) Ap. J., 150, 733.

Danziger, I. J. and Conti, P. S. (1966) Ap. J., 146, 383.

Danziger, I. J. and Vaughn, A. H. (1969) quoted in Wallterstein and Conti (1969).

Dworetsky, M. M. (1970) private communication (see Preston 1971).

Engvold, O., Moe, O. K., and Maltby, P. (1970) Astron. and Astrophys., 9, 79.

Feast, M. W. (1970) MNRAS, 148, 489.

Fujita, Y. (1970) Interpretation of Spectra and Atmospheric Structure in Cool Stars, (Tokyo, University of Tokyo Press), pp. 107.

Greenstein, J. L. and Richardson, R. S. (1951) Ap. J., 113, 536.

Griem, H. R. (1964) Plasma Spectroscopy, (New York, McGraw-Hill), pp. 455.

Griffin, R. F. (1968) A Photometric Atlas of the Spectrum of Arcturus, (Cambridge, Cambridge Philosophical Society).

Herbig, G. H. (1962) in Advances in Astron. and Astrophys., 1, ed. Z. Kopal (New York, Academic Press), pp. 47.

Herbig, G. H. (1964) Ap. J., 140, 702.

Herbig, G. H. (1965) Ap. J., 141, 588.

Herbig, G. H. (1968) Zt. f. Ap., 68, 243.

Herbig, G. H. (1970) private communication.

Herzberg, G. (1944) Atomic Spectra and Atomic Structure (New York, Dover Publications), pp. 59.

Hoffleit, D. (1964) Yale Catalogue of Bright Stars, (New Haven, Yale University Press).

Huang, S. S. and Struve, O. (1953) Ap. J., 118, 463.

Hudson, R. D. and Carter, V. L. (1967) Jrl. Opt. Soc. Am., 57, 651.

Iben, I. (1965) Ap. J., 141, 993.

Kodak Publication P-9 (1967) Eastman Kodak Co, Rochester, N.Y.

Kohl, K. (1964) Zt. f. Ap., 60, 115.

Kraft, R. P. (1965) Ap. J., 142, 681.

Kraft, R. P. (1967) Ap. J., 150, 551.

Kuhi, L. V. (1964) Ap. J., 140, 1409.

Kuhi, L. V. (1965) PASP, 77, 253.

McKellar, A. (1960) Stellar Atmospheres, ed. J. L. Greenstein, (Chicago, University of Chicago Press), pp. 569.

Mendoza, V., E.E. (1966) Ap. J., 143, 1010.

Mendoza, V., E.E. (1968) Ap. J., 151, 977.

Merchant, A. E. (1967) Ap. J., 147, 587.

Minnaert, M., Mulders, V. F. W., and Houtgast, J. (1940) Photometric Atlas of the Solar Spectrum, (Utrecht, Sterrewacht Sonnenborgh).

Moore, C. E. (1959) A Multiplet Table of Astrophysical Interest, NBS Technical Note 36.

Moore, C. E., Minnaert, M. G. J., and Houtgast, J. (1966) The Solar Spectrum, NBS Monograph 61.

Mugglestone, D. (1965) in SAO Special Report No. 174, 357 pp.

Oke, J. B. and Conti, P. S. (1966) Ap. J., 143, 135.

Oke, J. B. and Schild, R. E. (1970) Ap. J., 161, 1015.

Peach, J. V. (1968) MNRAS, 139, 403.

Pearce, J. A. (1924) LOB, 11, 131.

Peimbert, M. and Wallerstein, G. (1965a) Ap. J., 141, 582.

Piembert, M. and Wallerstein, G. (1965b) Ap. J., 142, 1024.

Peterson, D. M. and Scholz, M. (1971) Ap. J., 163, 51.

Petrie, R. M. (1962) in Astronomical Techniques, ed. W. A. Hiltner, (Chicago, University of Chicago Press), pp. 75.

Preston, G. W. (1971) Ap. J., 164, L41.

Reeves, H. (1969) Nuclear Reactions in Stellar Surfaces and their Relations with Stellar Evolution, lecture notes, U. of Tel Aviv Winter School.

Reeves, H., Fowler, W. A., and Hoyle, F. (1970) Nature, 226, 727.

Ritschl, R. and Schober, H. (1937) Phys. Zeit, 38, 6.

Sargent, W. L. W. and Jugaku, J. (1961) Ap. J., 134, 777.

Schadee, A. and Davis, D. N. (1968) Ap. J., 152, 169.

Schmahl, G. and Schroter, E. H. (1965) Zt. f. Ap., 62, 143.

Smak, J. (1964) Ap. J., 139, 1095.

Strom, S. E. and Avrett, E. H. (1964) Ap. J., 140, 1381.

Strom, S. E. and Avrett, E. H. (1965) Ap. J. Supl., 12, 1.

Strom, S. E. and Peterson, D. M. (1968) Ap. J., 152, 859.

Traub, W. and Roesler, F. L. (1971) Ap. J., 163, 629.

van den Bos, W. H. (1927) Danske Videnskabernes Selskab, 12, 295.

Vaughn, A. H. (1967) Ann. Revs. Astron. and Astrophys., 5, 139.

Vaughn, A. H. (1971) private communication.

Waddell III, J. (1962a) Ap. J., 136, 223.

Waddell III, J. (1962b) Ap. J., 136, 231.

Wallerstein, G., Herbig, G. H., and Conti, P. S. (1965) Ap. J., 141, 610.

Wallerstein, G. and Conti, P. S. (1969) Ann. Revs. Astron. and Astrophys., 7, 99.

Wiese, W. L., Smith, M. W., and Glennon, B. M. (1966) Natl. Standards Reference Data Series 4, Atomic Transition Probabilities, 1.

Wilson, O. C. (1963) Ap. J., 138, 832.

Wilson, O. C. (1966) Ap. J., 144, 695.

Wright, K. O., Lee, E. K., Jacobson, T. V. and Greenstein, J. L. (1964) Publ. D.A.O. 12, 173.